Assessment of multi-sensor data assimilation for improved land surface model heat flux prediction

Robert Carl Pipunic

September, 2014

Submitted in total fulfilment of the degree of

Doctor of Philosophy

Department of Infrastructure Engineering

The University of Melbourne

ABSTRACT

This thesis focuses on Land Surface Model (LSM) data assimilation for optimising latent (*LE*) and sensible (*H*) heat flux prediction. These fluxes influence cloud formation (hence precipitation) and atmospheric thermodynamics, therefore predicting them accurately is important for initialising Numerical Weather Prediction (NWP) forecasts. Applying data assimilation to update prognostic LSM state variables (typically soil moisture and soil temperature) with observed information can improve *LE* and *H* predictions. Furthermore, any overall improvement to modelled water balances will also have broader benefits in a water management context (i.e. for agriculture, water accounting etc.).

Options for initialising LSM states includes assimilating screen-level atmospheric variables, and various remotely sensed land surface variables. Soil moisture and skin temperature data have been demonstrated as useful for directly impacting soil moisture and temperature states. The potential benefits of assimilating remotely sensed *LE* and *H* products into LSMs, for optimising *LE* and *H* prediction, have yet to be explored in detail.

Evaluating *LE* and *H* assimilation is therefore a major objective of this thesis. It is examined in relation to assimilating different combinations of remote sensing data types, including soil moisture and skin temperature. Three main studies were undertaken: a synthetic-twin study; a one-dimensional study assimilating in-situ field observations; and a study assimilating remotely sensed data, including *LE* and *H* products. Field collection of *LE* and *H* (eddy covariance system), multi-depth soil moisture and temperature, and meteorological data over a full year was integral to this research. These data played a significant role in most experiments.

The point scale proof-of-concept synthetic study demonstrated improved *LE* and *H* prediction from assimilating *LE* and *H* observations over a three month period, similar to improvements from skin temperature, and surpassing improvements made by soil moisture assimilation which produced the best root-zone soil moisture prediction. Assimilation frequency was important, with *LE*, *H* and skin temperature data representing cloud-free conditions, and approximating twice-daily MODIS thermal data, producing better fluxes than when representing the nearly fortnightly repeat time of Landsat.

For the one-dimensional field data study, assimilation spanned one year with the time series of thermal related data filtered based on cloud-cover at the field site. Combined assimilation of different data types was also included. This study showed strong improvement to *LE* prediction from assimilating observed *LE* and *H*. While combined skin temperature and soil moisture assimilation improved *LE* the most, and also balanced this with simultaneous improvements to soil

moisture and temperature states. Improved soil moisture prediction from assimilating only near-surface soil moisture data translated to smaller *LE* improvement than from assimilating *LE* and *H*, or combined skin temperature and soil moisture.

The remotely sensed data study examined the assimilation of 25 km AMSR-E soil moisture data and of 5 km *LE* and *H* products derived from AQUA satellite based thermal observations. Experiments were performed with 5 km resolution model simulations spanning a year. Relative to data from 10 point scale in-situ stations, AMSR-E assimilation degraded the root-zone moisture predictions overall – with an average increase in RMSE of >100% compared to no assimilation. However, relative to single point-scale eddy covariance data, it improved *LE* prediction compared to no assimilation (RMSE reduced by 15%), with marginal improvement to *H* (reducing RMSE by ~1%). Assimilation of *LE* and *H* data derived from remote sensing improved both *LE* and *H*, reducing RMSE by ~13% and ~9% respectively compared to no assimilation. Repeated assimilation experiments using a range of increasing observational error for *LE* and *H* data (upwards from σ=50 Wm^{-2}) showed improvements to *LE* and *H* predictions with observational error of between 80 and 90 Wm^{-2}.

Validating results from spatial remote sensing studies is limited with sparsely distributed in-situ point-scale data. Furthermore, scale discrepancies between assimilated remotely sensed data, simulation resolution and point validation data make it challenging to understand the cause of the apparent poorer moisture predictions from the AMSR-E assimilation. The most important finding from this thesis is that assimilating *LE* and *H* can improve LSM predictions of *LE* and *H* beyond improvements from soil moisture, and beyond improvements from assimilating skin temperature alone. Another key finding was the potential of combined near-surface soil moisture and skin temperature data assimilation to improve *LE* predictions beyond what assimilating *LE* and *H* data can, while also improving the root-zone state predictions. This is important to verify in follow-up studies given that remotely sensed *LE* and *H* require additional effort for derivation which is based on skin temperature data in the first place. The right combination of multiple data types may therefore be the best solution in the long run for optimising heat fluxes and improving water balance predictions.

DECLARATION

This is to certify that:

i) the thesis comprises only my original work towards the PhD except where indicated in the Preface;

ii) due acknowledgement has been made in the text to all other material used;

iii) the thesis is fewer than 100,000 words in length, exclusive of tables, maps, bibliographies and appendices.

Robert C. Pipunic

PREFACE

Chapters 5 of this thesis has previously been published as:

Pipunic, R. C., Walker, J. P., & Western, A. W. (2008). Assimilation of remotely sensed data for improved latent and sensible heat flux prediction: A comparative synthetic study. *Remote Sensing of Environment*, 112, 1295–1305 (data assimilation special issue).

Chapters 6 of this thesis has also previously been published as:

Pipunic, R. C., Walker, J. P., Western, A. W., & Trudinger, C. M. (2013). Assimilation of multiple data types for improved heat flux prediction: A one-dimensional field study. *Remote Sensing of Environment*, 136, 315–329.

These journal articles each present part of the full series of complimentary experimental studies making up this thesis. As lead author at least 80% of the work for both publications was carried out by myself, which includes the background research, experimental work, analysis of results, and editing in response to journal editor and co-author reviews. The co-authors provided specific advice on some aspects of experiment design, with most of their input being in the form of manuscript review.

Elsevier Inc., the publisher of both articles, permits the author to republish them as part of a PhD thesis or other work for which there is no financial gain.

ACKNOWLEDGEMENTS

The primary funding for this research was an Australian Postgraduate Award Scholarship from the Australian Federal Government. Sincere thanks go to my supervisors, Professors Andrew Western and Jeffrey Walker. Professor Western's openness and intellectually stimulating contribution to discussions, and his generosity of time and ongoing support have been extremely valuable throughout this process. Professor Walker provided valuable input with the many discussions, the feedback on manuscripts, and financial support in the form of scholarship top-up and for the field work I undertook for this research – via a University of Melbourne-CSIRO Collaborative Research Support Scheme grant, for collaboration between himself and Dr Cathy Trudinger from CSIRO Marine and Atmospheric Research.

I also thank my various other colleagues and friends from over the years at The University of Melbourne. Including Dr Dongryeol Ryu for the discussions and useful advice on many aspects of land surface modelling and data assimilation, and Rodger Young for his technical and field work support, and his good conversation on those long drives during field trips. My appreciation also extends to Cressida Savige for giving me an introductory crash course on setting up eddy covariance systems.

From CSIRO Marine and Atmospheric Research, I am grateful to Dr Ying-Ping Wang who provided me with the CBM code used for this thesis and useful advice along the way, and to Dr Cathy Trudinger for helpful discussion and feedback on manuscripts.

Most importantly a big thank you to my family, especially my parents Ivan and Ingrid, their love and support over the years has meant a great deal to me. Time spent with family and friends throughout this process always reminded me of what's most important in life, and they have all contributed in some way to my achievements.

TABLE OF CONTENTS

LIST OF FIGURES

LIST OF TABLES

1 INTRODUCTION

Fluxes of latent (*LE*) and sensible (*H*) heat from the land surface influence the dynamics of the lower atmosphere, thus playing a key role in our weather and climate. Initialising Land Surface Models (LSMs) for optimal heat flux prediction is therefore important for weather forecasting. The overarching aim of this thesis is to contribute to existing knowledge on the best ways to optimise predictions from LSMs using remotely sensed information in a data assimilation framework. In addition to the climate and weather forecasting context, improving heat flux prediction is also relevant for a range of other problems that depend on accurate and timely land surface water and energy balance information for their solution.

This thesis evaluates the relative merits of assimilating different remote sensing data types into a LSM, in the context of yielding the most accurate land surface heat flux feedbacks (*LE* and *H*) to the atmosphere. Specifically, observed *LE* and *H*, surface skin temperature (the radiative temperature of the land surface, from here on referred to as skin temperature), and near-surface soil moisture are evaluated as the remotely sensed land surface observation types most likely to positively impact on LSM heat flux feedbacks. The individual and joint assimilation of these variables has been evaluated in terms of their impact on predictions of soil moisture and temperature states, together with the resultant *LE* and *H* predictions which characterise the land-atmosphere interaction.

Using an early version of the LSM that is a component of Australia's climate modelling and Numerical Weather Prediction (NWP) system, an ensemble Kalman filter (EnKF) was applied to assimilate both synthetic and in-situ observations representing typical remote sensing data types in a series of numerical experiments. The thesis concludes with a data assimilation application using actual remote sensing data products derived from MODIS and AMSR-E observations. Consequently, the trade-off between data type, temporal repeat and spatial scale have been explored through the use of these different observations.

1.1 RESEARCH MOTIVATION

LSM data assimilation research has received increased attention over the past 1 to 2 decades, driven largely by its potential for improving predicted land surface energy and water balance quantities for applications such as climate and NWP modelling (Balsamo *et al*., 2007; Mahfouf, 2010; Reichle *et al*., 2007; Van Den Hurk *et al*., 2002). Also facilitating this growth is the availability of different observation types from remote sensing that are related to the land surface water and energy balances – including near-surface soil moisture from microwave sensors (Kerr, 2001; Owe *et al*., 2008), skin temperature based on thermal infra-red imagery (Kumar & Kaleita, 2003), and instantaneous *LE* and *H* products derived using skin temperature (Bastiaansen, 1998; Su, 2002). Some of these data types have not been comprehensively explored for LSM assimilation applications and, in particular, there are very few published examples assimilating *LE* and/or *H* nor are there many studies looking at different combinations of these four variables.

An important LSM in the Australian context is the Community Atmosphere Biosphere Land Exchange model (CABLE: Kowalczyk *et al*., 2006, 2013), which is part of the Australian Community Climate Earth-System Simulator (ACCESS) set up for Australia's climate and NWP modelling (Kowalczyk *et al*., 2013; Law *et al*., 2012; Puri *et al*., 2013). The CSIRO Biosphere Model (CBM: Wang & Leuning, 1998; Wang *et al*., 2001, 2007) is an earlier version that was developed and used in-house by CSIRO researchers and has a similar structure for water and energy balances as CABLE – it was made available at the beginning of this research and hence for consistency has been used for all experimental work presented in this thesis. LSM data assimilation is seen as an integral part of any NWP within ACCESS (Puri *et al*., 2013), yet its application to CABLE and the CBM has not previously undergone rigorous testing.

Consequently, the main motives for this thesis are:

1) The need to better understand the relative impacts on LSMs from assimilating different observation types, or combinations of different observation types, that have not been comprehensively tested; and,

2) To understand the impacts from data assimilation specifically on the CSIRO Biosphere Model (CBM) and determine how suitable different observation types are for this model in terms of improving state variables and heat fluxes. This is important for informing future model development and data assimilation research into CABLE.

The ability to consistently improve *LE* and *H* prediction through the assimilation of key remote sensing observations will ultimately lead to better LSM initialisation for optimal weather and seasonal forecasts. Moreover, examining assimilation impacts on soil moisture and temperature state variables in conjunction with the related heat fluxes is expected to highlight limitations related to LSM physics and parameterisation, informing improvements that can be made for them. Scrutinising the impacts on CABLE from assimilating different data types and understanding the associated limitations is important prior to using it for operational NWP and performing assimilation in the more complex land-atmosphere coupled mode. Hence with CBM and CABLE sharing the same general structure for state variable and heat flux relationships, data assimilation experiments performed with CBM in this thesis will contribute knowledge relevant to the ongoing development of ACCESS and Australia's NWP and climate prediction.

1.1.1 IMPORTANCE OF LAND-ATMOSPHERE FEEDBACK PREDICTION

The main function of a LSM in climate and weather prediction systems is to quantify latent and sensible heat flux feedbacks to the lower atmosphere. These fluxes characterise the transfer of energy as latent heat in the form of water vapour (*LE*) and sensible heat (*H*) from the land surface to the atmosphere (Brutsaert, 2005). Subsequent condensation of the evaporated/vegetation-transpired water into cloud – leading to precipitation – is associated with a release of heat energy, which together with near surface heat conductance contributes to atmospheric convection, thus driving the thermodynamics of the atmosphere and hence our weather and climate (Brutsaert, 2005; Pitman, 2003).

With atmospheric processes strongly dependent on land surface *LE* and *H* feedbacks, these fluxes are the lower boundary conditions for atmospheric model equations, hence the importance of LSM initialisation to optimise predicted heat flux accuracy for climate modelling and NWP (Balsamo *et al*., 2007; Dirmeyer *et al*., 2009; Viterbo & Beljaars, 1995; Viterbo & Beljaars, 2004). As a key water supply for evapotranspiration (*ET*), soil moisture content is an important water balance component linking in with the energy balance. It regulates the proportions of net radiation available at the land surface that are converted into *LE* and *H*, and therefore soil moisture state variables are typically the target of LSM initialisation (de Rosnay *et al*., 2013; Dharssi *et al*., 2011; Koster *et al*., 2004). Soil temperature is also an important part of the land surface energy balance, with heat transfer and storage through the soil profile directly linked to skin temperature and therefore *LE* and *H*, so it is also recognised as an important state for LSM initialisation (Balsamo *et al*., 2007; Chen *et al*., 2007; Entekhabi *et al*., 1994).

1.1.2 PROBLEMS WITH LAND MODELS

The partitioning of available net radiation energy at the land surface into *LE* and *H* feedbacks to the atmosphere is a process that depends on a range of factors: soil moisture content, soil temperature, various soil physical properties, vegetation cover, and physical and biological properties relating to particular vegetation types. LSMs are an attempt to relate these factors in a mathematical framework, together with meteorological variables, for predicting water evaporation from soil and/or its transpiration through vegetation (*LE*) and the transfer of sensible heat (*H*) into the lower atmosphere on a continuous time scale.

LSMs are limited in that they represent highly variable and complex physical systems with simplified and/or empirically derived mathematical relationships. Another major shortcoming is that parameter values are often difficult to set because there is not enough data on model soil and vegetation properties to accurately represent the high temporal and spatial variation of these quantities (Franks & Beven, 1999; Yates *et al.*, 2003). While field measurements can assist in parameterising models at the point scale with considerable effort (Mertens *et al.*, 2005), this is more challenging when modelling across spatially heterogeneous landscapes without measurements on a scale or of an extent relevant to a particular application (e.g. spatial remotely sensed soil moisture data is not of a depth that can provide direct information on root-zone soil hydraulic properties). The complexity of many models means they often contain too many parameters for them all to be optimised with unique solutions given a limited number of relevant types of field measured data (Franks & Beven, 1999). Errors in meteorological forcing data also impact on the quality of model output. Overall, LSM predictions are inherently uncertain, with prediction uncertainty typically increasing through time.

Data assimilation is well suited for improving LSM predictions (e.g. Crosson *et al.*, 2002; Reichle *et al*., 2008) by sequentially updating/correcting prognostic state variables through time whenever new observed information becomes available. A key feature of assimilation is the factoring in of estimates of uncertainty inherent in both models and observed data, in order to appropriately weight the degree of model state adjustment for improved predictions. Estimates of errors in different related model variables provide information to relate the updates made directly to one variable from an observation with updates to other related model variables. Global coverage and regular temporal repeat of emerging remote sensing data streams, related to land surface state and flux quantities, improves the prospects for routinely improving LSM predictions over different spatial scales via data assimilation.

The hypothesis put forth in this thesis is that due to imperfect model structure and parameter estimates, the greatest improvements to predictions of any particular LSM state or flux from data assimilation would come from assimilating observations of the same variable or one that is most closely related to it. Under this hypothesis, model states would best be adjusted by the observation chosen to suit the variable of interest in spite of structural inaccuracies. In addition, this would not necessarily result in the most physically realistic values for all states. If the aim for NWP is to optimise *LE* and *H* prediction, then it seems intuitive to test the assimilation of *LE* and *H* observations. Very little research has focused on the assimilation of remotely sensed instantaneous estimates of these quantities, perhaps partly due to the fact that these are emerging products (derived using remotely sensed skin temperature observations). Validation of such products and development of standard uncertainty estimates required for data assimilation are still major challenges, which are exacerbated by the sparseness and scale differences of independent flux measurement sites distributed across the world.

In the context of getting the best predictions possible from imperfect models for a specific purpose, understanding whether assimilating *LE* and *H* data is a better strategy than assimilating soil moisture or skin temperature for improving *LE* and *H* predictions is important. It is also important to consider how assimilating different combinations of data types, to target different parts of the LSM water and energy balance, can simultaneously impact on states and fluxes. If the structure of LSMs cannot ensure that optimal improvements made to any variable will cause optimal improvements to all related quantities, more pragmatic data assimilation strategies targeted at particular applications are necessary.

1.2 OBJECTIVES AND SCOPE

The overall objective of this research was to conduct modelling experiments for examining the impacts of assimilating different data types – all of which are available from remote sensing – on CBM state and heat flux predictions.

This broader objective was broken down into the components listed below, the first few of which were necessary for facilitating the experiments:

- Undertake a field study to obtain data to support the study, including the set-up and management of in-situ *LE*, *H*, soil moisture, soil temperature and meteorological data collection for at least a full seasonal cycle over a year. These provided for experiments in a simpler one-dimensional modelling scenario, prior to more complex spatial experiments with remotely sensed data, while also providing for validation of different experiment results;

- Source available remote sensing data products for assimilation. Most importantly, instantaneous *LE* and *H* products, so that assimilation of these could be tested in a real spatial modelling scenario alongside that of a near-surface soil moisture product representing a more commonly assimilated remotely sensed data type;

- Develop an EnKF for the CBM which includes model error specification and an associated ensemble generation strategy, as well as applying a technique for removing/minimising systematic bias between model state predictions and real observed data prior to their assimilation.

The model experiments progressed from one-dimensional synthetic-twin and real in-situ field data modelling scenarios, followed by a more realistic spatial application scenario using remotely sensed data. The one-dimensional studies were more controlled in terms of there being more reliable uncertainty estimates for models and observations at the point scale, such that model impacts could be understood with greater certainty before carrying out the spatial study. The specific objectives were:

- Carry out a proof-of-concepts study over a short period, via synthetic-twin experiments, ensuring the EnKF algorithm works correctly with the CBM and whether assimilating the different data types show promising results worthy of further investigation using real observation-based data sets;

- Perform a one-dimensional study assimilating the data types used in the synthetic-twin study – with additional joint assimilation of different combinations of those data – but using real point scale data from independent in-situ field measurements that traverse major seasonal changes, for a more robust examination of impacts on the CBM;

- With knowledge from the previous studies on how assimilating *LE* and *H* observations may impact the CBM compared to a more commonly assimilated product such as soil moisture, undertake a study assimilating remotely sensed *LE*, *H*, and soil moisture data products. Validate results with independent in-situ data available for the study region and assess whether similar conclusions can be drawn as per results for the one-dimensional studies.

By addressing this list of specific objectives which involves experimental simulations and quantitative analyses, a better understanding is gained about which data assimilation strategies are most beneficial for improving the prediction of heat flux feedbacks to the atmosphere. In particular, whether assimilating remotely sensed *LE* and *H* data is promising. General insight was also gained into some current limitations of remotely sensed LSM data assimilation, including limitations LSMs themselves can pose – in terms of the relationships between key prognostic state variables and diagnostic heat fluxes – to applying data assimilation effectively.

The scope of this research was confined to a series of data assimilation experiments performed using a specific LSM and assimilation algorithm. Using the objectives above as a guide, the primary focus was on assimilating different observation types and analysing the impacts each had on predictions from that LSM. The scope of the research does <u>not</u> include:

- Improving the physics of the LSM (the CBM was used on an "as is" basis);

- A comparison and/or evaluation of the diverse range of data assimilation algorithms, or of a broad variety of techniques that can be applied in implementing the EnKF; or

- LSM assimilation within a coupled land-atmosphere model system.

1.3 THESIS ORGANISATION

This thesis is arranged into eight chapters including this introduction chapter.

Chapter 2: Covers a review of literature and provides a synthesis of background information underpinning the work in this thesis. This includes summaries of: Energy and water interaction between the land surface and atmosphere; In-situ measurement methods and remote sensing observations related to the data types used in experiments in this thesis; Characteristics of LSMs and how formulations have changed over time; and, Data assimilation background including some of the different methods. The chapter concludes with a survey of past LSM data assimilation applications highlighting knowledge gaps that motivated the experimental work in this thesis.

Chapter 3: Provides specific details on the modelling tools used – the CSIRO Biosphere Model (CBM) and the Ensemble Kalman Filter (EnKF) algorithm. It details the CBM structure including key relationships between state variables and fluxes relevant to data assimilation. Details are also given on the EnKF/CBM implementation including ensemble generation methods.

Chapter 4: All of the data sets that were used are presented here including maps showing geographic locations of measurement sites and the spatial extent of products. Reference to data sources and methods used for deriving products are also included in addition to the particular experiment in this thesis that they were used for.

Chapter 5: The synthetic-twin study is presented here. As a proof-of-concept, this study examines the impacts from assimilating synthetically derived *LE*, *H*, skin surface temperature and near-surface soil moisture data on the CBM.

Chapter 6: This covers the one-dimensional field data assimilation study, where real *LE*, *H*, skin surface temperature and near-surface soil moisture data from point-scale field measurements were assimilated.

Chapter 7: Presented here is the spatial data assimilation study using real remotely-sensed products – namely near-surface soil moisture derived from AMSR-E observed microwave data, and instantaneous *LE* and *H* derived from MODIS surface temperature data.

Chapter 8: The conclusions chapter where the over-arching findings across the three experimental studies are discussed. Specifically in terms of the potential for improving heat flux and soil state predictions by assimilating *LE* and *H* data, compared to assimilating other remotely sensed land surface data types. Challenges to performing optimal data assimilation for LSMs are also discussed along with directions for further research.

2 BACKGROUND AND LITERATURE SURVEY

This chapter is a synthesis of background information underpinning the experimental work carried out for this thesis. It is based on a review of literature and sets the context for the following chapters. Included are brief descriptions of the land surface in terms of key water and energy balance components. Approaches to quantifying some of these components – both from in-situ and remote sensing observations – which are relevant to observations used in this research are also discussed. A general overview is then given of the main features of LSMs and how their development has evolved through time into the typical modern day models such as the one used in this research. This is followed by a summary of data assimilation and evolution of its application to LSMs, highlighting how the research in this thesis contributes to a broader body of work.

2.1 THE LAND SURFACE

The term 'land surface' used here refers broadly to the earth's landscapes at the interface with the atmosphere, inclusive of vegetation and the unsaturated soil zone between the soil surface and the groundwater table. Water and energy exchanges between the land surface and the atmosphere are linked, and the fundamentals of the science behind our current understanding of these continuous processes can be found in introductory texts on hydrology such as those of Beven (2012), Ladson (2008) and Brutsaert (2005). These texts were drawn upon for much of the generic background information summarised in this section with other sources referenced where relevant.

2.1.1 THE ENERGY BALANCE

Fig. 2.1 is a schematic of the major land surface energy balance components described here. Land cover influences surface albedo which represents the fraction of total incoming shortwave (solar) radiation that is reflected away from it, while the remaining fraction is absorbed. Some generic albedo values given by Brutsaert (2005) for different surfaces include: ~0.8-0.9 (highly reflective) for fresh snow; ~0.05-0.15 (minimal reflection and high absorption) for moist dark soil; and, ~0.15-0.25 for green grass. Longwave radiation (or thermal infrared energy) plays a key role in the energy balance, with the land surface emitting it and absorbing it from the atmosphere. Emitted longwave radiation from the land surface can be described by the Stefan Boltzmann law

$$\uparrow LW = \varepsilon \sigma T_{sk}^{\ 4}, \qquad (2.1)$$

where $\uparrow LW$ represents the emitted longwave radiation, ε the emissivity, σ the Stefan Boltzmann constant ($= 5.67 \times 10^{-8} Js^{-1}m^{-2}K^{-4}$) and T_{sk} the radiative temperature of the land surface (representing contributions from soil and vegetation surfaces), which is referred to hereon in as the skin temperature. For a perfect black body the value of ε is 1 and approximate values for some different surfaces from Brutsaert (2005) include: ~0.99 for fresh snow; ~0.95-0.98 for bare soil; 0.96-0.97 for tree vegetation; and, ~0.97-0.98 for grassy vegetation.

The total sum of the major vector quantities of radiation – incoming shortwave ($\downarrow SW$), incoming longwave ($\downarrow LW$), reflected shortwave ($\uparrow SW$) and emitted longwave ($\uparrow LW$) – defines the net radiation (R_N) that is available to the land surface, so

$$R_N = \downarrow SW - \uparrow SW + \downarrow LW - \uparrow LW . \qquad (2.2)$$

The terrain, soil type, and vegetation type and cover of the land surface typically varies over a range of spatial scales (Richter *et al*., 2004; Yates *et al*., 2003) which translates to variations in albedo and emissivity. This spatial heterogeneity implies that there can be significant variation in R_N across landscapes which receive similar amounts of incoming radiation. Most

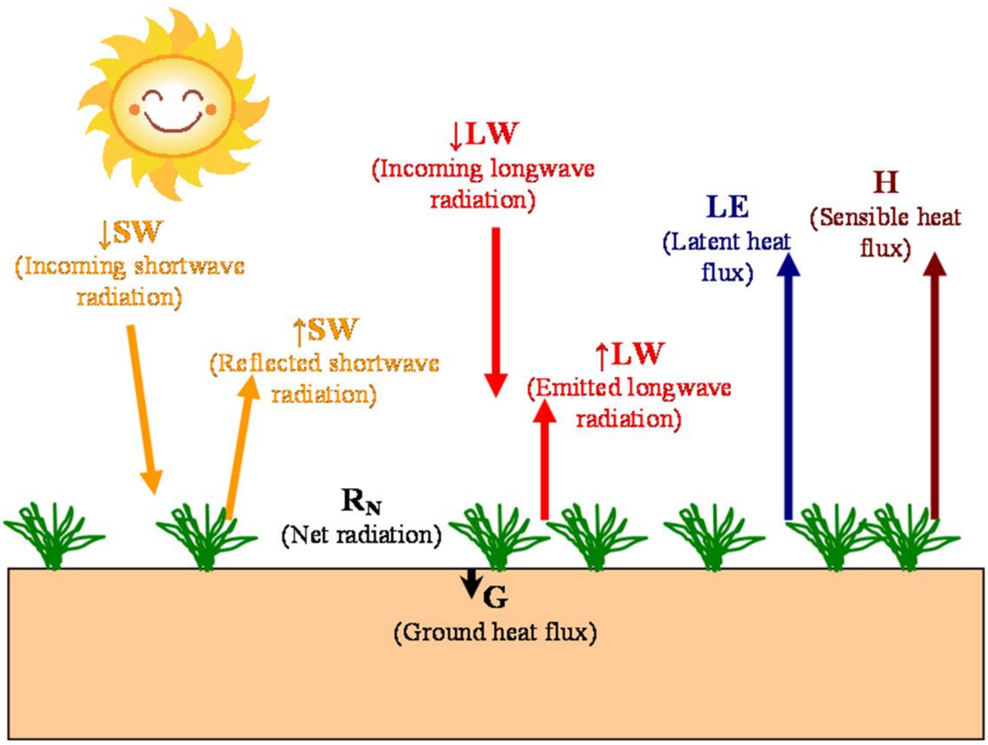

Figure 2.1: *Schematic of the major energy balance components at the land surface.*

of the R_N available to the land surface is subsequently partitioned to produce either latent (LE) or sensible (H) heat flux feedbacks to the atmosphere, in addition to a residual (typically smaller) energy flux into the soil termed the soil heat flux (G) as illustrated in Fig. 2.1. From Hsieh *et al.* (2009), G can be up to 50% of the R_N for dry soil surfaces in some conditions. Soil temperature (T_{Soil}) shares a strong relationship with G and is an important state of the land surface energy balance (De Ridder, 2009). The governing equation for soil temperature and heat transport is

$$\rho_s c_s \frac{\partial T_{Soil}}{\partial t} = -\frac{\partial G}{\partial z}, \qquad (2.3)$$

where the expression for heat transport after Fourier is

$$G = -k \frac{dT_{Soil}}{dz}. \qquad (2.4)$$

The terms t and z in Eqs. (2.3) and (2.4) are time and the depth below the surface respectively, whereas ρ_s and c_s are the soil properties of bulk density and specific heat capacity respectively, and k is the soil thermal conductivity. These equations illustrate that G is proportional to the magnitude of the vertical soil temperature gradient. The variation in T_{Soil} at the near-surface (which relates to T_{sk}) has a strong diurnal component, resembling the diurnal variation of R_N driven by day-time/night-time maximum/minimum of $\downarrow SW$ forcing incident upon the land surface (Eq. (2.2)). As soil depth increases, the temperature variation increasingly represents only seasonal time scale changes. Fig. 2.2 illustrates the contrasting temporal variation of T_{Soil} at different depths via a data series measured for this research at Kyeamba Creek in Australia.

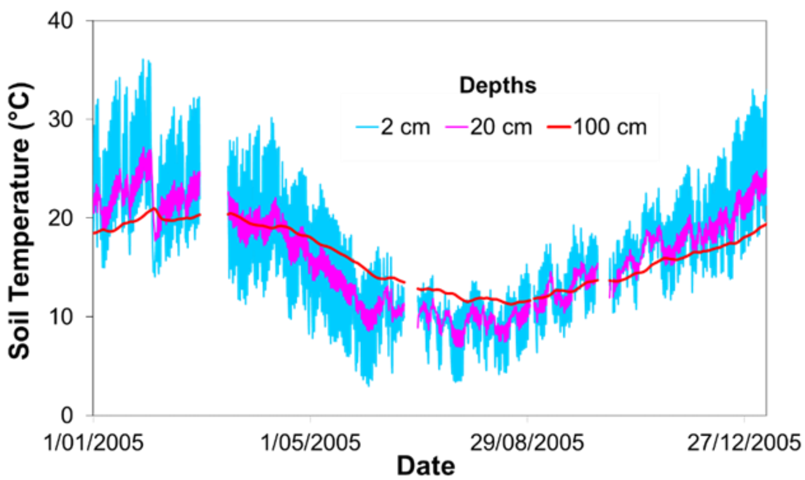

Figure 2.2: *Soil temperature variation at three depths – Kyeamba Creek, Australia.*

As summarised throughout much of the literature (e.g. Beven, 2012; Brutsaert, 2005; Ladson, 2008; and many others), LE, H and G are the main quantities resulting from R_N partitioning at the land surface (Fig. 2.1. and Eq. (2.2)) and therefore the energy balance can be represented as

$$R_N = LE + H + G\,. \qquad (2.5)$$

A major factor controlling the partitioning of R_N, and an important link between the land surface energy and water balances, is the amount of soil moisture available for soil evaporation (E) and plant transpiration via root uptake (in combination referred to as evapotranspiration or ET), where ET is the expression of LE as a quantity of vaporised/transpired water over a given time interval. As soil moisture content (θ) approaches zero, LE becomes minimal and a greater portion of available energy at the land surface is fed-back to the atmosphere as conductive heat with an increase in H. Hence θ regulates R_N partitioning into the major heat flux components (Reichle *et al*., 2002), thus influencing the Bowen ratio (Bowen, 1926):

$$Bo = H/LE\,. \qquad (2.6)$$

2.1.2 THE WATER BALANCE

The natural water supply to the land surface is from precipitation in the form of rainfall or snow. Only rainfall is considered relevant here due to the snow-free environments for which the modelling experiments were carried out. Rain water either directly reaches the soil surface or is intercepted by vegetation cover from where it can evaporate or drip through to the soil surface. At the soil surface it either evaporates, infiltrates into the soil or becomes gravity-driven surface runoff which flows into topographic depressions or waterways. For rainfall to become surface runoff there needs to be a sufficient surface gradient and the rate of rainfall needs to exceed the rate of infiltration (which typically decreases with increasing θ), and if the soil is saturated (maximum θ) there is no infiltration and practically all rainfall becomes runoff (Beven, 2012). Therefore θ is a very important state in the overall water balance given its effect on different hydrologic processes, including its key role in determining LE and H.

The definition of θ in this thesis is the volumetric soil moisture content, which using the notation from Brutsaert (2005),

$$\theta = \lim_{V_{H2O} \to \theta_{sat}} \left(\frac{V_{H2O}}{\Delta \forall} \right), \qquad (2.7)$$

is the total volume of water (V_{H2O}) contained in the pore space of a given bulk soil sample, per total volume of that sample ($\Delta\forall$). The maximum possible θ (being for saturated soil: θ_{sat}) is equivalent to the soil porosity, or the volume of pore space between solid particles (with volume V_{solids}) where

$$\theta_{sat} = 1 - \left(\frac{V_{solids}}{\Delta\forall}\right). \qquad (2.8)$$

Pore space varies with soil type due to differing proportions of different sized soil particles (i.e. sand, clay and silt) and it is a pathway for infiltrated water to percolate through. The rate of infiltration is dependent on the soil hydraulic conductivity (K), potential gradient (ψ) and rainfall rate. For ψ, the holding force between water and the soil matrix (e.g. capillarity) is the dominant factor, with the terms pressure head, matric potential or soil suction commonly used for it. As soils drain post saturation, a balance between gravity and the capillary forces in the pores is eventually reached, and the term for θ when this occurs is the field capacity (θ_{FC}). Wilting point (θ_{Wilt}) refers to a lower limit of θ beyond which plants can no longer extract water and they wilt. The range of θ between θ_{FC} and θ_{Wilt} defines the available water capacity, which is generally accepted as an approximation of the range within which water is available for extraction by plant roots (McKenzie *et al*., 2000), and is therefore important with regard to *ET*.

A well-established mathematical formulation for vertical water flux through pore space of unsaturated soils, as a function of key soil properties, is Richards' equation (Richards, 1931):

$$\frac{\partial\theta}{\partial t} = -\frac{\partial}{\partial z}\left(K(\theta) + D(\theta)\frac{\partial\theta}{\partial z}\right). \qquad (2.9)$$

The term z represents the vertical distance below the land surface while $D(\theta)$ is the soil moisture diffusivity where,

$$D(\theta) = -K(\theta)\frac{\partial\psi(\theta)}{\partial\theta}. \qquad (2.10)$$

Solving Eq. (2.9) therefore relies on relationships between θ, ψ and K such as that of Brooks and Corey (1964), with

$$\frac{\theta - \theta_{res}}{\theta_{sat} - \theta_{res}} = \left(\frac{\psi_{aep}}{\psi}\right)^{b}, \qquad (2.11)$$

and,

$$\frac{K}{K_s} = \left(\frac{\theta - \theta_{res}}{\theta_{sat} - \theta_{res}} \right)^{3+2b} . \qquad (2.12)$$

In Eq. (2.11), ψ_{aep} represents air entry potential (also referred to as the suction at saturation) and K_s in Eq. (2.12) is the hydraulic conductivity at saturation, while θ_{res} is the residual or air-dry soil moisture content (for ψ approaching infinity). The term b is a non-dimensional constant, sometimes called the pore size index (Beven, 2012) or Campbell b parameter (Williams *et al.*, 1992) in relation to the work of Campbell (1974) where the following was used:

$$\psi = \psi_{aep} \left(\frac{\theta}{\theta_{sat}} \right)^{-b} . \qquad (2.13)$$

Eq. (2.13), in addition to

$$K = K_s \left(\frac{\theta}{\theta_{sat}} \right)^{3+2b} , \qquad (2.14)$$

are the relationships of Clapp and Hornberger (1978) for solving Richards' equation. They are a slight variation on the Brooks and Corey (1964) relationships (Eqs. (2.11) and (2.12)), with the difference being that θ_{res} is made redundant for a smoother parabolic function relating the full range of values for θ, ψ and K. The van Genucthen (1980) model is another representation of soil-water retention that is widely referenced in the literature, and is expressed as:

$$\theta = \theta_{res} + \frac{\theta_{sat} - \theta_{res}}{\left[1 + (\alpha \psi)^n \right]^{1-1/n}} . \qquad (2.15)$$

The parameters α and n in Eq. (2.15) relate to ψ_{aep} and pore size distribution respectively.

As noted previously, the heterogeneity of the land surface includes variation in soil type and hence some of the key properties such as θ_{sat}, K, ψ, θ_{FC} and θ_{Wilt} can vary both laterally and with depth down to sub 1 metre scale. This can contribute to high spatial variability of θ, which in combination with varying vegetation type and cover, and associated plant water use, may also contribute to the spatial variability of heat fluxes (Kalma *et al.*, 2008; Western *et al.*, 2004). Spatial variability of these quantities adds to the challenge of estimating them over large spatial regions and over long time periods, particularly where observed data are sparse or do not support the spatial scale of information that is required.

2.2 OBSERVING LAND SURFACE QUANTITIES

The availability of different spatially distributed data types related to land surface water and energy balance quantities, as observed from a range of satellite based sensors, is a motivating factor behind much of the data assimilation research over the past couple of decades aimed at improving LSM prediction. Hence it is also a motivator for the research in this thesis, where the assimilation of observation types that have yet to be widely tested in LSM assimilation studies (i.e. *LE* and *H*) is examined, along with that of T_{sk} and soil moisture observations for which there is a larger body of published work. An important component of this research includes assimilation of in-situ field observed data at the point scale, prior to examining the more complex scenario of remotely sensed data assimilation.

If carefully managed, in-situ field observations can generally be made on flexible time scales and calibrated such that their uncertainty is better understood compared to remotely sensed data. A higher degree of confidence in estimated observational uncertainty for in-situ point scale data makes them valuable for better understanding the relative impacts that different data types can have on a LSM when assimilated. This is particularly true when the model simulation, the assimilated observations, and the validation data all represent approximately the same spatial scale – which is relatively easy to achieve with point scale field monitoring.

By contrast, remotely sensed data assimilation for spatially distributed modelling, which is ultimately of most interest for applications such as operational NWP and catchment water balance studies, involves greater complexity and therefore greater uncertainty. The processing of raw remotely sensed observations to produce specific data products is done with algorithms/models which can be complex, imperfect and introduce errors. Also, varying degrees of landscape heterogeneity can occur within remotely sensed measurement footprints, where spatial disparity between in-situ validation data and remotely sensed data (and the relative sparsity of in-situ monitoring across the world) presents a challenge for properly characterising uncertainty (Glenn *et al.*, 2007; Kalma *et al.*, 2008), and which also limits the ability for robust validation of model/assimilation output.

Spatial resolution and temporal repeat differs between remote sensing data types, which may add to the level of complexity when different remotely sensed data types are assimilated together. As an example, repeat times for observations of thermal energy related to T_{sk} (and therefore instantaneous *LE* and *H* estimates) can be as sparse as every 16 days from Landsat-7 ETM with ~60 m resolution, or as frequent as twice-daily (for daytime *ET* active times) from Moderate Resolution Imaging Spectroradiometer (MODIS) with ~1 km resolution (Li *et al.*, 2004). The temporal repeat of passive microwave observations for deriving near-surface soil moisture data products is typically more frequent, from sub-daily to every 3 days, but the spatial resolution is much broader in the order of 10's of km (e.g. Owe, *et al*., 2008).

With two separate studies presented in this thesis based on assimilating real data observations – a one-dimensional modelling study where point scale field measurements are assimilated, and a spatial study where remotely sensed data products are assimilated – the following sub-sections give an overview of observation methods relevant to the data that were used. For each data type, in-situ field measurement techniques are discussed first, followed by discussion of the remotely sensed data.

2.2.1 SOIL MOISTURE

Techniques for ground based soil moisture content measurements includes gravimetric and in-situ dielectric based reflectometry techniques – techniques used to collect soil moisture data that were available for this research.

Determining soil moisture via the gravimetric method (Black, 1965) involves weighing a field collected soil sample of known volume as soon as possible after collection and weighing the same sample after it has been oven dried at 105°C for >24 hours. Thus the total volume, the mass of water and mass of dry soil particles for a sample are all known and with some basic calculations the soil moisture content can be determined using Eq. (2.7). This is a relatively accurate method of determining soil moisture if done carefully due to the direct use of an actual field sampled volume of soil and simplicity of the measurements and calculations involved. A drawback of the gravimetric method is the destructive sampling (at the point-scale) and the human effort required for it, which limits the temporal frequency and the spatial coverage that can be achieved.

Dielectric based techniques are used to measure soil moisture in-situ and are also limited to the point-scale, but can be set up for continuous measurement over time. They provide non-destructive measurements where probes of a known length are inserted in the soil and act as waveguides for transmitted electromagnetic pulses (Topp *et al.*, 1980). The propagation time of a pulse along the waveguides is a function of the dielectric constant of soil surrounding them. Since liquid water has a high dielectric constant relative to dry soil the electromagnetic pulse travel time is a strong function of soil moisture content, thus time measurements from these instruments can be converted to soil moisture content via a calibration equation.

Commonly used sensor types relevant to the soil moisture data used in this research include conventional Time Domain Reflectometry (TDR) systems such as the TRASE TDR (Soil Moisture Equipment Corp., 1989), and those termed water content reflectometers such as the Campbell

Scientific CS615 sensor (Campbell Scientific Inc., 1996) and its successor the CS616 (Campbell Scientific Inc., 2002). With these latter types from Campbell Scientific, the frequency at which the pulse is reflected from the end of the waveguides is measured and the pulse period usually recorded. They differ from the conventional TDR (e.g. the TRASE system) for which multiple reflections along the length of the waveguide are detected so the entire waveform can be analysed and the pulse travel time determined.

In a field based comparative study by Walker *et al.* (2004), a number of ground based soil moisture sensors were compared including the TRASE TDR and the CS615. The TRASE connector-type TDR yielded the most accurate soil moisture content using the manufacturer supplied Topp calibration equation (Topp *et al.,* 1980) when compared against gravimetrically determined standard measurements – its measurements were within the manufacturer specified uncertainty interval. Western and Seyfried (2005) note that a CS615 type sensor is generally less accurate and more sensitive to variations in soil properties and temperature than a conventional TDR instrument, which is likely related to the lower operating frequency (Seyfried & Murdock, 2001, 2004). They also demonstrate a general soil temperature correction and soil moisture content calibration relationship for the CS615 that can cater for soil type variability. Establishing such a relationship requires soil temperature measurements and several independent soil moisture measurements (with both gravimetric and conventional TDR based measurements included in their demonstration examples) for different soil type/locations. The newer CS616 sensor operates at a higher frequency to the CS615 and Rudiger *et al*. (2010) have developed generalised calibration equations for them where soil texture information from particle size analysis are used in soil moisture calculations. Gravimetric, TDR and CS615/6 measurements of soil moisture were used in this research.

The work of Ulaby *et al*. (1982) and Ulaby *et al*. 1986) provides details on background theory and some practical aspects of remote sensing for soil moisture which is based on measuring microwave radiation. As presented by Wagner *et al*. (2007), key microwave bands in the electromagnetic spectrum that are relevant for soil moisture retrieval (with specific frequency (f) and wavelength (λ) ranges) are: L-band (f = 1-2GHz, λ = 30-15cm), C-band (f = 4-8GHz, λ = 7.5-3.8cm) and X-band (f = 8-12GHz, λ = 3.8-2.5cm). Microwave remote sensing can typically provide measurements for soil moisture estimation for the top few centimetres of soil, where the penetration depth into the soil is ~0.1-0.2 times the wavelength (Moran *et al.,* 2004). Analogous to the basic principles behind the in-situ methods mentioned previously, microwave emissions from soil are sensitive to the soil dielectric constant which varies greatly with soil moisture content (Jackson *et al*., 1996; Moran *et al*., 2004). Passive and active microwave remote sensing are two distinct approaches relating to soil moisture retrieval.

For the passive approach a radiometer sensitive to natural microwave emissions from the land surface is used with the brightness temperature (T_B) being the actual quantity measured. T_B is a product of the emissivity of a surface and its physical temperature (Jackson *et al*., 1996). Independent measurement of physical temperature enables emissivity to be determined, which then provides the link to estimate soil moisture content. Some examples detailing soil moisture retrieval from T_B measurements can be found in works by Gao *et al*. (2006) and Owe *et al*. (2008) amongst others. Surface roughness and increased vegetation cover can hamper the ability to retrieve soil moisture from the measurements, but this becomes less of a problem with increased wavelength (Jackson *et al*., 1996; Moran *et al*., 2004). Active sensing techniques are radar based where microwave pulses are transmitted to the land surface and a backscattering coefficient (σ^o) is determined by comparing transmitted and received signals (Jackson *et al*., 1996). Soil moisture can be retrieved using σ^o which is related to emissivity and hence is sensitive to contrasts in dielectric properties between wet and dry soil (Jackson *et al*., 1996; Ulaby *et al*., 1986).

The appeal of active techniques is that they can provide higher spatial resolution data than passive techniques (Entekhabi *et al*., 2010). However, algorithms for retrieving soil moisture from σ^o are more complicated than from passive radiometer data (Jackson *et al*., 1996), with issues of sensitivity to surface roughness and vegetation still needing to be fully overcome (Moran *et al*., 2004; Wagner *et al*., 2007). Change detection algorithms (e.g. Wagner *et al*., 1999) are a promising approach for addressing the challenges of active sensor moisture retrieval. The basis of these is that noise in the measured signal is assumed to either be constant over time (bare ground roughness and topography) or have seasonal periodicity (vegetation). The challenge is to adequately quantify and correct for the noise, and while some algorithms may do a reasonable job at this, vegetation may not always have the same seasonal variation over time in some regions. The soon to be launched Soil Moisture Active Passive (SMAP) mission satellite combines both a passive radiometer and active radar that will provide data with the best features of both sensing techniques – the greater overall certainty associated with passive microwave data retrieval and higher spatial resolution of active data (Entekhabi *et al*., 2010).

The C-band Advanced Microwave Scanning Radiometer (AMSR-E) on the NASA AQUA satellite (Njoku *et al*., 2003) is a prominent passive sensor which recently ceased operation (in October 2011), having provided approximately two repeat observations per day from descending and ascending overpasses at ~01:30-02:00 and ~13:30-14:00 respectively (local times). Observations represent ~1-2 cm soil depth and derived moisture products can have a spatial resolution down to ~25 km (Owe *et al*., 2008). Close to a 10 year observation series exists from AMSR-E and it has been replaced by its successor AMSR2 (Imaoka *et al*., 2010) which has similar measurement specifications. Another passive sensor is the L-band Microwave Imaging

Radiometer with Aperture Synthesis (MIRAS), which is on the European Space Agency (ESA) managed Soil Moisture and Ocean Salinity (SMOS) satellite (Kerr *et al*., 2010). Moisture data from this sensor represents the top ~5 cm of soil with ~40-50 km spatial resolution, and a temporal repeat of ~3 days corresponding to ascending and descending overpasses at ~06:00 and ~18:00 respectively for local times. A prominent active sensor is the C-band Advanced Scatterometer (ASCAT; Wagner *et al*., 2013) on the Meteorological Operational satellite (MetOp), which has approximately twice daily repeat coverage for Australia at ~08:30 (ascending overpass) and ~21:30 (descending overpass) local times (Su *et al*., 2013). ASCAT soil moisture data represent the top ~1-2 cm with spatial resolution down to ~12.5 km (Wagner *et al*., 2013), and are typically produced as a scaled wetness index from 0-100% as opposed to explicit volumetric moisture content quantities.

Moisture products from these particular passive and active sensors have been validated against in-situ moisture observations across different regions world-wide. Most recently, Su *et al*. (2013) assessed SMOS, AMSR-E and ASCAT over south-eastern Australia, and Albergel *et al*. (2012) assessed both SMOS and ASCAT (together with a blended observation/model product) for parts of Africa, Europe, the USA and Australia. From these studies, the overall error in the passive and active sensor products appear relatively comparable. While there is variation in the temporal repeat, spatial resolution and observation depths between them, they each contain information which can potentially contribute to improved model prediction via data assimilation. However, incorporating the full range of moisture products available from the different sensors and based on various retrieval algorithms into data assimilation experiments was beyond the scope of this research.

For the spatial remotely sensed data assimilation experiments in this thesis, the AMSR-E soil moisture product derived using the Land Parameter Retrieval Model (LPRM), developed jointly by the Vrije Universiteit Amsterdam and NASA (VUA-NASA: Owe *et al*., 2008) was used. An evaluation of this product by Draper *et al*. (2009a) over south eastern Australia determined root mean square differences (RMSD) of ~0.02-0.04 vol/vol relative to most in-situ validation data sites used, after systematic biases between them and AMSR-E estimates were removed. The evaluation also found that moisture estimates from the local night time (descending) overpass were generally more accurate than for day time, which is supported by the more recent work of Su *et al*. (2013).

2.2.2 SKIN TEMPERATURE

Skin temperature (T_{sk}) is a key variable linked to land surface physical processes (Wan & Dozier, 1996), sharing a relationship with energy and water fluxes as is evident through Eqs. (2.1), (2.2) and (2.5). Testing the assimilation of real T_{sk} data was done in the one-dimensional in-situ field data experiments (chapter 6) for this thesis. The T_{sk} observations used were derived via Eq. (2.1) using measurements of remotely sensed $\uparrow LW$ from a CNR1 four-way net radiometer (Kipp & Zonen, 2002), installed ~1 m above the ground at a field monitoring site discussed in chapter 4.

Satellite remotely sensed T_{sk} data is based on measured thermal infrared emissions from the land surface (Li *et al*., 2004; Wan & Dozier, 1996) with λ in the range of ~3-15 μm on the electromagnetic spectrum. From Kustas *et al*. (2003) and Li *et al*. (2004) some of the key data sources and their specifications include: Landsat Thematic Mapper (ETM) which provides ~60 m resolution imagery with an approximate fortnightly temporal repeat; Moderate Resolution Imaging Spectroradiometer (MODIS) providing coarser ~1 km resolution imagery, but with higher maximum temporal repeat of twice per day in daytime *ET* active periods – once daily from each of the Terra and Aqua platforms at ~10:00-10:30 and ~13:30-14:00 local overpass times respectively; and, there are also geostationary satellites such as the Geostationary Operational Environmental Satellites (GOES) measuring at 4km resolution with temporal repeat of ~30 minutes over a fixed geographic region.

In reality, satellite-based T_{sk} data timescales are often irregular and less than the above mentioned frequencies as cloud cover obscures the measurement of thermal infrared emissions (Wan *et al*., 2004). With T_{sk} related to emissivity (Eq. (2.1)), which varies with surface roughness and vegetation type, supplementary sensor data on emissivity is essential for reliable spatially distributed retrievals (Snyder *et al*., 1998), as is correcting the raw thermal data for atmospheric effects for satellite measurements of T_{sk} (Li *et al*., 2004).

Temporal repeat times associated with Landsat and MODIS remote sensors were used as the basis for T_{sk} assimilation frequency in the synthetic and one-dimensional field data experiments (chapters 5 and 6). A more frequent GOES data time scale was not imposed in these experiments in the interests of testing assimilation impacts for more conservative data availability scenarios (i.e. where assimilation frequency is less than the forcing data frequency and model integration time step). Uncertainty for Landsat T_{sk} data are assumed to be in the range of ~1-2 K based on the work of Li *et al*. (2004) and Sobrino *et al*. (2004), which is the same range assumed for data from MODIS based on Wan *et al*. (2004) and Wang and Liang (2009), while an uncertainty estimate of ~2 K is given for data from GOES by Sun *et al.* (2004).

2.2.3 LATENT AND SENSIBLE HEAT FLUXES

As discussed in the introduction, Latent (*LE*) and sensible (*H*) heat fluxes are the land surface processes most crucial for NWP initialisation. Hence the interest here in testing the assimilation of observation-based estimates of these quantities, an approach not well published in the scientific literature compared to the assimilation of other observation-based quantities such as soil moisture.

Shuttleworth (2007) and Wang *et al*. (2012) provide reviews of the science that has contributed to the understanding of *ET*/*LE* and different measurement techniques developed over preceding decades. Brutsaert (2005) also covers the principles behind different techniques for quantifying *LE* and *H*, and two main approaches are distinguished: i) aerodynamic or mass transfer formulations describing air and water vapour transport in the Atmospheric Boundary Layer (ABL); and ii) energy balance formulations focusing on the energy available to the land surface. Although it is noted that these approaches will nearly always need to be considered in combination. In the context of turbulent flow and mass transfer in the ABL, a general assumption is that the largest gradients of phenomena of relevance to *LE* and *H* (such as humidity and temperature) are in the vertical direction and by contrast the horizontal gradients are approximated to be zero (Brutsaert, 2005). As such, formulations typically involve mean values of measurements over a given time interval from different points in a vertical profile. An example illustrating the general form of using mean vertical profile values is the following representation of the Bowen ratio (Eq. (2.6)) as presented by Brutsaert (2005):

$$Bo = \frac{c_p\left(\overline{T_1} - \overline{T_2}\right)}{L_e\left(\overline{q_1} - \overline{q_2}\right)}. \qquad (2.16)$$

Here, T and q represent temperature and specific humidity respectively, the overbar represents the mean value for a given time interval, c_p is the specific heat capacity of air and L_e the latent heat of vaporisation for water. The subscripts 1 and 2 represent measurements from two separate levels in the vertical direction. Energy balance approaches rely on relationships (or variations of them) shown in Eqs. (2.2) and (2.5), and energy balance component measurements that are available, to define the fluxes that are of interest.

It can be assumed that for a wet surface the value of q is the saturation value at the surface temperature (T_s), as is the water vapour pressure (e) value, which is linked to q and air pressure (p) by the following from Brutsaert (2005):

$$q = \frac{0.622\,e}{p}. \qquad (2.17)$$

The work of Penman (1948) is significant in that it permeates some of the present day techniques for estimating *LE* and *H* from measurements and involves a combination of energy balance and aerodynamic formulations. Underpinning his work is an approximation describing the change in saturation vapour pressure (e^{sat}) with temperature which can be summarised as

$$\Delta = \frac{e_s^{sat} - e_a^{sat}}{\overline{T}_s - \overline{T}_a}. \qquad (2.18)$$

Where subscripts *s* and *a* represent the surface and air (at some reference level) respectively, and where e_s^{sat} and e_a^{sat} are saturation vapour pressure values as a function of the respective temperatures of the surface and the air. The formulation for evaporation (*E*) from Penman (1948) is

$$E = \frac{\Delta(R_N - G) + E_a\gamma}{\Delta + \gamma}. \qquad (2.19)$$

E_a is a term for the drying ability or evaporative demand of the air and is a function of: i) the saturation vapour pressure deficit ($e_a^{sat} - \overline{e}_a$) which represents the ability of air to take on water vapour, where $\overline{e}_a$ is the mean ambient vapour pressure; and, ii) the wind speed which influences the movement of saturated air away from, and drier air to, an evaporating surface. The term γ is the psychrometric constant

$$\gamma = \frac{c_p p}{0.622 L_e}. \qquad (2.20)$$

The Penman-Monteith method (Monteith, 1965) is an extension of the earlier work by Penman for calculating *ET*/*LE* from surfaces with vegetation as follows

$$LE = \frac{\Delta(R_N - G) + \rho c_p \frac{(e_a^{sat} - e_a)}{r_a}}{\Delta + \gamma\left(1 + \frac{r_s}{r_a}\right)}, \qquad (2.21)$$

where ρ is the air density, and r_a and r_s are terms for aerodynamic and surface (incorporating vegetation) resistances respectively. Eq. (2.21) is the basis for the standard method adopted by The United Nations Food and Agricultural Organisation (FAO) to calculate reference *ET* (or equivalent *LE*) – otherwise known as the FAO-56 Penman-Monteith equation – for a hypothetical grass crop treated as being well watered (i.e. for representing potential *ET*) and of uniform height (Allen *et al*., 1998). The FAO-56 method incorporates formulations for the resistances r_a and r_s which are functions of wind speed and Leaf Area Index (*LAI*) respectively, where standard meteorological observations are required as input. Limitations exist of course where the extent of such information is sparse relative to the spatial scale of interest and land cover variation. Moreover, effort is required to calibrate calculated reference/potential *ET* for different environments/vegetation cover which is dependent on additional direct measurement and/or ancillary data. Likewise the estimation of actual *ET* for a real water limited scenario from this process requires measured soil moisture content to adjust potential *ET* for water availability.

Observations of *LE* and *H* can be made on fine time scales (e.g. ~sub-hourly to hourly) via the eddy covariance method (Brutsaert, 2005; Burba, 2013), one of the most direct ways currently available to measure these fluxes. Ground based observations from this method, which were made and used for experimental work in this thesis, can only be made at small scales, usually ranging from 100's of metres to a few kilometres. Swinbank (1951) is one of the earliest published examples demonstrating the potential of measuring heat fluxes by sampling eddies at a fixed point as they move through the atmosphere. More recent work by Brutsaert (2005) outlines the theoretical detail behind the eddy covariance method, along with Burba (2013) who presents a thorough background summary on it, which includes practical aspects related to present day measurement technology and data processing. These sources were the basis of much of the information presented in the following paragraphs.

Eddy covariance theory is predicated on mass transfer, where the net positive vertical component of flux in turbulent air flow that occurs within the ABL describes the movement of latent and sensible heat from the land surface. This is represented by the following equations for latent and sensible heat flux:

$$LE = \rho_a \overline{q'w'}; \qquad (2.22)$$

and,

$$H = \rho_a C_p \overline{T'w'}. \qquad (2.23)$$

In Eqs. (2.22) and (2.23) q' and T' are fluctuations in specific humidity (water vapour concentration) and temperature of the air respectively, and w' is the vertical velocity of the air, all of which are measured at a given rate (10 or 20 Hz are commonly used rates), with the overbar denoting the calculation of cross-correlations over some averaging period (e.g. 30 minutes). The term ρ_a is the air density and C_p the specific heat capacity for air.

Eddy covariance instrumentation developed over recent decades can make the continuous rapid measurements required to determine flux quantities. As one of the most direct and detailed heat flux measurement methods, it is therefore one of the most accurate currently available. The system used for eddy covariance data collection in this research consisted of the Campbell Scientific CSAT 3D sonic anemometer (Campbell Scientific Inc., 1998) and a Licor 7500 open path gas analyser (LI-COR Inc., 2003). The CSAT 3D sonic anemometer measures wind speed along three non-orthogonal axes from which the vertical component of wind speed (w' in Eqs. (2.22) and (2.23)) is determined. It also measures the speed of sound (or sonic virtual temperature) for the term T' in the sensible heat flux calculation (Eq. (2.23)). The Licor 7500 measures the concentrations of water vapour (for q' in Eq. (2.22)) and carbon dioxide in the air.

The complexity of eddy covariance systems and of the turbulent flow which they measure means there are different potential sources of error in final period averaged values for *LE* and *H*. Burba (2013) outline a series of detailed processes for error correction using raw high frequency data if it is available, prior to period averaging. The energy balance (Eq. (2.5)) is routinely used to quality check period averaged heat flux values against direct in-situ observations of R_N and *G*. To satisfy Eq. (2.5), $LE + H$ and $R_N - G$ should theoretically share a 1:1 linear relationship, indicating perfect energy balance closure. However, gaps in energy balance closure due to underestimated eddy covariance fluxes are a recognised problem (Shuttleworth, 2007), a problem Twine *et al.* (2000) investigated in an experimental study. They suggest that errors in R_N and *G* from in-situ instruments are minimal overall compared to errors in eddy covariance *LE* and *H* data. Moreover, the Bowen Ratio (*Bo*: Eq. (2.6)) for these data were assumed reliable. Under this assumption a reasonable approach for correcting *LE* and *H* data is to adjust it against R_N and *G* data, while maintaining *Bo* as constant, to force closure of the energy balance as represented by Eq. (2.5).

Reviews of different techniques for quantifying *LE* and *H* from remote sensing have been presented by Kustas and Norman (1996) and more recently by Kalma *et al.* (2008). Instantaneous estimates of these quantities from remotely sensed observations are of particular interest with regards to assimilation for LSMs run on hourly to sub-hourly time scales. The techniques best suited for providing such estimates include the surface energy balance methods as summarised by Kalma *et al*. (2008) which rely on T_{sk} data. Examples of these include the Surface Energy Balance Algorithm (SEBAL) (Bastiaanssen *et al.*, 1998), the Surface Energy Balance System (SEBS) by Su (2002) and the two-source model (TSM) approach (e.g. Norman *et al*., 1995).

The general approach of these techniques is to estimate *H* as accurately as possible and then in combination with R_N and *G*, which are relatively easy to determine (Kalma *et al*., 2008), *LE* can be calculated via Eq. (2.5). Estimating *H* is the main challenge and is dependent on vertical differences between the aerodynamic surface temperature (T_{aero}) and near surface air temperature (T_a) at a reference height, and on aerodynamic resistance to heat transfer (r_{ah}), via the following (Boulet *et al*., 2012)

$$H = \frac{\rho_a C_p (T_{aero} - T_a)}{r_{ah}}. \qquad (2.24)$$

The Monin-Obukov Similarity Theory is relevant for heat flux formulations factoring vertical aerodynamic and mass transfer, and specifically for the terms r_{ah} and T_{aero}, as described by Kustas *et al*. (2007) and Liu *et al*. (2007). This theory relates turbulent fluxes in the lower atmosphere with vertical wind and temperature profile differences. From Liu *et al*. (2007) some of the key quantities include the zero-plane displacement *d* (the mean height above ground where wind speed becomes zero due to vertical structure such as trees) and separate stability parameters terms which are a function of: i) the reference height *z* (e.g. height from top of the vegetation canopy; ii) roughness length for momentum transfer *z0m* (the height at which wind speed reaches the surface value); and, iii) the roughness length for heat transfer *z0h* (the height at which temperature reaches the surface value).

The aerodynamic resistance to heat transfer r_{ah} can be calculated using local wind speed and T_a for the reference height *z*, and also the different roughness lengths *z0m* and *z0h* for atmospheric stability terms as outlined in Liu *et al*. (2007). The term T_{aero} is complex, representing temperature related to a mix of air, soil and vegetation surfaces (Boulet *et al*., 2012). It is described specifically by Boulet *et al*. (2012) as the average air temperature close to vegetation, within its canopy, and at the aerodynamic level height which is defined as the sum of the displacement height (*d*) and the roughness length for momentum (*z0m*). Determining T_{aero} is difficult and it cannot be measured by remote sensing so T_{sk} is often used as a proxy, although the discrepancy between T_{aero} and T_{sk} can be relatively large for non-uniform vegetation cover (Boulet *et al*., 2012; Kalma *et al.*, 2008; Kustas & Norman, 1996). This could potentially be a major source of error for estimated heat fluxes.

A TSM approach is where an explicit distinction between fluxes from the soil and from the vegetation is made – with the total fluxes being the sum of fluxes from each surface. For approaches such as SEBAL or SEBS, the fluxes between soil, vegetation and the atmosphere are treated as a single combined surface (Kalma *et al*., 2008). The TSM approach presented by Norman *et al*. (1995) can account for possible differences between T_{aero} and measured T_{sk}. It is based on using directional remotely sensed T_{sk}, along with the fraction of vegetation cover or *LAI* data and other standard meteorological data to help determine separate soil surface and vegetation canopy surface temperature values. Both of these are used in resistance calculations and thus heat fluxes which are subsequently determined have the separate contributions from soil and vegetation incorporated.

The SEBAL algorithm (Bastiaanssen *et al*., 1998) involves a calibration technique aimed at dealing with possible discrepancies between T_{aero} and measured T_{sk}. An assumption is made that the vertical temperature gradient (difference between T_{aero} and T_a – in the numerator of Eq. (2.24)) has an approximate linear relationship with observed T_{sk}. The premise for the calibration technique is that the temperature gradient is assumed zero for a wet extreme (where $LE >> H$ and H approximates to zero) and assumed to be at a maximum for a dry extreme where LE approximates to zero and H reduces to a function of R_N and G (Eq. (2.5)). From remotely sensed data for a region of interest, an extreme wet ($H \approx 0$) and extreme dry ($LE \approx 0$) pixel are identified. They represent anchors in the T_{sk} data coverage between which values for the temperature gradient term ($T_{aero} - T_a$) can be calculated for all pixels based on the assumed linear relationship between the temperature gradient and T_{sk}. A limitation with this algorithm is the reliance on subjective decision making by users to identify extreme wet and dry anchor points for a particular remote sensing scene (Gokmen *et al*., 2012).

The SEBS approach (Su, 2002) involves a range of remote sensing data for key quantities including T_{sk}, albedo, ε and for vegetation cover and characteristics, in addition to commonly available meteorological data. It is rigorous with several modules for estimating R_N and G, and depending on the range of meteorological and vegetation data available, the displacement height d and roughness height for momentum *z0m* (required for Monin-Obukhov based calculations) can be determined via methods of either Massman (1997) or Brutsaert (1999). In addition to detail discussed in Kalma *et al*. (2008), examples of studies using SEBS heat flux estimates include McCabe and Wood (2006) and Su *et al*. (2005, 2007).

Kalma *et al*. (2008) noted that spatially distributed heat flux data had yet to be used effectively for routine evaluation and improvement of LSMs. At present there is still no known wide-spread and routine use of instantaneous heat flux estimates (as per satellite overpass times) for this purpose. Kalma *et al*. (2008) also note that for remote sensing based data the inability to evaluate it in a distributed manner is a serious limitation. An obvious reason is the limited number of locations where direct in-situ measurements of heat fluxes are made (with instruments such as eddy covariance systems) over multi-year time scales.

Both Glenn *et al*. (2007) and Kalma *et al*. (2008) discuss the assessment of remotely sensed LE and H data using in-situ measurements. The main challenges include scale disparities between station measurements and remotely sensed pixel resolution, and how meaningful assessments are for locations far removed from a station when the landscape is heterogeneous or the possibility of varying meteorological conditions exists. Kalma *et al*. (2008) state that from about 30 published works involving validation of remotely sensed LE and H against independent ground data there is an average root mean squared error value of ~50 Wm^{-2}. With remotely sensed T_{sk} being the main input for deriving these heat fluxes, the temporal repeat imposed on the assimilated *LE* and *H* data series in the experiments that did not involve satellite remote sensing data (chapters 5 and 6) was identical to that for T_{sk}.

2.3 LAND SURFACE MODELS (LSMs)

It is well established that soil moisture and temperature states share a link with weather and climate through regulating the partitioning of available energy at the land surface into *LE* and *H* (Beljaars *et al*., 1996; Koster *et al*., 2004; Koster *et al*., 2011; Pielke *et al*., 1998; Pitman, 2003; Ridder, 2009; Sellers *et al*., 1997; van den Hurk *et al*., 2010). LSMs are designed to represent these state/flux processes, which relate to the water and energy balance components summarised in section 2.1, in order to support tasks such as Numerical Weather Prediction (NWP) and climate modelling. By definition a LSM is a mathematical framework representing mass, momentum and energy transfer in the lower boundary of the atmosphere over continental areas via processes such as *LE* and *H* (Levis, 2010). They include energy balance calculations for quantifying these fluxes, which factor in physical characteristics of the land such as vegetation cover and associated plant transpiration, along with formulations linking soil state dynamics (Ek *et al*., 2003; Overgaard *et al*., 2006).

From Pitman (2003), typical calculations of *LE* and *H* in LSMs are of the form incorporating water vapour and temperature gradients between the land surface and a reference level in the vertical, along with resistance terms (as in Eqs. (2.16) to (2.21)). For example, in using the saturation vapour pressure difference ($e_s^{sat} - e_a$) for *LE*, e_s^{sat} is the saturation vapour pressure at the surface temperature (T_s) and e_a the vapour pressure of the air at a reference level. Likewise, using the temperature difference between the land surface (T_s) and a reference level air temperature (T_a) is typical for *H*.

Running LSMs requires time series meteorologic forcing data inputs which provide values for water and energy supply to the land surface (as precipitation and incident radiation quantities) along with values for near surface atmospheric conditions with which calculations are made for evaporative demand. Model specific parameter data is required to quantify soil and vegetation properties which influence water and energy fluxes, and a list of inputs specific to the Australian CBM/CABLE model (Kowalczyk *et al*., 2006, 2013; Wang & Leuning, 1998; Wang *et al*., 2001, 2007) is provided in chapter 3. For a coupled LSM and atmosphere in NWP and climate modelling systems, meteorological forecasts within the system provide the forcing. Alternatively, uncoupled/stand-alone LSMs can be forced with meteorological variables which are usually routinely observed by meteorological agencies. This latter approach was used for this research as experiments focused on impacts on the LSM used (CBM), without the added complexity and uncertainties of a coupled system (progressing towards future research in such systems which are used operationally is essential however).

Important soil parameters in LSMs are those relating to the water retention/mobility properties of soils which impact on water availability to plants and hence available energy partitioning (key properties are given in section 2.1: porosity, field capacity, wilting point and hydraulic conductivity). Data on these properties suitable for global or continental scale model applications are generally available from databases associated with broad scale global or national soil type maps (e.g. McKenzie *et al*., 2000; Batjes, 2002). Key vegetation parameters can include (amongst others depending on the complexity of the particular model being used) time varying *LAI* from remote sensing, the distribution of roots in the soil and the vegetation canopy height (relating to land surface roughness and aerodynamic resistances), all of which impact on heat fluxes (Pitman, 2003). As with soil, there are also databases of vegetation parameters associated with global scale maps of vegetation or biome types (e.g. Potter *et al*., 1993). Spatially and/or temporally varying soil and vegetation parameters enable landscape heterogeneity to be represented in LSMs so that the variability of energy and water balance components are better predicted – although such variability is limited by the scale and accuracy of the available parameter data.

In contrast to parameters, prognostic state variables require initial conditions to be prescribed and subsequent values are calculated as a function of previous model time step values. Hence they retain some memory relating to water and energy balances as they change with new forcing data at each time step. Key state variables in LSMs typically include soil moisture content and soil temperature (e.g. Dai *et al*., 2003; Kowalczyk *et al*., 2006).

The level of detail that has been incorporated into LSMs over the past few decades has increased in an attempt to improve their accuracy with more realistic representations of soil, vegetation and atmospheric interactions. To set the context and give an overview, the following paragraphs provide a synthesis of the work of Pitman (2003) and Sellers *et al*. (1997) who categorised models as first, second or third generation in their reviews of LSM development.

First generation models are the most simplistic, with the bucket model from Manabe (1969) being a prime example. A single 15cm soil layer is used in this model – it fills from precipitation, after filling any precipitation becomes surface runoff and water depletion from the soil occurs via *ET*. For determining *ET* a potential value is calculated (using the vapour pressure gradient form as described earlier) and then a simple linear soil moisture availability factor (β) based on the bucket water content ($0 \le \beta \le 1$ from completely dry to saturation) is used as a multiplier to determine actual *ET*. An aerodynamic resistance term is used in *ET* calculations and vegetation canopy (stomatal) resistance is not included. This is a major limitation since plant stomatal control on transpiration in the presence of freely available water has an influence on *ET* (Milly & Shmakin, 2002). Stomatal resistance describes the regulation of water vapour transpiration through stomates in plant leaves.

With the exception of surface albedo which is linked to vegetation distribution, the Manabe (1969) model uses globally uniform values for surface parameters (Milly & Shmakin, 2002) thus spatial water and energy balance variations may not be represented as realistically as possible. This situation is improved with newer models (second and third generation). Pitman (2003) notes that only 1 or 2 soil layers are generally included in first generation models and that soil temperature variations might also not be adequately represented from short term to multi-annual time scales. Milly and Shmakin (2002) note that neglect of ground heat storage in the Manabe (1969) model is a limitation for modelling at sub-daily time scales, whereas net change in heat storage on daily or longer time scales can be considered negligible. Sub-daily heat storage changes are a function of *G* and soil temperature changes through the vertical soil profile, which are important components of the land surface energy balance as discussed in sub-section 2.1.1. The importance of good soil temperature representation in LSMs for weather and climate modelling is discussed by Ridder (2009).

Second generation (or biophysical) models according to Sellers *et al*. (1997) have more advanced vegetation representation than first generation ones which are described as representing vegetation as passive, spongelike structures separating the soil and atmosphere. The aim for second generation models was said to represent a soil-vegetation system for interacting with the atmosphere. Some of the advances in these models include differentiating between soil and vegetation cover for representing spatial variation in albedo, dealing with absorption of visible bands from incoming radiation (in the photosynthetic range) and reflection of near infrared wavelengths by vegetation, representing the impact of vegetation on momentum transfer which relates to *LE* and *H*, and, the inclusion of a biophysical control on *ET* via the representation of stomatal resistance for the vegetation canopy (Pitman, 2003; Sellers, 1997). Thus unlike first generation models, vegetation canopy resistance was incorporated and according to Sellers *et al*. (1997) it was possible to calculate heat fluxes more accurately overall due to the more realistic biophysically based model structure.

Second generation models usually contain multiple soil layers with root distribution and improved soil temperature and moisture representation (Pitman, 2003). In terms of hydrology, they include canopy interception (and evaporation) with a more complex representation of soil moisture dynamics typically using Richard's equation (Pitman, 2003). Some examples of second generation models are the Biosphere-Atmosphere Transfer Scheme (BATS) by Dickinson (1984), the Simple Biosphere Model (SiB) by Sellers *et al*. (1986) and the VB95 model (Viterbo & Beljaars, 1995) developed for European Centre for Medium Range Weather Forecasts (ECMWF) and which was the LSM implemented in Australia's NWP system in 1999 (Richter *et al*., 2004).

Despite an explicit representation of vegetation in second generation models, Pitman (2003) notes a limitation with them is that stomatal resistance is based on empirical relationships. In developing third generation (or physiological) models the mechanisms of plant stomatal functioning driven by photosynthesis were considered in more detail. Thus explicit representation of photosynthesis and the use of CO_2 by vegetation in relation to stomatal resistance and transpiration is a typical feature of them (Pitman, 2003; Sellers *et al*. 1997). Other processes in third generation models such as soil hydrology and soil temperature are usually similar to representations used in second generation models (Pitman, 2003).

Examples of third generation models include the Simple Biosphere Model 2 (SiB2) by Sellers *et al*. (1996), the CSIRO Biosphere Model (CBM: Wang & Leuning, 1998; Wang *et al*., 2001, 2007) used in this research and its successor the Community Atmosphere Biosphere Land Exchange model (CABLE: Kowalczyk *et al*., 2006; Kowalczyk *et al*., 2013). The CBM was made available for the research in this thesis and its use was continued in all of the studies carried out after the release of CABLE for the sake of consistency. A detailed description of the CBM structure and operation is provided in chapter 3. It has similar formulations for the energy balance and hydrology as the current version of CABLE, which is distributed as a community based model and as such is continually evolving (Law *et al*., 2012).

Despite advancement over the years that has improved the representation of some complex physical processes in contemporary models compared to earlier models, imperfect model structure and errors in input data are ubiquitous with modelling, contributing to prediction uncertainty. Uncertainty in initial state conditions, meteorological forcing data and parameter data are all sources of input error, both in terms of measurements accuracy and representation of spatial and temporal variability. Hence techniques such as data assimilation can play an important role in improving model predictions when additional information from independent observations are available.

2.4 DATA ASSIMILATION

Estimating the true state of a physical system for a given time is referred to in the geophysical sciences as the analysis (Holm, 2003). Data assimilation is described by Holm (2003) as being an analysis which combines time distributed information from observations and a dynamic model of the physical system. Data assimilation and the statistics underpinning it are covered in detail by Evensen (2009) where the important point is made that there are infinitely many equally likely solutions from a model's integration through time (due to the different sources of uncertainty mentioned in the preceding section). Thus it makes more sense to consider the probability distribution function (*pdf*) for a model variable than single deterministic predictions. With knowledge of the *pdf* we can estimate the most likely value (the mean) and uncertainty (the variance) for a particular variable(s) of interest.

From Evensen (2009), data assimilation is the computation of the *pdf* of the model solution conditioned on measured observations. Essentially, observed quantities which can be on a variety of spatial and time scales and are related to model variables, are used to update model variables in a way which factors in the uncertainty of both observed and modelled quantities. From Houser *et al*. (2010; pg. 549-550), land surface data assimilation is an approach which: "...aims to utilise both our knowledge of land surface processes as embodied in a LSM, and information that can be gained from observations, to produce an improved, continuous land surface state estimate in space and time". Model data fusion is sometimes used as an umbrella term for the different approaches to combining observed and modelled information for improving predictions, encompassing both parameter optimisation and state updating (e.g. Keenan *et al*., 2011; Wang *et al*., 2009). The term data assimilation is considered to be more specific based on much of the literature referenced throughout this thesis and its use here refers exclusively to model state updating.

2.4.1 WHY DATA ASSIMILATION

Using independently observed information to improve model predictions is not new. Model calibration is well published particularly for hydrological applications, where discussion of and reference to some different approaches can be found in Vrugt *et al*. (2006). A typical strategy is to calibrate for a particular variable (or variables) by optimising model parameter values so that some objective function for differences between predictions and observations of the variable(s) of interest is minimised. Wang *et al*. (2001, 2007) applied optimisation to the CBM (the LSM used in this research) with model vegetation parameters adjusted based on eddy covariance measurements to improve heat and CO_2 flux predictions for an Australian eucalypt forest site.

Vrugt *et al*. (2006) highlight that in contrast to optimisation with a focus limited to parameters, data assimilation adds specific value in sequentially updating model state variables through time whenever new measurements become available, to continuously improve predictions and estimate prediction uncertainty. The time step dependency of prognostic state variables enables the impact of updates to be carried forward to modelling time steps where observations are not available. Evensen (2009) indicates there are differences in opinion between research communities about which approach – data assimilation or identifying parameters via optimisation – is best for providing proper scientific knowledge and improving modelled outcomes.

Mitchell *et al.* (2004) noted that decades long improvements to atmospheric state initialisation for NWP and seasonal climate prediction using data assimilation had set the scene for LSM data assimilation research. This has progressed over recent years and the United Kingdom Meteorology Office (UK Met) is one institution where operational LSM assimilation of remotely sensed soil moisture has been implemented within a NWP system (Dharssi *et al*., 2011). LSM state updating with data assimilation is therefore recognised as being extremely valuable for NWP initialisation.

Parameter optimisation may also be of value in the NWP context, however for a remotely sensed product such as soil moisture which represents only the top few centimetres of soil there is no direct comparison for finding optimal soil properties over the deeper rooting zones which fluxes depend on. Robust data assimilation techniques require the factoring in of model uncertainty and therefore state updating can be beneficial where there is sub-optimal input data. Data assimilation can also update other unobserved model variables (e.g. root-zone moisture states) based on their relationship with the observed model variable. For Australia's current NWP system, broad scale global soil and vegetation parameters are used directly in the LSM with no optimisation applied to them (Dr P. Steinle, Data Assimilation Team Leader, Australian Bureau of Meteorology, *pers. comm.*, May 2011). The strengths of data assimilation with its recognised benefits for NWP initialisation has informed the research scope for this thesis – it is confined to testing the assimilation of different observation types and using fixed parameter data directly as they were available, as is done in Australia's weather prediction system.

2.4.2 DATA ASSIMLATION TECHNIQUES

Walker and Houser (2005) distinguish between dynamic observer and direct observer data assimilation techniques. Dynamic observer assimilation is aimed at finding the best fit between predicted model states and observations, constrained only by the initial state uncertainty and the observation uncertainty. It is likened to a calibration approach where the initial state values for a given assimilation period are optimised based on the full series of observations over that entire period. Four-dimensional variational (4DVAR) assimilation is an example of a dynamic approach and a limitation is that no model error is assumed (Bouttier & Courtier, 1999; Holm, 2003).

Walker and Houser (2005) summarise direct observer assimilation as using the innovation – defined as the difference between an observation and a model prediction of the observation – to sequentially update model predicted state variables, whenever observations are available. The product of the innovation and a weighting factor – where the weighting represents the relative uncertainty in the observation and model predictions – is added to the predicted state variables in order to update them. Holm (2003) lists optimal interpolation (OI), three-dimensional variational assimilation (3DVAR) and the Kalman filter as common data assimilation algorithms, which are all direct observer approaches. Walker and Houser (2005) also list these along with nudging, as used for soil moisture in Australia's NWP system (Draper & Mills, 2008), statistical correction, successive correction and analysis correction. The early approach of direct insertion is also mentioned.

With direct insertion, predicted model states are simply replaced with available observed information. Model or observation uncertainty is totally disregarded (the observation is treated as being perfect) and this approach is therefore very limited. Differences between most of the other aforementioned approaches relate largely to how their respective weighting factors are defined.

For nudging the weighting is a function of both space and time (relating to the influence an observation has on model predictions in terms of proximity and time lag), of the estimated observation quality and of a nudging factor which is typically chosen to ensure any state adjustment is realistic relative to rates of change of physical processes in the model (Stauffer & Seaman, 1990). The weighting for OI is based on estimated observation error and a simplified approximation of model prediction error covariance that remains constant for all time steps – it is often a prescribed estimate incorporating spatial correlation with an assumption that any location in a modelled region is only influenced by observations within a limited/fixed surrounding area (Bouttier & Courtier, 1999; Holm, 2003; Walker & Houser, 2005). This way of dealing with model error is typically the same for the 3DVAR approach (Walker & Houser, 2005). The strategy behind 3DAVR avoids directly determining a weighting factor. Instead the predicted states, the innovation, and estimates of observation and model prediction error are used in a cost function and its gradient to iteratively solve for updated states by minimising the cost function (Bouttier & Courtier, 1999; Holm, 2003).

The Kalman Filter (KF), first presented by Kalman (1960), forms the basis of more modern variations such as the extended Kalman filter (EKF) and ensemble Kalman filter (EnKF). The weighting factor for KF approaches (called the Kalman gain) is based on estimates of observation error and on the model prediction error covariances being propagated forward in time along with the predictions themselves. With the standard KF a linearisation of non-linear models such as LSMs (through determining the tangent linear of the model) is used to estimate error covariances at each assimilation time (Bouttier & Courtier, 1999). By definition the EKF is where the model prediction is linearised using a Taylor's series expansion (Walker & Houser, 2005). While error covariances can be propagated forward and estimated at assimilation times, actually defining the total model error in the first place – consisting of errors from initial conditions, forcing data, model physics and parameters – is extremely difficult (for any assimilation approach) and ad-hoc estimates are often made (Bouttier & Courtier, 1999; Walker & Houser, 2005).

Unlike the EKF, the EnKF (Evensen, 1994; Evensen, 2009) is a much more robust assimilation approach that avoids the need for computationally expensive propagation of error covariances through time and determining tangent linear models (Reichle *et al*., 2002). Instead a Monte-Carlo approach is used where an ensemble of parallel model predictions is used to represent model prediction error. Ensembles can be generated by applying random perturbations to different inputs and/or model states to represent errors relevant to each. Estimating prediction error covariances for determining the Kalman gain weighting factor is done using the ensemble spread at each assimilation time step.

Reichle *et al*. (2002) compared the EKF and EnKF and noted that the EnKF was more robust and flexible in covariance modelling with slightly superior performance, thus it is well suited for LSM applications. The flexibility in prescribing error perturbations to model inputs for the EnKF means that some error ensembles can propagate naturally through the model making it possible to achieve more realistic dynamic error covariances through time than for approaches such as OI or 3DVAR where more rigid structures are used. However as mentioned previously, accurately defining total model error from all sources (especially model physics) is still a major challenge for any approach.

From this review of common data assimilation approaches, the EnKF was chosen as the technique to use for experiments in this thesis due to its robustness – it is easy to implement, efficient and has been shown to perform strongly against the EKF. It has also been used in its own right for various published assimilation studies (with some of these referenced in following sections here and in following chapters). A description of the EnKF and its implementation for experiments in this thesis is presented in chapter 3, while the generic KF formulation on which it is based is as follows:

$$\mathbf{X}_k^a = \mathbf{X}_k^f + \mathbf{K}(\mathbf{Z}_k - \mathbf{Z}_k^f), \qquad (2.25)$$

where subscript k refers to the assimilation time step, superscript f refers to a prediction and superscript a refers to an analysis (from an update). The model state vector is denoted by $\mathbf{X}$ and the observation is denoted by $\mathbf{Z}$. The difference between an observed value and a model predicted value of the observation – i.e. the innovation $(\mathbf{Z}_k - \mathbf{Z}_k^f)$ – is weighted by the Kalman gain ($\mathbf{K}$) which determines the correction added to the predicted state vector. In addition to projecting from $\mathbf{Z}$ to $\mathbf{X}$ space, $\mathbf{K}$ is the weighting factor that represents the relative uncertainty of model predicted and observed values based on their covariances and is given by

$$\mathbf{K} = \mathbf{P}_k^f \mathbf{H}^\mathbf{T} (\mathbf{H}\mathbf{P}_k^f \mathbf{H}^\mathbf{T} + \mathbf{R}_k)^{-1}, \qquad (2.26)$$

where **P** represents the error covariance of the predicted model states and **R** is the error covariance of the observation. The matrix **H** is a nonlinear operator that relates the state vector **X** to the observation **Z,** with superscript T denoting the matrix transpose. Therefore, if **P** is large compared to **R** (i.e. observations more trustworthy than model prediction), then **K** will approximate to 1 when **X** and **Z** are the same scalar quantity (i.e. **H** = 1), and the innovation will be relied upon heavily to adjust the predicted states due to the small relative observation error. Alternatively, where **R** is large compared to **P**, **K** will approach 0 and the observation will not be trusted sufficiently leaving the final analysis vector $\mathbf{X}_k^a$ relatively unchanged, since the model's prediction is likely to be more reliable in this case.

Evensen (2009) and Maybeck (1979) present comprehensive detail on the KF including its statistical basis. It is discussed with reference to Bayes' theorem, given it is designed to determine the most likely value of a model state (the analysis) based on the *pdf* for an *a priori* model prediction conditioned on the *pdf* for some observed estimate of the modelled quantity. The *pdf* variances for predictions and observations are the quantities used for **P** and **R** respectively in Eq. (2.26). As highlighted by Evensen (2009) and Maybeck (1979), amongst others, the statistical assumptions about the prediction and observation error distributions for an optimal KF are that they are zero mean (unbiased), independent of each other, represent random white noise, and are Gaussian. Errors may not be strictly Gaussian in reality, however it is often the case that only the mean and variance of error processes are known, and without clear knowledge of higher moment statistics a Gaussian distribution is the best assumption for the KF to minimise error in the analysis (Maybeck, 1979).

2.4.3 THE BIAS PROBLEM

The KF is a linear combination of modelled and observed information (Eq. (2.25)), and based on the error distribution properties discussed in the previous section it deals specifically with correcting for random error in finding an optimal model prediction. Therefore systematic biases between modelled and observed time series represent a challenge for data assimilation, which is an issue covered in numerous publications such as Drusch *et al.* (2005) and Reichle and Koster (2004).

For observations of a state variable such as soil moisture from remote sensing or in-situ instrumentation, the dynamic range is a function of the measuring instrument(s) and algorithm (with associated uncertainty) used to derive it. This range, along with the mean state over longer time periods (e.g. multi-annual or at least a full annual seasonal cycle) is likely to differ to that from a LSM which has its own inherent uncertainty issues arising from different sources, including structural error and poor information on soil parameters such as wilting point and field capacity (amongst others), which influence moisture dynamics (Koster & Milly, 1997).

Moreover, observation depths for remotely sensed microwave based data such as AMSR-E (~1-2 cm) are 2 to 5 times thinner than the surface soil layer in some LSMs resulting in disparate temporal dynamics (Drusch *et al*., 2005). However this was not an issue for soil moisture assimilation in this research where observed depths could be approximately matched to equivalent CBM soil layer depths. Remotely sensed data with a broad spatial scale (10's of km) can also be difficult to validate over extended regions where well calibrated in-situ data is sparse, adding to the uncertainty in relation to bias. While bias between LSM states and remotely sensed observations of them is recognised as a problem, which must be dealt with in some way for meaningful comparisons to be made in the context of data assimilation, the relative contribution to overall bias from the model and observations is difficult to define. Without independent information enabling the source(s) of bias to be accurately identified and quantified, treating it remains a challenge.

A tractable and therefore typical approach to treating the bias problem is to rescale observations prior to assimilation such that the observed data series matches the model climatology. This can be done via matching the cumulative distribution function (*cdf*) of the observed series to the modelled one (e.g. Draper *et al*., 2009b; Drusch *et al*., 2005; Reichle *et al*., 2007; Reichle & Koster, 2004), or matching the observed series mean and standard deviation to that of the modelled series – as done by Draper *et al*. (2009a) in minimising bias between AMSR-E and in-situ soil moisture data series. Although such approaches aimed at bias removal are relatively well published they are not necessarily optimal. Reichle and Koster (2004) defined a relationship for rescaling remotely sensed soil moisture to model predictions over a one year period, and when applied to a nine-year long data series it reduced the bias but did not completely remove it. This highlights the difficulty of thoroughly understanding bias relative to true climatology, especially where only short data series are available.

Despite the rescaling approach to treat observation/model state bias having limitations, it is the best known option at present for when there is a lack of additional information independent of the assimilated observations and model state predictions. Holm (2003) discusses bias as a serious issue impeding the full potential of data assimilation but states that it must be dealt with in some way given that assimilation is based on merging independently sourced and unbiased information. Rescaling was applied in this thesis for experiments which involved real data assimilation and with clear bias between observed and modelled states over a one year period (i.e. bias could be determined for a full cycle of seasons).

2.4.4 SYNOPSIS OF LSM DATA ASSIMILATION RESEARCH

An early example of investigating the ability of data assimilation to improve model soil moisture and temperature state predictions is a synthetic study by Entekhabi *et al.* (1994). This study demonstrated the potential for improving soil moisture and temperature predictions over a 1 m deep soil profile by assimilating data that is representative of remotely sensed skin temperature and soil moisture observations of only the top few centimetres of soil (the typical depth range of real remotely sensed soil moisture data).

Synthetic studies are based on model outputs from some benchmark simulation designated as the "truth", and on a "degraded" simulation which is a result of prescribing different/erroneous inputs (either initial conditions, forcing data, parameters, or any combination of these) compared to those used for the "truth". Synthetic observations are obtained by sampling data from the "truth" output series for the desired variable(s) at the desired temporal resolution. By assimilating these into the "degraded" simulation, the data assimilation performance can be assessed based on its ability to retrieve the original "truth" output series. Given that such studies are very controlled, with a known "truth" and known error(s) as prescribed for the "degraded" simulation, they are valuable as a proof-of-concept when examining the feasibility of new data assimilation strategies.

In addition to the work of Entekhabi *et al.* (1994) there are a range of synthetic LSM data assimilation studies in the literature from over the years, including the work of Balsamo *et al.* (2007), Kumar *et al.* (2009), Reichle *et al.* (2008), and Walker and Houser (2004). Across these examples there is clear indication that assimilating near-surface soil moisture and/or skin temperature observations has potential for improving model predictions of soil moisture (including over the deeper root-zone), soil temperature and heat fluxes.

Testing LSM data assimilation with real observed data is essential towards developing and having confidence in real-world assimilation applications, although it entails certain challenges which are not encountered in synthetic studies. Specifically, in dealing with real data it is unlikely that the truth is perfectly known (hence the purpose of assimilation in the first place) where the best estimate of it relies on well defined observational and model prediction errors. Therefore, in the absence of reliable data independent of the assimilated observations and model predictions, this is difficult to achieve – as is performing robust validation of assimilation results to assess the viability of particular assimilation strategies. This also relates to the difficulty in understanding the true source of any bias between observations and model predictions as discussed in the previous section.

Various studies assimilating real one-dimensional point-scale data have been published, such as those by De Lannoy *et al.* (2007), Heathman *et al.* (2003), Li & Islam (1999) and Sabater *et al.*

(2008) which involve soil moisture assimilation, and further demonstrate the potential for improving root-zone soil moisture prediction. There is also the work of Meng *et al*. (2009) where the focus was on skin temperature assimilation and the potential for improving *LE* prediction is shown. One-dimensional studies using real observations are also a valuable part of the process of testing LSM assimilation, as at point-scale monitoring sites (the source of data used in the studies referenced above) different data sets can be collected and quality controlled relatively easily to support both assimilation and validation for site based simulations. Moreover, testing the impacts on a model with real independently measured data is done without the added uncertainty from large discrepancies in spatial scale between data sets. By contrast, spatially distributed modelling with remotely sensed data assimilation is more susceptible to the challenges of defining error and performing validation – given the overall lack of global coverage of independent data at a range of spatial scales.

Ultimately though, the aim of LSM assimilation in NWP and many hydrological applications is to use remotely sensed observations for improved spatially distributed modelling. Therefore, in progressing beyond synthetic studies and one-dimensional studies using point-scale field data to test the viability of particular LSM assimilation strategies, research into remotely sensed data assimilation is imperative despite the challenges. Many of the published remotely sensed data assimilation studies for LSMs have focused on assimilating microwave data, or the near-surface soil moisture products derived from them. These include Draper *et al*. (2012), Liu *et al*. (2011), Margulis *et al*. (2002), Peter-Lidard *et al*. (2011), Reichle *et al*. (2007) and Reichle and Koster (2005). While Huang *et al*. (2008), Lakshmi (2000), Reichle *et al*. (2010) and Xu *et al*. (2013) present examples of assimilating remotely sensed thermal infrared based skin temperature into LSMs.

Most LSM assimilation studies in the literature appear to involve soil moisture and/or skin temperature observations. This is reflected in the range of example references presented in the preceding paragraphs, for which the works associated with them collectively show the benefits that assimilating these data types can have for either soil moisture, soil temperature and/or heat flux predictions. Assimilating other data types has also been examined in some studies, such as *LAI* (e.g. Sabater *et al*., 2008), and also heat fluxes for which the only known published examples – outside of the research conducted for this thesis – are the assimilation of remotely sensed *LE* data by Schuurmans *et al*. (2003) and by Pan *et al*. (2008). Schuurmans *et al*. (2003) showed impacts on modelled *ET* which appeared promising but there was no validation with independent data, while Pan *et al*. (2008) assessed assimilation results using independent model predictions and showed improvement to soil moisture with no improvement to *ET*.

Hence separate to the experimental work in this thesis, published research into the assimilation of heat flux data is limited, with inadequate validation of resulting flux predictions in studies where it was assimilated (i.e. without using independent observations – as outlined above). Consequently, the question of whether assimilating heat flux data has merit for improving heat flux predictions, in comparison to assimilating other more commonly used data types, is largely unanswered – with this thesis aimed at making a contribution towards answering it.

Of the other (non heat flux assimilation) studies referenced previously in this sub-section, some involved validation of heat flux predictions (Margulis *et al*., 2002; Meng *et al*., 2009; Peter-Lidard *et al*., 2011; Reichle *et al*., 2010; Xu *et al*., 2013), with some potential shown for improving them. Most of the soil moisture assimilation studies referenced herein focused primarily on how soil moisture prediction is impacted, particularly over the root-zone for which any improvement is often assumed to increase the likelihood of improved heat flux predictions. Mahfouf (2010) notes that of the various studies into assimilating near-surface soil moisture, relatively few have examined the impact that the resulting root-zone moisture predictions have on atmospheric model forecasts of screen-level (2 m above ground) air temperature and relative humidity. While the scope of the work in this thesis is limited to assimilation into a stand-alone LSM, the focus on heat flux predictions is key given their influence on air temperature and relative humidity.

In the context of NWP, Mitchell *et al.* (2004) note that in contrast to assimilation for atmospheric models which has been established since the late 1970s, LSM assimilation is a much newer practice. They attribute some of the earliest examples of real-time assimilation in coupled land-atmosphere systems as being carried out at the National Centers for Environmental Prediction (NCEP) in the USA and the European Centre for Medium Range Weather Forecasts (ECMWF), with reference to Kalnay *et al*. (1996) and Gibson *et al*. (1997) respectively. LSM assimilation in NWP has typically involved adjusting soil moisture states via nudging or OI, driven by differences between observed and modelled screen-level air temperature and humidity (de Rosnay *et al*., 2014; Douville *et al*., 2000; Mahfouf, 2010). This approach does not always lead to improved soil moisture states (Drusch *et al*., 2009). Research has seen progress towards the use of more optimal data assimilation techniques such as the KF, motivated by a need to take advantage of the increasing availability of different remotely sensed information on the land surface such as soil moisture (de Rosnay *et al*., 2013; Drusch *et al*., 2009; Mahfouf, 2010).

Operational assimilation of remotely sensed land surface data (as opposed to only screen-level data) for soil state analysis in NWP is rare at present, with UK Met believed to be the only institution where it is carried out. It was implemented there in mid-2010 after it was demonstrated that assimilating soil moisture data along with screen-level data, using an existing UK Met nudging scheme, lead to improvements in both soil moisture and screen-level forecasts for various regions of the world (Dharssi *et al*., 2011). It is noted by de Rosnay *et al*. (2013) that the use of a simple nudging scheme at UK Met might limit the ability to optimally include other land surface observation types in the assimilation. Testing of remotely sensed soil moisture data assimilation by de Rosnay *et al*. (2013) in the ECMWF forecasting system, with the KF land surface assimilation scheme that was implemented there in late-2010, showed neutral impacts on soil moisture and screen-level forecasts. They assert that ongoing improvement in the moisture data product they used (ASCAT) is expected to result in improved soil moisture analysis. They also mention the longer-term value of the KF scheme is in the ability to include additional land surface data products, and that the analysis of other model variables such as soil temperature and those related to vegetation and snow cover needs to be investigated.

The CABLE LSM is a component of the Australian Community Climate and Earth System Simulator (ACCESS) which is used for climate prediction and Australia's NWP (Kowalczyk *et al*., 2013; Puri *et al*., 2013). There is currently no operational land data assimilation implementation within ACCESS although it is planned as part of ongoing development (Puri *et al*., 2013). As previously mentioned, the CBM used in this thesis for LSM assimilation experiments shares similar water and energy balance formulations with CABLE. Not only is there currently no operational LSM assimilation within ACCESS, there is no known published work involving assimilation into CBM/CABLE outside that which is presented in this thesis, or that of Pipunic *et al*. (in press) which focused exclusively on assessing the ability of remotely sensed soil moisture assimilation to improve root-zone moisture prediction.

2.5 CHAPTER SUMMARY

Based on a survey of the literature, this chapter has provided detailed background information relevant to the work carried out to meet the objectives of this thesis as outlined in the introduction chapter. This includes highlighting knowledge gaps within the broader context of LSM data assimilation research, which the experiments in following chapters make some contribution towards narrowing.

It is well established in the literature that soil moisture and temperature are key states related to the exchange of water and energy between the land surface and atmosphere via *LE* and *H*, which in turn influence air temperature and humidity in the lower atmosphere. Varying soil and vegetation properties impact the spatio-temporal dynamics of soil moisture and temperature, and hence also of *LE* and *H*. There are different ways in which data related to key land surface quantities – such as near-surface soil moisture, skin temperature and heat fluxes (*LE* and *H*) – can be observed, either in-situ or from remote sensing. Characterising the spatio-temporal variation of such quantities across broad regions (catchments, continents etc.) is best served with remote sensing. Various published studies provide generalised quantitative error estimates for these land surface data types which are valuable for data assimilation, and were used to guide observational error for experiments in this thesis. Some of the literature surveyed outlined practically useful techniques for quality control and correction of raw data collected in-situ with certain instruments. These were informative for managing some of the in-situ field data collected for this thesis.

LSMs have evolved over the past few decades towards more physically based representations of the land surface – including soil moisture mobility based on Richards' equation and representation of plant CO_2 use and photosynthesis as a function of stomatal conductance. The CBM used for this thesis is a physically based LSM with these features, and was the basis for the CABLE model which is part of Australia's climate prediction and NWP system (ACCESS). Errors in the input data and imperfect model structure are typical sources of error in LSM predictions. While assimilation of different land surface data types available from remote sensing has shown potential for improving soil state and heat flux predictions across various publications.

Many of the published LSM assimilation studies have examined the assimilation of soil moisture data, with skin temperature assimilation also having been tested in a range of studies. By contrast, research into the assimilation of *LE* and *H* data is limited in the literature, and the potential that using these data may have for improving predictions of *LE* and *H* – which is important for NWP (and water management more generally) – remains unclear. Hence this thesis has sought to contribute to a better understanding of the possible merits of assimilating *LE* and *H* data, in comparison to the use of data types for which a broader body of published research exists.

LSM data assimilation is clearly recognised as important for state initialisation in NWP and climate modelling. Operationally it has usually relied on observed screen-level atmospheric variables to adjust LSM soil states using OI or nudging schemes. With a growing body of research showing the benefits of directly assimilating emerging land surface data products for soil state prediction, there is a move towards assimilating such products operationally in NWP systems – UK Met implemented the assimilation of remotely sensed soil moisture with its nudging scheme in mid-2010. There is also suggestion in the literature of a need to progress towards using more optimal LSM data assimilation schemes such as the KF for NWP systems, to better handle the different land surface data products becoming available. The EnKF is therefore a suitable choice to use for comparing the assimilation of different data types in this thesis, with its use here based on research showing it to be computationally more efficient than the EKF but without the filter performance being degraded.

In addition to focusing on knowledge gaps surrounding the potential value of assimilating *LE* and *H* data, this thesis also plays an important role in examining data assimilation with the CBM as the results have implications for the CABLE model (which shares similar water and energy balance formulations) within ACCESS. LSM assimilation is planned for ACCESS but is not yet implemented, moreover the work presented herein is believed to be the first published work on sequential assimilation of land surface related data into the CBM/CABLE model.

As with many of the published research studies, the experiments here are applied to a stand-alone implementation of the CBM, to assess and understand impacts on the model in its own right without the added complexity of a coupled atmospheric model. Also in the literature are many examples where assimilation is assessed in simplified/controlled synthetic-twin studies or point-scale one-dimensional studies. The value of such studies as a proof-of-concepts is recognised here. Hence the sequence of experimental work that is presented – starting with the synthetic study, followed by the one-dimensional field data study, and culminating in the remotely sensed data assimilation study which by comparison is more complex given the added spatial uncertainty.

3 MODEL AND ASSIMILATION IMPLEMENTATION

All experimental studies in this thesis were performed using the CSIRO Biosphere Model (CBM: Wang & Leuning, 1998; Wang *et al*., 2001, 2007). As discussed in previous chapters this model was the basis for (and shares similar water and energy balance formulations) with the CABLE model (Kowalczyk *et al*., 2006, 2013) which is part of Australia's NWP and climate simulator (ACCESS: Kowalczyk *et al*., 2013; Puri *et al*., 2013). Plans for LSM data assimilation within ACCESS (Puri *et al*., 2013) requires a greater understanding of how data assimilation can be best utilised to consistently improve CABLE predictive skill of *LE* and *H* feedbacks to the atmosphere – starting with its uncoupled performance in the first instance. Thus the assimilation experiments performed with the CBM that are presented here make an important contribution towards developing this understanding.

The EnKF data assimilation algorithm was applied in all experiments where the key technical aspect involved generating ensembles of parallel model simulations and of observations in order to represent the relative uncertainties of each. As discussed in chapter 2, this algorithm was chosen because it is relatively easy to implement and is economical with the use of computing resources compared to other techniques such as the EKF. This chapter provides details on the CBM and EnKF implementation.

3.1 CSIRO BIOSPHERE MODEL (CBM)

Scientists at Australia's Commonwealth Scientific and Industry Research Organisation (CSIRO) developed the CBM (Wang & Leuning, 1998, Wang *et al*., 2001, 2007), which has become the Community Atmosphere Biosphere Land Exchange (CABLE) model. It was designed to quantify the vertical exchange of heat, water and CO_2 fluxes between the land surface (consisting of bare soil, snow and vegetation surfaces) and the atmosphere. Heat and water fluxes are of primary interest in this research and thus details relating to CO_2 are not included here. Much of the model details presented in this section are sourced from the CABLE technical report (Kowalczyk *et al.*, 2006), through personal communication with Dr Ying-Ping Wang (one of the model developers at CSIRO Marine and Atmospheric Research), and from working knowledge of the CBM source code. Fig. 3.1 summarises some of the main features of the CBM to provide a general reference for descriptions that are given.

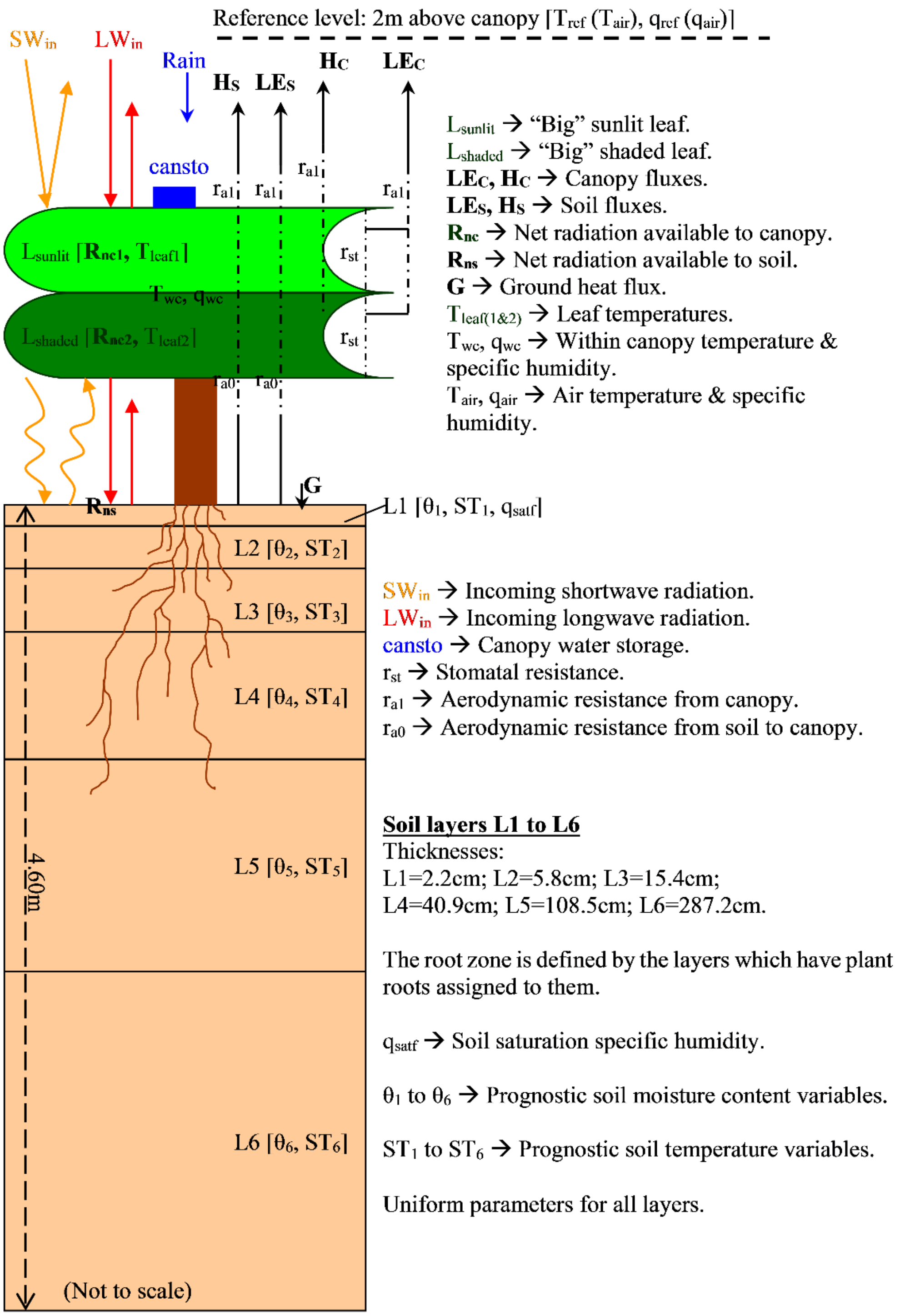

Figure 3.1: *Schematic of CBM showing two-leaf canopy scheme and six layer soil scheme with key features relating to the energy and water balance.*

3.1.1 GENERAL STRUCTURE

The CBM consists of a detailed canopy scheme with vegetation placed above the ground enabling aerodynamic and radiative interaction between the ground and the vegetation (Raupach, 1997). In addition to the canopy scheme there is a snow scheme for representing snow-pack and a soil scheme for representing the hydrology of the unsaturated soil zone. Vegetation roots are placed within the soil profile to provide a link between the vegetation and soil moisture content. Snow cover was not a relevant feature of the environments that were modelled in this research and thus details on the snow scheme are not presented.

Vegetation is represented using a two-leaf sub-model (Wang & Leuning, 1998) that differentiates between a "big" sunlit and a "big" shaded leaf, where *LE* and *H* from the canopy to the atmosphere (LE_C and H_C) are calculated separately for the two leaves as are other related quantities such as photosynthesis, stomatal conductance and leaf temperature. There is a canopy storage term representing rainfall interception such that LE_C and H_C are determined for dry and wet fractions of the canopy. Calculations of *LE* and *H* from the soil underneath the canopy (LE_S and H_S) are also made, thus the total quantities of *LE* and *H* calculated by the CBM are the respective sums of the components from the soil and from the canopy.

The soil scheme consists of six computational layers for calculating the fluxes of water and heat transfer. It is a one-dimensional scheme with no lateral movement or topographic effects accounted for. Darcy's law describes water flux through soil as a function of unsaturated hydraulic conductivity (K) and matric potential (ψ), and together with the relationships of Clapp and Hornberger (1978) (Eqs. (2.13) and (2.14)) it is used to form Richard's equation, which calculates soil moisture over time in the CBM. Calculations of soil moisture for the soil layers includes a term for root extraction for evapotranspiration (LE_C). The top soil layer includes representation of infiltration which depends on rainfall, runoff and evaporation, while for the bottom layer gravitational drainage works to restore soil moisture to its field capacity (θ_{FC}). Both soil moisture and soil temperature from the previous model time step, and fluxes from the current time step, are used in solving for soil moisture and soil temperature at the current time step.

A heat conduction equation (combination of Eqs. (2.3) and (2.4)) is used for calculating the vertical soil temperature over time. This incorporates volumetric heat capacity terms for the portions of dry soil, soil moisture and ice content, in addition to a thermal conductivity term based on Johansen (1975), which is a function of soil moisture and weighted by a normalised thermal conductivity term (Kersten number). At the soil surface, the net heat flux is given by G (Fig. 3.1, Eqs. (2.4) and (2.5)) with the lower boundary condition being zero heat flow. Soil moisture content and soil temperature of each of the six soil layers are prognostic state variables, which are initialised via user input at the first model time step and updated at subsequent time steps as a function of the previous time step value.

The general form of the land surface energy balance as represented by Eq. (2.5) is key to determining *LE* and *H* (with change in canopy heat storage not considered). In the CBM, the portion of total land surface R_n that is available to the vegetation canopy is a function of vegetation cover – as quantified by the leaf area index (*LAI*) parameterisation – which determines the amount of LE_C and H_C. Hence the *LAI* will influence the relative proportion of total *LE* and *H* coming from the canopy to that from the soil by regulating the amount of R_n that is available to each of the surfaces.

Calculations of *LE* and *H* can be summarised using the following general form:

$$LE = \rho_a \left(q_{surf} - q_{ref} \right) / r_E \qquad (3.1)$$

and

$$H = \rho_a c_p \left(T_{surf} - T_{ref} \right) / r_H \ , \qquad (3.2)$$

where T_{ref} and q_{ref} are air temperature (T_{air}) and specific humidity (q_{air}) at the reference level, T_{surf} and q_{surf} are the surface (i.e. soil or leaf) values, ρ_a is air density, c_p is the specific heat, r_H is the total resistance for heat and r_E the total resistance for water exchange between the surface and a reference level. The calculation of r_E is the sum of aerodynamic resistance, boundary layer resistance and stomatal resistance for water vapour, and r_H is the sum of aerodynamic resistance and boundary layer resistance for heat. Determining values of T_{surf} is an important task in the CBM heat flux calculations. For soil fluxes T_{surf} is represented by the soil temperature of the top-most soil layer (ST_1) which is a prognostic state variable, and for canopy fluxes it is represented by a leaf temperature variable (T_{leaf}), which is determined iteratively assuming thermodynamic equilibrium at each model time step after being initialised with meteorological forcing data. Specific detail on the sequence of calculating *LE* and *H* for the canopy and soil, including their relationship with prognostic model state variables, is given in section 3.1.3.

3.1.2 METEOROLOGICAL FORCING DATA AND PARAMETERS

The meteorological forcing data inputs for the CBM are:

- Incoming shortwave radiation;

- Incoming longwave radiation;
- Air temperature;
- Rainfall
- Specific humidity;
- Wind speed;
- Air pressure; and,
- Atmospheric CO_2 concentration.

In each modelling experiment, the CO_2 concentration was set to a uniform value of 370 ppm as an approximation of current atmospheric concentrations, with all other forcing variable values taken from measured time series data that were available. Data sources are summarised in chapter 4 and descriptions of the data use are included in the experimental chapters.

Key physical properties of soil and vegetation that influence the water and heat fluxes between the land surface and the atmosphere are represented by model parameters. Soil parameter values are essential for solving Richard's equation and for calculating heat transfer through the soil profile, affecting the moisture content in soil layers that is available for *LE*, along with the value of ST_1 required for soil fluxes. The CBM can only be parameterised with the same set of soil parameters for all six soil layers. This limits the ability to represent depth varying properties that can occur with contrasting soil horizons. Some major impacts from key vegetation parameters include determining the amount of R_n that is available to the vegetation canopy, linking available soil moisture and transpiration through the root distribution, and regulating transpiration efficiency based on properties relating to photosynthesis. Important vegetation and soil parameters are summarised in Tables 3-1 and 3-2 respectively. The different sources of key parameter data used in this research are presented in chapter 4 and the assignment of parameter values for different experiments is discussed in the relevant experimental chapters.

Table 3-1: *Key vegetation parameters in the CBM relevant to LE and H.*

PARAMETER	DESCRIPTION	UNITS
LAI (Leaf Area Index)	Area of vegetation cover per unit area of bare ground	-
froot	Fraction of plant roots in each soil layer	-
canst1	Maximum amount of water intercepted by the canopy	mm/LAI
ejmax	Maximum potential electron transport rate of the top leaf	$mol/m^2/s$
vcmax	Maximum RuBP carboxylation rate of the top leaf	$mol/m^2/s$
Hc	Height of the canopy	m
TVJmin	Minimum temperature for the start of photosynthesis	°C
TVJmax	Maximum temperature for the start of photosynthesis	°C
Taul	Leaf transmissivity for 3 wavelength bands – visible, near infra-red (NIR) and thermal infra-red (TIR)	-
Refl	Leaf reflectance for 3 wavelength bands – visible, NIR and TIR	-
tauw	Woody tissue transmissivity for 3 wavelength bands – visible, NIR and TIR	-
Refw	Woody tissue reflectance for 3 wavelength bands – visible, NIR and TIR	-

Table 3-2: *Key soil parameters in the CBM affecting the water balance and heat transfer through the soil profile, and hence LE and H.*

PARAMETER	DESCRIPTION	UNITS
c3	Fraction of soil moisture content above field capacity in bottom-most layer (L6) which drains	-
c_s	Heat capacity of soil minerals	J/kg/C
ρ_s	Soil density	kg/m^3
K_s	Hydraulic conductivity at saturation	m/s
Ψ_{aep}	Air entry potential (termed soil suction at saturation in CBM parameter file)	m
b	b parameter from Campbell (1974)	-
θ_{FC}	Volumetric soil moisture content at field capacity	vol/vol
θ_{sat}	Volumetric soil moisture content at saturation (porosity)	vol/vol
θ_{Wilt}	Volumetric soil moisture content at wilting point	vol/vol
Refsbare	Bare soil reflectance	-

3.1.3 DETAILS OF FLUX CALCULATIONS

Parameter and initial state variable values are input into the CBM by the user and other key model variables are initialised at the beginning of each model time step. The calculation of canopy fluxes are made prior to soil fluxes, which are both performed within an iterative loop for a stability parameter (Fig. 3.2). The stability parameter is necessary for applying the far field and near field theory to estimate aerodynamic resistance between the reference height and the canopy, and between the canopy and soil surface (see Raupach *et al.* 1997). These aerodynamic resistance values from the soil to the canopy (r_{a0}) and from the canopy (r_{a1}) are needed for flux calculations. Four iterations are used to determine a final stability parameter value and hence also resistances, other flux related variables and of course fluxes themselves. An iterative approach is used due to a number of the quantities involved being interdependent and therefore needing to be solved simultaneously.

Determining R_{nc} is done prior to canopy heat fluxes (LE_C and H_C) and plays a part in their calculation. It is a function of key parameters (including *LAI*, *taul*, *tauw*, *refl* and *refw*, see Table 3-1) and meteorological forcing for the current time step. Since the true value of R_{nc} requires knowledge of T_{leaf} which is unknown, isothermal conditions are assumed for R_{nc} where $T_{leaf} = T_{ref} = T_{air}$ (from the meteorological forcing data). Values of LE_C and H_C are calculated for both L_{sunlit} and L_{shaded} between the canopy and the reference level within the T_{leaf} iterative loop (Fig. 3.2, where for the canopy $T_{surf} = T_{leaf}$). Preceding the T_{leaf} loop, aerodynamic and vegetation boundary layer resistances are defined. Isothermal R_{nc} values remain unchanged within each T_{leaf} loop iterations where the following sequence occurs:

1) $T_{leaf} = T_{air}$ and leaf surface vapour pressure deficit (D_{leaf}) is set to D_{air} (from meteorological forcing) for the initial iteration;

2) Either one or both of T_{leaf} and D_{leaf} are used in the calculations of photosynthesis and canopy conductance values for heat (G_h), radiation (G_r) and water (G_w, which is a function of stomatal conductance for water). The link between soil moisture and stomatal conductance is an indirect one tracing back through the photosynthesis calculation to a soil water availability term given by,

$$rwater = froot \times \left((\theta - \theta_{Wilt}) / (\theta_{FC} - \theta_{Wilt}) \right), \qquad (3.3)$$

where *rwater* is a fraction representing the total soil moisture available for transpiration across all soil layers (denoted by *i*), given the current values of soil moisture (θ_i) and the associated parameter values (Tables 3-1 and 3-2);

3) LE_C is calculated using a Penman-Monteith combination equation,

$$LE_C = \frac{\Delta R_{nc} + \rho_a c_p D_{air} (G_h + G_r)}{\Delta + \gamma (G_h + G_r) / G_w}, \qquad (3.4)$$

which is of the form represented by Eq. (2.21) with Δ and γ and given by Eqs. (2.18 and 2.20) respectively. Here in Eq. (3.4) R_{nc} is the isothermal net radiation ($T_{leaf} = T_{air}$) for the radiation energy absorbed by the canopy, the vapour pressure deficit is represented by D (described in step 1)), and conductance terms (G_h, G_r and G_w) are used instead of resistances (i.e. r_a and r_s);

4) Based on the land surface energy balance relationship (Eq. (2.5), excluding the soil heat flux term since this is for the canopy), the isothermal R_{nc} and the value of LE_C from Eq. (3.4) are used to determine H_C with the following,

$$H_C = (R_{nc} - LE_C) \times G_h / (G_h + G_r); \qquad (3.5)$$

5) Using H_C from Eq. (3.5), a new value of T_{leaf} is calculated based on the form of Eq. (3.2) where $T_{leaf} = T_{surf}$ and conductance terms are used instead of the resistance r_H,

$$T_{leaf} = T_{air} + H_C / (\rho_a c_p G_h); \qquad (3.6)$$

6) With values determined at previous steps in the loop, a new value for D_{leaf} is calculated;

7) Thus with new values of T_{leaf} and D_{leaf}, the loop repeats from steps 2) through to 6) until the difference between the new T_{leaf} value from step 5) and the one prior to its calculation is less than 0.1.

At the end of the above iteration process when the T_{leaf} difference condition in step 7) has been met, the final canopy flux calculations are then performed based on wet and dry canopy portions. The term *cansto* (Fig. 3.1) represents the canopy water storage resulting from rainfall interception and is a function of *LAI* and *canst1* (Table 3-1) – it is used to calculate a wet canopy fraction. Wet canopy fluxes are subsequently determined using similar calculations to Eqs. (3.4) and (3.5) except that heat, radiation and water conductance terms for a wet canopy are used instead, and the calculations are weighted by the wet canopy fraction. The dry canopy fraction is multiplied by the final LE_C and H_C values from the T_{leaf} loop to obtain dry canopy flux values. Therefore, the total calculated canopy fluxes, LE_C and H_C, for the current model time step are the sums of the wet and dry components.

Calculation of R_{ns} follows the canopy flux calculations, as do calculations for LE_S and H_S (Fig. 3.2) which are based on the form of Eqs. (3.1) and (3.2) respectively where the resistance terms in each (r_E and r_H) are both represented here by $r_{a0} + r_{a1}$ (see Fig. 3.1). The result from Eq. (3.1) is essentially a potential evaporation term and is thus weighted by an available water factor (*wetfac*) for the top soil layer to get LE_S where

$$wetfac = (\theta_1 - \theta_{Wilt}) / (\theta_{FC} - \theta_{Wilt}). \qquad (3.7)$$

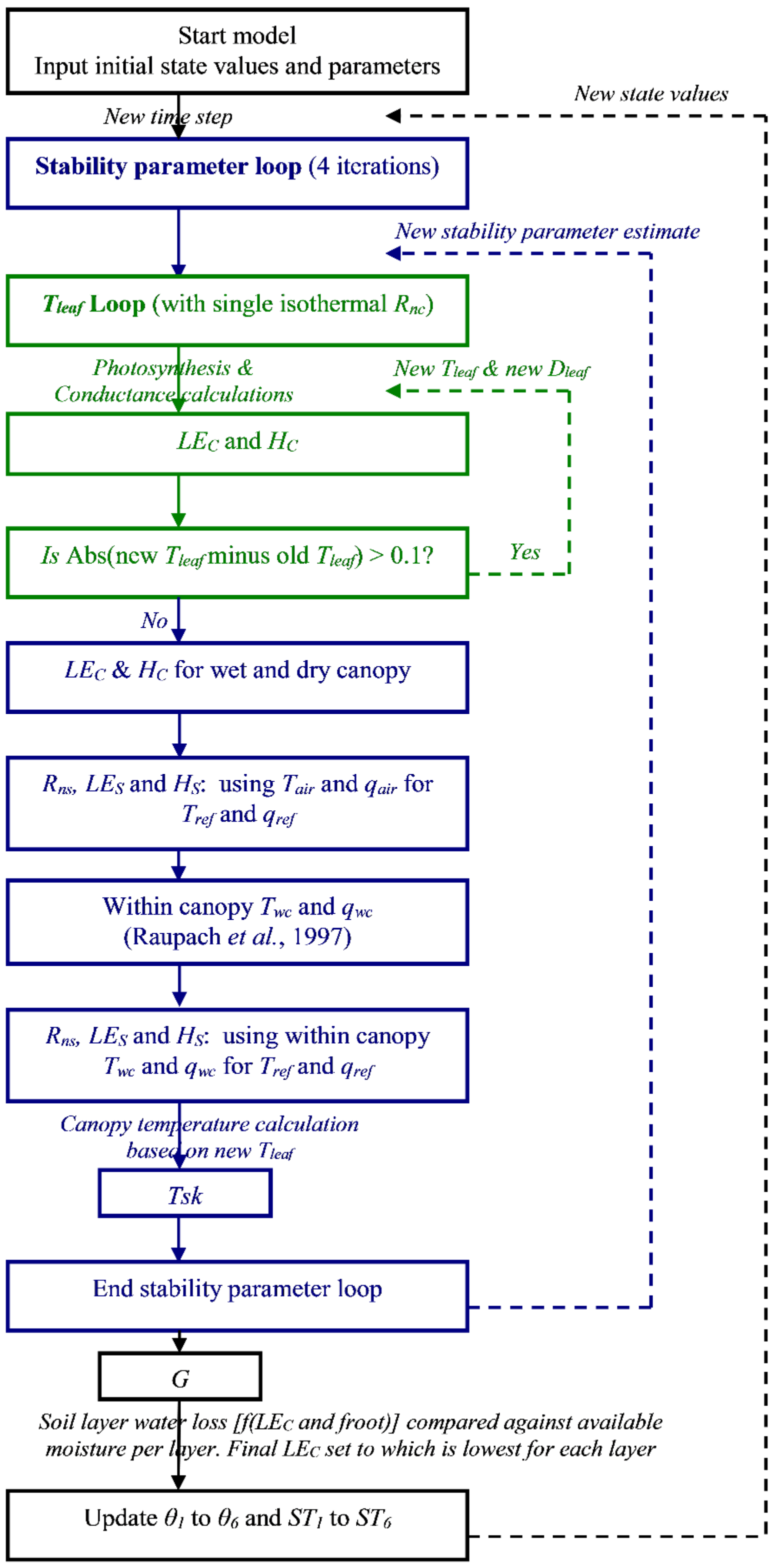

Figure 3.2: *Flow diagram summarising the order of major processes involved in calculating heat fluxes, skin temperature and model states in the CBM. See Kowalczyk et al. (2006) for more comprehensive detail. Refer to Fig. 3.1, and Tables 3-1 and 3-2 for variable name descriptions.*

Also for LE_S, the q_{surf} term is the soil specific humidity at saturation which is a function of the top soil layer temperature (ST_1). Whilst for H_S, the current time step value of ST_1 is used for T_{surf}. Values for both LE_S and H_S are calculated twice, with the first calculation using the reference level values of T_{air} and q_{air}. Subsequent to this is a complex formulation from Raupach *et al.* (1997) which is used to determine values for within canopy temperature and specific humidity (T_{wc} and q_{wc}). Thus the second and final calculations of LE_S and H_S for the current time step use these values of T_{wc} and q_{wc} for T_{ref} and q_{ref}.

The total skin temperature (*Tsk*) of the land surface is the sum of the canopy and soil components of radiative temperature from the longwave radiation balance which is calculated for each surface. For soil, ST_1 is the temperature term used in the longwave radiation balance, and for the canopy it is a canopy temperature term (T_C) which is derived using the final T_{leaf} value determined from the T_{leaf} iterative process. The contribution from each component to the total skin temperature value is a function of *LAI* – where a very small *LAI* value (i.e. minimal vegetation cover) results in a larger contribution from the soil and *vice-versa* as summarised by the following:

$$Tsk = \left[\left(f(LAI) \times ST_1^{\,4}\right) + \left(\left(1 - f(LAI)\right) \times T_C^{\,4}\right)\right]^{1/4} . \qquad (3.8)$$

In Eq. (3.8), *f(LAI)* represents a variable that is a function of *LAI* and describes the fraction of total radiation that can get through to the soil surface.

In the final steps of the sequence outlined in Fig. 3.2, the soil heat flux *G* is calculated based on the energy balance equation (Eq. 2.5) and using R_{ns}, LE_S and H_S. Prior to final soil moisture and temperature state value updates by the soil scheme, LE_C for the current time step is used to determine soil moisture loss from vegetation transpiration. The fractions of vegetation roots assigned to each soil layer (*froot* parameter) are used as weighting factors to divide the total transpired water amount between layers. A comparison is then made to check if the calculated transpiration water loss from each layer exceeds the available soil moisture content. If it does, the value for transpired water loss is then reset to the amount of available soil moisture for the respective layer(s) where this occurs. A final update is then made to LE_C for the current time step by summing all the transpiration water loss amounts determined for each soil layer with roots. The final transpiration water loss amounts are also deducted from the current soil moisture content values for each layer. Final updates to soil moisture and soil temperature state values are then made which are carried forward to the beginning of the next model time step.

3.1.4 SUMMARY OF KEY CBM CHARACTERISTICS

The most important feature regarding all heat flux calculations in terms of this research is the relationship that the fluxes share with the twelve prognostic model state variables – θ_1 to θ_6 and ST_1 to ST_6. These are the variables updated and re-initialised by the data assimilation and thus observations must be able to relate and impact on them, and in turn, they need to impact on the modelled heat fluxes in a way that reflects the real world relationships between the states and fluxes in order for there to be any potential benefits from performing the assimilation.

Formulations for LE_S and H_S have the most direct link with the CBM states through *wetfac* (Eq. (3.7)) and the use of ST_1 for both fluxes. Alternatively, the canopy scheme for vegetation fluxes is considerably more complex where the strongest link to model states is between soil moisture and LE_C via the root distribution in the soil layers (e.g. the *rwater* term, Eq. (3.3)). There is no direct link between soil temperature and the canopy fluxes (only indirectly via the soil moisture and soil temperature relationship), with the non-prognostic T_{leaf} variable (initialised with meteorological forcing data and determined iteratively at each time step) representing the surface temperature in energy balance calculations for the vegetation canopy. Similarly for the skin temperature calculation, the soil surface contribution is linked directly to the ST_1 state variable but the canopy contribution is dependent on T_{leaf} (Eq. (3.8)). Thus for increasing vegetation cover (i.e. increasing *LAI*) the direct connection between total skin temperature and soil state variables will decrease.

With some relationships between state variables and heat fluxes in the CBM being more complex and/or weaker than others, an additional benefit of this research is identifying any limitations there may be to constraining CBM heat flux predictions with certain observed data types via data assimilation.

3.2 ENSEMBLE KALMAN FILTER (EnKF) IMPLEMENTATION

Chapter 2 covered the general background of data assimilation and Kalman filtering, followed by a summary of different assimilation applications to LSMs from the literature. The specifics of the EnKF and its implementation in this research are presented here.

The general form of the Kalman Filter is summarised by Eqs. (2.25) and (2.26) in Chapter 2. A Monte Carlo approach forms the basis of the EnKF, where an ensemble of randomly perturbed model simulations run in parallel for the same time period is used, and the ensemble spread represents prediction uncertainty for determining the model error covariance **P**, as required for calculating the Kalman gain **K** (Eq. (2.26)). Formulation of the EnKF as used in this research can be summarised as follows (Evensen, 1994; Houtekamer & Mitchell, 1998; Walker & Houser, 2005). The background state covariance matrix for determining the model error covariance at assimilation times, with *f* denoting a prediction and *k* denoting the current time step, is defined as

$$\mathbf{P}_k^f = \frac{(\mathbf{x}_k^f - \overline{\mathbf{x}}_k^f)(\mathbf{x}_k^f - \overline{\mathbf{x}}_k^f)^{\mathbf{T}}}{m-1}, \qquad (3.9)$$

where **x** are individual ensemble members of the state prediction matrix **X**, and the over-bar represents the ensemble mean across all members. With the EnKF it is the ensemble mean which is taken to be the true value of the state. The number of ensemble members is denoted by *m* and the choice of this number for the experiments is discussed in chapter 5 (proof-of-concepts synthetic study). However, explicit calculations of $\mathbf{P}_k^f$ are not actually required and the analysis equation for state updating (Eq. (2.25)) can be written as

$$\mathbf{X}_k^a = \mathbf{X}_k^f + \mathbf{B}_k^{\mathbf{T}}\mathbf{b}_k, \qquad (3.10)$$

where

$$\mathbf{B}_k^{\mathbf{T}} = \mathbf{P}_k^f \mathbf{H}_k^{\mathbf{T}}, \qquad (3.11)$$

and

$$\mathbf{b}_k = (\mathbf{H}_k \mathbf{P}_k^f \mathbf{H}_k^{\mathbf{T}} + \mathbf{R}_k)^{-1}(\mathbf{y}_k - \mathbf{Z}_k^f). \qquad (3.12)$$

In Eq. (3.12), **y** is the observation **Z** with an error term as follows

$$\mathbf{y}_k = \mathbf{Z}_k + \zeta, \qquad (3.13)$$

where ζ represents random observational error with zero mean and covariance **R**. Estimates of error ranges for observed variables were used to define the covariance **R** – values used in each study are presented in respective experimental chapters. An ensemble of *m* random perturbations were generated within the estimated error ranges and added to the observed data values to produce observation ensembles **y** with covariance **R** as per Eq. (3.13).

The first term in brackets of Eq. (3.12) is calculated as

$$\mathbf{H}_k \mathbf{P}_k^f \mathbf{H}_k^{\mathbf{T}} = \frac{\mathbf{q}_k \mathbf{q}_k^{\mathbf{T}}}{m-1}, \qquad (3.14)$$

where

$$\mathbf{q}_k = \mathbf{H}_k(\mathbf{x}_k^f - \overline{\mathbf{x}}_k^f) = (\mathbf{z}_k^f - \overline{\mathbf{z}}_k^f), \tag{3.15}$$

and $\mathbf{z}$ are individual ensemble members of the predicted observation ($\mathbf{Z}_k^f$) and the over-bar denotes the ensemble mean. Hence, it is unnecessary to solve for $\mathbf{H}$ and therefore $\mathbf{B}$ can be calculated as

$$\mathbf{B}_k^{\mathbf{T}} = \frac{(\mathbf{x}_k^f - \overline{\mathbf{x}}_k^f)}{m-1}\mathbf{q}_k^{\mathbf{T}}. \tag{3.16}$$

In summary $\mathbf{b}_k$ is calculated using Eqs. (3.13), (3.14), (3.15) and $\mathbf{R}$ (with predicted observation ensemble members $\mathbf{z}$ used for $\mathbf{Z}_k^f$ in Eq. (3.13)), and $\mathbf{B}_k^{\mathbf{T}}$ is calculated using Eq. (3.16). Then substitution of $\mathbf{b}_k$ and $\mathbf{B}_k^{\mathbf{T}}$ into Eq. (3.10) updates the ensemble members for each state variable at assimilation time steps. For all experiments in this research the model's soil moisture and soil temperature were updated, so the state prediction matrix $\mathbf{X}$ consisted of the CBM state variables θ_1 to θ_6 and ST_1 to ST_6 (Fig. 3.1).

In addition to generating ensembles for observed data (as mentioned on the previous page), the EnKF implementation also involved generating ensembles of model inputs by perturbing estimated state initial conditions and the time series of each meteorological forcing variable in order to represent modelling errors introduced by each. Using these ensembles of inputs resulted in ensembles of CBM predictions for approximating prediction uncertainty. Inaccurate model physics and uncertain parameters also contribute to model error, but these contributions have not been specifically treated in this thesis.

For the year-long simulations in the one-dimensional and remotely sensed data assimilation studies (chapters 6 and 7), state variables were also directly perturbed just prior to the state update calculations, as a form of covariance inflation to counter the potential for filter divergence (e.g. Anderson & Anderson, 1999). Over extended periods spanning seasonal changes, maintaining good approximations of model error with the EnKF can be very challenging, with filter divergence a potential symptom of progressively degraded error representation by ensembles (Anderson & Anderson, 1999; Li *et al.*, 2009). This is where a narrowing of predicted ensembles reduces model error covariances $\mathbf{P}$ to a point where the EnKF is sub-optimal, and poor model predictions could potentially persist with negligible corrective impact from observations. As an example, an ensemble spread for soil moisture state error, as a consequence of an ensemble of perturbed rainfall forcing, may narrow towards a single moisture value after a prolonged period of drying without further rainfall. To reduce this risk, one approach is to slightly inflate the spread of ensemble members about the ensemble mean prior to state updating, using multiplicative or additive inflation (Anderson & Anderson, 1999; Anderson, 2007; Li *et al.*, 2009).

Accurate ensemble representation of model prediction error as it evolves through time for different variables is non-trivial, particularly for complex models such as the CBM. Investigating model error and quantifying it in terms of all of its intricate detail, and due all possible sources, is beyond the scope of this research. Ensemble representations of error here are approximations where the focus is on comparing the merits of assimilating different observation types via three separate studies. The treatment of model error for assimilation experiments was the same within each respective study, therefore differences in experiment results within each study were due only to the observation data assimilated.

All perturbations used for ensemble generation were from a random number generator, which produced random numbers from a Gaussian distribution with zero mean (μ=0) and standard deviation of 1 (σ=1). Uncertainty range estimates for the data being perturbed (e.g. initial state variables) were used for multiplying with the generated random numbers, and the resulting perturbations added to the data values – resulting in an approximate Gaussian ensemble spread representative of the data error (with the original data value the ensemble mean).

The approach of Turner *et al.* (2008) was used as a guide for creating ensembles of time series meteorological forcing data. It involves prescription of two types of error for creating ensemble members, with i) separate random perturbations generated at each model time step in the experiment period and added to the data value (time dependent random measurement error), and ii) a single random perturbation generated once and applied at each time step in the period (offset or spatial representative error from using point scale forcing data). Using notation from Turner *et al*. (2008), where for a measured forcing variable value h_k^o at time step *k*, the value of the *j*th ensemble member is determined as

$$h_k^j = h_k^o + \zeta_k^j + \beta^j . \qquad (3.17)$$

From Eq. (317) ζ_k^j is the time dependent (with time step *k*) measurement error for each ensemble member *j* resulting from random perturbations created with a standard deviation σ_1. The term β^j is the offset error term from perturbations generated once for each ensemble member *j* (note no time step index) with a standard deviation σ_2. Hence the overall standard deviation σ of the ensemble spread about the ensemble mean μ for the time series data is approximately the value for σ_2 (given it represents the offset of members from μ).

The standard deviations (σ_1 and σ_2) of generated perturbations can vary with time in some cases. Their variation is dependent on the forcing variable data type – categorised by Turner *et al.* (2008) as either unrestricted, semi-restricted or restricted – and their values are also defined by Turner *et* *al.* (2008) using the parameters ξ and χ, which are constants relating to measurement and offset error respectively. Estimating values for ξ and χ to provide appropriate standard deviations for error perturbations is ideally done by comparing multiple sets of observed forcing data, if available, from the region that is of interest for modelling (assuming only point scale data sets are available).

Regarding data type categories, unrestricted variables are described as measured on a scale with no maximum or minimum bounds, and errors are considered independent at any point on the measurement scale and so perturbations are added directly to each data value. Perturbation standard deviations are represented by

$$\sigma_1 = \xi , \qquad (3.18)$$

and

$$\sigma_2 = \chi . \qquad (3.19)$$

Semi-restricted data are described by Turner *et al.* (2008) as having a lower or upper bounding limit and errors are assumed to be proportional to measurements (multiplicative) with perturbations added as a percentage of measured values. Therefore if a particular variable has a minimum bound of zero then there is assumed to be no error if the measured value is zero (such as with rainfall) – a measurement of zero rainfall may indeed be erroneous in reality (i.e. a detection error) although this adds another level of complexity to generating error perturbations that is not dealt with here. For measured values h_k^o of a variable that has an upper bound $h_{\max}$ or a lower bound $h_{\min}$, measurement error standard deviation can be represented by

$$\sigma_1 = \left(h_{\max} - h_k^o\right)\xi \quad \text{or} \quad \sigma_1 = \left(h_k^o - h_{\min}\right)\xi , \qquad (3.20)$$

and for the offset

$$\sigma_2 = \left(h_{\max} - \hat{h}_k\right)\chi \quad \text{or} \quad \sigma_2 = \left(\hat{h}_k - h_{\min}\right)\chi . \qquad (3.21)$$

Restricted data are described by Turner *et al*. (2008) as measured on a scale with an upper and lower bound. An example is cloud cover fraction where at the end points of the measurement domain, the sky is either completely clear or completely covered (low/no uncertainty) and more uncertain in the middle. Turner *et al*. (2008) note that the perturbations can be generated via a variable approach where error is a function of the measurement, and the maximum error is added at the mid-point of the measurement domain and reduces linearly to zero at the domain boundaries. Or simply with an approach similar to that used with unrestricted data (Eqs. (3.18) and (3.19)) with error perturbations treated as independent of measurements, but where values are truncated at the boundaries of the measurement scale to avoid ensemble values occurring outside of realistic value bounds.

For their work, Turner *et al.* (2008) drew upon multiple sets of point scale forcing data from sites scattered around the region where their modelling was focused. Having a range of data sets available should enable better characterisation of offset or spatial representation error for point data and is hence valuable for assisting the choice of ξ and χ values. Turner *et al.* (2008) describe how choosing these parameter values and associating data type categories with variables can be guided by analysing scatter plots with: i) the standard error between the values of a variable from different neighbouring data sets, plotted against, ii) the average of the values across the data sets. Generally, the average standard error from scatterplots for unrestricted data is a reasonable estimates for ξ and χ (where the spread of scatter over standard error values can also provide a general estimate for χ). While the slope of the mid-point line through such scatterplots for semi-restricted data provides an approximation for ξ and χ. At most there were two complete forcing data sets from the region where modelling was focused for the research in this thesis, and the error perturbation techniques summarised here from Turner *et al*. (2008) were drawn upon as a guide.

For the synthetic study (chapter 5) a single regional forcing data set was used that was available at the time of the study. The ensemble generation process discussed here was loosely followed in that work for simplicity. No complimentary data sets were used to help estimate parameters for defining σ_1 and σ_2, and the semi-restricted data type category was applied for generating ensembles for all variables except air temperature where the unrestricted category was applied. Guiding the choice of ξ and χ values were estimates of instrument measurement uncertainty along with choices ensuring that offset error would provide a broader ensemble spread than the instrument error range. Two forcing data sets were available from the area where the real data assimilation studies (chapters 6 and 7) in this research were focused. A single set of forcing data was used to run the CBM in each study, while the two sets enabled differences between values from each to be analysed and assist with defining the overall ensemble spread σ for each variable.

The covariance inflation applied for experiments in chapters 6 and 7 was additive. Perturbations were added to each *a priori* soil state ensemble member at assimilation time steps, to slightly increase their spread about the ensemble mean. The value of σ used for these perturbations was chosen based on the CBM soil layer. Specifically, for the top-most soil layer, moisture perturbations with σ=0.01 vol/vol and soil temperature perturbations with σ=1°C were added. For subsequent soil layers, these values of σ used for the top-most layer were scaled down, based on the fraction of the top-most layer thickness (2.2 cm) to the layer thickness of the respective states being perturbed. For example, the second layer is 5.8 cm thick, therefore the scaling applied to σ

used for the top-most soil layer was 2.2/5.8 (=0.38), and for the 15.4 cm thick third layer the scaling applied was 2.2/15.4 (=0.14), and so on. This scaling is an attempt to factor in that for deeper/thicker soil layers, random error is likely to be increasingly dampened compared to the near-surface.

3.3 CHAPTER SUMMARY

This chapter describes key features of the CSIRO Biosphere Model (CBM), the precursor to the Community Atmosphere Biosphere Land Exchange (CABLE) model which shares much of the same structure for the water and energy balance and is part of Australia's weather and climate simulation system. Features pertinent to this research are the formulations for latent and sensible heat fluxes (*LE* and *H*) and skin temperature – each consisting of soil and vegetation canopy components – and any relationship they may share with the soil moisture and soil temperature prognostic state variables for the six CBM soil layers. These state variables are the target of data assimilation updates with the Ensemble Kalman Filter (EnKF) aimed at improving *LE* and *H* predictions. Implementing the Monte-Carlo based EnKF was also described, with ensembles for initial state condition and meteorological forcing data uncertainty used to produce estimates of uncertainty for model predictions, and with additive perturbation applied to state ensembles as a form of covariance inflation in some experiments. A description of study sites and data sets that were used in this research are presented in the next chapter.

4 STUDY REGION AND DATA PROVENANCE

The data used in this research have been measured within, or in the vicinity of, the Kyeamba Creek catchment in south eastern Australia. Kyeamba Creek is a tributary of the Murrumbidgee River, a major waterway in the southern portion of the Murray Darling Basin. Fig. 4.1 provides a contextual view of the region containing all of the ground based monitoring locations from where experimental data were sourced, set against a back-drop of false colour Landsat imagery. A close-up in the lower right of Fig 4.1 shows the location of the Murray Darling Basin within Australia and the relative location and scale of the Kyeamba Creek catchment. The city of Wagga Wagga is located ~30 km to the north west of the catchment and is a major urban centre that has a Bureau of Meteorology (BoM) weather station (ID 072150) located on its outskirts (Fig. 4.1). Reference to BoM data in this chapter refers to data from that particular station.

Based on statistics for the Wagga Wagga BoM weather station observations (http://www.bom.gov.au/climate/averages/tables/cw_072150.shtml), the annual average rainfall in the region for the period 1941-2014 is ~570 mm/year, and annual average minimum and maximum air temperatures over a similar period are 9.0°C and 22.1°C respectively. A Digital Elevation Model (DEM) is displayed in Fig. 4.2 to provide an overview of the elevation variation across the Kyeamba Creek catchment region.

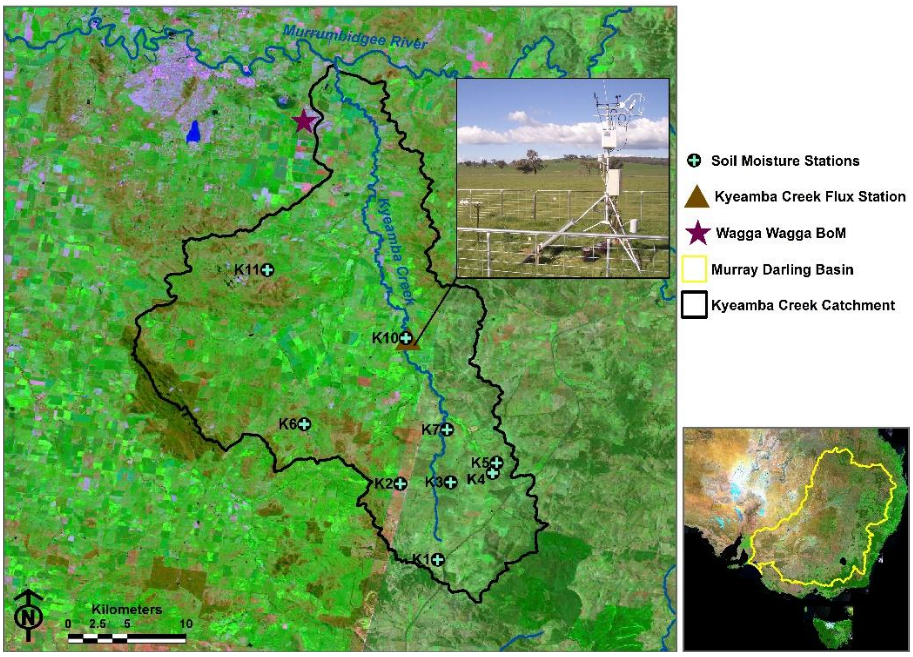

Figure 4.1: *A map of the region where all experimental data originated. South eastern Australia is shown in the panel on the bottom right of the main map with the Murray Darling Basin coverage and relative location of the Kyeamba Creek catchment (black spot) for reference.*

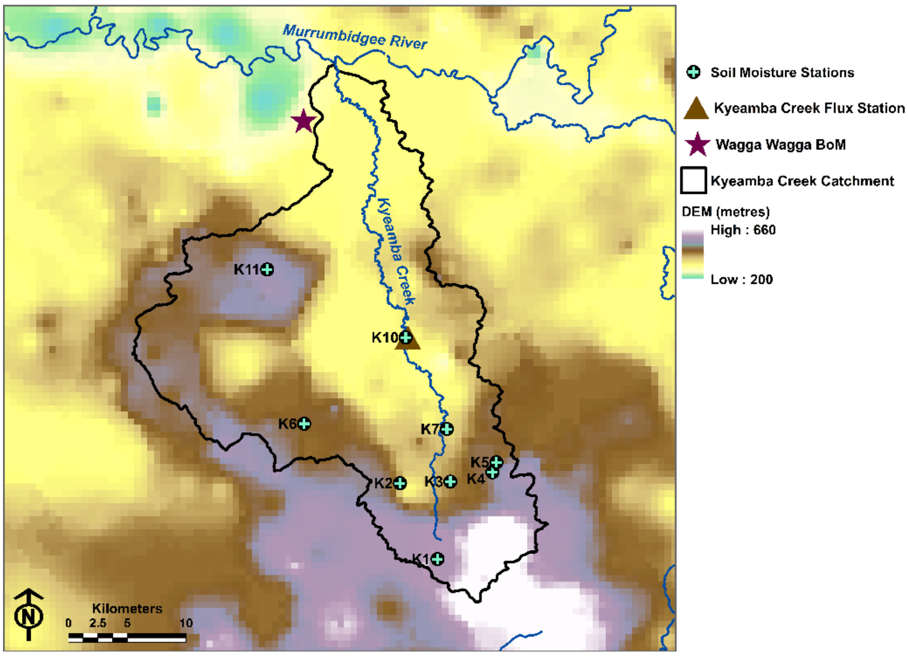

Figure 4.2: *Elevation variation across the Kyeamba Creek catchment, with sites relevant to the data used in this research also displayed.*

Soil moisture data monitoring sites within the Kyeamba Creek catchment shown in Fig. 4.1 (and the other maps of the catchment presented in this chapter) were originally set-up and managed by the Department of Infrastructure Engineering (formerly Civil and Environmental Engineering) at The University of Melbourne. Currently they form part of the OzNet monitoring network (Smith *et al*., 2012) which is jointly supported by The University of Melbourne and Monash University in Australia.

A range of in-situ water balance, energy balance and meteorological observations have been made across the different sites shown in Figs. 4.1. They are summarised in the following sections, as are the remotely sensed products and sources of parameter data used in the CBM for this research. Monitoring station locations shown in the above-referenced figures are relevant to the different experimental studies in this thesis. For the synthetic-twin study (chapter 5) most of the forcing used was based on Wagga Wagga BoM station data, along with data from some OzNet stations. The one-dimensional field data study (chapter 6) relied mostly on Kyeamba Creek flux station data, with some BoM station and OzNet station data used. While the remotely sensed data study (Chapter 7) also relied on flux station site and BoM station data, together with data from all soil moisture stations (Figs. 4.1). The particular OzNet stations relevant to the respective experimental studies are specified in following sections.

4.1 KYEAMBA CREEK SOIL MOISTURE STATIONS

Data from nine of the Oznet soil moisture monitoring stations (Smith *et al*., 2012; www.oznet.org.au/kyeambasm.html) were used in this research and are shown with their respective Oznet labels in Fig. 4.1. Measurements of interest made at the stations include rainfall, soil moisture and soil temperature. These particular stations fall within the spatial domain of the remotely sensed products (section 4.5) used in the remotely sensed data assimilation study (Chapter 7) and were thus used for ground validation. The meteorological forcing dataset used in the synthetic-twin study (see section 4.2) includes rainfall from the K2 and K3 stations. Rainfall data from K10 station was used to fill gaps in the rainfall series recorded at the Kyeamba Creek flux station (~200 m distant), as used for the one-dimensional field data and remotely sensed data studies.

Data from the nine stations had been previously processed and made available on the Oznet website (referenced above) from where they were sourced. Stations K1 to K5 have been operating since 2001 and the available data processed to a 30 minute time step, while the newer installations of K6, K7, K10 and K11 have been in operation since 2004 with the available data processed to a 20 minute time step.

In-situ measurements of soil moisture at all of the stations cover a depth profile down to 90 cm via three separate 30 cm long Campbell Scientific water content reflectometer probes installed at consecutive depth intervals from the surface. This is illustrated in Fig. 4.3 taken from the Oznet website – CS615 probes (Campbell Scientific Inc., 1996) were used at the older monitoring sites and CS616 probes (Campbell Scientific Inc., 2002) at the newer ones. Surface soil moisture has also been measured over the 0-8 cm depth range at the older monitoring stations (with a CS615 probe inserted at a small angle from the surface), and over the 0-5 cm range at the newer stations with a Hydraprobe sensor (Vitel Inc., 1994). The soil temperature measurements at the older stations (Fig. 4.3) cover depths of 4 cm, 15 cm, 45 cm and 75 cm, while at the newer stations they are made for 2.5 cm and 15 cm.

Periodic soil moisture measurements were also made at the stations using Time Domain Reflectometer (TDR) probes (Trase system, Soil Moisture Equipment Corp., 1996), along with gravimetrically determined soil moisture, to assist with calibrating Campbell Scientific probe and Hydraprobe sensor data. Calibration of the CS615 and CS616 probe data was based on the work of Western and Seyfried (2005) and Yeoh *et al*. (2008) respectively, and Hydraprobe calibrations were based on the work of Merlin *et al*. (2007).

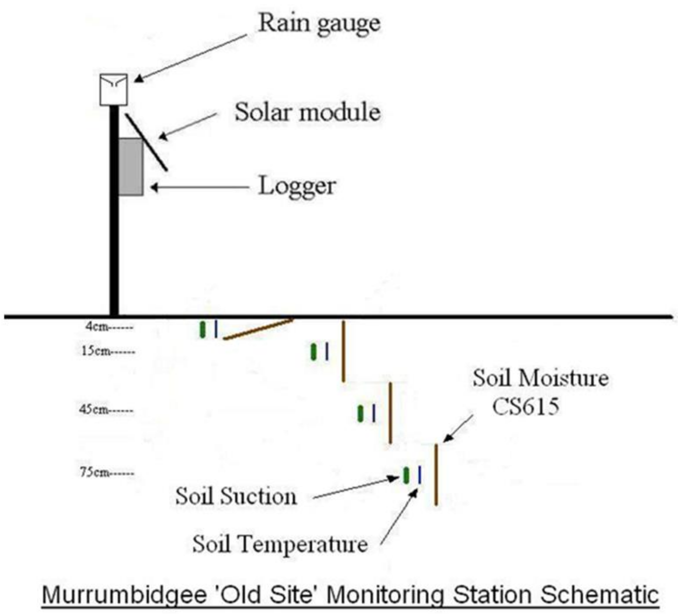

Figure 4.3: *A schematic of the above and below ground monitoring at the older soil moisture stations (K1 to K5). For newer stations (K6, K7, K10 and K11), Hydraprobe sensors (0-5 cm) were used for the near-surface moisture and CS616 probes for the three deeper moisture.*

4.2 KYEAMBA CREEK REGIONAL FORCING DATA

A 30 minute time scale data set compiled from meteorological observations relevant to the Kyeamba Creek catchment region has been produced by The University of Melbourne for the years 2000-2007, with details described by Siriwardena *et al.* (2003). It was aimed at providing a ready-made meteorologic forcing dataset for conducting LSM experiments applied around the catchment and has been utilised for modelling in the synthetic-twin data study. The variables making up the dataset are:

- Incoming shortwave radiation;
- Incoming longwave radiation;
- Rainfall;
- Air temperature;
- Wind speed; and,
- Specific humidity.

Data for each of these variables except rainfall are based on Wagga Wagga BoM weather station observations. The rainfall data is taken from the K2 soil moisture monitoring station (Fig. 4.1) – in the synthetic study the K2 rainfall was replaced by the rainfall data series from K3 as part of producing a "degraded" model input (chapter 5).

This Kyeamba Creek forcing data set was also used to help estimate representative uncertainty for Kyeamba Creek flux station site meteorological data used in the one-dimensional and remotely sensed data studies. Estimates of forcing data uncertainty ranges for implementing the EnKF in each experimental study are presented in the respective experimental chapters.

4.3 KYEAMBA CREEK FLUX STATION SITE

Elevation at the site (147.56°E, -35.39°S) is approximately 230m above sea level. The site is on the alluvial flats of the creek valley (Fig. 4.2), approximately 30 km south east of the Wagga Wagga BoM weather station and only about 200 m distance from the K10 soil moisture station in a non-irrigated grass pasture area – with cleared farmland representative of most the creek catchment (Fig. 4.1). Heat fluxes, meteorological forcing, soil moisture and soil temperature were measured at various rates and were all processed to a 30 minute time step.

These data sets were collected primarily for this research, to facilitate modelling experiments for the one-dimensional study and also for use in the remotely sensed data assimilation study. Therefore, considerable effort was spent for a period spanning >1 year to set-up and manage an eddy covariance system for heat flux measurements, along with instrumentation for the other above and below ground data listed in the previous paragraph. Unlike the readily-available data sets related to the other stations, some of the data collected from this site required processing, quality checking and calibration before use in the experiments.

4.3.1 SUB-SURFACE MONITORING

Soil moisture related data were recorded once per a 30 minutes at this site over four depths – 0-8 cm, 0-30 cm, 30-60 cm and 60-90 cm – using CS615 probes in an identical set-up as with the soil monitoring stations illustrated in Fig. 4.3. The actual data recorded were period measurements of the probe waveguide signals in ms (related to moisture content of surrounding soil via the dielectric constant). Soil temperature was measured at six depths at the site – 2 cm, 5 cm, 10 cm, 20 cm, 50 cm and 100 cm – using UNIDATA 6507A temperature thermistor probes (Unidata Australia, 1997). Two HFT3 heat flux plates (Campbell Scientific Inc., 2004) were also installed at 8 cm from the surface to measure ground heat flux (G), accompanied by temperature thermocouple probes installed above them at 6 cm and 2 cm from the surface.

To facilitate calibration and conversion of period measured CS615 probe data to a volumetric moisture content value, TDR soil moisture measurements coinciding with the depths of the installed CS615 probes were also made throughout the year for wet and dry conditions, as were gravimetric measurements using collected soil samples. Literature on field based studies presented in chapter 2 (section 2.2.1) indicated that TDR systems are generally more accurate than the CS615 probes. For the TDR data at this site the system was set to directly collect volumetric moisture content values (i.e. using the standard installed calibration equation; Topp *et al.*, 1980). The gravimetric method used to determine volumetric moisture for soil samples is based on mass differences between a soil sample of known volume just after collection and after being oven dried at 105°C for >24 hours.

The first part of the calibration process involved correcting the raw CS615 moisture probe period data for temperature effects (using site measured soil temperature data) as outlined by Western and Seyfried (2005), to produce period measurements relative to a temperature of 25°C. Temperature corrected period data were then plotted against the available independent moisture measurements for the times that they coincide, to establish the linear relationships for conversion to volumetric moisture content values as shown in Fig. 4.4. After rearranging the equations for these fitted linear relationships to solve for x (soil moisture content), they were then applied to the full 30 minute series of temperature corrected period measurements (y) to produce moisture data series used in some of the experiments (Fig.4.5).

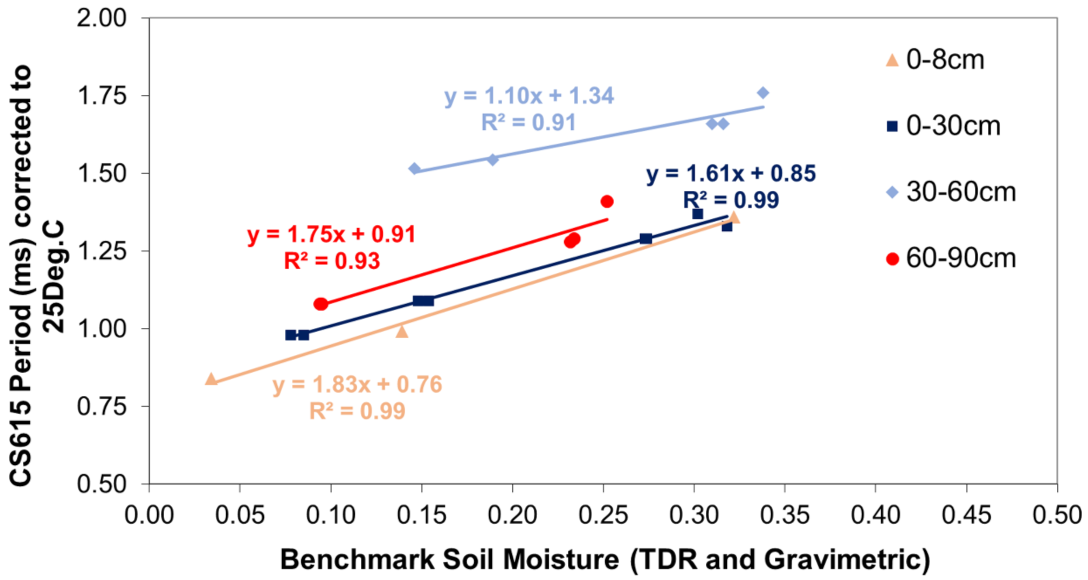

Figure 4.4: *Calibration of CS615 soil moisture probe data from the Kyeamba Creek flux station site. Shown are the relationships for calculating volumetric soil moisture content (x) from temperature corrected soil moisture probe period measurements (y).*

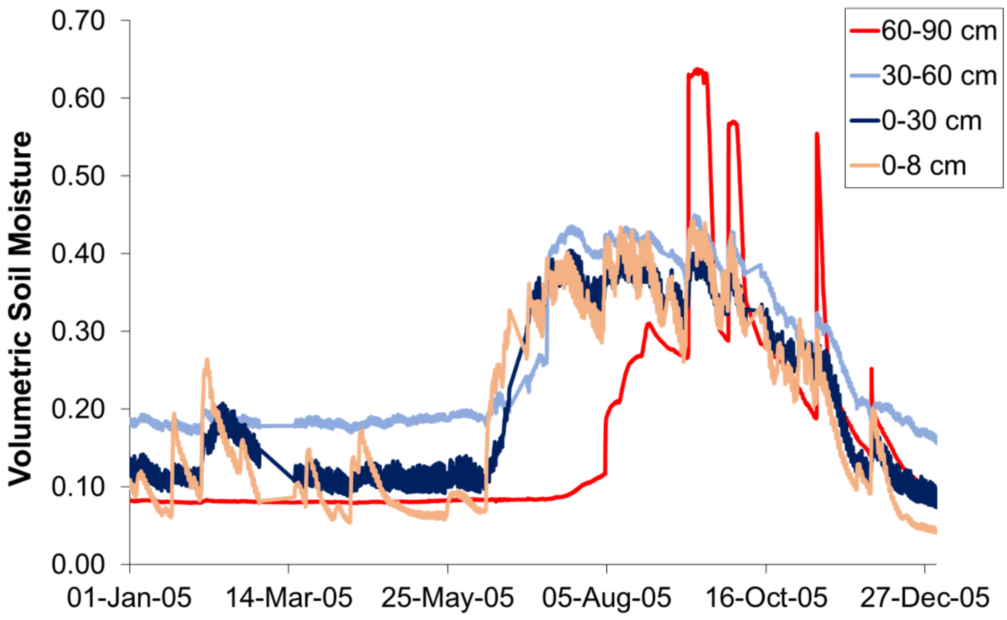

Figure 4.5: *Soil moisture content data series for 2005 from CS615 probe period measurements at Kyeamba Creek flux station site, calculated using calibration relationships shown in Fig. 4.4.*

With only twenty-one independent moisture measurements (from the TDR and gravimetric methods combined) across all four probe depths, there is no additional data independent of those used for calibration with which to verify the calculated CS615 moisture series plotted in Fig. 4.5. The Root Mean Squared Difference (RMSD) between the twenty-one moisture measurements used for calibration and the calculated values from CS615 data across all depths is 0.017 vol/vol. The data series in Fig. 4.5 show the seasonal soil moisture dynamics for different depth ranges at the flux station site, with the increased austral winter/spring moisture storage from ~June-November. A number of spikes in the series for the 60-90 cm depth range is a notable feature and they have been interpreted as indicative of elevated groundwater for brief periods, though no other data are available to directly verify this. While the moisture data for this depth is not used for any quantitative modelling or analysis, it provides additional information to consider when interpreting results for this site in some of the real data experiments.

Measured values for *G* at 8 cm depth were post processed in order to produce values representative of the fluxes at the soil surface. This involved using the temperature thermocouple data measured over the top 8 cm above the heat flux plates (i.e. each record is the temperature difference over preceding previous 30 minute period), together with the calibrated 0-8 cm soil moisture data series, to calculate heat storage in the top 8 cm of soil with which to correct measured *G* data to represent fluxes at the surface. Details of this procedure are presented in the instrument manual for the HFT-3 heat flux plates (Campbell Scientific Inc., 2004).

4.3.2 ABOVE GROUND MONITORING

The 3D eddy covariance instrumentation, which consisted of a CSAT 3D sonic anemometer (Campbell Scientific Inc., 2003) and Licor 7500 open path gas analyser (LI-COR, Inc., 2003), was elevated 3 m above the ground for an approximate fetch of 300 m with raw data measured at 10 Hz and processed online by the data logger to 30 minute block averaged *LE* and *H* values. Visits to the site were limited to approximately once per month because of proximity to Melbourne and funding, hence the 10 Hz flux data were not stored.

A CNR1 four-way net radiometer (Kipp and Zonen, 2003) measured the incoming and outgoing components of short and longwave radiation from which the total net radiation (R_N) at the surface was calculated. Other meteorological data recorded were rainfall using a tipping bucket rain gauge (0.2 mm resolution with 30 minute totals calculated), screen-level (2 m above ground) air temperature and relative humidity with a Vaisala HMP45C probe and radiation shield (Campbell Scientific Inc., 2004), atmospheric pressure with a CS105 barometric pressure sensor (Campbell Scientific Inc., 2004), and wind speed and direction using a 03001-5 R.M. Young cup and vane wind sentry (Campbell Scientific Inc., 1996) mounted on the station mast at just above 3m height. All of these meteorological data, except for rainfall were recorded at a rate of 0.5 Hz and aggregated to the 30 minute as with the rest of the site data. These data were the main source of meteorological forcing in both one-dimensional and remotely sensed data studies (chapters 6 and 7).

In filtering of the 30 minute eddy covariance data, obvious spurious data points from visual inspection were removed as a first pass, including extreme valued records of >1,000 Wm^{-2}. While records for conditions that can affect data quality were also removed. This includes periods of rainfall, as water beading on the open path CO_2/H_2O gas analyser lens will interfere with measurements. Also periods where the overall wind direction (averaged over the 30 minute block) was through the instrument mounting infrastructure – the eddy covariance system was oriented to point directly south (180°), therefore the filtered records coincided with wind from between 60° and 300° relative to north. With a maximum possible 18,000 covariance samples used to calculate the 30 minute flux averages (with 10 Hz sampling), diagnostic data for the number of covariance samples in each 30 minute flux average were also used to remove any record calculated with less than 15,000 samples (83%). Advection and a lack of turbulence at night time may compromise eddy covariance data quality, hence only records from between 6:00 am and 6:00 pm were used.

The energy balance of *LE+H* (after filtering) versus R_N-*G* indicates 82% closure (Fig. 4.6). Based on the work of Twine *et al*. (2000), 100% closure was forced by adjusting *LE* and *H* data (while maintaining a constant Bowen Ration (Eq. (2.6)) to match *LE+H* to R_N-*G*. This resulted in the filtered and energy balance corrected *LE* and *H* data used for experiments in this research.

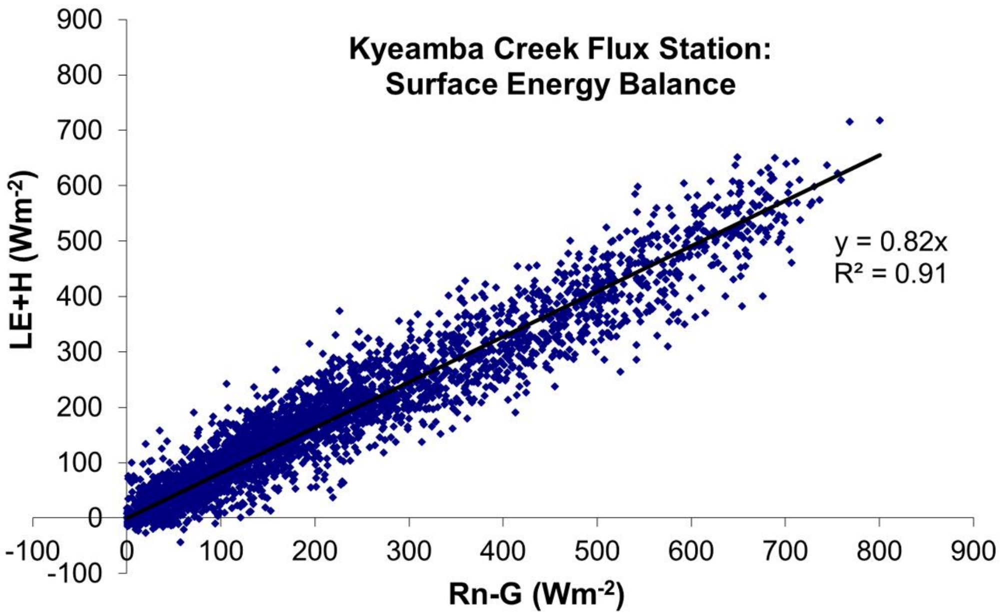

Figure 4.6: *Scatterplot showing the energy balance gap for eddy covariance measured LE and H (post filtering) against measured R_N and G data from the Kyeamba Creek flux station site. Prior to forcing closure based on Twine et al. (2000).*

4.4 ASSIMILATED REMOTELY SENSED PRODUCTS

The remotely sensed data assimilation study (Chapter 7) focussed on a portion of the Kyeamba Creek catchment corresponding to a single 25 km pixel of soil moisture data derived from AMSR-E passive microwave brightness temperature observations (Figure 4.4). The particular AMSR-E soil moisture product used in the study was derived using the Land Parameter Retrieval Model (LPRM) developed by Vrije Universiteit Amsterdam (VUA) in collaboration with NASA (Owe *et al.*, 2008). The data are on a once daily timescale corresponding to the AQUA satellite descending overpass of approximately 2:00 am local time, and they represent a spatially averaged value sampled to a 25 km pixel for the top ~1-2 cm of soil. Based on examination of this product against in-situ moisture data across a broader region of south east Australia (incorporating Kyeamba Creek) by Draper *et al*. (2009a) and Su (2013), data from the descending satellite over pass was found to be of better quality than from the ascending overpass (~2:00 pm local time), hence the choice of the 2:00 am data for use in this research.

The remotely sensed instantaneous *LE* and *H* data products used for the work in chapter 7 were derived via the SEBS algorithm (Su, 2002) and provided by Prof. Eric Wood and Dr. Raghuveer Vinukollu (Princeton University, *pers. comm.*, October 2008). They are based on a range of remotely sensed meteorological and energy balance observations including skin temperature from the AQUA platform (Dr. Raghuveer Vinukollu, Princeton University, *pers. comm.*, October 2008).

Details of SEBS instantaneous heat flux retrieval by Prof. Eric Wood's research group at Princeton University, who provided the data, are given by Vinukollu *et al*. (2011). The temporal repeat of the products that were provided is once-daily for 2:00 pm local time. Figure 4.7 illustrates the 5 km spatial resolution of the provided data covering the study domain (the single AMSR-E pixel extent) – note the relative uniformity of the agricultural/grassland environment over this domain highlighted by the Landsat image.

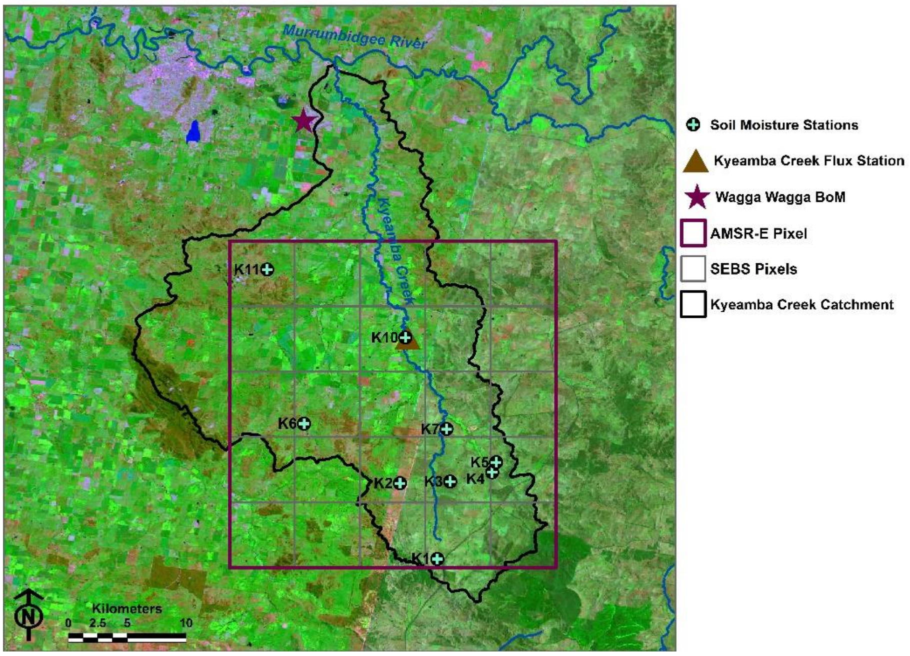

Figure 4.7: *Extent of the remotely sensed data study domain marked out by a 25 km AMSR-E soil moisture data pixel, with pixels of the finer resolution (5 km) SEBS LE and H coverage.*

4.5 MODEL PARAMETER DATA SOURCES

Tables 3-1 and 3-2 (Chapter 3) list key vegetation and soil parameters in the CBM. Parameter data used for modelling in each study are described in the experimental chapters, with all parameter data used for this thesis drawn upon from a variety of sources. This included a combination of third party data sets that were provided, default global data values from the CBM/CABLE model documentation and field estimates from the Kyeamba Creek region. In the case of the synthetic-twin study, some of the values were randomly chosen.

Vegetation parameter values provided in the CABLE user guide (Abramowitz, 2006), for the agricultural/C3 grassland classification from Potter *et al.* (1993) were chosen as representative of the Kyeamba Creek region. While field estimates of the percentage of roots in each CBM soil layer (*froot*) and average canopy height (*hc*) were made at the Kyeamba Creek flux station site and assumed representative of the entire catchment. These are: 10%, 40%, 45% and 5% for *froot* in layers 1 through to 4 respectively (refer to Fig. 3.1 for depths); and, 25 cm for *hc*.

Two separate data sets were used for Leaf Area Index (*LAI*) values: 1) An older one from Lu *et al.* (2003) on an approximate 5 km spatial scale used for the synthetic-twin experiments (values from within the Kyeamba Creek catchment were used); and, 2) A newer one on an approximate 1 km spatial scale based on the fraction of Photosynthetically Active Radiation (fPAR) data product from Donohue *et al.* (2008) that was used in the one-dimensional and remotely sensed data studies. The older data set 1) consists of monthly averaged values determined using visible and near infra-red reflectance data from the Advanced Very High Resolution Radar (AVHRR) for the period 1981-1994. Data were averaged over this entire period for each month resulting in single monthly *LAI* values. In the newer data set 2), *LAI* is based on fPAR derived from AVHRR red and near infra-red reflectance data and the values are unique monthly averages per year (as opposed to single monthly values averaged over several years). Randomly chosen examples of *LAI* from the two data sets are shown in Fig. 4.8 highlighting the different spatial scales between them.

Key soil parameter values used as representative of the Kyeamba Creek region were determined from a combination of soil samples taken at the flux station site and soil property interpretations (McKenzie *et al.*, 2000, 2003) relating to a 1:100,000 scale soil landscape map of the region (Chen & McKane, 1997) – the mapped soil units are displayed in Fig. 4.9. Available data for these soil units based on interpretations from McKenzie *et al.* (2003) consists of A and B horizon values for wilting point (θ_{Wilt}: moisture content at 15 bar), field capacity (θ_{FC}: moisture content at 0.1 bar), saturated hydraulic conductivity (K_s) and bulk density (ρ_s). These are all inputs to the CBM, and they were also used to derive values for the other following CBM soil parameters for which there was no data: moisture content at saturation (θ_{sat}), air entry potential (ψ_{aep}) (also termed soil suction at saturation) and the Campbell *b* parameter. These properties and their relationships with soil moisture mobility are described in section 2.1.2 of chapter 2.

From the available soil property data listed above, θ_{sat} was determined as

$$\theta_{sat} = [1 - (\rho_s/2650)], \qquad (4.1)$$

where the value 2,650 kg/m^3 is a standard value for density of mineral solids. Values for ψ_{aep} and *b* were then determined from θ_{Wilt}, θ_{FC} and θ_{sat} using Eq. (2.13) from Campbell (1974) which relates ψ_{aep} and *b* with the fraction of moisture content to solve for the pressure head (ψ). Thus given the value of ψ is 150 m for θ_{Wilt} and 1 m for θ_{FC} (and θ_{sat} is determined), these two known values for ψ and the corresponding two known soil moisture values (θ) of θ_{Wilt} and θ_{FC} were used to solve for both ψ_{aep} and *b* simultaneously with Eq. (2.13).

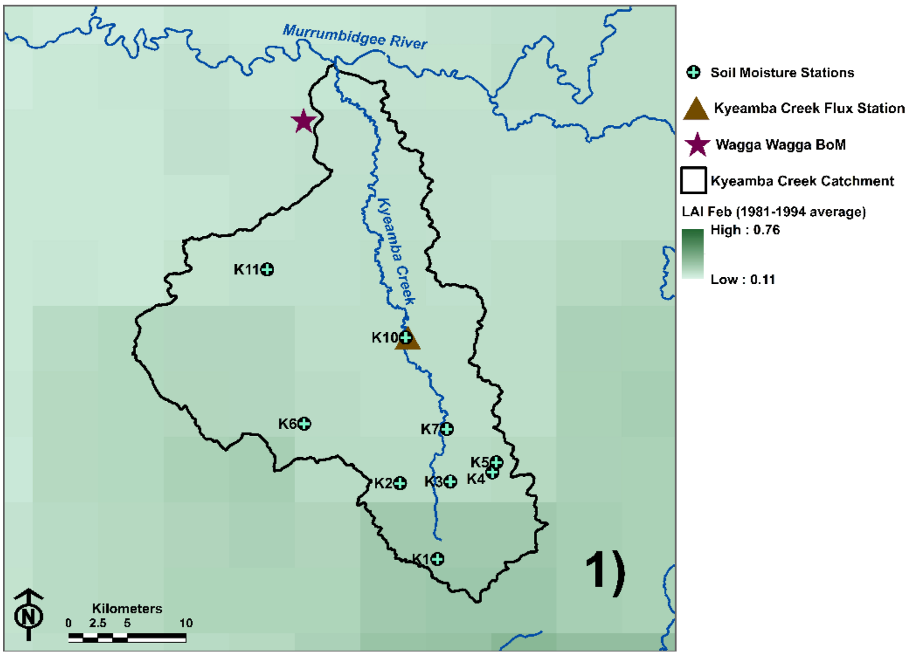

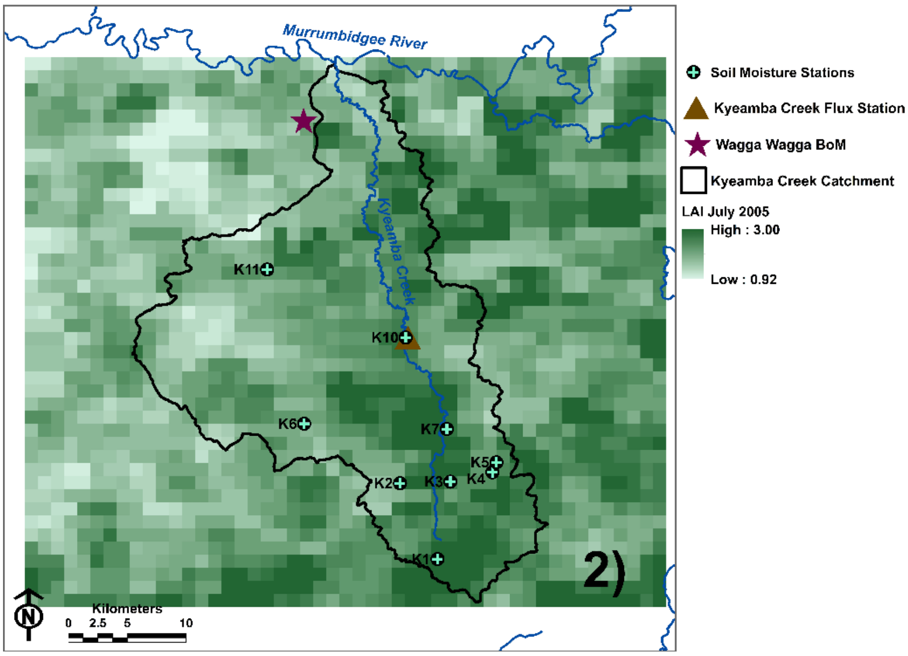

Figure 4.8: ***1)*** *Example of Older LAI data at 5 km resolution from Lu et al. (2001) used in the synthetic-twin study; and,* ***2)*** *Example of a newer 1 km LAI dataset based on fPAR data from Donohue et al. (2008), used in the one-dimensional field data and remotely sensed data assimilation studies.*

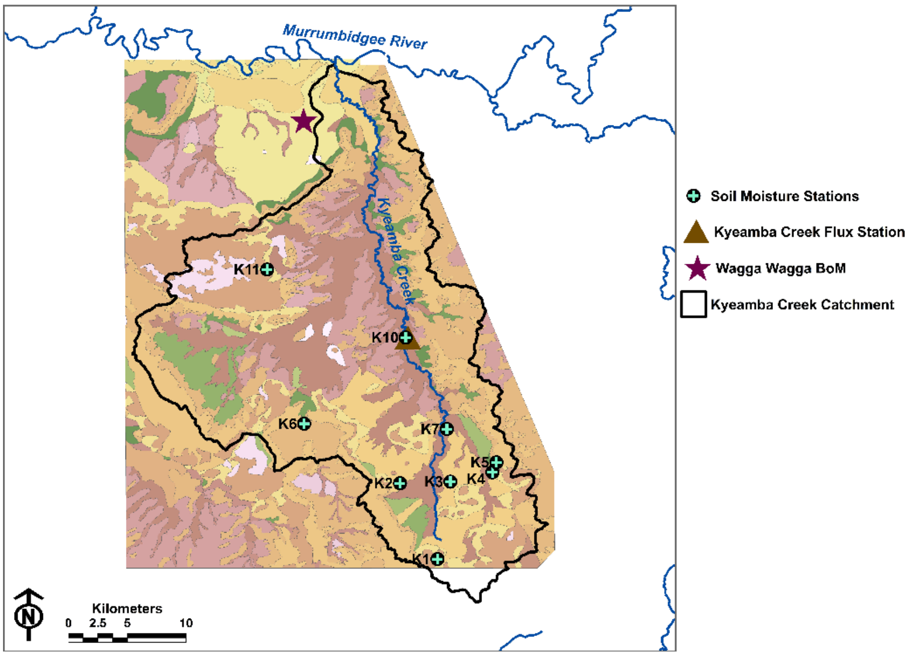

Figure 4.9: *Map of different soil units in the Kyeamba Creek region (Chen & McKane, 1997), each associated with interpreted parameter values for both A and B soil horizons (McKenzie et al., 2003).*

Comparing Figs. 4.7 and 4.9, the spatial domain for the remotely sensed data study (chapter 7) is not completely covered by the 1:100,000 scale mapped soil units (with associated model parameter data) for the Kyeamba Creek catchment. The missing coverage is mostly in the north eastern region of the remotely sensed data study domain. Therefore soil parameter data from McKenzie *et al*. (2000), which are associated with broader scale mapped soil units from the Atlas of Australian Soils (Northcote *et al*., 1960-1968) and also soil type interpretation from Northcote (1979), was used to supplement the missing coverage for this particular study.

4.6 DATA PROVENANCE SUMMARY

The Kyeamba Creek region, including the Wagga Wagga BoM station 072150, is the geographic focus for this research and hence the origin of all field data that were used. Where the *LE* and *H*, soil moisture and temperature, and meteorological data from the different monitoring sites described, in addition to remotely sensed products and parameter data sets which were sourced for the region, were the basis for the data assimilation experiments presented throughout this thesis. The Kyeamba Creek flux station site with the eddy covariance system and associated monitoring was the only site set-up and managed especially for this thesis research, which included quality control and data processing work. All of the other data used were sourced and used "as is".

Specific details on the use of the different data sets for experiments are included in the following three chapters.

5 SYNTHETIC DATA ASSIMILATION

This chapter has been published as:

Pipunic, R. C., Walker, J. P., & Western, A. W. (2008). Assimilation of remotely sensed data for improved latent and sensible heat flux prediction: A comparative synthetic study. *Remote Sensing of Environment*, 112, 1295–1305 (data assimilation special issue).

The numbering of sections, figures and tables in the original publication have been altered for this chapter, to be consistent with the thesis chapter numbering. Also the references have been incorporated into the full list of references at the end of this thesis.

5.1 ABSTRACT

Predicted latent and sensible heat fluxes from Land Surface Models (LSMs) are important lower boundary conditions for numerical weather prediction. While assimilation of remotely sensed surface soil moisture is a proven approach for improving root-zone soil moisture, and presumably latent (*LE*) and sensible (*H*) heat flux predictions from LSMs, limitations in model physics and over-parameterisation mean that physically realistic soil moisture in LSMs will not necessarily achieve optimal heat flux predictions. Moreover, the potential for improved *LE* and *H* predictions from the assimilation of *LE* and *H* observations has received little attention by the scientific community, and is tested here with synthetic twin experiments. A one-dimensional single column LSM was used in 3-month long experiments, with observations of *LE*, *H*, surface soil moisture and skin temperature (from which *LE* and *H* are typically derived) sampled from truth model run outputs generated with realistic data inputs. Typical measurement errors were prescribed and observation datasets separately assimilated into a degraded model run using an Ensemble Kalman Filter (EnKF) algorithm, over temporal scales representative of available remotely sensed data. Root Mean Squared Error (RMSE) between assimilation and truth model outputs across the experiment period were examined to evaluate *LE*, *H*, and root-zone soil moisture and temperature retrieval. Compared to surface soil moisture assimilation as will be available from SMOS (every 3 days), assimilation of *LE* and/or *H* using a best case MODIS scenario (twice daily) achieved overall better predictions for *LE* and comparable *H* predictions, while achieving poorer soil moisture predictions. Twice daily skin temperature assimilation achieved comparable heat flux predictions to *LE* and/or *H* assimilation. Fortnightly (Landsat) assimilations of *LE*, *H* and skin temperature performed worse than 3-day moisture assimilation. While the different spatial resolutions of these remote sensing data have been ignored, the potential for *LE* and *H* assimilation to improve model predicted *LE* and *H* is clearly demonstrated.

5.2 INTRODUCTION

The land surface provides a continuous feedback of latent (*LE*) and sensible (*H*) heat flux to the atmosphere, which drives our weather and climate. Hence the accuracy of heat flux outputs from land surface models (LSMs) plays an important role in the accuracy of weather and climate forecasts from coupled atmospheric prediction models (Pitman, 2003). *LE* and *H* result from the partitioning of available net radiation energy at the land surface, and this feedback is related to a combination of soil moisture content, soil temperature, various soil physical properties, vegetation cover, and physical and biological properties relating to particular vegetation types. LSMs are an attempt to relate these factors in a mathematical framework, together with meteorological variables, for predicting water evaporation from soil and/or its transpiration through vegetation

(*LE*) and conductance of heat (*H*) to the atmosphere on a continuous time scale. The CSIRO Biosphere Model (CBM) is one such model (Wang *et al*., 2001) and was used for undertaking the experiments in this study.

Models such as CBM are limited in that they represent highly variable and complex physical systems with simplified and/or empirically derived mathematical relationships. Another shortcoming of LSMs is that they are often over-parameterised – there is not enough data on model soil and vegetation parameters to accurately represent the highly variable temporal and spatial variation of these quantities (Crosson *et al*., 2002; Franks & Beven, 1999; Yates *et al*., 2003). While field measurements can assist in parameterising models at the point scale with considerable effort (Mertens *et al*., 2005), accurate parameterisation becomes increasingly difficult when modelling across spatial regions. Model predictions are therefore inherently uncertain, with prediction uncertainty typically increasing through time. Data assimilation is one technique commonly used to correct LSM predictions (e.g. Crosson *et al*., 2002). This is where observed quantities of a particular variable with known uncertainty are used to adjust predicted model state variables such as soil moisture and temperature, and hence other related quantities such as *LE* and *H* at the observation time (Walker & Houser, 2001). The data assimilation process compares the uncertainty in the observation with that in the model prediction to determine the correction required; the data assimilation technique applied in this research is the Ensemble Kalman Filter (EnKF) algorithm (Evensen, 1994).

Many examples exist in literature where data assimilation has been used to improve LSM predictions with efforts mainly focussing on improving soil moisture prediction. An early example by Entekhabi *et al*. (1994) demonstrates the ability to retrieve the true soil moisture profile of a model from an initial poor guess by assimilating remotely sensed passive microwave and thermal infrared data. The study uses a simplified soil scheme and is a synthetic experiment primarily aimed at testing the assimilation algorithm. Walker and Houser (2001) present a synthetic study on surface soil moisture assimilation motivated by the need to improve soil moisture initialisation for climatological and hydrological predictions. Synthetically generated surface soil moisture observations were assimilated into a catchment based LSM with degraded initial moisture values. Observations were assimilated every 3 days to replicate the temporal scale of surface soil moisture data that would be available from satellite sensors. It is shown that the assimilation could retrieve the true soil moisture content for the entire soil profile. To augment past synthetic studies, Crow and Wood (2003) mention the need to further test assimilation applications using real data to better understand the challenges of data assimilation in an operational context. In their study, airborne measurements of 1.4GHz surface brightness temperature (equivalent to the data that will be available from the SMOS satellite sensor) were assimilated into a LSM to correct soil moisture predictions. Surface state and flux predictions from assimilation outputs were found to be more accurate than predictions from open loop modelling.

Some early studies (Bouttier *et al*., 1993; Mahfouf, 1991) have shown that assimilating screen level (2 m above ground) air temperature and relative humidity observations can correct soil moisture for improved numerical weather prediction. Seuffert *et al*. (2003) assimilated a combination of synthetic 1.4GHz brightness temperature observations together with screen level air temperature and relative humidity measurements to test the potential for improving soil moisture. Assimilation of all of these variables was shown to result in the greatest improvement in soil moisture and heat flux predictions compared to assimilating the screen level variables or brightness temperature data alone. McNider *et al*. (1994) showed using two experiments that assimilation of surface skin temperature had a positive impact on model predictions. A one-dimensional experiment was conducted with field measured thermal infrared data from a downward-looking radiometer, and a spatial experiment was performed using GOES satellite thermal infrared observations. A more recent example by Margulis and Entekhabi (2003) examined the assimilation of skin temperature together with screen level air temperature and relative humidity into a coupled land surface-atmospheric boundary layer model with both a synthetic experiment and a one-dimensional application using field measured radiometer data. Again, the results showed that assimilating multiple observation types allowed for more robust estimation of model states and fluxes.

The aim of most of these assimilation experiments was to correct root-zone soil moisture prediction and hence indirectly correct the heat flux predictions, but achieving physically correct soil moisture estimates through data assimilation does not guarantee improved heat flux prediction feedbacks to the atmosphere. Consequently, this study tests the hypothesis that assimilation of remotely sensed *LE* and *H* observations themselves could potentially produce better heat flux predictions than assimilation of soil moisture observations, or the skin temperature observations from which they are derived. Only one example can be found in literature dealing with *LE* assimilation (Schuurmans *et al*. 2003), which shows promising results. However, the results are largely unverified and more research is required to determine if and how well assimilation of *LE* and *H* can improve heat flux, soil moisture and soil temperature predictions from LSMs.

Different techniques for estimating *LE* and *H* from remotely sensed data have been developed and widely reported in literature over recent years (i.e. Bastiaanssen *et al*. 1998; Jiang & Islam, 2001; Kustas & Norman, 1996). The energy balance algorithms used to estimate these quantities, such as SEBAL (Bastiaanssen *et al*., 1998), are based on satellite observations of thermal infrared measurements of skin temperature, available from GOES, MODIS and Landsat sensors. Repeat coverage of these satellites over the same geographical location typically occur twice daily at 1km resolution for MODIS (morning and afternoon), approximately every fortnight at 30m resolution for Landsat and hourly at 4km resolution for the geostationary GOES satellite. These temporal scales for thermal infrared data are best case scenarios, which are unlikely over long periods due to cloud cover. In contrast, the soon to be launched SMOS satellite will provide data at 50km resolution on a three daily temporal scale irrespective of cloud cover (Kerr *et al*., 2001). While such variations in spatial resolution are potentially important, this paper presents a synthetic one-dimensional data assimilation study as a proof of concept. Moreover, this study demonstrates the relative impact of *LE*, *H*, skin temperature and surface soil moisture assimilation on LSM prediction of *LE*, *H*, and root-zone soil moisture and temperature, using the typical remote sensing repeat times for the respective data types, ignoring potential cloud impacts.

5.3 DATA ASSIMILATION

The original Kalman Filter (KF) is an optimal recursive data processing algorithm first presented by Kalman (1960), and forms the basis for more modern variations such as the EnKF (Evensen, 1994) which was applied in this study. A good introduction to the Kalman filter is presented by Maybeck (1979), and Walker and Houser (2005) provide a review of different data assimilation techniques relating to hydrology, land surface modelling and remote sensing. In terms of land surface modelling, data assimilation aims to use available observations of model variables with known uncertainty to correct model predictions which are not optimal due to a combination of uncertain initial conditions, errors in meteorological forcing data, errors in model physics, and poor knowledge of model parameters.

When applying the KF to nonlinear systems, the Extended Kalman Filter (EKF) results. This requires calculation of a tangent linear model which can result in poor state and error forecasts due to model non-linearities. The EnKF overcomes the linearization issue through a Monte Carlo approach, where an ensemble of parallel model runs is generated for the same time period. The model error covariance is then determined from the ensemble spread at the assimilation time step and the ensemble mean taken as the best estimate of the model state. Reichle *et al*. (2002) present a comparison between the EKF and EnKF in a synthetic soil moisture assimilation study and found the EnKF to be more robust and flexible in covariance modelling, and its performance slightly superior.

The EnKF is one form of a number of direct observer assimilation methods which differs from the EKF only in the way in which model covariances are estimated. It can be summarised as follows:

$$\mathbf{X}_k^a = \mathbf{X}_k^f + \mathbf{K}(\mathbf{Z}_k - \mathbf{Z}_k^f), \qquad (5.1)$$

where subscript k refers to the assimilation time step, superscript f refers to the forecast value and superscript a refers to an analysis (updated) value. The model state vector is denoted by **X** and the observation is denoted by **Z**. The difference between an observed and model predicted value $(\mathbf{Z}_k - \mathbf{Z}_k^f)$ is the innovation and is weighted by the Kalman gain (**K**). Together they determine the correction added to the forecast state vector. In addition to projecting from **Z** to **X** space, **K** is a scaling factor that represents the relative uncertainty of model predicted and actual observations based on the covariance matrices. Therefore

$$\mathbf{K} = \mathbf{P}_k^f \mathbf{H}^\mathbf{T} (\mathbf{H}\mathbf{P}_k^f \mathbf{H}^\mathbf{T} + \mathbf{R}_k)^{-1}, \qquad (5.2)$$

where **P** represents the error covariance of the forecast model states and **R** is the error covariance of the observation. The matrix **H** is a nonlinear operator that relates the state vector **X** to the observation **Z**, with superscript T denoting the matrix transpose. Therefore, if **P** is large compared to **R** (i.e. observations more trustworthy than model prediction), then **K** will approximate to 1 when **X** and **Z** are the same scalar quantity (i.e. **H** = 1), and the innovation will be relied upon heavily to adjust the forecast states due to the small relative observation error. Alternatively, where **R** is large compared to **P**, **K** will approach 0 and the observation will not be trusted sufficiently leaving the final analysis vector $\mathbf{X}_k^a$ relatively unchanged, since the model's forecast is understood to be more reliable in this case.

Implementation of the EnKF in this study can be summarised as follows (Evensen, 1994; Houtekamer & Mitchell, 1998; Walker & Houser, 2005). The background state covariance matrix for determining the model error covariance at assimilation times is defined as

$$\mathbf{P}_k^f = \frac{(\mathbf{x}_k^f - \overline{\mathbf{x}}_k^f)(\mathbf{x}_k^f - \overline{\mathbf{x}}_k^f)^\mathbf{T}}{m-1}, \qquad (5.3)$$

where **x** are individual ensemble members of the state forecast matrix **X** and the over-bar represents the ensemble mean across all members. The number of ensemble members is denoted by m. However, explicit calculations of $\mathbf{P}_k^f$ are not actually required and Eq. (5.1) can be written as

$$\mathbf{X}_k^a = \mathbf{X}_k^f + \mathbf{B}_k^\mathbf{T} \mathbf{b}_k, \qquad (5.4)$$

where

$$\mathbf{B}_k^\mathbf{T} = \mathbf{P}_k^f \mathbf{H}_k^\mathbf{T}, \qquad (5.5)$$

and

$$\mathbf{b}_k = (\mathbf{H}_k \mathbf{P}_k^f \mathbf{H}_k^{\mathbf{T}} + \mathbf{R}_k)^{-1} (\mathbf{y}_k - \mathbf{Z}_k^f) . \qquad (5.6)$$

A perturbed observation **y** replaces the actual observation **Z** in Eq. (5.1) and is defined as

$$\mathbf{y}_k = \mathbf{Z}_k + \zeta , \qquad (5.7)$$

with ζ being a random observation error term that has zero mean and covariance **R**. For each observation variable, the typical uncertainty for remotely sensed measurements is used to determine its error range, representing covariance **R**. Prior to assimilation, a random number generator, which generates numbers with a normal distribution and zero mean is used to generate a single number within this error range which is then added to the observation resulting in a perturbed observation value **y**. The random number generator is then used again to generate an ensemble of observation values about **y** resulting in an observation ensemble with covariance **R** (more details on observations are given later). Also

$$\mathbf{H}_k \mathbf{P}_k^f \mathbf{H}_k^{\mathbf{T}} = \frac{\mathbf{q}_k \mathbf{q}_k^{\mathbf{T}}}{m-1} , \qquad (5.8)$$

and

$$\mathbf{q}_k = \mathbf{H}_k (\mathbf{x}_k^f - \overline{\mathbf{x}}_k^f) = (\mathbf{z}_k^f - \overline{\mathbf{z}}_k^f) , \qquad (5.9)$$

where **z** are individual ensemble members of the perturbed observation and the over-bar denotes the ensemble mean. Hence, it is unnecessary to solve for **H** and therefore **B** can be calculated as

$$\mathbf{B}_k^{\mathbf{T}} = \frac{(\mathbf{x}_k^f - \overline{\mathbf{x}}_k^f)}{m-1} \mathbf{q}_k^{\mathbf{T}} . \qquad (5.10)$$

Therefore calculation of $\mathbf{b}_k$ using Eqs. (5.6), (5.7) and (5.8), and $\mathbf{B}_k^{\mathbf{T}}$ using Eq. (5.10), then substituting into Eq. (5.4) will update each individual ensemble member at assimilation time steps. Ensemble generation used the approach developed by Turner *et al*. (2008), which is discussed further on.

5.4 EXPERIMENT DATA AND METHODOLOGY

A synthetic experiment was set up as a proof of concept for the assimilation of remotely sensed *LE* and *H*, and inter-comparison with the assimilation of skin temperature and surface soil moisture. Synthetically derived observations of *LE*, *H* (including a joint combination of *LE* and *H*), surface

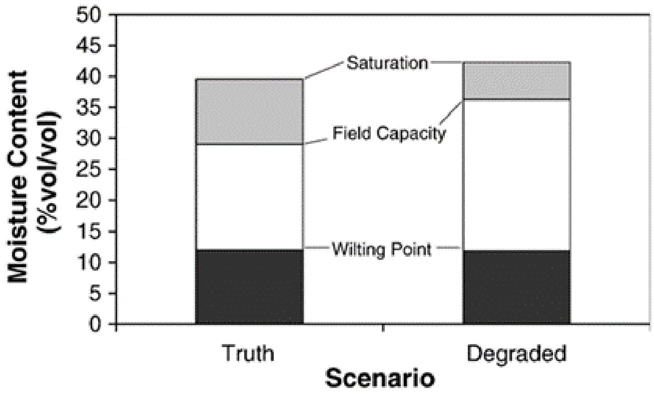

Figure 5.1: *A comparison between key soil parameter values used in truth and degraded scenarios that were derived from an available catchment data set. Truth values are from a point location and degraded values are catchment area weighted averages.*

soil moisture and skin temperature were separately assimilated into the CBM forced with data from the first three months of 2003 (January 1 to April 1), and the results compared to see which approach produced the more accurate prediction of *LE*, *H*, root-zone soil moisture and temperature. Two model scenarios were used in the experiments – a truth scenario where knowledge of meteorological forcing, state initial conditions and parameters is assumed to be perfect, and a degraded scenario which used degraded meteorological forcing, initial conditions and parameters. Fig. 5.1 shows key soil parameter values used in each scenario. In addition, saturated hydraulic conductivity values of 4.3×10^{-6} ms^{-1} for the truth and 1.1×10^{-5} ms^{-1} for the degraded scenario were applied, as were monthly averaged Leaf Area Index *LAI* values for January, February and March (0.30, 0.31 and 0.35 for the truth scenario and 0.33, 0.33 and 0.39 for the degraded scenario). All input data required to run the models was taken from the Kyeamba Creek catchment in South Eastern Australia to provide realistic input values. However, the modelling is not intended to represent a particular geographical location.

5.4.1 THE CSIRO BIOSPHERE MODEL (CBM)

The CBM is a single column model dealing with the exchange of energy, water and CO_2 between a vertical profile represented computationally using six soil layers with uniform soil properties, the land surface, vegetation and the atmosphere (Wang *et al.*, 2001). The thicknesses of the soil layers from top to bottom are 2.2, 5.8, 15.4, 40.9, 108.5 and 287.2 cm respectively with a total soil column thickness of 4.60 m. Each layer has a value for soil temperature and moisture for calculating evaporation, respiration and soil heat flux. Moisture movement through the layers is governed by Richards' equation, the snow scheme is that of Kowalczyk *et al.* (1994), and a bulk aerodynamic formulation is used to model soil evaporation (Mahfouf & Noilhan, 1991). Amongst the input (forcing) data required to run the CBM are air temperature, downward short and long wave radiation, specific humidity, wind speed, precipitation and barometric pressure.

Four surface types are represented including bare soil, snow (snow does not occur in this study) and a two-leaf canopy model (Wang & Leuning, 1998) which calculates fluxes of *LE*, *H* and CO_2 for a 'sunlit' and 'shaded' leaf canopy. A formulation for canopy turbulence is also included based on theory developed by Raupach (1989). Some important vegetation parameters in the model include *LAI*, canopy height, canopy water storage capacity per unit *LAI*, average leaf size, the fraction of roots by mass in each soil layer and a number of other parameters related to plant photosynthesis. Vegetation properties for uniform grassland were applied in this study which included typical monthly averaged *LAI* values for grassland in south eastern Australia and a canopy height of 20 cm. Total values of *LE* and *H* calculated by the model represent the respective sums of *LE* and *H* for the soil surface and for the vegetation canopy. Using *LAI* values and a radiation extinction coefficient, the fraction of radiation transmitted through the vegetation canopy is calculated from which *LE* and *H* can be calculated for both the soil surface and the canopy.

5.4.1.1 MODEL INPUT DATA

Input forcing data used by this study includes a continuous series of half hourly meteorological data compiled for the Kyeamba Creek catchment from 2000 to present (Siriwardena *et al*., 2003). It consists of point scale data recorded at the nearest Bureau of Meteorology (BOM) station (Wagga Wagga, ~30 km distant) and precipitation data measured at one of the University of Melbourne monitoring sites within the Kyeamba Creek catchment. Given the half hourly temporal resolution of meteorological forcing data, the model was run at half hourly time steps for all of the experiments. Soil parameter data have been estimated by Dr. Neil McKenzie (CSIRO Land and Water, *pers. comm*., 2005) based on different soil units across the catchment. These soil units have associated values for field capacity, wilting point, soil bulk density and hydraulic conductivity at saturation, all required as inputs to the CBM. Leaf area index data was sourced from a monthly average, 0.05˚ by 0.05˚ spatial resolution publicly available data set derived from remotely sensed Advanced Very High Resolution Radiometer visible infrared and near infrared images (Lu *et al*., 2001).

5.4.1.2 TRUTH SCENARIO

The half hourly Kyeamba Creek meteorological dataset (Siriwardena *et al*., 2003) was used directly in its available form for the truth scenario. It includes incoming short wave and long wave radiation, air temperature, wind speed, and specific humidity for the catchment. As no data was available for atmospheric pressure or CO_2 concentration, generic values of 980 mbar and 370 ppm were assigned respectively for the entire time series of the experiment period. Precipitation data used for the truth forcing was sourced from a University of Melbourne monitoring site in the Kyeamba Creek catchment. This location was also used to obtain point estimates of soil and vegetation parameter input into the truth model. Soil moisture content and temperature profiles were not available at the same site for the start of the modelling period (January 1, 2003, 00:30 hours). Therefore initial moisture and temperature values were estimated for the six CBM layers based on University of Melbourne data measured at nearby sites for the same time in other years. While arbitrary initial conditions could have been assumed for this synthetic study, these observed quantities were used to provide a set of realistic and internally consistent values.

5.4.1.3 DEGRADED SCENARIO

This scenario represents the model prediction results anticipated from the use of erroneous and/or averaged forcing and parameters which is a likely situation when modelling with real data. Hence, spatial input data was averaged within the Kyeamba Creek catchment boundary, or in the absence of spatially distributed data either random perturbations were added (within known uncertainty limits) to the data used in the truth scenario or data was taken from an alternative location within the catchment.

Meteorological forcing inputs were generated by adding random perturbations within determined error ranges to each meteorological data variable used in the truth scenario. The error range for each variable was determined through personal communications with Dr. John Gorman (March 7th, 2006) from the BoM National Climate Centre who is knowledgeable on the typical quality of BoM data. Precipitation was taken from an alternate University of Melbourne monitoring location in the Kyeamba Creek catchment to that used for the truth scenario. Table 5-1 summarises the error ranges within which the BoM forcing data variables and the University of Melbourne precipitation data were perturbed including the average daily standard error between truth and degraded scenario variables over the 91 day experiment period.

Area weighted averages of available soil and vegetation parameter data within the Kyeamba Creek catchment boundary were calculated for the degraded scenario. Poor initialisation of model states through either lack of data or high uncertainty in the data is a common source of model error which can increase model uncertainty over time, even with accurate forcing and parameters. Initial moisture and temperature values were set to extreme values (higher soil moisture content and lower temperature) compared to the typical summer time values at the start of the experiment period in the truth scenario. This would test the assimilation in a worst case scenario where no information is available to initialise model states. Fig. 5.2 shows initial soil moisture and temperature value differences between the truth and degraded scenarios, as well as the ensemble ranges.

Table 5-1: *Model forcing variables with associated uncertainty ranges, daily standard errors between truth and degraded values, data type category and values for calculating measurement and offset error standard deviations used in ensemble generation (from Turner et al., 2008).*

Forcing variable	Quoted uncertainty	Daily Average Std Error	Category	*h* domain	ξ	χ
SW Radiation (W m^{-2})	$\pm$2%	2.2	Semi-restricted	(0, ∞)	0.01	0.04
LW Radiation (W m^{-2})	$\pm$3%	3.1	Semi-restricted	(0, ∞)	0.003	0.05
Precipitation (mm)	$\pm$0.2	0.2	Semi-restricted	(0, ∞)	0.2	0.2
Air Temp. (˚C)	$\pm$0.5	0.4	Unrestricted	(-∞, ∞)	0.9	0.4
Wind Speed (m s^{-1})	$\pm$1.03	0.4	Semi-restricted	(0, ∞)	1.0	0.3
Sp. Humidity (g kg^{-1})	$\pm$5%	1.2×10^4	Semi-restricted	(0, ∞)	0.0025	0.06

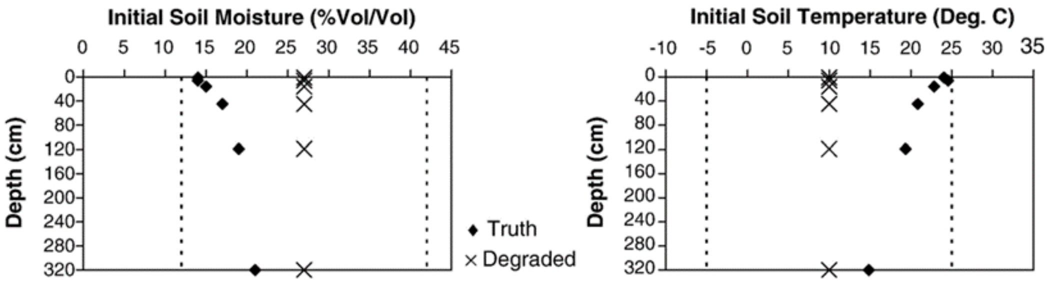

Figure 5.2: *Truth and degraded scenario initial conditions for soil moisture and temperature. Dashed lines show the minimum and maximum of the ensemble ranges for initial soil moisture and temperature.*

Fig. 5.3 highlights the effect of degraded inputs on the truth model. This shows corresponding *LE* and *H* outputs from partial open loop simulations resulting from individually using degraded scenario meteorological forcing, initial condition and parameter data into the truth model, with the truth and full open loop (degraded) simulation outputs included for comparison. The degraded forcing and parameters each cause slight but noticeable differences in model output compared to the truth, with degraded parameters having a greater effect on *LE* than on *H*. In contrast, the degraded initial conditions cause the greatest deviation from the truth and account for most of the error represented by the full open loop simulation, as they had the greatest uncertainty imposed.

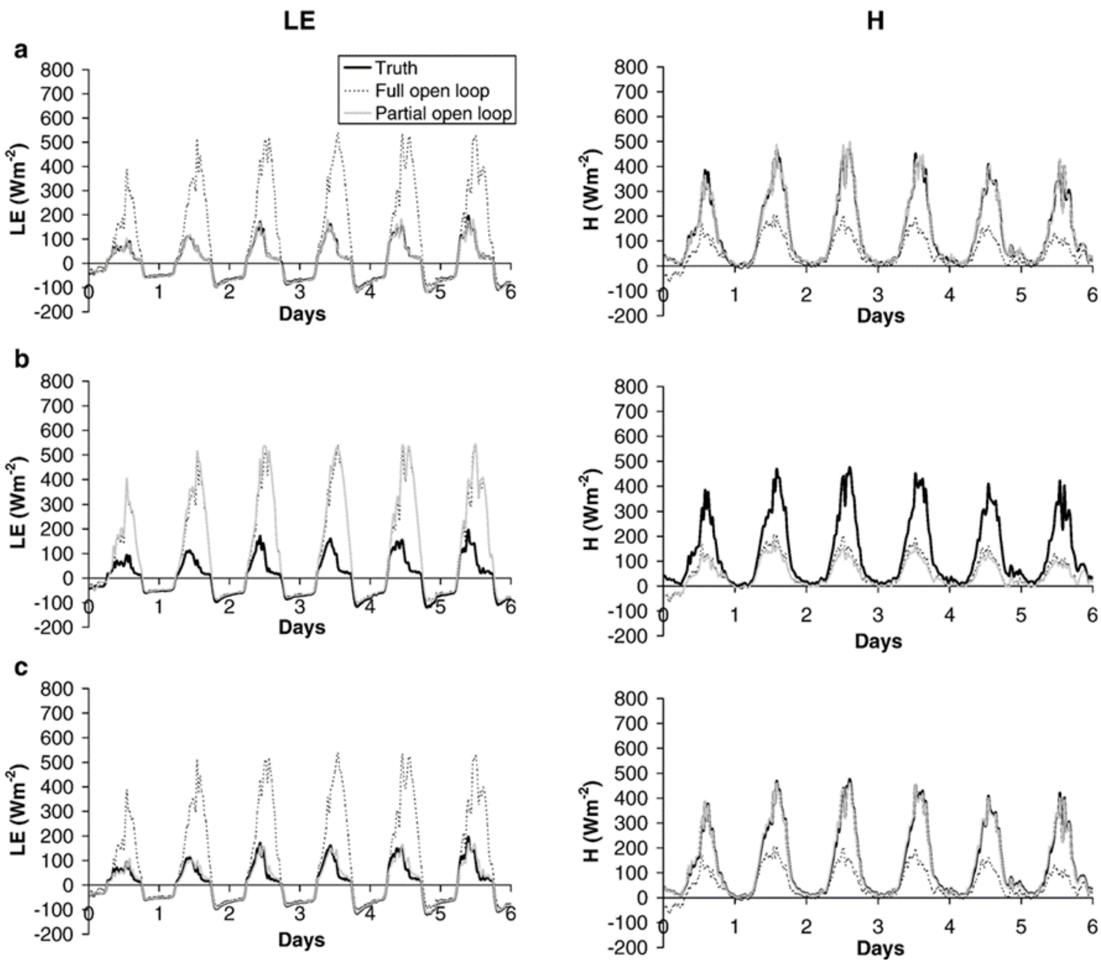

Figure 5.3: *Outputs of LE and H showing the effect on the truth predictions from 3 separate partial open loop simulations – a) Truth simulation with degraded meteorological forcing, b) Truth simulation with degraded initial conditions, and c) Truth simulation with degraded parameters.*

5.4.2 SYNTHETIC OBSERVATION DATA

Truth scenario outputs were sampled at selected time intervals to create synthetic observation data sets of *LE*, *H*, joint *LE* and *H*, surface soil moisture (from the upper-most 2.2cm thick soil layer in the CBM) and skin temperature. The time intervals used to sample these variables correspond with the temporal scales of remote sensing platforms that provide information on these quantities (see Table 5-2). Hence, assimilation of each observation set into the degraded model scenario was intended to emulate the assimilation of available observations.

Two separate observation data sets were created for each of *LE*, *H*, joint *LE* and *H*, and skin temperature from the truth scenario outputs; twice daily to emulate MODIS observations and fortnightly to emulate observations from Landsat. The top soil layer moisture content was sampled once every three days to generate a surface soil moisture observation data set emulating SMOS

Table 5-2: *Key characteristics of remotely sensed data types tested in this synthetic study*

Observed quantity	Quoted accuracy	Corresponding satellite/sensor	Temporal resolution	Spatial resolution
LE (Wm^{-2})	± 50	MODIS, Landsat	Twice daily, fortnightly	$1km^2$, $30m^2$
H (Wm^{-2})	± 50	MODIS, Landsat	Twice daily, fortnightly	$1km^2$, $30m^2$
Surface soil moisture (%vol/vol)	± 4	SMOS	Every 3 days	$50km^2$
Skin temperature (K)	± 2	MODIS, Landsat	Twice daily, fortnightly	$1km^2$, $30m^2$

observations. Uncertainty for remotely sensed estimates of these four variables varies throughout the literature with typical estimates being those given in Table 5-2 for skin temperature (Kaleita & Kumar, 2000; Sun *et al*., 2004), LE and H (French *et al*., 2005), and surface soil moisture (Kerr *et al*., 2001). These uncertainty ranges were used to prescribe error perturbations to observations and generate observation ensembles during the assimilation experiments. Prior to each assimilation step, a random error value was added to observations within the respective uncertainty range for each observation to generate an observation ensemble as required by the EnKF.

5.4.3 MODEL ENSEMBLE GENERATION AND ERRORS

The EnKF uses an ensemble of model trajectories to represent likely uncertainty in a model prediction. The main sources of error in a model prediction include i) erroneous initial conditions, ii) erroneous meteorological forcing data, and iii) limitations in model physics. The uncertainty in model physics and inclusion of biases has not been treated in this study. Normally distributed random numbers with zero mean and unit variance were generated and used to calculate error perturbations for initial conditions and meteorological forcing data within desired ranges when creating ensembles.

Soil moisture and temperature state initial condition values across the six CBM layers for the degraded scenario were perturbed within a selected range to generate ensembles that reflected the uncertainty in initial conditions. The uncertainty range was chosen such that the true values (i.e. truth scenario initial conditions) were captured within the ensemble (Fig. 5.2). As a result, degraded scenario initial soil moisture (27% vol/vol) was perturbed with random error within a possible range of $\pm$15% vol/vol, which spans most of the range between wilting point (11.9%

vol/vol) and porosity (42.3% vol/vol). The initial soil temperature value (10˚C) was perturbed with random values within $\pm$ 15˚C for ensemble generation. Generating initial condition ensembles with a large spread about the chosen value is especially important when assimilating with real data if a priori knowledge of initial conditions is poor, as it increases the likelihood of including the true value. The techniques described by Turner *et al*. (2008) were employed here to assign random errors to degraded scenario meteorological forcing data and generate each forcing data ensemble, using the parameters specified in Table 5-1.

5.5 RESULTS AND DISCUSSION

Statistically, a greater number of ensemble members results in an ensemble mean and covariance which is closer to reality. However, this comes with increased computation burden. Consequently, it is desirable to use the minimum number of ensemble members while still obtaining a satisfactory estimate of the ensemble mean and covariance. Therefore the first assimilation experiment undertaken was to determine the minimum number of ensemble members required to achieve optimal results from application of the EnKF to the CBM, so as to optimise the computing power available for the subsequent assimilation experiments. An observation data set consisting of once daily *LE* values sampled from the truth scenario output was used for this purpose, with *LE* observation errors assigned as in Table 5-2.

Assimilation over the experiment period with this set of observations was performed separately using five different ensemble sizes – 10, 20, 30, 50 and 100 members. Root mean square error (RMSE) values were calculated between *LE* outputs from the truth simulation and from assimilation runs performed with each ensemble size to determine an optimal number of ensemble members. Fig. 5.4 is a plot of the number of ensemble members against RMSE values between *LE* outputs. The value corresponding to 0 ensembles is the RMSE value between the truth and full open loop outputs for reference. As the declination in RMSE was minimal for more than 20 ensembles, an ensemble size of 20 members was chosen as adequate for carrying out the remaining assimilation experiments.

Fig. 5.5 shows a series of plots comparing outputs for the first 6 days of the joint assimilation of *LE* and *H* twice per day, with that of surface soil moisture once every 3 days.. The plots show the initial impacts of the assimilation on four specific CBM outputs – *LE*, *H*, root-zone soil moisture and root-zone soil temperature. Root-zone soil moisture and temperature are taken as the average values across the top four soil layers in the model, weighted by each layer's thickness (2.2, 5.8, 15.4 and 40.9 cm), covering a total depth of 64.3 cm.

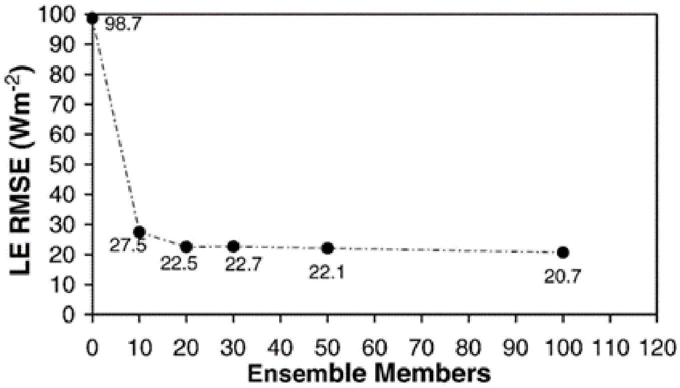

Figure 5.4: *Ensemble size comparison results for the 91 day experiment period, showing RMSE between truth and assimilated LE outputs for different number of ensemble members.*

Based on Fig. 5.5, heat flux outputs for the first 6 days of the experiment period showed that the twice daily *LE* and *H* (proxy for MODIS derived data) assimilation retrieved truth *LE* and *H* outputs more quickly and accurately than soil moisture assimilation every 3 days (SMOS observation proxy). The assimilation frequency is the most likely reason for this. However, this is an idealised case that assumes cloud-free conditions. While it is unrealistic to expect twice-daily coverage continually, results from the fortnightly assimilation of *LE* and *H* (proxy for Landsat derived data) show the corresponding loss of skill that could be expected when extended cloud cover periods exist. In contrast to the *LE* and *H* results, it is evident in this initial 6 days that soil moisture assimilation is better than *LE* and *H* assimilation for retrieving the true soil moisture, as expected. A reason for this is that *LE* and *H* assimilation has a direct impact on model *LE* and *H*, which is used to adjust both soil moisture and temperature states accordingly, whereas assimilating surface soil moisture has a direct impact on the model soil moisture alone. Consequently, the soil temperature is not impacted directly and thus *LE* and *H* predictions are initially degraded by soil moisture assimilation.

A full comparison of all the assimilation results over the entire 91 day experiment period is given in Fig. 5.6, which summarises the RMSE between the truth and all of the assimilation outputs for *LE*, *H*, root-zone soil moisture and temperature. Of the heat flux and skin temperature assimilation experiments, assimilating twice a day (MODIS) achieves better retrieval of truth predictions than fortnightly assimilation (Landsat). This result is due to temporal resolutions; results may be different if spatial resolution effects are taken into account. The spatial resolution differs greatly between MODIS and Landsat, which have 1 km and 30 m pixels respectively. If there is significant heterogeneity at scales less than 1 km in the landscape, this would have potentially significant impacts on the assimilation accuracy.

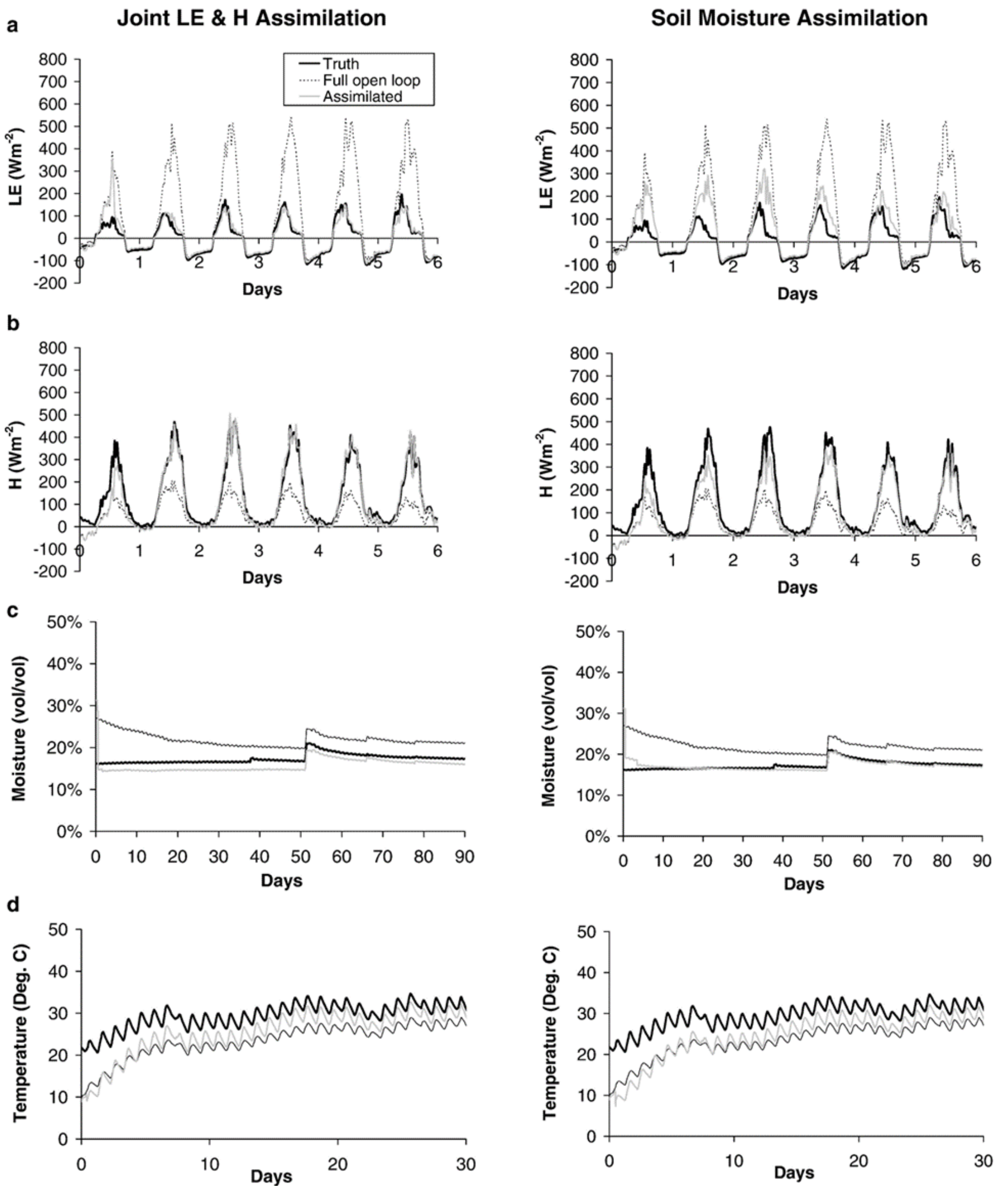

Figure 5.5: *Outputs from joint LE and H and surface soil moisture assimilation, for estimating a) LE, b) H, c) root-zone soil moisture, and d) root-zone soil temperature.*

Of the twice daily assimilations, the RMSE values indicate that *LE* assimilation achieves slightly better *LE* predictions than *H* assimilation and vice-versa. The root-zone soil moisture predictions for *LE* assimilation are slightly worse than for *H* assimilation. Also evident is the considerably lower root-zone soil temperature RMSE from *H* assimilation, as *H* is more closely related to soil temperature in the model formulation than *LE*. On the fortnightly time scale, *LE* assimilation results in better predictions for both *LE* and *H*, while also producing better root-zone soil moisture predictions but poorer soil temperature than *H* assimilation. Comparing the individual *LE* and *H*

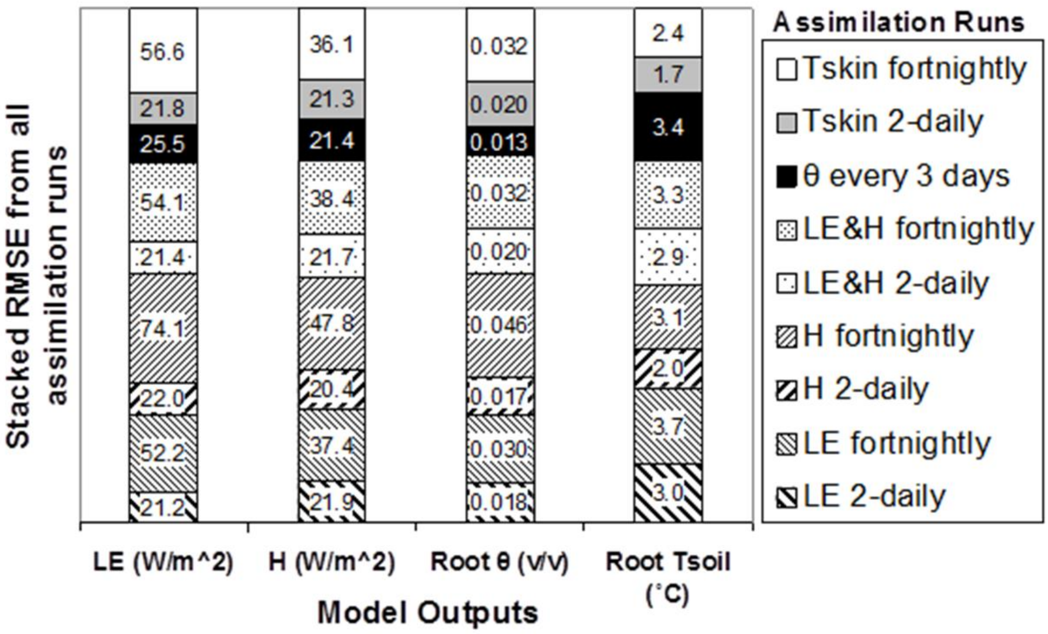

Figure 5.6: *RMSE values for the difference between assimilation and truth outputs of LE, H, root-zone soil moisture (θ) and root-zone soil temperature (T_{soil}) covering the 91 day experiment period from assimilating LE, H, surface soil moisture (θ) and skin temperature (T_{skin}) combinations. *Note that the RMSE between Open Loop and truth outputs (not included in the published paper) are: 98.7 Wm^{-2} for LE; 64.1 Wm^{-2} for H; 0.049 vol/vol for root-zone soil moisture; and, 4.2° C for root-zone soil temperature.*

assimilation results for the two time scales, *LE* assimilation produces the best *LE* results in both cases, and whichever assimilation produces the best soil moisture prediction also achieves the better *H* prediction; *H* assimilation achieves the best soil temperature in both cases as expected. Joint *LE* and *H* assimilation twice daily achieves similar improvements to both *LE* and *H* predictions compared with assimilation of each variable individually on a twice daily time scale. On a fortnightly scale, joint *LE* and *H* assimilation produces similar improvements in *LE* and *H* as fortnightly *LE* assimilation, and greater improvements than fortnightly *H* assimilation.

Assimilating surface soil moisture every 3 days resulted in poorer *LE* predictions than any of the twice daily heat flux assimilation experiments but had considerably lower RMSE for root-zone soil moisture prediction than any other experiment, reinforcing the qualitative interpretations of the initial 6 days of assimilation shown in Fig. 5.5. Regarding *H* predictions, soil moisture assimilation produced outputs that have ~1-2% vol/vol lower RMSE than from twice per day joint *LE* and *H*, and *LE* assimilation, but higher RMSE than from twice per day *H* assimilation. When considering the spatial resolution of remotely sensed observation data available (~1 km × 1 km for *LE* and *H* from MODIS and ~50 km × 50 km for surface soil moisture from SMOS), assimilation of *LE* and/or *H* could potentially produce better overall heat flux predictions from a LSM such as the CBM for a period that is relatively cloud free, compared with soil moisture assimilation based on the results here. However, more detailed analyses are required for a range of different initial conditions, parameter inputs, temporal and spatial resolutions in order to show definitively that assimilating a particular variable can consistently produce better *LE* and *H* predictions.

The assimilation of skin temperature twice a day resulted in predicted heat flux accuracies that were very similar to those from twice daily heat flux assimilation experiments. Fortnightly skin temperature assimilation achieved similar predictions of *LE* and *H* to fortnightly *LE* and joint *LE* and *H* assimilation, and better predictions than fortnightly *H* assimilation. When compared with the heat flux assimilation experiments for corresponding time scales, skin temperature assimilation has a strong impact on improving root-zone soil temperature, as shown by the small RMSE values.

The ability of skin temperature assimilation to match the predictive accuracy of heat fluxes from the heat flux assimilation experiments is likely to be related to the strong relationship that skin temperature has with the surface net radiation, which directly impacts on the surface energy balance and thus strongly influences both *LE* and *H* in the model. An interesting implication of these results is the apparent lack of benefit in assimilating *LE* and *H* estimates representing quantities that would be derived from remotely sensed skin temperature observations as compared to direct skin temperature assimilation. However, these results may be an artefact of how the *LE* and *H* estimates were derived in this synthetic study, as the same skin temperature – *LE*/*H* relationships are used in the assimilation as for *LE* and *H* observation generation, which will not be the case with actual remote sensing data. Therefore *LE* and *H* derived from real remotely sensed skin temperature using an algorithm (such as SEBAL) must be assimilated and compared with direct skin temperature assimilation to make definitive statements in this regard. A key question is whether an energy balance model such as SEBAL can provide better *LE* and *H* estimates than an LSM through skin temperature assimilation.

5.6 CONCLUSIONS

This paper has compared the assimilation impact of *LE*, *H*, skin temperature and surface soil moisture observations, representing typically available remotely sensed data and temporal repeat (MODIS, Landsat and SMOS), to understand the relative impact on LSM predictions of *LE*, *H*, root-zone soil moisture and temperature, in a synthetic experiment framework. Soil moisture assimilation is the more traditional approach for improving LSM predictions, and as expected, showed the most direct impact on root-zone soil moisture. While it also improved heat flux predictions, the other approaches performed comparatively in terms of *H* predictions and slightly better in terms of *LE* predictions, when assimilated on a twice daily time scale, as these variables share more direct relationships with *LE* and *H* in the model. Moreover, they were able to have a direct impact on soil temperature predictions, which is not possible with direct soil moisture assimilation.

While this study clearly demonstrates that assimilation of *LE* and/or *H* has the potential to improve *LE* and *H* predictions to at least a similar degree as soil moisture assimilation, when tested under idealised conditions, the results may be different when cloud impacts and contrasting spatial resolutions are taken into consideration. Moreover, assimilating *LE* and *H* on a fortnightly temporal scale that is comparable to Landsat, resulted in significantly poorer *LE* and *H* predictions compared to twice daily *LE* and *H* assimilation that would be available from MODIS, and 3 day soil moisture assimilation that would be available from SMOS. This shows that if cloud cover reduces the temporal quality of remotely sensed *LE* and *H* observations (also of skin temperature), it can reduce the predictive performance of *LE* and *H* considerably. Hence, further research is required to make definitive conclusions regarding the best variables to assimilate for improved *LE* and *H* prediction. This includes assimilating over a range of different time scales, soil moisture conditions, soil and vegetation parameters, and using real remotely sensed observations so that the different spatial scales and error sources can be considered. Since *LE* and/or *H*, and skin temperature assimilation has shown promise for improving predictions of *LE* and *H* in these experiments, further field-based studies are warranted. Moreover, assimilation of a combination of the available data may provide the best results, complementing the different spatial and temporal characteristics with the different land surface variables that are observed.

5.7 ACKNOWLEDGEMENTS

This work has been funded by a University of Melbourne-CSIRO Collaborative Research Support Scheme grant. The authors are grateful to Dr. Ying Ping Wang and Dr. Cathy Trudinger from CSIRO Marine and Atmospheric Research Division for supplying and permitting the use of CBM for this research and also providing valuable discussion on details of the model. Also Dr. Neil McKenzie from CSIRO Land and Water Division for supplying soils data. Dr. John Gorman from the Bureau of Meteorology assisted with queries relating to Bureau of Meteorology data used by this study. Robert Pipunic is supported by an Australian Postgraduate Award Scholarship.

6 ONE-DIMENSIONAL FIELD DATA ASSIMILATON

This chapter has been published as:

Pipunic, R. C., Walker, J. P., Western, A. W., & Trudinger, C. M. (2013). Assimilation of multiple data types for improved heat flux prediction: A one-dimensional field study. *Remote Sensing of Environment*, 136, 315–329.

The numbering of sections, figures and tables in the original publication have been altered for this chapter, to be consistent with the thesis chapter numbering. Also the references have been incorporated into the full list of references at the end of this thesis.

6.1 ABSTRACT

Accurate latent (*LE*) and sensible (*H*) heat flux partitioning from Land Surface Models (LSMs) is important for numerical weather prediction. Land data assimilation can play a key role in improving heat flux prediction by merging information from a range of remotely sensed products with LSMs. This paper demonstrates this potential for an open grassland site in Australia via one-dimensional experiments spanning a year-long period. With a focus on how a LSM is impacted, in-situ field observations were assimilated. Data types as available from passive microwave and thermal infra-red remote sensors were tested for their impact, with individual and joint assimilation of *LE* and *H*, near-surface soil moisture, and skin temperature observations – all on time scales approximating satellite overpass intervals. Assessed against independent data from field observations, the multi-observation approach of joint near-surface soil moisture and skin temperature assimilation made the greatest improvements to *LE* (expressed as daily evapotranspiration; *ET*), being slightly better than for joint *LE* and *H* assimilation. This result questions the value of using *LE* and *H* retrievals from thermal imagery within an assimilation context. Individually, skin temperature assimilation was one of the best performers for soil temperature estimates but with degraded root-zone soil moisture estimates and minimal *ET* improvements. Likewise, near-surface soil moisture assimilation produced the greatest root-zone soil moisture improvement but with relatively modest *ET* improvement. Combined near-surface soil moisture and skin temperature assimilation balanced the improvements to both soil moisture and temperature states along with strong improvements to *ET* estimates, highlighting the benefits of multi-observation assimilation.

6.2 INTRODUCTION

Land Surface Models (LSMs) require careful initialisation in order to achieve accurate latent (*LE*) and sensible (*H*) heat flux prediction. Relative humidity and temperature in the lower atmosphere are influenced by *LE* and *H* from the land surface (Denman *et al*., 2007), and hence LSM state initialisation impacts Numerical Weather Prediction (NWP) model skill (Beljaars *et al*., 1996; Case *et al*., 2008; Chen *et al*., 2001, 2007; Koster *et al*., 2004). Due to spatial and temporal land surface heterogeneity and the resulting complexity of water and energy exchanges between soil, vegetation, and the atmosphere, characterising these interactions with LSMs is inherently uncertain. Thus a challenge for NWP is to obtain the most accurate *LE* and *H* predictions from LSMs whilst maintaining realistic model physics and state estimates. Global coverage and regular temporal repeat of land surface state and flux quantities from current and emerging remote sensing data provides an opportunity to meet this challenge through data assimilation, the process whereby such information is combined with model estimates (factoring in uncertainty estimates for each) to produce the best predictions possible.

Remotely sensed information relevant to LSMs includes microwave brightness temperature, which is related to soil moisture content (e.g. Gao *et al*., 2006; Njoku & Entekhabi, 1995) and forms the basis of global soil moisture data products such as those derived from Advanced Microwave Scanning Radiometer (AMSR-E/AMSR2) data (Imaoka *et al*., 2010; Owe *et al*., 2008) or the European Space Agency's Soil Moisture and Ocean Salinity (SMOS) data (Kerr, 2001). Active microwave sensor data such as from the Advanced Scatterometer (ASCAT) are also valuable for deriving soil moisture content (Wagner *et al*., 1999) and have been used for assimilation research in an NWP context (e.g. Mahfouf, 2010), including use for testing a newly implemented assimilation scheme in an operational system (de Rosnay *et al*., 2013) and for operational forecasting (Dharssi *et al*., 2011). Thermal infra-red (TIR) data provide information on skin temperature and hence model soil temperature states, which are an important part of the land surface energy and water balance (Entekhabi *et al*., 1994; Viterbo & Beljaars, 1995). Moreover, skin temperature based on data from sensors such as the Moderate Resolution Imaging Spectroradiometer (MODIS: e.g. Wan & Li, 1997) and Landsat Thematic Mapper (TM: e.g Sobrino *et al*., 2004) can be combined with other remote sensing data to derive spatially distributed *LE* and *H* data products using algorithms such as METRIC (Allen, *et al*., 2007), SEBS (Su, 2002), and SEBAL (Bastiaanssen, *et al*., 1998).

In many coupled NWP systems soil moisture is treated as a tuning variable and adjusted in non-physical ways to produce fluxes that are congruent with atmospheric observations (Douville *et al.*, 2000; Mahfouf, 1991; Rhodin *et al*., 1999; Seuffert *et al*., 2004). With the aim of achieving more physically realistic LSM predictions of soil states (i.e. soil moisture and temperature) and heat fluxes (i.e. *LE* and *H*), a common assumption is that more accurate root-zone soil moisture should lead to improved heat fluxes, due to the role of profile soil moisture in regulating the partitioning of available energy at the land surface (Reichle *et al*., 2007). To this end, and spurred by the emergence of remotely sensed soil moisture products, there has been considerable LSM assimilation research focusing on soil moisture.

The potential for improving root-zone soil moisture predictions with near-surface soil moisture assimilation (remote sensing products characterise the top few centimetres of soil at most) has been demonstrated via synthetic studies (Entekhabi *et al*., 1994; Kumar *et al*., 2009; Pipunic *et al*., 2008; Reichle *et al*., 2008; Walker and Houser, 2004). Real data on near-surface moisture has been assimilated in one-dimensional in-situ field experiments (Li and Islam, 1999; Sabater *et al*., 2008; Walker *et al*., 2001a). Experiments using remotely sensed products have also shown some potential in terms of improving root-zone soil moisture (Draper *et al*., 2009b; Reichle & Koster, 2005; Reichle *et al*., 2007), but few have demonstrated impacts on atmospheric prediction (Mahfouf, 2010). Skin temperature assimilation has also been investigated via synthetic experiments (e.g. Entekhabi *et al*., 1994; Pipunic *et al*., 2008) and real data experiments involving both in-situ field and remotely sensed data (Huang *et al*., 2008; Lakshmi, 2000; McNider *et al*., 1994; Meng *et al*., 2009; Reichle *et al*., 2010), showing promise for the improvement of model states and/or heat fluxes.

Assimilating combinations of different observation types is expected to provide better overall model constraint through direct impact on different variables simultaneously. Research into such strategies is important as the availability of different remotely sensed data increases. Examples include synthetic experiments for combined assimilation of observations relating to remotely sensed soil moisture and skin temperature by Entekhabi *et al*. (1994) and Balsamo *et al*. (2007) for an NWP context (whose study also incorporated screen-level variables). While Balsamo *et al*. (2007) assessed the contribution to atmospheric screen-level prediction from different observations, and highlighted the importance of soil state and land surface heat fluxes to screen-level prediction, neither study explicitly assessed land surface flux predictions.

Pan *et al*. (2008) assimilated both remotely sensed microwave brightness temperature (linked to soil moisture) and an *LE*/*ET* product. Assessed against independent model predictions there was improvement to soil moisture but not to *ET*, leading them to conclude that improvement from assimilating remotely sensed *ET* remains challenging. The strategy of assimilating heat flux observations has received minimal attention in literature. Other examples are limited to Schuurmans *et al.* (2003) who assimilated remotely sensed *ET* retrievals from the SEBAL algorithm (Bastiaanssen *et al*., 1998), showing impacts on modelled *ET* that appeared promising but with no independent data for validation, and the assimilation of both *LE* and *H* in a synthetic study by Pipunic *et al*. (2008) which showed improved flux predictions. Hain *et al*. (2012) assimilated soil moisture estimates which they retrieved using an *ET* product derived from TIR remote sensing, along with microwave based soil moisture estimates. However they did not explicitly assimilate *ET* itself and only evaluated assimilation impacts on modelled soil moisture, with the soil moisture data derived from the *ET* product making the best improvements to modelled root-zone moisture.

Current challenges with remotely sensed data assimilation include disparate spatial and temporal resolution between data sources available for model input, assimilation and validation, and considerable errors in both remotely sensed products and models (Reichle *et al*., 2007). From an operational NWP perspective, the ultimate aim is to utilise available land surface and screen-level meteorological observations for assimilating into a system where the LSM and atmospheric model are coupled. The scope of this study covers only LSM assimilation, as it is important to thoroughly test a LSM offline first and understand the impacts (and limitations) from assimilating different data types – starting with point-scale scenarios where observational uncertainties from in-situ measurements are better understood, prior to testing in more complex spatial scenarios and coupled systems involving greater uncertainty.

This paper examines the impact from assimilating different data types on soil states and heat fluxes for the CSIRO Biosphere Model (CBM, Wang *et al*., 2001, 2007) – a version of the Community Atmosphere Biosphere Land Exchange (CABLE) model (Kowalczyk *et al*., 2006; Wang *et al*., 2011). The work presented here is an extension to the synthetic twin experiments of Pipunic *et al.* (2008) which demonstrated the potential of assimilating remotely sensed product types other than soil moisture to improve heat flux predictions. That study was based on simulations limited to a 3 month period forced with data from summer/early-autumn and with relatively uniform/sparse vegetation cover (LAI ~0.30-0.40). While it demonstrated that *LE*, *H* and skin temperature assimilation could provide comparable and/or better improvement to heat fluxes than near-surface soil moisture assimilation alone, it also showed that improved soil moisture predictions from near-surface soil moisture assimilation did not translate to the best overall *LE* and *H* predictions.

Here we extend on the proof-of-concept study of Pipunic *et al.* (2008) via year-long experiments spanning the full vegetation growth cycle and using real in-situ observations of *LE, H*, near-surface soil moisture and skin temperature. This includes combinations of observations that represent multi-sensor data assimilation approaches not examined in the synthetic study. While different temporal scales are taken into account, including the masking of optical data by cloud, this paper does not address the important issue of the contrasting spatial scales between optical and passive microwave products.

6.3 MODELLING AND ASSIMILATION

The CSIRO Biosphere Model (CBM, Wang *et al*., 2001, 2007) used in this study was developed in Australia by scientists at the Commonwealth Scientific and Industry Research Organisation (CSIRO), Marine and Atmospheric Research division. It was used for the synthetic study by Pipunic *et al*. (2008), and for consistency, was used in the extension of that work presented here. As a precursor to the current Community Atmosphere Biosphere Land Exchange (CABLE) model (Kowalczyk *et al*., 2006; Wang *et al*., 2011), which is planned for use as the LSM for Australia's NWP (Law *et al*., 2012), the CBM shares similar formulations for the land surface water and energy balances. The data assimilation scheme used for all experiments in this study was the Ensemble Kalman Filter (EnKF, Evensen, 1994).

A description of the CABLE model by Kowalczyk *et al*. (2006) provides details on the energy balance and soil scheme, which are very similar in the two versions (CBM and CABLE). The CBM soil profile has a total depth of 4.60 m and consists of six layers of fixed thickness which are (from the uppermost to the bottom layer): 2.2, 5.8, 15.4, 40.9, 108.5 and 287.2 cm. Soil moisture movement is only in the vertical direction between layers and is calculated based on Richard's equation, with individual prognostic soil moisture and soil temperature state variables being associated with each layer. However, only a single set of soil parameter values can be specified for all soil layers, resulting in uniform properties over the whole soil profile. Linking with the vegetation scheme is through the plant root distribution, where the percentage of roots in each soil layer can be specified by the user. Vegetation in the CBM is represented by a detailed two leaf canopy model – a "big" sunlit and a "big" shaded leaf (Wang & Leuning, 1998) – which includes aerodynamic and radiative interaction between the ground and the vegetation (Raupach *et al*., 1997). Also included in the CBM are calculations for photosynthesis, leaf temperature, and stomatal conductance.

The Leaf Area Index (*LAI*) parameter plays a key role in determining the relative fraction of canopy cover to bare soil. Net radiation is calculated separately for the vegetation canopy and soil surface, as is *LE* and *H* where total *LE* and *H* outputs are the sum of the canopy and soil components. Total skin temperature from the CBM is based on a combination of the soil and canopy surface temperature components involved in longwave radiation balance calculations and is summarised as follows:

$$\sqrt[4]{[\{1.0 - f(LAI)\} \times Tcan^4] + [f(LAI) \times Tsoil^4]}. \qquad (6.1)$$

The soil component (*Tsoil*) is the temperature state variable of the top-most soil layer (0-2.2 cm), while the canopy surface component (*Tcan*) is based on a non-prognostic leaf temperature variable which is determined iteratively at every model time step (after initialisation with air temperature from meteorological forcing) as part of the vegetation canopy energy balance calculations. Relative contributions from soil and vegetation components to the total skin temperature are determined by a weighting factor *f*(*LAI*), which is a function of *LAI* that describes the fraction of radiation (from 0 to 1) transmitted through the canopy.

The aim with sequential data assimilation techniques, such as the EnKF used in this work, is to update and correct prognostic state variables, with an expectation that key diagnostic variables, such as heat fluxes, will consequently be improved. Updates were applied here to soil moisture and soil temperature states for each of the six CBM soil layers. In relation to heat fluxes, the top-most soil layer moisture and temperature states are closely related to the soil component of *LE*, while the soil moisture states for layers which have roots are used in a water availability term linked to the vegetation component of *LE*, and hence also indirectly linked to leaf temperature. The temperature state variable of the top-most soil layer is closely linked to calculations for the soil component of *H*, whereas the vegetation canopy component results from vegetation energy balance calculations, involving the vegetation component of *LE* and the non-prognostic leaf temperature variable (both indirectly linked to soil moisture). Details of the EnKF and its application to the CBM are contained in Pipunic *et al.* (2008).

For meaningful comparisons to be made between observation-based and LSM predicted state data as part of data assimilation, systematic biases must be removed (Drusch *et al*., 2005; Reichle & Koster, 2004). Bias can be due to representative differences, such as differences in soil depth or spatial scale between observations and model estimates, and also uncertainties specific to different sources of information. These include uncertain LSM parameters such as wilting point and field capacity (amongst others) which influence moisture dynamics (Koster & Milly, 1997), while observation-based data may have different dynamics as a results of a particular observing instrument or algorithm used to estimate final quantities from remotely sensed observations. Although instrument bias is typically of limited concern for well calibrated in-situ installations, the correct treatment of bias remains a challenge, particularly using LSMs and remotely sensed products in the absence of adequate information enabling its source(s) to be accurately identified and quantified.

Rescaling approaches such as cumulative distribution function (*cdf*) matching of observed data series to LSM state climatology prior to assimilation are now considered de rigueur for bias removal (e.g. Draper *et al*., 2009b; Drusch *et al*., 2005; Reichle & Koster, 2004). Reichle and Koster (2004) demonstrated that rescaling remote sensing derived surface soil moisture to model predictions for a one year period reduced observation-model bias over a subsequent nine year series, but did not fully remove it. This highlights the difficulty in thoroughly understanding and dealing with such bias, especially if only short data series are available. Keeping in line with current standard practice, observation-model bias for land surface states in this study were eliminated by rescaling the observed data series prior to assimilation, by matching the mean and standard deviation to that of the CBM predicted series. In the long-term however, research effort should focus on better understanding and treating bias in LSMs which may involve improvements to model physics and/or better parameterisation – likewise for remotely sensed land data products given the ultimate aim is operational assimilation.

6.4 STUDY SITE AND DATA

The one-dimensional modelling experiments presented in this paper were carried out for a flux station site in south eastern Australia, located on non-irrigated pasture within a mainly agricultural area at Kyeamba Creek (Fig. 6.1). Site instrumentation consisted of an eddy covariance system, meteorological sensors, soil moisture and soil temperature sensors. Smith *et al*. (2012) summarises the main instruments used and briefly describes the landscape of the Kyeamba Creek catchment. Key environmental characteristics and CBM parameter values that were used for modelling experiments here are summarised in Table 6-1.

This site was managed by this paper's lead author and no details have previously been published on the basic processing for this data, thus some are included herein. Kyeamba Creek is a tributary of the Murrumbidgee River, located in the south of Australia's Murray Darling Basin. The flux station location was on the alluvial flats of the creek valley approximately 20 km south east of an Australian Bureau of Meteorology (BoM) automatic weather station in the town of Wagga Wagga (Fig. 6.1). Heat fluxes, meteorological variables, soil moisture and soil temperature data were all measured for a full year period from January 1st to December 31st 2005 and processed to a 30 minute time-step. The total percentage of instrument down-time at the site was approximately

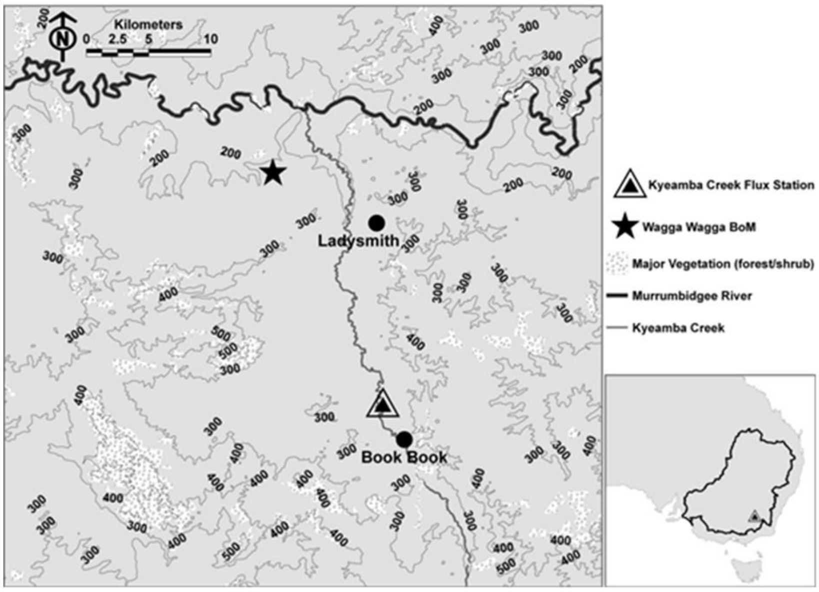

Figure 6.1: *Map showing locations of the Kyeamba Creek flux station study site, Wagga Wagga BoM automatic weather station, and NSW Office of Water discharge gauges for Kyeamba Creek near Ladysmith and Book Book. Grey elevation contour lines in metres. The Oznet soil moisture and rainfall monitoring site is situated ~200 m west of the flux station. A broad scale overview of the Kyeamba Creek site location in south eastern Australia is shown in the bottom right hand corner with the black boundary delineating the Murray Darling Basin.*

Table 6-1: *Summary of Kyeamba Creek flux station site characteristics and key model input data relevant to numerical experiments.*

Managing institution	The University of Melbourne
Location (WGS84)	147.56°E, -35.39°S
Elevation – metres above sea level	~233
Vegetation	Grass pasture (non-irrigated)
*** LAI Range**	~0.25 (Summer/Autumn) – 3.0 (Spring)
Average canopy height (m)	~0.25
Dominant soil type	Silty loam
Soil bulk density (kg/m^3)	1,475
Soil porosity (vol/vol)	0.450
Soil field capacity (vol/vol)	0.360
Soil wilting point (vol/vol)	0.070
Soil hydraulic conductivity at saturation (m/s)	8.33×10^{-6}
Soil suction at saturation (m)	0.505
^ Long term average annual rainfall (mm/yr)	~575
§ Spinup period (simulation repeated 12 times) ***Total rainfall (mm):***	Jan 1st 2004 – Dec 31st, 2004; ***585***
† Experimental period ***Total rainfall (mm):***	Jan 1st 2005 – Dec 31st, 2005; ***595***

* Based on AVHRR-derived monthly data used for simulations over the 2004 and 2005

^ For the period 1941-2012 at the Australian Bureau of Meteorology (BoM) Wagga Wagga station (http://www.bom.gov.au/climate/averages/tables/cw_072150.shtml) shown in Fig. 6.1.

§ Most of the meteorological forcing generated from BoM Wagga Wagga station data (Siriwardena *et al.*, 2003), with rainfall data from the K10 Oznet station (Smith *et al.*, 2012) ~200m from the flux station site.

† All data are site measured, with small gaps in the forcing in-filled using Wagga Wagga BoM data and rainfall gaps in-filled using the nearby K10 Oznet data (Smith *et al.*, 2012).

10%, with the longest consecutive gap being about 16 days from day of year (DoY) 59 to 75. Meteorological data gaps were in-filled using 30 minute meteorological data compiled from BoM Wagga Wagga automatic weather station data (Siriwardena *et al.*, 2003), with the exception of rainfall for which supplementary data was available from an adjacent OzNet monitoring station (Smith *et al.*, 2012) approximately 200 m away (see http://www.oznet.org.au/k10.html). Corresponding gaps in the *LE*, *H*, soil moisture and soil temperature data series were not in-filled.

The *LE* and *H* were measured with an eddy covariance system consisting of a CSAT 3D sonic anemometer (Campbell Scientific Inc., 1998) and LI-7500 open path gas analyser (LI-COR Inc., 2003). They were elevated 3 m above ground giving an approximate maximum fetch of 300 m.

A CNR1 four-way net radiometer (Kipp and Zonen, 2002) measured the incoming and outgoing components of short and longwave radiation for determining the total net radiation at the land surface (R_N). Ground heat flux (G) was also measured using two HFT3 ground heat flux plates (Campbell Scientific Inc., 1999) buried 8 cm below the surface, and corrected to represent G at the land surface using temperature thermocouple and soil moisture measurements in the 0-8 cm layer of soil as outlined in the HFT3 manual (Campbell Scientific Inc., 1999).

The LE and H data were filtered for spurious values and conditions known to compromise the quality of 3D eddy covariance measurements (e.g. rainfall), and night time data (from 6pm to 6am) were discarded. The energy balance gap between $(LE+H)$ and (R_N-G) was approximately 20% and the technique of Twine *et al.* (2000) was applied to achieve closure. This method adjusts LE and H to achieve a closed energy balance against measured (R_N-G) while maintaining a constant Bowen Ratio (H/LE). The root mean square error (RMSE) between the LE and H data before and after closing the energy balance was just under 40 Wm^{-2} for each.

Soil moisture observations were made over depths of 0-8 cm, 0-30 cm, 30-60 cm and 60-90 cm using CS615 water content reflectometer probes (Campbell Scientific Inc., 1996), and calibrated using a number of independent gravimetric and TRASE Time Domain Reflectometer (TDR, Soil Moisture Equipment Corp., 1989) volumetric soil moisture measurements made under wet and dry conditions. After soil temperature correction of raw CS615 data following Western and Seyfried (2005), a calibration relationship was established with an accuracy of ~0.02 vol/vol (section 4.3.1). Soil temperature was measured at depths of 2 cm, 5 cm, 10 cm, 20 cm, 50 cm and 100 cm with Unidata 6507A temperature thermistor probes (Unidata Australia, 1997).

The meteorological variables measured at the station include incoming short and longwave radiation, rainfall, air temperature, wind speed, saturation vapour pressure and station level barometric air pressure – specific humidity was derived from barometric air pressure and saturation vapour pressure. These were all used for model forcing over the experimental period (2005). Incoming short and longwave radiation used for forcing were measured with the two CNR1 upward facing sensors, whereas all four separate CNR 1 sensor measurements (upward and downward facing for both short and longwave) were combined for R_N to correct the LE and H data used for assimilation as described above. Thus the corrections to LE and H partly involved the same incoming radiation data used for CBM forcing, but also the separately measured outgoing short and longwave radiation and G which were not used for any model input or results validation. Also, measurements from only the downward facing outgoing longwave radiation sensor, independent of the forcing data, were used to construct the assimilated skin temperature data set.

A separate meteorological series spanning 2004 from Wagga Wagga BoM data (Siriwardena *et al*., 2003), with rainfall data from the adjacent OzNet station (Smith *et al*., 2012; http://www.oznet.org.au/k10.html), was used as forcing for spinning up the model. The total rainfall used for the 2004 spin up and for the 2005 experiment periods are both close to the long term average of annual rainfall for the region, based on comparison with data from BoM records as shown in Table 6-1.

An actual evapotranspiration (*ET*) series was also derived for 2005 to provide a data set independent to the eddy covariance measurement series. This derived *ET* series was used for assessing *LE* predictions, as the assimilated heat flux observations were sampled from the eddy covariance series. The site specific data available to achieve this were rainfall – also used for model forcing – and root-zone (estimated to be within the top 60 cm for the grassland) soil moisture data consisting of both 0-30 cm and 30-60 cm deep probe measurements, which are independent of the 0-8 cm measurements used for soil moisture assimilation.

This *ET* series was based on calculating differences between rainfall totals and root-zone soil moisture storage changes over time. It was calculated on a fortnightly time scale to minimise excessive noise in the series from moisture probe data, which is likely to be more prominent with respect to small moisture changes over shorter time scales. Potential *ET* calculated from meteorological data was used as an upper-bound for truncating any of the calculated actual *ET* that exceeded it. Of the twenty fortnightly *ET* totals that could be calculated from the available data, 35% of them clearly exceeded the corresponding potential *ET* and were hence reset to the potential value – all of these reset totals occurred consecutively in time spanning from the DoY 169 total through to DoY 302, in the austral winter and spring (mid-June to end of October). Deep drainage (below the 0-60 cm root-zone) and/or saturation excess surface runoff are the most likely reasons for the calculated *ET* exceeding its potential in this wetter/cooler period of the year when soil moisture was high. The total for DoY 316 immediately following this period exceeded the potential *ET* by a negligible amount (57.8 mm compared to 57.4 mm).

Outside the period from the DoY 169 total to DoY 316, where calculated *ET* exceeded potential *ET*, all of the fortnightly totals were considerably below potential. Within one of the driest periods of the year (late autumn) the calculated *ET* for the fortnight ending at DoY 141 was -4.1 mm. This negative value is attributed to soil moisture probe measurement errors in the dry conditions. Over the 60 cm measurement depth, 4.1 mm of water represents approximately 0.007 vol/vol moisture content, which is well within the moisture probe data error of ~0.02 vol/vol. Any *ET* occurring in the fortnight ending DoY 141 is therefore likely to be at or near the minimum for the year and close to zero.

This *ET* series provides for validation, enabling comparisons to be made between *ET* determined in two independent ways using the same rainfall data – from a complex model (CBM prediction with and without assimilation) and calculated from direct field measurements of soil moisture storage (supplemented with potential *ET* where appropriate). A regression between fortnightly rainfall and the calculated *ET* resulted in an R^2 of 0.07, indicating that the storage processes in the soil largely remove any dependence of the calculated *ET* on rainfall at a fortnightly time step. In constructing this series there was an assumption that, outside the period where calculated *ET* was limited to potential *ET*, there was no surface run-off over unsaturated soil in the pasture field where measurements were made.

From the station site there was no visually discernible gradient for at least a few hundred metres surrounding it. Where calculated *ET* totals were below potential, the near-surface and root-zone moisture were below saturation and 30 minute rainfall intensities (maximum observed was 8.4 mm in 30 minutes) were less than the estimated saturated hydraulic conductivity (Table 6-1), which equates to a 30 minute total of 15 mm. The hydraulic conductivity estimate comes from regional soil data analysis by McKenzie *et al*. (2000, 2003). Hence all of the rainfall for these periods is likely to have infiltrated into the soil.

The period of high root-zone soil moisture storage in the experimental year spans most of winter and spring with the main increase towards maximum storage beginning in June from ~DoY 160. By ~DoY 190 the storage approaches its maximum, and moisture content levels persist close to field capacity through to ~DoY 290 in mid-October, sometimes peaking near saturation (values for these properties are in Table 6-1 and their origin discussed later in this section). The highest root-zone storage occurs within the period where potential *ET* dominates the constructed *ET* validation series, with rainfall that exceeded the potential assumed to have been balanced by percolation below the 60 cm root-zone depth and/or run-off. The 60-90 cm soil moisture probe data – which were not used for modelling or quantitative validation in this study – shows no notable change in moisture content below the root-zone from the beginning of the year until ~DoY 200.

Possible groundwater interaction at the site is evident in the form of three separate extreme spikes in the 60-90 cm moisture data series that correspond with flow events (Table 6-2) in Kyeamba Creek at Book Book and Ladysmith (Fig. 6.1). This is indicative of lateral recharge of groundwater, followed by discharge (i.e. bank storage processes), related to flow events in Kyeamba Creek located ~350 m to the west of the study site. There are no independent measurements to verify the peak values of these moisture data spikes (up to and above ~0.55 vol/vol) which have only been interpreted qualitatively as indicators of groundwater influence, and while root-zone soil moisture data show some increases at these times they are not similarly extreme.

Table 6-2: *Summary of major spikes in soil moisture data for below the root-zone (60-90cm) corresponding to spikes in Kyeamba Creek discharge both upstream and downstream from the point in the creek closest to the study site.*

	Period 1 60-90 cm Soil Moisture Spike			**Period 2 60-90 cm Soil Moisture Spike**			**Period 3 60-90 cm Soil Moisture Spike**		
Data Set	***Increase to Peak***	***Days at Peak***	***Consecutive Days Rain Total to Peak***	***Increase to Peak***	***Days at Peak***	***Consecutive Days Rain Total to Peak***	***Increase to Peak***	***Days at Peak***	***Consecutive Days Rain Total to Peak***
60-90 cm Soil Moisture at Flux Station	DoY 252-253 0.26-0.63 vol/vol (~110 mm)	9	DoY 252-253 ~56 mm	DoY 270-272 0.29-0.57 vol/vol (~80 mm)	Data Gap	DoY 269-272 ~40 mm	DoY 310-311 0.19-0.55 vol/vol (~110 mm)	1	DoY 311 27 mm
Discharge at Ladysmith (~14 km Upstream)	DoY 251-253 17-5,588 Ml/day	1	-	DoY 270-272 77-2,046 Ml/day	1	-	DoY 310-311 38-1,106 Ml/day	1	-
Discharge at Book Book (~4 km Downstream)	DoY 251-253 11-1,754 Ml/day	1	-	DoY 270-271 32-937 Ml/day	1	-	DoY 310-311 23-291 Ml/day	1	-

Groundwater interaction could have implications for the fortnightly *ET* validation series, particularly following the final 60-90 cm moisture data spike shown in Table 6-2 (DoY 311) leading into the spring/summer transition – the few days after this and beyond is where *ET* calculated from changes in root-zone moisture storage were maintained in the final data series as they were either equal to or less than the potential *ET*. In this period there might have been a small groundwater contribution to *ET* via capillary rise into the root-zone, which would be captured in the total *ET* of the validation series via soil moisture data, but which could not be quantified separately to it.

Soil parameters used in the CBM (see Table 6-1) were determined from a combination of samples collected at the site as part of this study, and soil property interpretations (McKenzie *et al*., 2000, 2003) relating to a 1:100,000 scale soil landscape map of the region (Chen & McKane, 1997). Particle size analysis performed on site samples determined that the top 60 cm of soil is fairly uniform and predominantly silty loam with clay and sand contents of ~12% and ~33% respectively (CSIRO particle analysis, May, 2007). A-horizon values from the map related soil interpretations (McKenzie *et al*., 2003) were used for wilting point (assumed to be the moisture content at 15 bar), field capacity (assumed to be the moisture content at 0.1 bar) and saturated hydraulic conductivity. Bulk density and porosity were determined using volumetric soil samples taken from the top 60 cm at the site, and together with the map related values for wilting point and field capacity, soil suction at saturation and the Campbell's *b* parameter were calculated.

Vegetation canopy height and the percentage of roots in each model soil layer were estimated from field observations. Leaf Area Index (*LAI*) values used for the site were monthly averages derived from 0.01° resolution Advanced Very High Resolution Radaiometer (AVHRR) fPAR (Photosynthetically Active Radiation) data of Donohue *et al*. (2008). The fPAR data were converted through a fractional cover estimate (fPAR/0.95; see Lu *et al*., 2003) from which *LAI* was estimated (Choudhury, 1989). Values of *LAI* from such estimates are known to become less reliable when they are greater than ~3.0 (Carlson & Ripley, 1997; Lu *et al*., 2003). Moreover, McVicar *et al*. (1996) found that more than 90% of field sampled *LAI* values from a similar pasture environment in south east Australia were below 3.0. Therefore, any of the *LAI* estimates made for this site greater than 3.0 (for August through to November) were set to 3.0. Other parameter values used were provided with the CBM/CABLE model (default values; see Abramowitz, 2006) pertaining to the agricultural/C3-grassland category from a global vegetation dataset based on Potter *et al.* (1993).

6.5 METHODOLOGY

A one-dimensional CBM set-up was used following Pipunic *et al*. (2008) but with real field observations from point scale in-situ measurements, approximately representing overpass times of remotely sensed product types that can be derived from MODIS and AMSR-E observations. The grassland site where observations were made represents a land-cover for which remotely sensed microwave and thermal infra-red measurements are typically reliable. CBM simulations were performed using fixed parameters (derived from site specific information where possible or from regional datasets as outlined at the end of the previous section) and with the model uncalibrated, as is the case with the current LSM in Australia's NWP system (Dr P Steinle, Data Assimilation Team Leader, Australian Bureau of Meteorology, *pers comm.*, May 2011).

Numerical experiments performed for this study included model simulations for 2005 with: i) no assimilation (denoted as "Open-Loop"); ii) *LE* and *H* observations assimilated together (denoted as "LEH_Assim"); iii) near-surface soil moisture observations assimilated (denoted as "SM_Assim"); iv) skin temperature – derived from observed outgoing longwave radiation – assimilated (denoted as "Tsk_Assim"); v) a combination of all observations assimilated – *LE*, *H*, near-surface soil moisture and skin temperature (denoted as "ALL_Assim"); and, vi) a combination of near-surface soil moisture and skin temperature assimilated (denoted as "SMTsk_Assim"). Available field observations of soil moisture and soil temperature, along with the calculated fortnightly *ET* estimates, were the independent data used for comparing with simulation outputs and assessing the impact of each assimilation option on predicted flux and state values.

Initial state conditions used for all the simulations were obtained from spinning up the CBM through repeated simulation using the one year meteorological forcing data series for 2004. The spin up was carried out until differences between model state values of soil moisture and temperature for the start of the year matched those at the end of the year for all soil layers to within 0.001 vol/vol and 0.01° C respectively. This took 12 iterations, with most of this time attributable to minimising the differences for the deeper soil layers. CBM simulation time steps are governed by the time scale of forcing data and are therefore 30 minutes in this study.

In implementing the EnKF data assimilation algorithm, error estimates of field measurements were used to define the uncertainty range for generating observation ensembles, and these are summarised in Table 6-3. Model uncertainty for the EnKF is defined from the spread of an ensemble of model predictions, which in this study was the result of performing simulations with ensembles of key model inputs. Specifically, these were ensembles of initial state conditions and forcing data variables that represented error range estimates of each, since these inputs contribute

Table 6-3: *In-situ observations of remotely sensed data types used in this study, with estimated additive error ranges used for ensemble σ values, and satellite sensor information that each observation represents.*

Observed quantity	Additive error (ensemble σ)	Corresponding satellite/sensor	Temporal resolution used	Spatial res. available
LE (Wm^{-2})	± 50	MODIS	Twice daily, filtered for cloud	~1km x 1km
H (Wm^{-2})	± 50	MODIS	Twice daily, filtered for cloud	~1km x 1km
Near-surface soil moisture (vol/vol)	± 0.04	AMSR-E	Once per day (am)	~25km x 25km
Skin temperature (K)	± 2	MODIS	Twice daily, filtered for cloud	~1km x 1km

to overall model error. Inaccurate model structure and parameterisation are also major sources of model error, which due to their complexity are very difficult to represent with ensembles. Hence they have not been treated directly in the ensemble generation for this study. Ensemble generation is discussed later.

In all simulations for numerical experiments spanning 2005, ensembles of model inputs included perturbed 2005 forcing data (Table 6-4) and perturbed initial state conditions, with covariance inflation applied to model state ensembles just prior to state update calculations. Fixed values of key parameters are included in Table 6-1. More detail on perturbing model inputs and states for ensemble generation follows. The ensemble mean of each simulation is taken as the modelled estimate of the truth.

Table 6-4: *Meteorological forcing variables perturbed for ensemble generation. Comparisons between Kyeamba Creek and Wagga Wagga BoM point measurements assisted with estimating the σ (as per Turner et al., 2008) for ensemble generation.*

Forcing variable	Estimated σ for ensembles
Short-wave in	~15%
Long-wave in	~35Wm^{-2}
Precipitation	~60%
Air Temperature	~2˚C
Wind Speed	~45%
Specific Humidity	~0.0007kg/kg

6.5.1 ASSIMILATION OBSERVATIONS

The field observations used for assimilation were sub-sampled from the original one-dimensional observation data sets, guided by daytime satellite overpass times of MODIS and the night-time overpass time of AMSR-E; while AMSR-E recently ceased operation its successor AMSR2 is expected to provide similar data (Imaoka *et al*., 2010). Other studies where the focus incorporated the Kyeamba Creek region found that AMSR-E soil moisture produced from local night-time overpass data was of superior quality to that from daytime data (Draper *et al*., 2009a; Su *et al*., 2013). Hence the soil moisture data were sampled daily at 2am local time, approximating the night-time AMSR-E overpass, while it is acknowledged that AMSR-E data would not always be available every day for this site.

Thermal infra-red related observations – *LE*, *H* and skin temperature – were sampled twice daily at 10am and 2pm local time to represent data available from MODIS for daytime when *ET* is most active. Sampling skin temperature for assimilation on the same time steps as *LE* and *H* provides an important insight into the relative merits of assimilating these different data types, given that the derivation of instantaneous remotely sensed *LE* and *H* uses remotely sensed skin temperature. While these data can also be derived at hourly (MTSAT1R) and bi-weekly (Landsat TM) timescales, only the MODIS timescale is explored here. Pipunic *et al.* (2008) explored the assimilation of bi-weekly *LE*, *H* and skin temperature and found that they resulted in much poorer results than for MODIS intervals. Since clouds can obscure remotely sensed TIR data, which relate to skin temperature and hence also *LE* and *H* observations, further sub-sampling of these observations at MODIS overpass times was performed for cloud free conditions (defined here as where incoming solar radiation for the site was greater than 90% of expected clear sky radiation for the day). Cloud screening for real MODIS data would likely involve greater complexity and uncertainty, especially with partial cloud cover, compared to the procedure using in-situ ground data adopted here. The frequency of assimilated observations is displayed on plots of simulation results in Figs. 6.2 through to 6.4.

The root mean square error between eddy covariance *LE* and *H* data before and after closing the energy balance is ~40 Wm^{-2} each. A review of derivation methods for TIR based remotely sensed heat fluxes by Kalma *et al*. (2008) found the average root mean square error for such data to be ~50 Wm^{-2} based on a survey of validation studies. Consequently, this value was used here for the assimilated *LE* and *H* uncertainty. For soil moisture, a value of 0.04 vol/vol was used. While in-situ calibration results indicated an uncertainty of ~0.02 vol/vol, this was increased for consistency with errors in satellite derived observations for a similar Australian environment (Draper *et al*., 2009a). As direct TIR data were not available, skin temperature observations were derived using measured outgoing longwave radiation by solving for the temperature term in the Stefan-

Boltzmann equation using an assumed emissivity of 0.98 (Wan & Dozier, 1996). The uncertainty range used for these observations was 2 K, based on some error range estimates for remotely sensed skin temperature quoted in literature (e.g. Kaleita & Kumar, 2000; Sun *et al.*, 2004; Wang & Liang, 2009).

The shallowest volumetric soil moisture measurements made were 0-8 cm and consequently these were the observations assimilated. They correspond exactly with the depth averaged values over the top two CBM soil layers (2.2 and 5.8 cm respectively) but exceed the observation depth of real AMSR-E soil moisture data (~1-2 cm), which might have implications for appropriately representing remotely sensed data assimilation.

In a synthetic study by Walker *et al*. (2001b) the depth of assimilated soil moisture data had no significant influence on the time taken to retrieve the deeper root-zone moisture profile, although the authors note that the ability to impact the deeper moisture profile from assimilating near-surface observations depends on the correlation between soil moisture states over depth. A more detailed synthetic study by Kumar *et al*. (2009) spanning multiple years, and using multiple LSMs with different subsurface physics and soil layer depths, found that when the coupling between the surface and root-zone is stronger the benefit of assimilating near-surface soil moisture observations to improve root-zone prediction is higher.

To the authors' knowledge, no studies using real data for a broad range of observation depths exist in the literature, thus it is not clear to what extent the measurement depth can influence root-zone impacts in real systems. The possibility exists that the 0-8 cm near-surface soil moisture used here might sometimes have a stronger correlation with the root-zone compared to the top ~1-2 cm, and thus its assimilation may also have an overstated impact on the root-zone compared to assimilating data for the shallower AMSR-E product depth. It was not possible to investigate this issue here as the 0-8 cm measurements were the shallowest available, hence why only satellite overpass repeat intervals were considered in relation to representing remotely sensed moisture data.

6.5.2 OBSERVATION MODEL BIAS REMOVAL

Prior to assimilation, the in-situ near-surface soil moisture used for assimilation was rescaled, to eliminate systematic differences relative to the CBM predicted near-surface soil moisture series from Open-Loop, both in terms of its annual mean and its standard deviation. For skin temperature there was no significant difference in terms of the mean and standard deviation between observations and comparable Open-Loop predictions (based on an F-Test for variances followed by a t-Test for means assuming equal variances) hence this data series was not rescaled. The soil moisture rescaling was applied using:

$$\theta_{Obs}^{'} = \left(\theta_{Obs} - \mu(\theta_{Obs})\right) \times \left(\sigma(\theta_{CBM}) \Big/ \sigma(\theta_{Obs}) \right) + \mu(\theta_{CBM}) \,, \tag{6.2}$$

where the rescaled near-surface soil moisture observations $\theta_{Obs}^{'}$ used for assimilation were calculated using the mean (μ()) and standard deviation (σ()) of the 0-8 cm observed series (θ_{Obs}), and of the series of CBM Open-Loop moisture predictions depth averaged over 0-8 cm (θ_{CBM}) for coincident time steps in the experiment period.

6.5.3 ASSIMILATION IMPLEMENTATION AND ASSESSMENT

Different ensemble sizes were tested with the EnKF and 20 ensemble members were found to be sufficient for use with the CBM, congruent with earlier findings from the synthetic-twin study by Pipunic *et al*. (2008). Ensemble generation involved adding random perturbations to model initial conditions and forcing data, and to observations as ensembles of observations were assimilated. Perturbations were derived from random numbers generated with a normal distribution around a mean (μ) of zero with a standard deviation (σ) equal to the estimate of the error standard deviation of the particular data being perturbed. Ensembles were produced such that members were spread within the 95% confidence interval (C.I.) as determined from the assumed data uncertainty.

For observations (treated as ensemble means), the σ values were based on the estimates of observational uncertainties in Table 6-3. Ensembles of initial model state conditions were generated from the spun-up initial soil moisture and temperature values. While initial state perturbations do not persist in contributing to long-term ensemble error representation (unlike forcing perturbations which apply throughout a simulation time series) they were used for initiating the ensemble spread with values of σ=0.03 vol/vol selected here for perturbing initial soil moisture and σ=3° C for perturbing initial soil temperature in each layer. The approach of Turner *et al.* (2008) was used as a guide for generating meteorological forcing ensembles, which factors in measurement error and representative errors when using forcing data from multiple point locations. Both flux station site forcing data and data from the ~20km distant Wagga Wagga BoM station (for gap filling) were used here – discrepancies between the full 2005 series of these two datasets were used to estimate representative error for each variable (based on Turner *et al.*, 2008). The approximate errors relating to ensemble generation are included in Table 6-4.

Given that model structural error or parameter uncertainty were not specifically accounted for in the ensemble generation, and with the potential for filter divergence to affect EnKF performance over time, covariance inflation (e.g. Anderson & Anderson, 1999) was applied prior to updating at assimilation times. It was applied by adding small perturbations to each state ensemble member to slightly increase the spread about the mean prediction. For the CBM near-surface soil layer (2.2 cm thick), soil moisture ensemble members were inflated by adding random perturbations generated with σ=0.01 vol/vol, while σ=1°C was used for soil temperature. These σ values ensured a small inflation of ensemble spreads to increase the likelihood that state error quantities associated with unknown parameter and model structure errors are factored in at update times. For additive inflation of subsequent deeper soil layer ensembles, σ values were scaled down fractions of the values used for the surface layer, with the scaling based on the ratio between the surface layer thickness and each subsequent layer's thickness. This was to account for the expectation that random state errors are dampened with the deeper/thicker soil layers, which has implications for state error correlations between layers, and hence EnKF error covariances and filter performance. The use of covariance inflation and basic assumptions about error correlations are employed here in the absence of a complete understanding of all errors that would enable optimal depictions of them with predicted ensembles. A detailed investigation for understanding all aspects of model error is a major task beyond the scope of this study.

Assessments of the model simulations were made by comparing predictions with independent field data for the variables of interest – *ET*, root-zone soil moisture, and surface and root-zone soil temperature. Root Mean Squared Error (RMSE) and Nash Sutcliffe coefficient of efficiency (E) metrics for quantifying magnitudes of error, and the coefficient of determination (R^2) for quantifying the goodness of fit in terms of variance, were used to assess simulation predictions against the independent field data. Prior to these assessments, state variable predictions from all simulations (Open-Loop and assimilation experiments) were rescaled so that their mean and standard deviation matched that of the corresponding time series of independent field observed states used for comparison (by substituting relevant values into Eq. (6.2)). This ensured that the subsequent state comparisons were bias free relative to the best available representation of the true states as observed with in-situ soil temperature probes and soil moisture probes that were calibrated for the site.

Soil moisture comparisons were made for two different depths, including the near-surface (0-8 cm) representing the depth of the assimilated soil moisture observations (as a sanity check) and the deeper 0-60 cm profile (an average of 0-30 cm and 30-60 cm field observations) corresponding to the estimated vegetation root-zone. For soil temperature, comparisons were made between the shallowest observation (2 cm) and the top soil layer in the model (0-2.2 cm), being the prognostic temperature variable linked to the *LE* and *H* soil component calculations. A weighted average of soil temperature measurements throughout the soil profile was used for comparison with the model root-zone (0-60 cm) prediction.

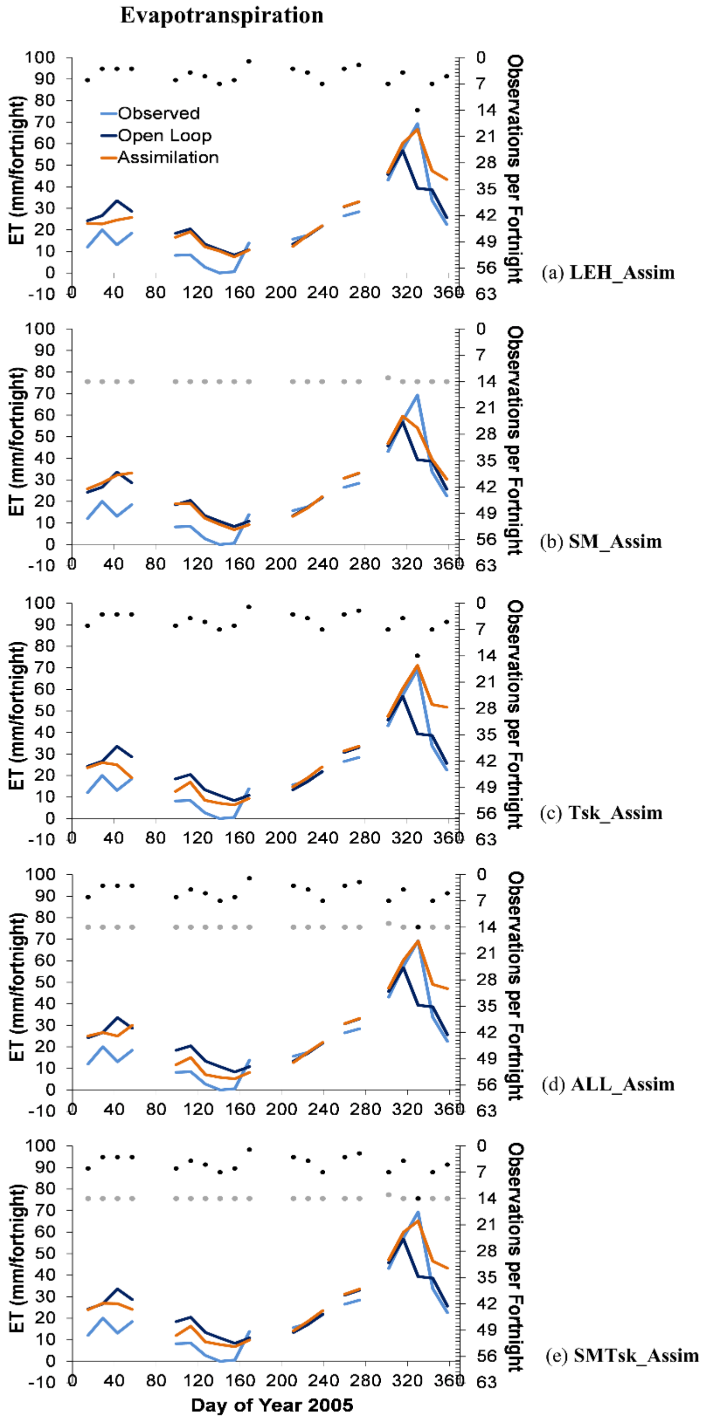

Figure 6.2: *Plots of fortnightly ET totals for Kyeamba Creek showing: Observed validation series, Open-Loop simulations, and from top to bottom the assimilation experiment outputs from a) LEH_Assim; b) SM_Assim; c) Tsk_Assim; d) ALL_Assim; and, e) SMTsk_Assim. Dots along the top of each plot correspond to the assimilation frequency (right hand axis) for LE, H and skin temperature observations (black), and soil moisture observations (grey).*

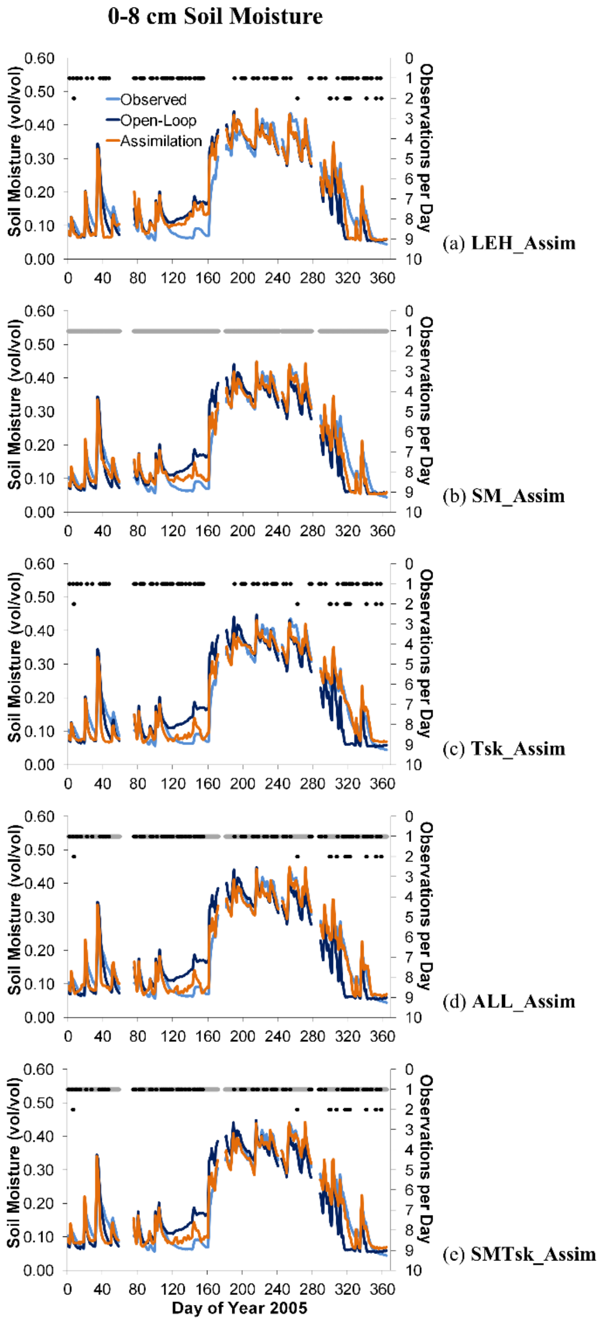

Figure 6.3: *Plots of daily averaged (midnight to midnight) soil moisture for Kyeamba Creek showing: Observed validation series, rescaled Open-Loop simulations and in each row the rescaled assimilation experiment outputs from a) LEH_Assim; b) SM_Assim; c) Tsk_Assim; d) ALL_Assim; and, e) SMTsk_Assim. Dots along the top of each plot correspond to the assimilation frequency (right hand axis) for LE, H and skin temperature observations (black), and soil moisture observations (grey).*

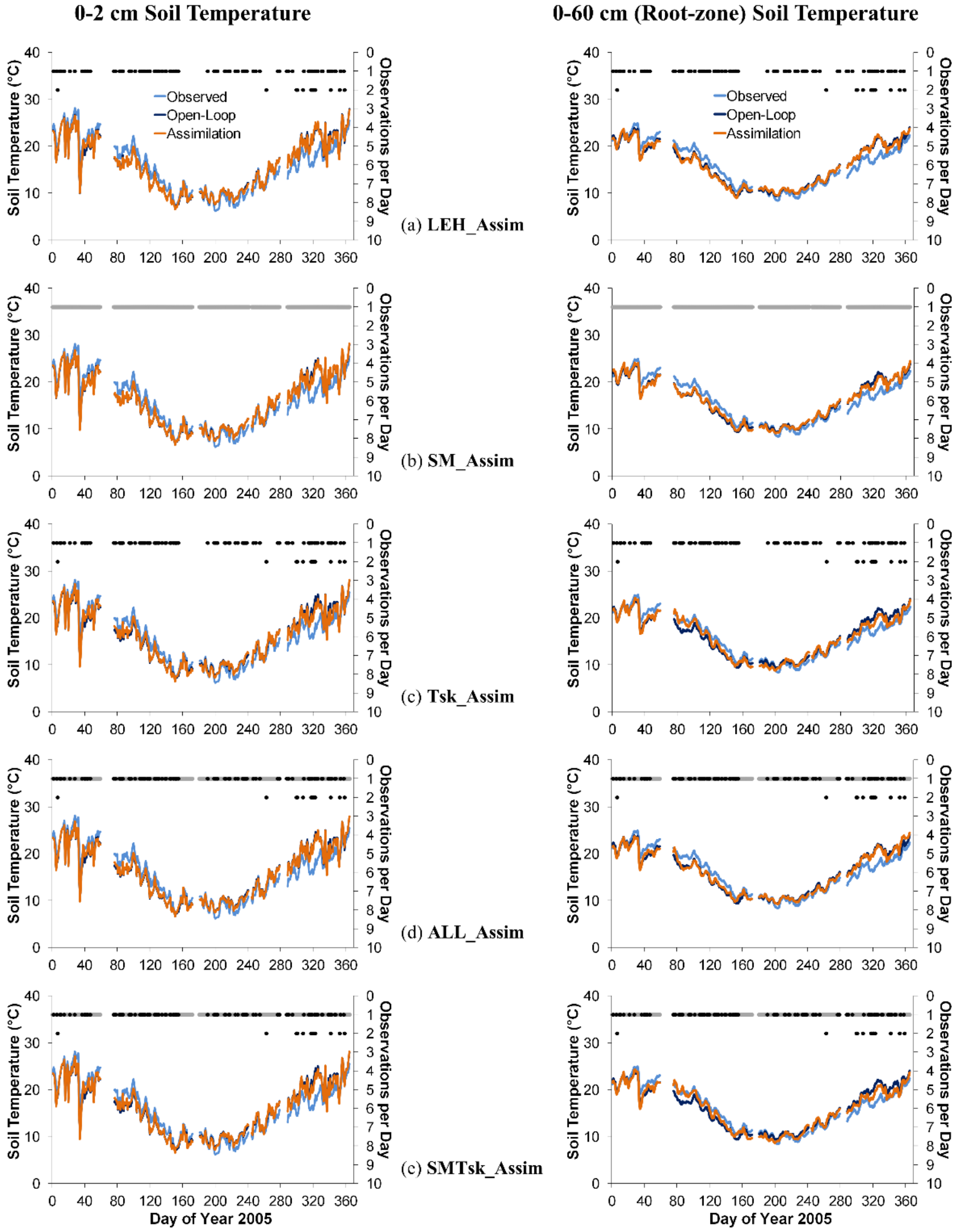

Figure 6.4: *Plots of daily averaged (midnight to midnight) soil temperature for Kyeamba Creek showing: Observed validation series, rescaled Open-Loop simulations and in each row the rescaled assimilation experiment outputs from a) LEH_Assim; b) SM_Assim; c) Tsk_Assim; d) ALL_Assim; and, e) SMTsk_Assim. Dots along the top of each plot correspond to the assimilation frequency (right hand axis) for LE, H and skin temperature observations (black), and soil moisture observations (grey).*

6.6 RESULTS

Fortnightly totals of *ET* were calculated from 30 minute simulation outputs in order to compare with the independent *ET* series that was derived directly from field observed data. Therefore a fortnightly scale was the smallest time unit for which *ET* comparisons were made. It is acknowledged that for NWP the diurnal surface heating is very important and hence comparisons for the full series of 30 minute heat flux predictions would be informative. However, it was not possible to make independent comparisons at a 30 minute time step here, given the available validation data. Comparisons for soil moisture and soil temperature were both made using daily averaged (midnight to midnight) values from the 30 minute observed and simulated series. Rescaling the simulated series of these states to match the observations was applied to the daily averages prior to any comparisons.

Figs. 6.2 to 6.4 are time series plots showing observed site data together with simulation predictions and the frequency of assimilated observations included across the upper horizontal axis. Each vertical sequence of five plots in the figures shows simulation results from a separate assimilation experiment. Qualitative descriptions comparing simulated and observed time series based on these plots are presented in following sub-sections. Quantitative comparisons for all experiments in the form of RMSE, E and R^2 values between observed and simulated values are provided in Table 6-5. These scores were calculated using the data on the same time scales on which they are plotted in Figs. 6.2 to 6.4 and highlight the best performing simulation(s) overall relative to observed validation data. Fig. 6.5 shows the changes made by each experiment in terms of RMSE between observations and predictions relative to RMSE between Open-Loop predictions and observations.

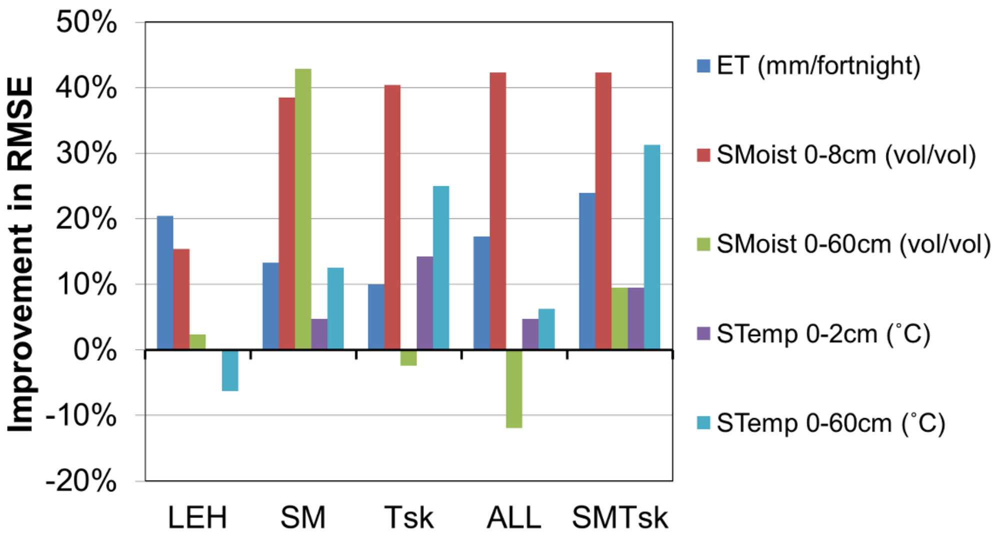

Figure 6.5: *Comparative improvements over Open-Loop made by each assimilation experiment in terms of RMSE reduction for heat flux and soil state predictions.*

Table 6-5: *Statistics for comparisons between simulations (rows) and independent observations over the 2005 experiment period, calculated after removing biases for state variables. Bold values indicate most improvement to simulated values of interest (Columns).*

	ET (mm/fortnight)			**SM 0-8cm (vol/vol)**			**SM 0-60cm (vol/vol)**			**ST 0-2cm (˚C)**			**ST 0-60cm (˚C)**		
	R^2	***RMSE***	***E***	R^2	***RMSE***	***E***	R^2	***RMSE***	***E***	R^2	***RMSE***	***E***	R^2	***RMSE***	***E***
Open-Loop	0.71	10.8	0.63	0.83	0.052	0.82	0.84	0.042	0.83	0.86	2.1	0.86	0.88	1.6	0.88
LEH_Assim	0.88	8.6	0.76	0.88	0.044	0.87	0.85	0.041	0.84	0.86	2.1	0.86	0.87	1.7	0.86
SM_Assim	0.83	9.4	0.72	**0.94**	0.032	0.93	**0.95**	**0.024**	**0.95**	0.87	2.0	0.87	0.90	1.4	0.90
Tsk_Assim	0.85	9.8	0.70	**0.94**	0.031	**0.94**	0.83	0.043	0.82	**0.89**	**1.8**	**0.89**	0.93	1.2	0.93
ALL_Assim	0.87	9.0	0.75	**0.94**	**0.030**	**0.94**	0.80	0.047	0.79	0.88	2.0	0.88	0.89	1.5	0.89
SMTsk_Assim	**0.89**	**8.2**	**0.78**	**0.94**	**0.030**	**0.94**	0.87	0.038	0.87	**0.89**	1.9	0.88	**0.94**	**1.1**	**0.94**

6.6.1 OPEN-LOOP COMPARISONS

6.6.1.1 OPEN-LOOP ET OUTPUT

Differences between predicted *ET* from Open-Loop and the estimates from observations vary across the experiment year (Fig. 6.2). From the austral summer at the start of the year through to early winter at around DoY 160, the observation derived *ET* was over-predicted by as much as ~20 mm/fortnight (~DoY 40). Therefore, possibly too much of the rainfall in this period became *ET* via the model, presumably due to inaccurate soil and vegetation parameters and/or physical processes in the model, and hence incorrect soil moisture (in both the near-surface and root-zone – Fig. 6.3). As noted in section 6.4 the observed 60-90 cm moisture series, beneath the root-zone as defined here, is static throughout this period ruling out any groundwater contribution. Another contributing factor may be that time invariant root distribution in the model over-states the amount of water drawn for transpiration from deeper soil in periods where grass is shorter and its growth is sparse around the site (especially where Open-Loop root-zone moisture is over-estimated). The vegetation cover in this period from the beginning of the year to ~DoY 160 is minimal where *LAI* values range from 0.39 to 0.85 with a mean of 0.53.

Through the winter and most of spring (from DoY 160 to 316) where most of the observation based *ET* values were set to the calculated potential *ET*, in what is predominantly an energy limited period with relatively high moisture storage in the soil profile for the year, Open-Loop *ET* predictions track the observation series closely with the only noticeable difference being negligible over-predictions of ~5 mm/fortnight occurring for the ~DoY 260 and 274 totals. This close match is not surprising given that with high water availability in the soil profile the CBM is expected to predict *ET* close to the potential rate.

After DoY 316 to the end of the year (most of November through December) is where the largest discrepancies occur, with observed *ET* under-predicted by Open-Loop by as much as 30 mm/fortnight. This period is characterised by warming where the high soil moisture storage of winter/spring transitions to a water limited scenario with increased incoming radiation, and where high vegetation cover for November (*LAI* of 3.0) declined in December (*LAI* of 1.21). As discussed in section 6.4 there is evidence indicating possible groundwater interaction around DoY 311 (refer to Table 6.2). Thus any water added to the soil profile as a result could have contributed to root-zone water availability for *ET* over the following days or weeks. This may explain the large under-prediction of *ET* by Open-Loop after DoY 316, as the only water supply information available for CBM calculations was from rainfall forcing data.

6.6.1.2 OPEN-LOOP SOIL MOISTURE OUTPUT

Plots in Fig. 6.3 also show variation in differences between Open-Loop soil moisture predictions and observations throughout the experimental period. Early in the year through summer and autumn (to ~DoY 120), the depletion of Open-Loop soil moisture compared to observations for the near-surface assimilation depth (0-8 cm) is from higher peak values and up to twice as fast in parts, particularly in early February (~DoY 35-40) where the peak is over-estimated by ~0.09 vol/vol. Following on, between ~DoY 120 and 160, the observations indicate a mostly dry period where they are increasingly over-estimated. Much of these discrepancies from the beginning of the year to ~DoY 160 are consistent with Open-Loop over-estimating *ET* in this period. The response of the Open-Loop near-surface soil moisture at ~DoY 160 in June to the beginning of the major increase in winter/spring moisture storage is accurately timed, with some over-estimation persisting through the first half of this period. In the spring/summer dry-down period there is another large discrepancy, with the Open-Loop under-estimating observations by as much as ~0.15 vol/vol, which is again consistent with the *ET* under-estimation in this period (Fig. 6.2).

Deeper root-zone (0-60 cm) soil moisture content from Open-Loop shows a similar relationship in terms of variation with respect to observations as for the near-surface moisture plots, albeit with the magnitude of variations being less pronounced. In particular, the over-estimation and more rapid depletion of root-zone moisture compared to observations for instances in the first ~100 days and under-estimation around ~DoY 320-330 (Fig. 6.3) are consistent with the respective over-estimation and under-estimation of *ET* for periods incorporating these times (Fig. 6.2). As noted in relation to *ET* predictions, inaccurate model parameters could have contributed to discrepancies between Open-Loop predictions and observations here, while the inability to prescribe different soil parameters with depth for different model layers might also be a contributing factor.

6.6.1.3 OPEN-LOOP SOIL TEMPERATURE OUTPUT

Surface soil temperature plots (0-2 cm) in Fig. 6.4 show a general pattern of Open-Loop predictions under-estimating observations in the drier austral summer/autumn period up to ~DoY 150. Then across the first half of winter from June to mid-July (~DoY 150-200) which includes some of the coolest temperatures of the year the Open-Loop tracks the observations very closely. From mid-winter until the end of the year as the temperature increases, predictions mainly over-estimated the observations with the largest differences (up to 6°C) occurring in November between ~DoY 310-330 – the period in which Open-Loop soil moisture and *ET* predictions under-estimated their respective observations by relatively large magnitudes (Figs. 6.2 and 6.3) and where groundwater interaction is a possibility (Table 6-2).

As with soil moisture, the deeper 0-60 cm root-zone soil temperature predictions from Open-Loop exhibit a similar pattern of discrepancy with observations as for the near-surface soil temperature. The main difference being the root-zone series has less day-to-day variation, as expected, and the differences with observations are sometimes slightly less in magnitude than the corresponding differences for near-surface soil temperature.

6.6.2 ASSIMILATION COMPARISONS

6.6.2.1 ASSIMILATION ET OUTPUT

From the beginning of the year up to early winter at ~DoY 160, where Open-Loop *ET* predictions over-estimate observations (Fig. 6.2), the best overall improvements to *ET* were from simulations where the assimilation involved skin temperature observations and combinations of variables (i.e. Tsk_Assim, ALL_Assim and SMTsk_Assim). The only notable impact from LEH_Assim here was in the summer with some improvement within the first ~60 days. When only soil moisture was assimilated (i.e. SM_Assim), no notable impact or improvement was made to *ET* estimates for this entire period.

Through the mainly energy limited period with increased moisture availability that covers most of winter/spring (between ~DoY 160 to 316), where observed and Open-Loop *ET* series are at or near potential *ET* with no notable differences between them, the predictions from every experiment were maintained at approximate potential *ET* values. While each assimilation experiment made clear improvements to *ET* in the period between DoY 316 and ~DoY 330-340, where Open-Loop under-estimated the observed series most. All of the experiments except for SM_Assim resulted in very close matches to the maximum observed *ET* at ~DoY 330 although unlike SM_Assim they caused over-estimation from ~DoY 340 onwards where Open-Loop and observations were relatively close.

6.6.2.2 ASSIMILATION SOIL MOISTURE OUTPUT

From the beginning of the year through to ~DoY 160, being before the major winter/spring moisture storage period, predictions of near-surface soil moisture (0-8 cm) were improved overall by each data assimilation approach compared with Open-Loop. SM_Assim improvements were the most consistent (Fig. 6.3) while for other approaches where either skin temperature or *LE* and *H* observations were involved in the assimilation, soil moisture was slightly degraded by over-correction at ~DoY 40-50 during the dry-down after high rainfall. Improvements to near-surface soil moisture were also made by each simulation over the remainder of the year after ~DoY 160, with simulations involving skin temperature observations (i.e. Tsk_Assim, ALL_Assim and

SMTsk_Assim) performing particularly well over the spring to summer dry-down period post ~DoY 310. The consistency of SM_Assim in making some improvement across all seasons of the experiment year in relation to near-surface moisture observations (the 0-8 cm series which assimilated observations were sampled from) instilled confidence in the assimilation scheme.

For root-zone soil moisture, SM_Assim produced the best overall improvement across the year. Predictions from the other simulations which involved skin temperature and/or heat flux observations in the assimilation were poorest and most degraded in drier periods within the first half of the year and at the end post ~DoY 320 (Fig. 6.3a, c, d and e). During the wetter winter/spring period these simulations performed reasonably well, improving parts of the root-zone moisture series and without any extreme degradation. In this period the moisture content was more uniform over the root-zone and near-surface moisture dynamics were more strongly correlated with dynamics through the root-zone depth.

A possible reason for the better and more stable results in the wetter period is that the ensemble generation might have produced more adequate error representations for predicted observations and predicted root-zone moisture states here. In which case the resulting EnKF error covariances would have been a good reflection of actual error correlations between these predictions, hence the more reasonable root-zone moisture state updates. Compared to wetter seasons, moisture dynamics were more weakly connected through the root-zone in drier periods where greater contrasts in moisture over depth occurred – e.g. such as wetter near-surface soil from isolated rain events compared to drier deeper soil. The degraded root-zone moisture in drier periods from most simulations may have been due to poorer error representations for these particular conditions, such that EnKF covariances did not adequately reflect error correlations between predictions of assimilated observations and the different root-zone soil moisture states.

6.6.2.3 ASSIMILATION SOIL TEMPERATURE OUTPUT

Fig. 6.4 illustrates soil temperature outputs from all simulations for the CBM surface soil layer (0-2.2 cm) and root-zone (0-60 cm). The relevance of the surface soil layer temperature here is its use in the soil component of the CBM calculated total skin temperature (Eq. (6.1)), and also in the calculation of soil components of *LE* and *H*. Assimilation impacts on the surface soil layer temperature appear relatively minor across all of the simulations, and any impacts that were made are most noticeable for warmer periods, including from ~DoY 40 to 100 in the first half of the year and towards the end of the year from ~DoY 300 to 340 where the impact on *ET* was greatest from all assimilation approaches. The best improvements for these periods were from Tsk_Assim, which is expected due to the surface soil layer temperature being linked directly to skin temperature in the CBM.

For periods of high vegetation cover, such as the second half of the year (where LAI is 2.4 for July, 3.0 from August through November, and 1.2 for December), the direct impact on heat fluxes from any surface soil layer temperature state adjustments were minimal. The adjustments to *ET* at the end of the year (> ~DoY 316) from Tsk_Assim are assumed to be related to impacts on soil moisture (compare Figs. 6.2c and 6.3c). This is likely due to the vegetation canopy components of *LE* and *H* in the CBM dominating the total predicted values of *LE* and *H* in this period, where the vegetation canopy surface temperature used in the CBM vegetation heat flux calculations (also for the vegetation component of skin temperature – see Eq. (6.1)) is based on the non-prognostic leaf temperature variable. Hence, for the LEH_Assim simulation there is very little impact on surface soil layer temperature for the period at the end of the year from ~DoY 316 onwards (Fig. 6.4a), which coincides with some of the greatest adjustments to *ET* predictions (Fig. 6.2a). While for ~DoY 40 where LEH_Assim had some noticeable impact on correcting surface soil layer temperature, coinciding with an adjustment to *ET*, there is minimal vegetation cover (LAI of 0.6) and therefore surface soil layer temperature values feature more prominently here in calculated *LE* and *H* totals from the CBM.

The experiments Tsk_Assim and SMTsk_Assim made the greatest changes/improvements to root-zone soil temperature predictions reinforcing that skin temperature observations are the main driver for soil temperature state impacts. From Figs. 6.4c and e, the greatest improvements were made in the first half of the year between ~DoY 80 to 160 where vegetation cover was low and the Open-Loop under-estimated observations, and also towards the end of the year post ~DoY 280 incorporating the period where vegetation cover was highest and also where *ET* adjustments were greatest. LEH_Assim and SM_Assim had minimal overall impact on root-zone temperature across the year by comparison (Figs. 6.4a and b), with root-zone soil temperature generally lacking a strong relationship with heat fluxes, particularly as vegetation cover increases (in the second half of the year).

6.7 DISCUSSION

Based on the results presented, the overall differences between simulations are summarised and interpreted here. From the R^2 and E scores for Open-Loop predictions (Table.6-5) the dynamics of the validation *ET* data series in this study were generally more difficult to simulate than near-surface and root-zone soil moisture and temperature observations. LEH_Assim was expected to produce amongst the best *ET* predictions given that state updates were driven only by heat flux observations. While it led to a strong reduction in RMSE of 20% compared to predictions from Open-Loop, the level of improvement trailed that made by SMTsk_Assim which reduced RMSE by 24% but was greater than improvements from ALL_Assim which reduced RMSE by 17%. The comparative improvements between these three simulations are supported by all of the metrics used. Although these were the top three performers for *ET* amongst all of the experiments, their impact on root-zone soil moisture predictions were varied, with ALL_Assim producing the most degraded results of all experiments, SMTsk_Assim making fairly solid improvements, and LEH_Assim making only minor overall improvement.

The relatively poor impact LEH_Assim had on state variables in contrast to strong *ET* improvements as per the quantitative scores highlights the challenge of simultaneously improving all state variables and heat fluxes given the inherent uncertainties associated with complex relationships between them in LSMs. Scores for SM_Assim and Tsk_Assim indicate they made amongst the greatest improvements to soil moisture and temperature state variables respectively along with SMTsk_Assim which performed well for both. This supports the expectation that assimilated observations will usually lead to strong improvements for the most directly related model variables.

Despite SM_Assim producing the best root-zone soil moisture with a reduction in RMSE of over 40%, the corresponding reduction in RMSE of 13% for *ET* indicates only a modest improvement relative to validation data compared with other experiments. When considered together with the top three experiments for *ET* improvement which had varied impacts on root-zone soil moisture, it is clear that specifically improving root-zone moisture will not necessarily optimise the heat flux predictions. Moreover, the inconsistency between quantitative soil temperature scores for SMTsk_Assim and LEH_Assim, which both strongly improved *ET*, and between the strong soil temperature and only modest *ET* improvements from Tsk_Assim compared to those from LEH_Assim, supports the qualitative time series interpretations (discussed in the previous section) that improved soil temperature prediction does not always make a strong contribution to *ET* improvement throughout the whole year – particularly as vegetation cover increases.

Comparing the impacts on *ET* from LEH_Assim and from experiments using skin temperature and no heat flux observations is of particular interest when considered in a remote sensing context. LEH_Assim represented the assimilation of *LE* and *H* data which would first need to be derived from thermal and visible remote sensing imagery using an energy balance model separate to the LSM. However, remotely sensed skin temperature represented in Tsk_Assim and SMTsk_Assim is more directly available from the thermal imagery used in deriving *LE* and *H*. The results for *ET* prediction from both SMTsk and LEH_Assim (Table 6-5 and Fig. 6.5) indicate that there may be no significant benefit from assimilating remotely sensed *LE* and *H* over using skin temperature together with an observation directly related to the water balance (i.e. soil moisture) for improving heat flux prediction, especially when considering the additional modelling required to produce remotely sensed *LE* and *H*.

Quantitative results for the SMTsk_Assim experiment highlight some clear benefits of multi-observation assimilation. It produced the greatest improvements to *ET* relative to validation data of any experiment, presumably due to cumulative positive impacts from the different observations used, which when assimilated separately each improved *ET* to lesser degrees (through Tsk_Assim and SM_Assim experiments). The multi-observation approach of ALL_Assim also produced relatively strong *ET* improvements, but was inconsistent in terms of state variable improvements, with root-zone soil moisture having been degraded more than from any other experiment. This may be due to the combined impact of *LE*, *H* and skin temperature (which produced poor or degraded root-zone soil moisture via LEH_Assim and Tsk_Assim) outweighing any beneficial impacts from the soil moisture observations. The worst impacts on root-zone moisture from ALL_Assim were mainly for drier periods, which is congruent with the worst impacts from LEH_Assim and Tsk_Assim (compare Figs. 6.3a, c and d).

The SMTsk_Assim multi-observation approach and SM_Assim were the only simulations in this study which simultaneously improved predictions of all of the assessed variables against validation data (Table 6-5 and Fig. 6.5). This demonstrates that assimilating soil moisture and directly impacting the model water balance improved soil state variables and *ET*, while incorporating an additional observation type linked directly to model energy balance calculations (skin temperature) could still lead to improved state variables, and most importantly in the NWP context, also produce optimal *ET* predictions. The added benefit of SMTsk_Assim is of course the potential for good *ET* prediction while avoiding the intermediate modelling step to estimate *LE* and *H* from thermal and visible imagery when assimilating remotely sensed data.

The varying assimilation results during the year, and particularly the degradation caused by some of the assimilation scenarios, point to the likelihood of systematic model errors. As an example, the root distribution in CBM soil layers is represented by user prescribed parameter values which are time-invariant. With a seasonally varying vegetation cover (see *LAI* range in Table 6-1) it is likely that rooting depth varies with different growth phases, and thus the connection between *ET* and deeper layer soil moisture in the model may be overstated for periods of sparse vegetation cover. This may also explain the excessive reduction in root-zone soil moisture from LEH_Assim and Tsk_Assim in the first half of the year, coinciding with reductions in *ET* (Figs. 6.2a-6.3a and 6.2c-6.3c). These errors are likely to be quite intricate and require more detailed data than is available here to properly address. It is also worth noting that in this respect uncertainties in the subsurface (soil properties, root water extraction profiles, etc.) are severe. Progress in this area may result in more accurate estimates of error covariances and hence better assimilation outcomes overall.

6.8 CONCLUSIONS

This paper has presented one-dimensional Open-Loop and various data assimilation runs of the CBM for a temperate grassland site in southern New South Wales, Australia. Comparisons between Open-Loop and validation data suggest that accurate modelling of heat fluxes is most difficult for water limited scenarios where *ET* rates are below potential. This is evident from the poorer Open-Loop predictions of *ET* in the first ~60 days of the year spanning late summer and through all of autumn where the soil profile is mostly at its driest, and for a period towards the end of the year around the spring/summer transition where moisture storage is below maximum. Exact causes of the poorer predictions are likely to be varied, including parameter uncertainty, model structural limitations, and possibly isolated instances of groundwater contribution where rainfall forcing data may not have accounted for the total water supply for the LSM water balance.

Five different assimilation runs were conducted using real field data for a selection of times corresponding to approximate satellite overpasses relevant to each data type: latent and sensible heat (LEH_Assim); 0-8cm soil moisture (SM_Assim); skin temperature (Tsk_Assim); all four of these (ALL_Assim); and 0-8cm soil moisture combined with skin temperature (SMTsk_Assim). It was demonstrated that the multi-observation approach of SMTsk_Assim produced the greatest improvements to *ET* relative to validation data constructed from independent field observations. This is to be contrasted with the traditional SM_Assim approach which led to the strongest root-zone soil moisture improvements but with relatively modest *ET* improvements. Thus accurate root-zone soil moisture prediction does not necessarily translate to optimal heat fluxes.

The LEH_Assim approach made strong improvements to *ET* as expected, second only to those from SMTsk_Assim. From a remote sensing perspective this implies that incorporating skin temperature from thermal imagery together with soil moisture observations in the data assimilation may be more beneficial to LSM heat flux accuracy than assimilating *LE* and *H* alone, which first needs to be derived using the same thermal imagery via a separate energy balance model. A major strength of SMTsk_Assim in this study was in balancing impacts on the model energy and water balances to improve both soil moisture and temperature states in addition to *ET*.

Consequently, this study demonstrates the value of multi-observation assimilation into a LSM using real observations. This provides a sound basis for further multi-observation assimilation studies using remotely sensed data products, including remotely sensed *LE* and *H* assimilation, to better understand and draw stronger conclusions about its potential benefits.

6.9 ACKNOWLEDGEMENTS

An Australian Postgraduate Award (APA) Scholarship from the Australian Federal Government provided the funds for the lead author Robert Pipunic to undertake this work as part of his PhD research. While at The University of Melbourne, Cressida Savige provided invaluable help in the initial set-up of the eddy covariance system and supporting instrumentation. A University of Melbourne-CSIRO collaborative research grant provided funds for maintenance of the Kyeamba Creek flux station site including operational support for Robert Pipunic's PhD work. The authors sincerely thank Fred Hulm, who allowed the Kyeamba Creek flux station to be installed on his property.

We are extremely grateful to Dongryeol Ryu from the Department of Infrastructure Engineering at The University of Melbourne, Australia, who made time for valuable feedback and provided important advice on key technical aspects of the research methodology. Thanks are also due to Vanessa Haverd at the CSIRO Land and Water division in Canberra, Australia, for helpful comments on the manuscript. From the same division, Tim McVicar provided the fPAR data product for deriving *LAI* values used in simulations. Ying-Ping Wang at the CSIRO Marine and Atmospheric Research division in Aspendale, Australia, provided the CBM code along with helpful advice.

7 REMOTELY-SENSED DATA ASSIMILATION

The one-dimensional study presented in chapter 6 reaffirmed some key findings from the synthetic-twin study (chapter 5) through the use of real field observations on approximate remote sensing timescales. Specifically, assimilating *LE* and *H* was again shown as being able to produce better CBM predictions of *LE* and *H* overall compared with assimilating only near-surface soil moisture. The value of assimilating skin temperature observations to improve *LE* and *H* prediction was also demonstrated in both chapters 5 and 6.

As the final phase in assessing the assimilation of *LE* and *H*, alongside that of data more commonly used in past LSM assimilation studies, this chapter presents assimilation experiments using real remotely sensed data. This has the most direct relevance to spatially distributed modelling as used in NWP (and most model applications for water resource management). There is a greater level of complexity (and hence uncertainty) in this context than for the point based scenarios, especially where the spatial resolution and/or spatial distribution of different data used for simulation input, assimilation and validation differs between variables. The experiments here are confined to comparisons between assimilating remotely sensed instantaneous *LE* and *H* products (the testing of which is a major objective in this thesis) and a near-surface soil moisture product (a product more commonly used for LSM data assimilation).

7.1 EXPERIMENTAL DATA

The *LE* and *H* data used were produced via the SEBS algorithm (Su, 2002) at 5 km spatial resolution and with a minimum time step of once-daily, corresponding to the MODIS AQUA overpass at ~2:00pm local time. They were produced and provided by Prof. Eric Wood and Dr. Raghuveer Vinukollu at Princeton University (*pers. comm.*, October 2008), with Vinukollu *et al*. (2011) describing the production of SEBS data. Near-surface soil moisture data that were assimilated are from AMSR-E observations (the descending satellite overpass at ~2:00am local time), derived via the LPRM algorithm (Owe *et al*., 2008). The model forcing and validation data used, the latter of which includes heat fluxes from the Kyeamba Creek eddy covariance system (used in experiments for chapter 6), and in-situ soil moisture and temperature data from OzNet monitoring stations across the Kyeamba Creek catchment (Smith *et al*., 2012), are described in chapter 4.

The simulation experiments were carried out for the full calendar year of 2005 (as per the experiments in chapter 6), given that *LE* and *H* validation data from the eddy covariance system cover this annual period. Marking out the study domain for assimilation experiments is the single

25 km by 25 km AMSR-E soil moisture data pixel covering most of the Kyeamba Creek catchment (Fig. 4.7). Modelling was performed at 5 km resolution within this domain (with the CBM run as a series of single columns for calculating vertical water and energy fluxes) corresponding to each SEBS data pixel. The meteorological forcing data set is the same as that used in the one-dimensional field data study (see chapter 6) and it was applied across the whole domain. Any spatial variation in CBM predictions (without assimilation) between the 5 km pixels is due to spatial variation in the parameter data (see Figs. 4.8 and 4.9).

Values used for the key model soil parameters of θ_{Wilt}, θ_{FC}, K_s and ρ_s (see Table 3-2, chapter 3), for each simulation pixel, are based on soil property interpretations (McKenzie *et al*., 2000, 2003) associated with soil units of the Wagga Wagga 1:100,000 soil landscape map (Chen and McKane, 1997) shown in Fig. 4.9 (chapter 4). Supplementary data from McKenzie *et al*. (2000) based on the broader scale Atlas of Australian Soils was also used where the 1:100,000 map had no coverage within the study domain, as described in section 4.5. Spatial analysis determined which mapped soil unit had the largest areal coverage within each pixel, and the associated soil parameter values were assigned to pixels accordingly. Values obtained for θ_{Wilt}, θ_{FC}, and ρ_s were used to determine θ_{sat}, ψ_{aep} and Campbell's b parameter values for each pixel using Eq. (2.13) from Campbell (1974) as discussed in section 4.5. For the simulation pixel collocated with the Kyeamba Creek flux station, the same parameter values as used for the one-dimensional field data study (chapter 6) were applied (where ρ_s was determined from analysis of site-sampled soil).

For the key vegetation parameter of *LAI*, values derived from the Donohue *et al*. (2008) fPAR product based on AVHRR data (Fig. 4.8 (2)) were used, where the ~1 km resolution data were spatially averaged within each 5 km simulation pixel. Conversion from the fPAR product to *LAI* is discussed in chapter 6. The plant root-zone was defined uniformly across simulation pixels as ~0-60 cm, with root presence assigned to the top four CBM soil layers (64.3 cm depth in total: see *froot* values in section 4.5) – the same as for experiments in chapter 6 where this depth was based on field estimates from the grass pasture at the flux station site, with pasture being a major land cover type across the study region presented in this chapter. A vegetation canopy height of 25 cm was also applied for all pixels, based on an estimate of the annual average pasture height at the flux station site. For all other parameters not mentioned above in this or the previous paragraph (see Tables 3-1 and 3-2), default values provided with the CBM/CABLE model (Abramowitz, 2006) were applied uniformly across simulation pixels. These include vegetation parameter values associated with the agricultural/C3-grassland category of a global vegetation dataset (Potter *et al*., 1993).

There is an obvious difference in spatial representation that limits the robustness of comparing/validating remotely sensed products and spatially distributed model output with a finite number of point-scale in-situ measurements. However, these are the only independent datasets that were available.

Four of the nine Kyeamba Creek OzNet soil moisture station datasets in the study domain (K6, K7, K10 and K11) are missing near-surface soil moisture records (0-8cm) over the 2005 experimental period, while root-zone soil moisture data (from 0-30 cm and 30-60 cm measurements) are available for all nine including the flux station site. The average of soil moisture for 0-30 cm and 30-60 cm is used to represent the 0-60 cm root-zone soil moisture profile. Fig. 7.1 illustrates the relative location of in-situ stations and simulation pixels, using separate plots that show which pixels are collocated with available in-situ near-surface and root-zone soil moisture data respectively.

Availability of in-situ soil temperature data over the experimental period varies for different depths across OzNet stations within the study domain. Only shallow/near-surface soil temperature data is considered in this study, for which availability is most consistent across the greatest number of sites (compared to ~60 cm root-zone data). As noted in chapter 6, near-surface soil temperature is most relevant to modelled fluxes as only the CBM top soil layer (0-2.2 cm) temperature is directly involved in energy balance calculations. Referring to Fig. 7.1, the shallowest temperature records available are at 4 cm depth at K1, K2, K3, K4 and K5, and for 2 cm depth at the flux station site.

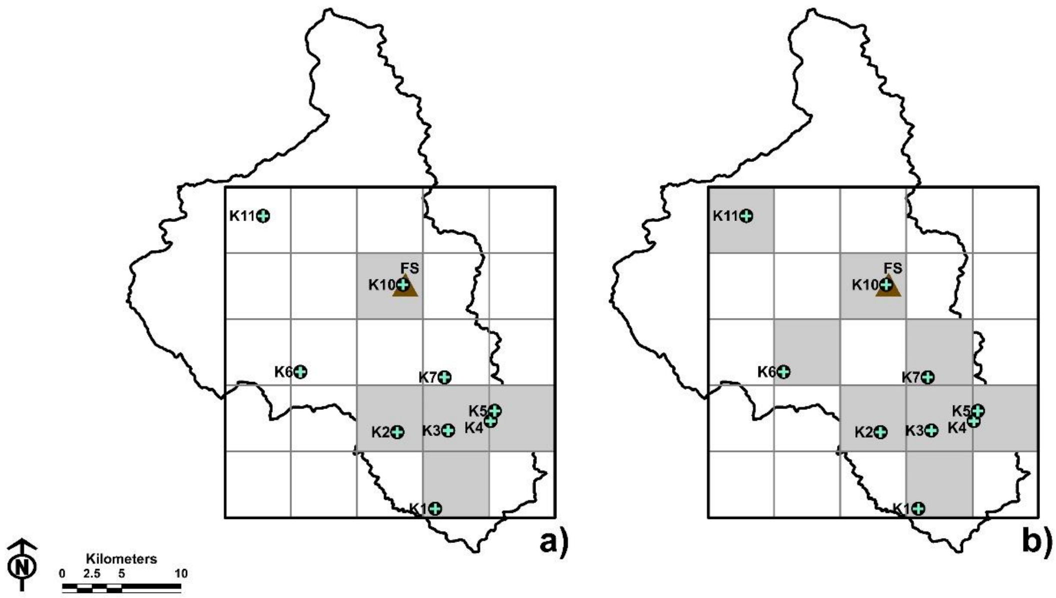

Figure 7.1: *The black 25 km by 25 km modelling domain boundary over the Kyeamba Creek catchment, matching a single AMSR-E pixel, with grey 5 km by 5 km simulation pixels within. Locations of the OzNet stations K1-K7 and K10-11 (Smith et al., 2012) and the flux station (FS) are shown. Shaded simulation pixels highlight coincidence with available in-situ station data for: a) near-surface soil moisture (0-8 cm) and temperature (4 cm at OzNet sites, and 2 cm at FS); and, b) root-zone soil moisture (0-60cm).*

7.1.1 AMSR-E SOIL MOISTURE PREPARATION

The choice to use AMSR-E soil moisture data from descending (~2:00 am local time) satellite overpass observations was based on the evaluation study by Draper *et al*. (2009a) over south eastern Australia (incorporating the study region in this chapter), which showed it had lower error than data from ascending overpasses. A 5-day moving average filter was applied to reduce random noise in the downloaded year-long AMSR-E moisture series, as done by Draper *et al.* (2009a). Most gaps in the once per day (at 2:00 am) series were consequently filled, except where there was fewer than two records within the 5-day averaging window (in which case the whole 5-day window period was left as a data gap). Prior to assimilation, bias was removed between the noise-reduced AMSR-E soil moisture data, and CBM predictions without assimilation (from this point on referred to as Open-Loop_sp) for the top soil layer moisture state (0-2.2 cm), by matching data series means and standard deviations (as done in chapter 6: Eq. (6.2)). Here the AMSR-E data series (for the 25 km by 25 km pixel defining the study domain: Fig. 7.1) was rescaled so that the mean and standard deviation over the year-long experiment period matched that of the Open-Loop_sp moisture series (from the spatial average of predictions across all 5 km simulation pixels within the study domain).

Fig. 7.2 illustrates the AMSR-E descending overpass (~2:00 am) moisture data series for the different stages in its preparation, from the original downloaded series to the final noise-reduced and rescaled series used for assimilation. The uncertainty estimated for the rescaled AMSR-E data (Fig. 7.2), as used for data assimilation, was informed by the AMSR-E moisture evaluation study of Draper *et al*. (2009a). They determined a Root Mean Square Difference (RMSD) of ~0.08 vol/vol for original/unscaled descending overpass data for the Kyeamba Creek region using in-situ data from a number of OzNet stations. Based on the rescaling applied here (Fig. 7.2), the standard deviation of the original AMSR-E moisture series (~0.12 vol/vol) was scaled down by a factor of 2.4 to fit that of the Open-Loop_sp series (~0.05 vol/vol). Applying this factor to the unscaled RMSD uncertainty estimate of ~0.08 vol/vol results in an uncertainty estimate of >0.03 vol/vol for the rescaled AMSR-E moisture series here – which was rounded up to the nearest whole percentage point of 0.04 vol/vol for use in data assimilation.

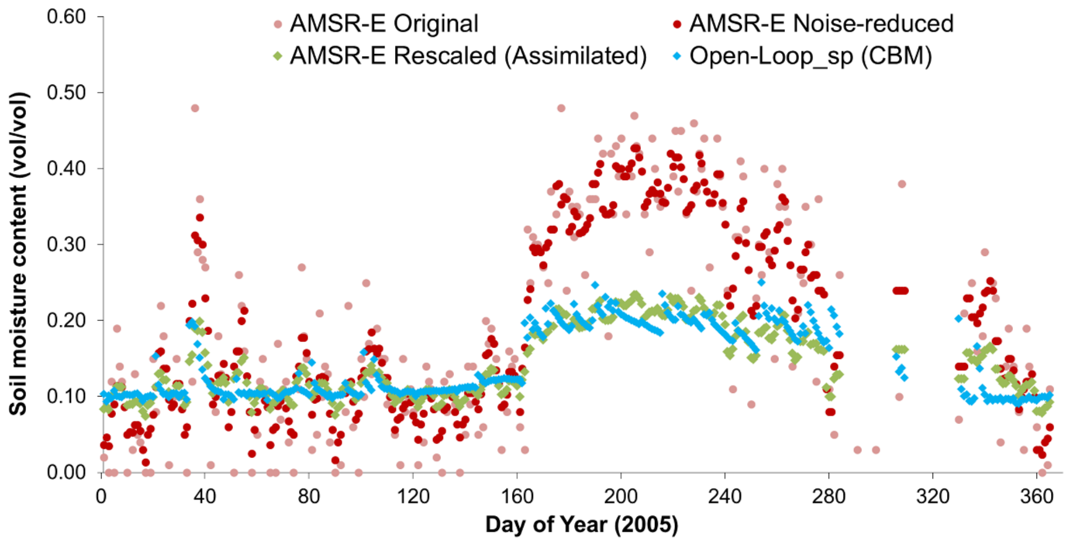

Figure 7.2: *Different series of the daily (~2:00 am) AMSR-E soil moisture data (~1-2 cm) over the experiment period in preparation for data assimilation. The series of Open-Loop_sp soil moisture predictions from the CBM (0-2.2 cm) is also shown, representing spatially averaged predictions across the 25km by 25km study domain, as used for rescaling the AMSR-E series.*

7.1.2 SEBS LE AND H DATA CHECKING

The SEBS estimates of instantaneous *LE* and *H* made available for this research are based on observations of the land surface (including skin temperature) from the AQUA satellite platform at ~2:00 pm (local time) overpasses, and therefore correspond to *ET* active times. Allowing for missing data for numerous days, there are a total of 157 days with 2:00 pm *LE* and *H* records over the 2005 experiment period, with a few pixels in the study domain missing data for some of these days. Prior to assimilation, the SEBS data were checked against eddy covariance flux data to ensure that they were reasonable estimates. The eddy covariance data provides the only independent direct measurements of *LE* and *H* in the study region and therefore comparison was only possible for a single 5 km SEBS pixel (see Fig. 7.1 with FS location marked).

Qualitatively the SEBS *LE* and *H* estimates represent seasonal dynamics reasonably well (Fig. 7.3). There appears to be greater scatter within the plotted data sets for both fluxes in approximately the first ~150 days of the year, which is the warmer/drier (water limited) part of the year, and within which a few relatively large rainfall events occurred (up to ~20 mm in some days). SEBS *LE* values are mostly higher than eddy covariance values across this period, being closer to Open-Loop_sp predictions at times, while SEBS *H* values slightly are lower than eddy covariance values but appear better matched overall, compared with *LE*.

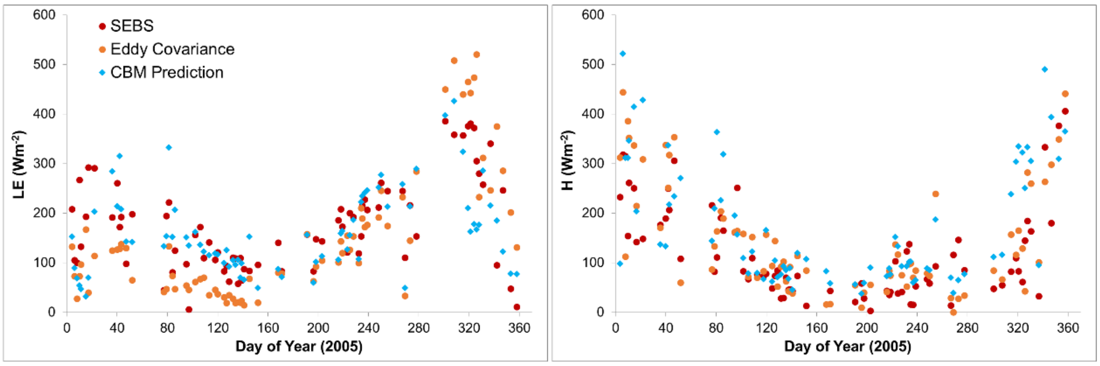

Figure 7.3: *LE (left) and H (right) data from: Kyeamba Creek flux station measurements, SEBS estimates and CBM Open-Loop_sp predictions for the collocated 5 km simulation pixel (Figure 7.1). Plotted points are for the 76 2:00 pm time steps in 2005 for which records coincide in each data set.*

For the austral winter period (DoY ~150 to ~240), much of which is energy limited with soil moisture storage mostly at or near maximum (refer to Fig. 6.3), there is less scatter overall and smaller differences between the three data sets for both *LE* and *H*, compared with other parts of the year (Fig. 7.3). This suggests that the different methods of quantifying *LE* and *H* are possibly most reliable during periods where water availability is not limited and *LE* is at or near its potential. Some of the largest differences for the year between the plotted datasets are in the spring/summer period from DoY ~240 to the end of the year, where evaporative demand increases eventually leading to depletion of the winter/spring soil moisture storage.

Despite some obvious differences between the SEBS and eddy covariance data sets in Fig. 7.3, SEBS appears to realistically represent fluxes (considering the scale discrepancies of a ~200-300 m measurement fetch vs a 5 km pixel) and therefore has potential to benefit LSM predictions through data assimilation. From these data, the coefficient of determination (R^2) between eddy covariance and SEBS *LE* is 0.55, compared to 0.38 between eddy covariance and Open-Loop_sp *LE*. For *H*, the R^2 between eddy covariance and SEBS is 0.60, compared to 0.57 between eddy covariance and Open-Loop_sp. Therefore SEBS represents annual seasonal heat flux variations for 2005 slightly better than the Open-Loop_sp, based on the 76 coincident samples (Fig. 7.3) from the full 157 days with both *LE* and *H* SEBS data for the pixel collocated with the flux station.

An important part of the year-long study period is the several days surrounding DoY 320, where eddy covariance *LE* values are at or near maximum and differences with Open-Loop_sp predictions are amongst the greatest for the year (Fig. 7.3). The very high eddy covariance *LE* (and low *H*) compared to Open-Loop_sp here is thought to follow temporary groundwater elevation (from lateral recharge related to spikes in the flow of nearby Kyeamba Creek) which may have provided water for *LE*, as discussed in chapter 6 (section 6.4). Such a process is not represented in the CBM which only receives water input as rainfall forcing, hence it would explain the large discrepancy between field-observed and Open-Loop_sp fluxes. SEBS *LE* (*H*) values are also greater (less) than Open-Loop_sp predictions for the days surrounding DoY 320 (with some closely matched to eddy covariance values). The SEBS data therefore supports the interpretation of the Open-Loop/observation discrepancy from chapter 6 for this short period, reinforcing confidence in SEBS as containing useful information for the region. If any groundwater interaction is only at the small/local scale within a few hundred metre range of Kyeamba Creek (no data is available to directly verify it or quantify its extent), the impacts may not be represented by the 5 km scale of the SEBS data. Therefore other factors may be contributing to the large differences between broader scale remotely sensed data and Open-Loop_sp around DoY 320 and following days, such as model inaccuracies related to depleting soil moisture at this time of year, coupled with the high vegetation cover and the complexities of vegetation heat flux calculations.

The observation uncertainty value used for SEBS *LE* and *H* assimilation was 50 Wm^{-2}, based on a survey by Kalma *et al*. (2008) of a range of remotely sensed heat flux validation studies. In the absence of a number of independent data sets distributed across the study domain, as was the case for AMSR-E validation in the region by Draper *et al*. (2009a), it is difficult to confidently assess how appropriate this uncertainty value is for this product in this environment. With 50 Wm^{-2} used for the main assimilation experiment, a number of additional assimilation runs were considered for a range of increasing observation uncertainty values (more detail is provided in the following section). This was to examine the sensitivity of assimilation output to different uncertainty values for the specific SEBS data set used here.

7.2 EXPERIMENTS AND METHODOLOGY

This remotely sensed data assimilation study includes spatially distributed CBM simulations at 5 km resolution, over the 25 km by 25 km AMSR-E pixel domain (Fig. 7.1), with:

- No assimilation (Open-Loop_sp) – predictions are plotted for data comparisons in Figs. 7.2 and 7.3 above;
- Joint assimilation of SEBS *LE* and *H* products (LEH_Assim_sp); and,
- AMSR-E near-surface soil moisture assimilation (SM_Assim_sp).

All simulations were run with a 30 minute time step as determined by the 30 minute meteorological forcing data. The Ensemble Kalman Filter (EnKF) assimilation algorithm, as described in chapter

3 (section 3.2) and applied in chapters 5 and 6 studies, was applied for LEH_Assim_sp and SM_Assim_sp. The experiments here involved comparing predictions from the simulations listed above with the in-situ validation data (from eddy covariance and OzNet soil moisture stations: Fig. 7.1), to assess assimilation impacts on CBM heat fluxes and state variables relative to Open-Loop_sp predictions. The specific variables assessed were mostly the same as for chapter 6 – *LE*, *H*, near-surface soil moisture (0-8 cm) and root-zone soil moisture (0-60 cm), while for soil temperature only the near-surface (~4 cm records for ~0-8 cm depth) was considered due to varied data availability for the OzNet stations in the study period. Assessments were made using R^2 and Root Mean Square Error (RMSE) metrics between simulation output and validation data, for summarising explained variance and quantifying overall differences respectively.

The first step was to set-up meteorological forcing and spatial parameter data for model input for the 5 km simulation pixels across the study domain – assigning spatially varying input data values to pixels is described in the first few paragraphs of section 7.1. No lateral/horizontal interaction was implemented between simulation pixels for forcing data or model processes, with modelling strictly representing vertical heat and water exchanges for each pixel using the same meteorological forcing.

All of the simulations – Open-Loop_sp, LEH_Assim_sp and SM_Assim_sp – were initialised with the same set of state variable values obtained from spinning-up the CBM. Spin-up consisted of repeated yearly simulations for each pixel with the 2005 experimental forcing data, until the differences between soil moisture and soil temperature state values for the initial/final time steps of the year were <0.001 vol/vol and <0.1 respectively. The number of spin up years varied between pixels – ranging from 6 to 12 years – due to spatially varying parameter values.

The approach to generating ensembles of simulations in implementing the EnKF was identical to that for experiments in chapter 6 and is described in section 6.5.3. With the spatially distributed modelling here, state perturbations (for initial conditions and covariance inflation) were generated separately for each 5 km simulation pixel in all assimilation experiments.

7.2.1 SEBS LE AND H ASSIMILATION

SEBS data and CBM simulation pixels have identical 5 km resolution coverage (shown in Fig. 7.1 with grey boundaries). The full series of available SEBS *LE* and *H* data for the experiment year (157 once per day records at 2:00 pm local time) were jointly assimilated pixel-for-pixel into the CBM over the study domain for LEH_Assim_sp. Innovations were calculated as differences between SEBS and CBM *LE* and *H*, and soil moisture and temperature states for all six CBM soil layers were updated. As previously mentioned, the main LEH_Assim_sp experiment was performed with an observational uncertainty value for SEBS data (both *LE* and *H*) of 50 Wm^{-2}. Assessments of the predicted states and fluxes from this simulation are compared with assessments of SM_Assim_sp predictions.

A number of repetitions of LEH_Assim_sp were also carried out separate to the main experiment, to examine the impact of different SEBS uncertainty values on improvements in *LE* and *H* predictions. This was done repeatedly with observational uncertainty increased by 10 Wm^{-2} each time until there was no improvement in *LE* and *H* prediction.

7.2.2 AMSR-E SOIL MOISTURE ASSIMILATION

The de-noised and rescaled series of 2:00 am (local time) AMSR-E soil moisture data that were assimilated for SM_Assim_sp are displayed in Fig. 7.2. As described in section 7.1.1, temporal averaging filled some gaps in the original series for days with missing data, while gaps remain where the number of consecutive days with missing data was too large for the 5-day averaging window (near the end of the year scattered between ~DoY 280 to 330). There are a total of 326 records in the AMSR-E data set that were assimilated using an observational uncertainty of 0.04 vol/vol.

Fig. 7.1 illustrates the discrepancy between AMSR-E data and simulation spatial resolutions, and comparisons in Fig. 7.2 are made using spatially averaged Open-Loop_sp predictions. Innovations for the EnKF were therefore calculated between AMSR-E values (representing ~1-2 cm depth) for the single 25 km by 25 km pixel (the study domain), and the spatial average of all 5 km by 5 km CBM moisture predictions (for the 2.2 cm deep top soil layer) within it. Updates to soil moisture and temperature state variables in CBM's six layers, based on the single innovation for the whole study domain, were subsequently applied to the individual 5 km simulation pixels.

7.3 DATA ASSIMILATION RESULTS

Results from the assimilation experiments are presented separately for the different predictions that are of interest – firstly for *LE* and *H*, followed by soil moisture and then soil temperature. Graphical time series comparisons between validation data and outputs from Open-Loop_sp, LEH_Assim_sp and SM_Assim_sp are included, as are the R^2 and RMSE quantities for differences between assimilation outputs and validation data, and differences between Open-Loop_sp outputs and validation data.

7.3.1 LE AND H PREDICTION

Assessing *LE* and *H* predictions relied on the eddy covariance data from the Kyeamba Creek flux station, hence the focus here is solely on predictions from the single simulation pixel within which it is located (Fig. 7.1). There are a total of 2,298 irregularly spaced 30 minute records for both *LE* and *H* in the eddy covariance validation series over the experiment period. The time series outputs from each simulation (also 30 minute time steps) were sampled to match the validation series, resulting in 2,298 temporally coincident records across all data sets with which comparisons were made. Weekly averages were calculated for each data set from the matching 30 minute records to enable clearer qualitative comparisons in annual time series plots (Fig. 7.4). For quantitative comparisons, R^2 and RMSE were calculated using all 2,298 matching records, with the results summarised in Table 7-1.

From Fig. 7.4, *LE* and *H* assimilations (LEH_Assim_sp) had a relatively minor impact on *LE* and *H* predictions compared with Open-Loop_sp for most of the year (week 1 to approximately week 44 (DoY ~305)). The *LE* series from LEH_Assim_sp shows slightly increased over-prediction relative to eddy covariance data for most of the period between weeks 11 and 24 (DoY ~75 to ~165), consistent with SEBS *LE* over-estimation for this period (Fig. 7.3). The impact on *H* in this same period appears smaller overall with both Open-Loop_sp and assimilation predictions being in better agreement with eddy covariance data than for *LE*, reflecting the closer match between SEBS and Open-Loop_sp *H* data here.

The greatest impact in the year from LEH_Assim_sp, for both fluxes, is between weeks 44 and 48 (DoY ~305 to ~335). This is the period within which differences between eddy covariance observations and Open-Loop_sp are greatest, with groundwater interaction (which CBM does not represent) interpreted as a possible contributor to large *LE* observations, as discussed in section 7.1.2 and in chapter 6 (section 6.4). The plots in Fig. 7.4 show clear improvements to *LE* and *H* in this period from assimilating the SEBS data.

Fluxes from SM_Assim_sp are also a relatively close match to those from Open-Loop_sp for most of the year, in this case from week 1 to approximately week 36. There are some slight improvements for the latter half of autumn (week ~16 to ~22), which is the driest part of the year at the flux station. During this period assimilation of soil moisture led to the best representation of eddy covariance data of the three simulations. The SM_Assim_sp fluxes are degraded for part of spring, most prominently from weeks ~40 to ~44 with a sharp reduction in *LE* (increase in *H*) coinciding with a large under-estimation of Open-Loop_sp soil moisture by AMSR-E data (see DoY ~280 to ~285 in Fig. 7.2). Despite gaps in the AMSR-E data series over the following few weeks, SM_Assim_sp then mostly improved the fluxes from week ~44 to the end of the year.

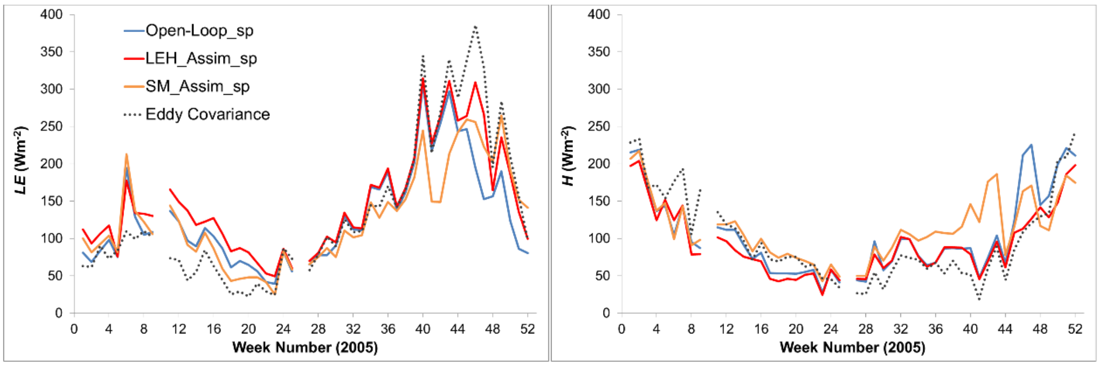

Figure 7.4: *Weekly averaged LE (left) and H (right) from the three main simulations and eddy covariance observations, for the 5 km simulation pixel collocated with the flux station (Figure 7.1). Weekly averages were calculated with the 2,298 matching time series records in each data series.*

Both LEH_Assim_sp and SM_Assim_sp had the strongest impact on modelled fluxes in the final few months of the year from austral spring to summer, where moisture storage in the soil profile declines from its annual maximum. The greatest improvements from both approaches are between weeks ~44 to ~48, where eddy covariance and Open-Loop_sp discrepancies are greatest and where there is some evidence for groundwater interaction (~DoY 320 at least locally around the flux station site as previously discussed). With reference to Fig. 7.4, it is the improvements in this short period which contribute to the bulk of the overall annual improvement to flux predictions – to *LE* from both LEH_Assim_sp and SM_Assim_sp, and to *H* from LEH_Assim_sp – as indicated by the quantitative results in Table 7-1.

The short period of degraded flux outputs from SM_Assim_sp (centred on weeks ~40 to ~44) is an obvious limitation on the level of improvement to *LE* in terms of R^2 and RMSE. While for *H* it appears to be the main factor in the overall poor results from these metrics, where the degraded prediction is more pronounced for slightly longer (from week ~36) than for *LE*. The negative impacts in this period are presumably related to the large footprint of AMSR-E and its under-estimation in relation to the spatially aggregated CBM predictions across the 25 km domain (e.g. DoY ~280-285 in Figure 7.2), which may not represent local conditions in the vicinity of the flux station. Alternatively, error in the AMSR-E data might be greater for this period, in which case the single observational error term used for the whole experiment period may not be appropriate. However this cannot be determined from any of the data available for this research.

Experiments examining the use of different SEBS data uncertainty values for LEH_Assim_sp consisted of four repeated simulations, additional to the main simulation using 50 Wm^{-2}. Fig. 7.5 illustrates the change in R^2 and RMSE scores for the full year predictions of *LE* and *H* from the various increased uncertainty values. These results indicate that SEBS data are still valuable for improving both *LE* and *H* prediction via assimilation, as implemented in this study, with observational uncertainty of up to 80-90 Wm^{-2}. It is noted that improvements with the larger uncertainty values examined here are mainly due to impacts made in relation to the very large discrepancy between Open-Loop_sp and observed data between weeks ~44 and ~48 (Fig. 7.4).

Table 7-1: *R^2 and RMSE for predicted LE and H time series from the main simulations relative to eddy covariance data. These were calculated from the 2,298 matching 30 minute records between data sets, for the single simulation pixel collocated with the flux station. Values indicating greatest improvement over Open-Loop_sp are in bold, and degraded impact is indicated by grey italics.*

	LE		**H**	
	R^2	***RMSE (Wm^{-2})***	***R^2***	***RMSE (Wm^{-2})***
Open-Loop_sp	0.56	81.5	0.55	73.6
LEH_Assim_sp	**0.69**	70.8	**0.60**	**66.9**
SM_Assim_sp	0.68	**69.3**	*0.53*	72.6

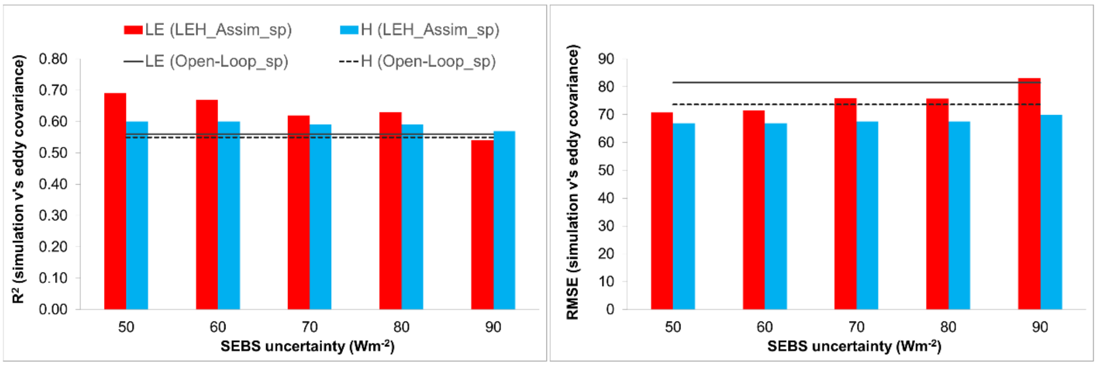

Figure 7.5: *R^2 (left) and RMSE (right) results for predicted LE and H over the experiment period, from repeats of LEH_Assim_sp using progressively increased observational uncertainty values – above the 50 Wm^{-2} used in the main experiment simulation that was assessed against SM_Assim_sp. Horizontal lines mark the R^2 and RMSE for Open-Loop_sp predictions, representing the limit beyond which (below for R^2 and above for RMSE) the LEH_Assim_sp results indicate no improvement.*

7.3.2 SOIL MOISTURE PREDICTION

As mentioned previously, the availability of in-situ soil moisture data from OzNet stations over the experiment period differs for the near-surface (0-8 cm) and root-zone (0-60 cm: the depth average of 0-30 cm and 30-60 cm measurements), with data available from six and ten stations respectively (see Fig. 7.1). Validation involved depth-weighted averaging soil moisture state predictions for relevant CBM soil layers to match the in-situ data depths. For 0-8 cm the top two CBM soil layers (2.2 and 5.8 cm thick respectively) were averaged, while for 0-60 cm the averaging calculation used the top three soil layers (2.2, 5.8 and 15.4 cm thick respectively: 23.4 cm in total) and a fraction (36.6/40.9) of the fourth layer from the surface (which is 40.9 cm thick). Furthermore, where there are more than one validation data series available within the same 5 km simulation pixel they were averaged to produce a single validation series for the pixel – this was done for stations K4 and K5 (for near-surface and root-zone data), and for station K10 and the flux station (for root-zone data, with near-surface data only available for the flux station site).

Time series comparisons for soil moisture are presented in Fig. 7.6 with plots of available near-surface and root-zone data for the simulation pixels that are collocated with validation data (greyed pixels in Fig. 7.1). The plots are of daily averaged (midnight to midnight) data, for which rescaling has been applied to match the means and standard deviations of simulation output series with in-situ observed series, in order to minimise annual biases between them resulting from soil parameter and structural errors in the model (as done with results in chapter 6). The daily averaged and rescaled data were used to calculate R^2 and RMSE for quantitative validation over the experiment year. Table 7-2 summarises average values for these metrics across all of the simulation pixels relevant to the validation.

There were no overall improvements to soil moisture predictions for the year from either LEH_Assim_sp or SM_Assim_sp, with near-surface and root-zone soil moisture predictions degraded in both experiments according to averaged R^2 and RMSE. While these metrics also indicated degraded results for all of the individual pixel validations from both experiments. The negative impacts from LEH_Assim_sp are less pronounced than from SM_Assim_sp, as evident in most of the time series plots (Fig. 7.6).

The flux station pixel results in Fig. 7.6 (associated with OzNet K10 for the near-surface and OzNet K10 & FS for the root-zone) show that LEH_Assim_sp moisture predictions track those from Open-Loop_sp fairly closely for most of the year, similar to heat flux predictions. The overall poor results from this simulation are due mainly to short periods of degraded soil moisture within the first ~160 days of the year. This is presumably related to a few large differences between SEBS and modelled fluxes in this period (mainly the earlier half of it – see Fig. 7.3) where some

SEBS/Open-Loop_sp differences are as high as 100-200 Wm^{-2}. Large rainfall events occurred at the flux station site for a few days scattered across this period. With the root-zone moisture here at or near its minimum for the year, the main effect of the high rainfall events was rapid wetting and drying of the near-surface soil (see in-situ moisture in Fig. 7.6).

Most notable for the flux station pixel is the improved soil moisture prediction from LEH_Assim_sp between DoY ~280 to ~320, for both the near-surface and root-zone. Here the moisture storage in the soil profile depletes from near the winter/spring maximum, with Open-Loop_sp predicting the depletion slightly too early compared to in-situ data, resulting in under-estimated moisture (Fig. 7.6). It is an important period within which groundwater is thought to have contributed to root-zone soil moisture (around DoY ~311 or soon after, see section 6.4 in chapter 6), which could not be represented by Open-Loop_sp. The scale of any such groundwater interaction is unknown, therefore the 5 km scale SEBS data may not necessarily contain strong information related to it. This implies the improved moisture here from LEH_Assim_sp could also be from correcting Open-Loop_sp prediction error related to model structure and parameter errors.

Degradation of soil moisture from SM_Assim_sp varies across the different plots in Fig. 7.6. In the first ~160 days, where moisture is mainly near its minimum for the year, there are clearly some poor root-zone results with examples of positive bias relative to Open-Loop_sp (e.g. K1, K2 and K3). A major contribution to the overall degraded results is the sharp reduction in soil moisture for most of the validated pixels around DoY ~280, which is where AMSR-E under-estimates Open-Loop_sp in Fig. 7.2. This, along with other incidences of sharp impacts from SM_Assim_sp in some plots, indicates possible issues with error representation that result in too much weight given to short-term variations in AMSR-E data, along with some deeper moisture state updates being too sensitive to the near-surface impacts. Specifically, AMSR-E error might be larger for some periods and not be well represented by the single observational uncertainty value used (0.04 vol/vol). For the flux station pixel (FS and K10&FS plots) SM_Assim_sp improved moisture prediction briefly between DoY~300 and ~330, which approximately coincides with some improvement it made to *LE* and *H* (see weeks ~44-48 in Fig. 7.4).

Table 7-2: *R^2 and RMSE for predicted soil moisture time series from the main simulations, relative to in-situ OzNet moisture data. These are averages of values calculated for all of the individual simulation pixel results plotted in Figure 7.6. Values indicating greatest improvement over Open-Loop_sp are in bold, and degraded impact is indicated by grey italics.*

	Near-Surface Moisture (0-8 cm)		**Root-Zone Moisture (0-60 cm)**	
	R^2	***RMSE (vol/vol)***	***R^2***	***RMSE (vol/vol)***
Open-Loop_sp	0.76	0.048	0.84	0.027
LEH_Assim_sp	*0.74*	*0.051*	*0.78*	*0.032*
SM_Assim_sp	*0.66*	*0.059*	*0.48*	*0.050*

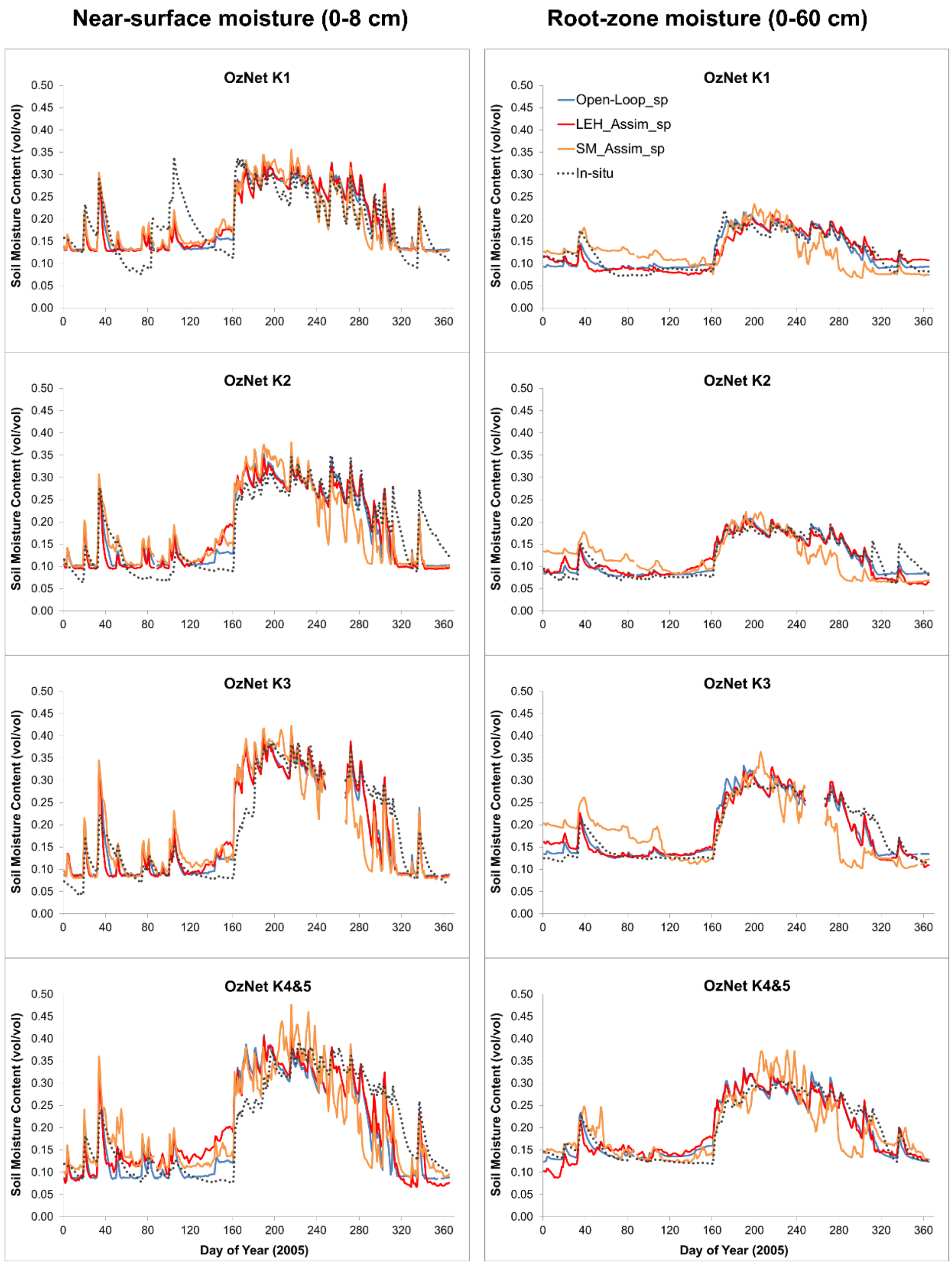

Figure 7.6: *Daily averaged (midnight to midnight) time series plots of available 0-8 cm near-surface (left) and 0-60 cm root-zone (right) soil moisture data from: OzNet in-situ observations, and the three main simulations performed for this study. All simulated data series have been rescaled by matching their means and standard deviations with those of the observed series, for bias-free comparisons. (Plots continue on next page).*

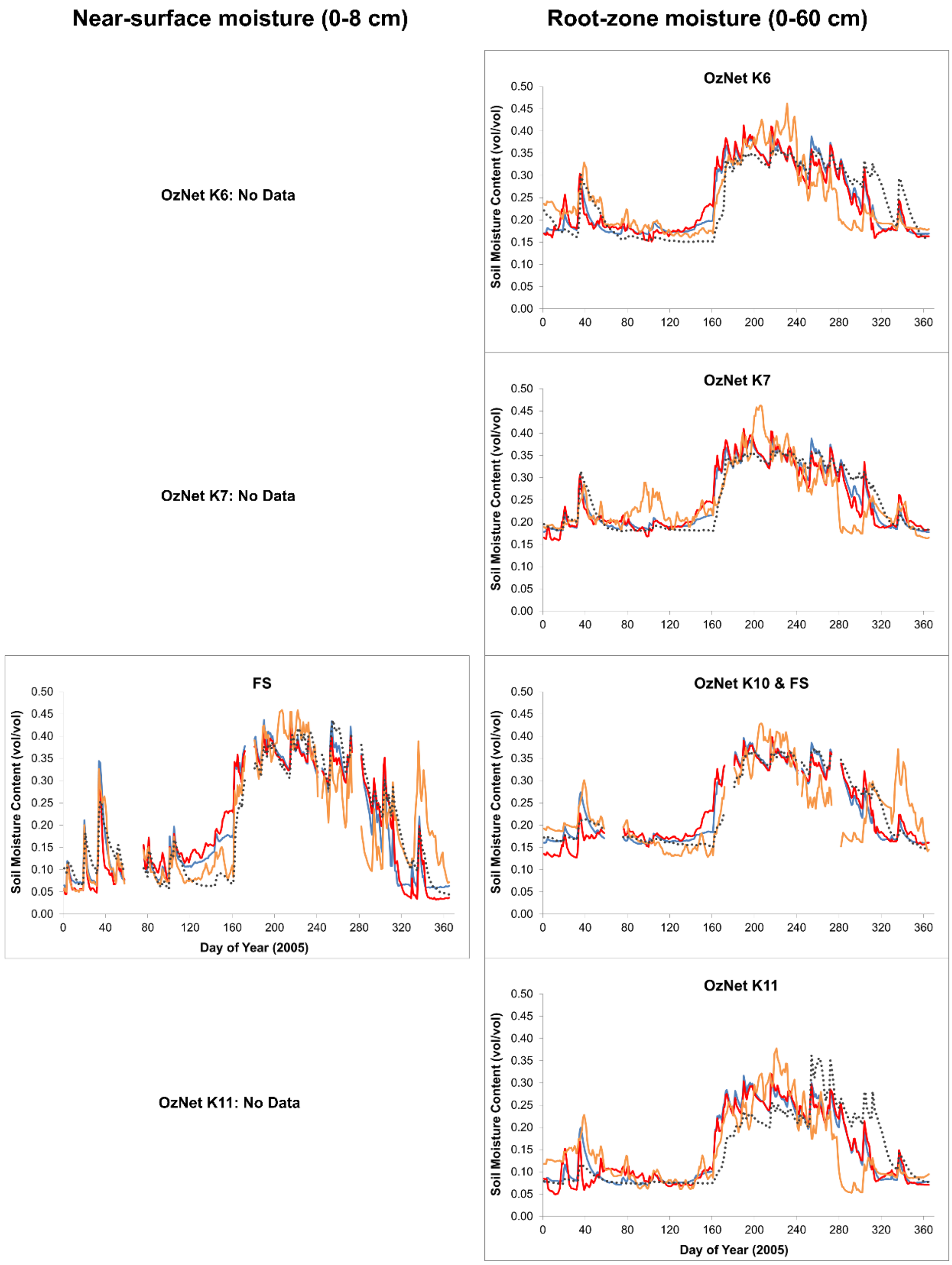

(Figure 7.6 continued)

7.3.3 SOIL TEMPERATURE PREDICTION

As with soil moisture, preparation of soil temperature predictions for validation involved averaging them over depth ranges where necessary so they are comparable to in-situ observations. For comparisons with the 4 cm deep measurements from OzNet sites K1 to K5, the depth-weighted average between the top CBM soil layer temperature (2.2 cm thick) and temperature of the second layer from the surface (5.8 cm thick) were used (for a 0-8 cm depth average, with 4 cm the mid-point). While for the 2 cm deep temperature measurements from the flux station site, direct comparisons were made with temperature of the top CBM soil layer. Temperature data were available from both K4 and K5 stations within the same 5 km simulation pixel (Fig. 7.1), hence the average of the two series (K4&5) were used for validating predictions for that pixel.

The final preparation of simulated and observed temperature series for validation also followed the same procedure as applied for soil moisture – daily averaging of each series (midnight to midnight), and in order to minimise bias, rescaling the annual mean and standard deviations of the simulated series to match those of the annual observed series. Time series plots of temporally averaged and rescaled series are shown in Fig. 7.7. While R^2 and RMSE metrics summarising the performance of simulations relative to observations are shown in Table 7-3 (which are averages of R^2 and RMSE calculated for the individual pixels corresponding to the separate plots in Fig. 7.7).

All of the time series comparisons and quantitative results, in Fig. 7.7 and Table 7-3 respectively, indicate an overall negligible impact on near-surface temperature predictions from LEH_Assim_sp and a minor impact from SM_Assim_sp. The most noticeable impacts are increased/degraded temperature from SM_Assim_sp in some plots for a short period around DoY ~280, coinciding with the reduced/degraded soil moisture prediction (Fig. 7.6) related to the dip in the assimilated AMSR-E soil moisture estimates (Fig. 7.2). The only noticeable impacts from LEH_Assim_sp

Table 7-3: *R^2 and RMSE for predicted near-surface soil temperature time series from the main simulations, relative to in-situ OzNet temperature data. These are averages of values calculated for all of the individual simulation pixel results plotted in Figure 7.7. Values indicating greatest improvement over Open-Loop_sp are in bold, and degraded impact is indicated by grey italics.*

	Near-Surface Temperature	
	R^2	***RMSE (°C)***
Open-Loop_sp	0.86	2.2
LEH_Assim_sp	0.86	**2.1**
SM_Assim_sp	*0.83*	*2.4*

are very minor, with a slight increase/improvement around DoY ~40 in some plots, and very slight decrease/improvement around DoY ~280 (opposite to the increased/degraded impact from SM_Assim_sp here for some plots).

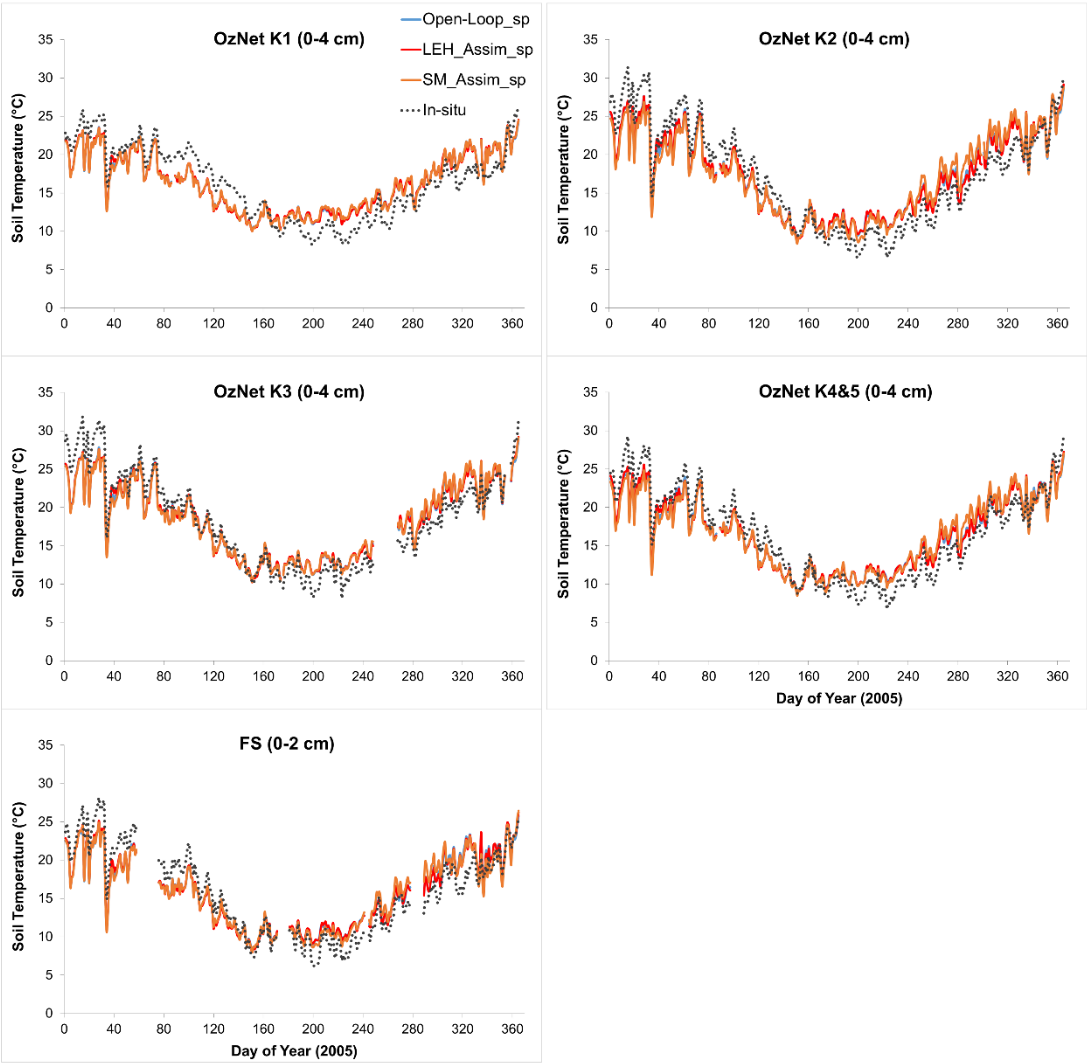

Figure 7.7: *Daily averaged (midnight to midnight) time series plots of available near-surface soil temperature data from: OzNet in-situ observations (4 cm), Kyeamba Creek flux station (FS) site observations (2 cm), and the three main simulations performed for this study. All simulated data series have been rescaled by matching their means and standard deviations with those of the in-situ observed series, for bias-free comparisons.*

7.4 DISCUSSION

Interpretations and possible implications of key results from the previous section are discussed here. Fig. 7.8 is included for reference, providing a summary of the overall change in RMSE between predicted and observed series as a consequence of the different data assimilation approaches.

The most important result from this study is that the remotely sensed heat flux data products were capable of positively impacting on CBM predicted heat fluxes via data assimilation, as was a remotely sensed near-surface soil moisture product. The reduction in RMSE from assimilation relative to Open-Loop_sp predictions (Fig. 7.8) shows clear improvements to *LE* for the single simulation pixel for which validation was possible, with reductions of ~13% and 15% from LEH_Assim_sp and SM_Assim_sp respectively. While the RMSE for *H* was reduced by ~9% from LEH_Assim_sp but only ~1% from SM_Assim.

The bulk of the annual improvement to heat fluxes, from both assimilation approaches, can be attributed to the period of DoY ~300-330 (~week 44-48; Fig. 7.4) where Open-Loop_sp predictions were poorest, under-estimating eddy covariance *LE* observations by nearly 200 Wm^{-2} and over-estimating *H* by nearly 100 Wm^{-2} (for weekly averages). This period is interesting due to the evidence of groundwater interaction (somewhere in the days post DoY ~311, as discussed in chapter 6) which is not represented in the CBM, providing a possible explanation for the poor Open-loop_sp predictions at least locally in the vicinity of the flux station site.

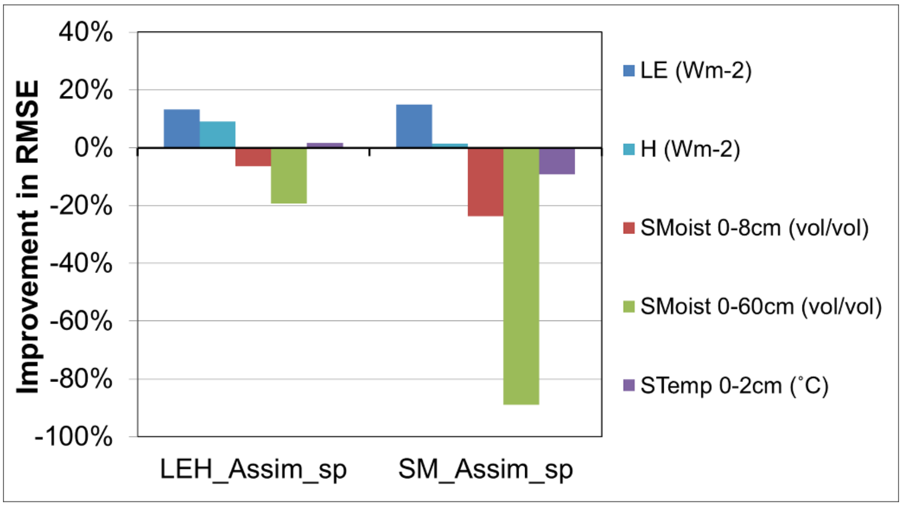

Figure 7.8: *Changes in RMSE from the assimilation experiment outputs compared to RMSE for Open-Loop_sp outputs. With RMSE calculated relative to in-situ validation data for the variables of interest. RMSE for each output variable are averages of values calculated for individual validation sites across the study domain. A positive change indicates improvement to the predictions over the experiment year, and a negative change indicates degradation.*

Any groundwater interaction is thought to be linked to lateral recharge from very large but isolated flow increases in Kyeamba Creek, which runs approximately north/south through the centre of the study domain shown in Fig. 7.1, and only a few hundred metres west of the flux station as shown in Fig. 6.1 in chapter 6. This would therefore have had to occur for a considerable area along the length of the creek valley in order for the broad scale remotely sensed data (5 km resolution for heat fluxes and 25 km for soil moisture) to contain any related information (namely, from increased root-zone soil moisture via capillary action).

There is the possibility that remotely sensed data here have large errors and that some improvements to *LE* and *H* from data assimilation are due to chance, which is not possible to test given the spatial discrepancies between >=5 km resolution spatial data and the few available independent field measured data sets at the point scale. However, testing LEH_Assim_sp with a series of increasing SEBS data uncertainty values, showed improvements to heat flux predictions could be made with uncertainty up to 80-90 Wm^{-2}. This suggests there is a real anomaly in the SEBS heat fluxes relative to Open-Loop_sp predictions (at least for the period of DoY ~300-330 or week ~44-48; Fig. 7.4), which is supported by other data sources (e.g. eddy covariance) as described throughout this chapter and in chapter 6.

Soil moisture predictions from both assimilation experiments show some improvements for the flux station site from DoY ~300 leading up to around DoY ~320, where the strongest improvements to heat flux predictions are made. It is unlikely that broader scale remotely sensed data (especially 25 km for AMSR-E) would contain considerable groundwater related information here in relation to recharge from high flows in Kyeama Creek. Therefore prediction errors related to model physics and parameters would likely play a role in the large discrepancies between Open-Loop_sp predictions and the remotely sensed products for this period leading into summer with high grass cover and depleting soil moisture. Aside from this period, soil moisture prediction was degraded overall in both experiments and across all of the pixels that were validated (Figs. 7.6). This was especially the case for SM_Assim_sp where the RMSE for near-surface and root-zone moisture is ~24% poorer and ~89% poorer respectively compared to Open-Loop_sp predictions, while for LEH_Assim_sp the RMSE is ~6% poorer and ~19% poorer for the near-surface and root-zone moisture respectively (Fig. 7.8).

Better soil moisture results were expected from SM_Assim_sp than those obtained here. The poor impacts on soil moisture vary over the annual experiment period (Fig. 7.6) and a number of possible factors may have contributed to the overall strongly degraded predictions. One of these factors possibly relates to the wilting point parameter in the CBM defining a rigid lower boundary for moisture state prediction. This is illustrated in the near-surface moisture series for stations K1, K2 and K3 over drier periods (e.g. the first ~160 days of the year), where in-situ data minimums drop below the fixed wilting point boundary in some instances (Fig. 7.6). When the mean of predicted moisture state ensembles for the EnKF approaches wilting point, any ensemble member values which would be less than the prescribed wilting point, as a consequence of applying Gaussian perturbations, will be set to the wilting point value by the CBM. The result can be a clumping of ensemble members with values at or close to wilting point, contributing to a positively biased ensemble mean away from this minimum moisture boundary. This may have contributed to biased impacts on moisture predictions in the earlier drier part of the year for K1, K2 and K3 root-zones. In addition, apart from the technical assimilation issues, in reality soil evaporation can cause drying below wilting point; however this is prevented in the model physics.

Other negative impacts from SM_Assim_sp on predicted soil moisture include some sharp and overly strong updates. The large negative impact at around DoY ~280 (which also limited the overall annual improvements SM_Assim_sp made to both heat fluxes) may relate to poorer AMSR-E estimation here, or to near-surface moisture variability at small spatial scales in which case there is the possibility of a mismatch in the moisture representation across the different spatial scales of individual 5 km simulations, 25 km AMSR-E data and the local/point scale in-situ measurements. Again, this cannot be accurately determined from the data available for this study. However this particular impact and some overly strong impacts of higher frequency variation (especially for the root-zone) indicate that more careful treatment of model error representation is required for future work – both in terms of achieving covariances between the predicted and the deeper moisture states that lead to more realistic state updates, and more sophisticated observational error representation (i.e. reflecting non-stationarity).

The overall negligible impact on near-surface soil temperature from LEH_Assim_sp highlights the minimal role it has in determining heat fluxes in the CBM where there is considerable vegetation cover, with the most direct links soil temperature has to *LE* and *H* being via the soil components of heat flux calculations. For days around DoY ~320 in the soil temperature plot for the flux station pixel (Fig. 7.7; denoted FS) where heat flux improvements were greatest (Fig. 7.4; weeks ~44-48) and vegetation cover high (LAI of 3.0), there is little noticeable impact on soil temperature. The greatest impact on soil temperature in most of the time series plots (Fig. 7.7) is from SM_Assim_sp, with degraded/increased temperature impacts coinciding with the decreased/degraded moisture and *LE* impacts around DoY ~280 (see also Fig. 7.8).

7.5 CONCLUSIONS

Assessing the assimilation of spatial remotely sensed data products is inherently difficult due to the lack of spatially distributed in-situ data for assessing remotely sensed data uncertainty or validating assimilation results. Here it was demonstrated that instantaneous *LE* and *H* products derived from the SEBS algorithm for ~2:00 pm each day, using remotely sensed skin temperature and other ancillary data from the AQUA platform, could improve heat flux predictions from a LSM via assimilation, based on validation for a single simulation pixel. While the ability to accurately assess standard published uncertainty estimates for assimilated data products is limited without adequate independent data, in this particular study the *LE* and *H* products still had beneficial impacts when assimilated with error estimates of 80-90 Wm^{-2}.

Assimilating an AMSR-E near-surface soil moisture product also improved heat flux predictions. But it strongly degraded soil moisture predictions for all validation sites over the experimental year, which in turn is likely to have hindered greater improvement to heat fluxes. The effects of sub-optimal error representation, for AMSR-E and model states, and spatial scale discrepancies between assimilated data and simulation outputs are likely to be factors in the poor results. Greater focus on these issues is therefore required to achieve better performance for soil moisture prediction.

Results for soil temperature support those from chapter 6, where it is clear that soil temperature generally does not play as much of a direct role in heat flux predictions as soil moisture state changes do where vegetation cover is high.

8 FINAL DISCUSSION AND CONCLUSIONS

This thesis has covered three distinct yet complimentary LSM data assimilation studies. When considering the findings of each in combination, a clear contribution towards understanding the requirements for better predictive skill of key land surface water and energy balance processes, using both models and observed information, has been developed.

8.1 SUMMARY OF ASSIMILATION STUDIES

8.1.1 SYNTHETIC DATA ASSIMILATION

The synthetic assimilation study in chapter 5 involved a series of short proof-of-concept experiments, where CSIRO Biosphere Model (CBM) derived synthetic observations of data types that are available from remote sensing were assimilated over a ~3 month simulation period. The ability of *LE* and *H* assimilation to improve *LE* and *H* predictions was examined, in comparison to assimilating near-surface soil moisture and skin temperature.

Synthetic observations were sampled from outputs of a CBM "truth" simulation and assimilated into a "degraded" simulation, with assimilation results assessed based on how closely they retrieved the "truth" output series. The "degraded" simulation was set-up using different inputs to those used for the "truth". This included degraded initial state values (extreme wet soil moisture and warm soil temperature by comparison), different values for key soil hydraulic parameters and LAI, rainfall data measured at an alternate site ~5 km distant, and for all other forcing variables a perturbed series of the "truth" data. The EnKF implementation was based on simulating the "degraded" scenario using ensembles of perturbations generated for initial state conditions, and forcing variables to represent error ranges for each. At assimilation update time steps, the synthetic observations were perturbed once before ensembles were generated to represent their respective measurement errors. This was guided by information from the literature on typical error characteristics for the remotely sensed products that each data type represented.

Synthetic *LE*, *H* and skin temperature observations, analogous to data from remotely sensed thermal infrared sensors, were assimilated on two different temporal scales – once every fortnight to represent using data from Landsat thermal imagery, and twice daily at 10 am and 2 pm (local *ET* active times) to represent using data from MODIS. Near-surface soil moisture observations were assimilated once every three days as an approximation of SMOS repeat coverage.

Results showed that assimilation frequency was important, with the twice daily assimilation of thermal related data types at approximate MODIS overpass times producing better *LE* and *H* predictions than for the ~fortnightly frequency corresponding to Landsat overpasses. The other major result was that assimilating *LE* and *H* at the twice daily MODIS frequency was roughly comparable to skin temperature assimilation (at the same frequency). The *LE* and *H* assimilation reduced the RMSE for *LE* prediction by 78% compared with no assimilation ("degraded" series), while the RMSE reduction for *H* from *LE* and *H* assimilation was 66%. Reductions in RMSE for both heat flux predictions from skin temperature assimilation were within 1% of the reductions from *LE* and *H* assimilation.

Compared with assimilating thermal related data types on the twice-daily time scale, near-surface moisture assimilation improved *LE* to a lesser degree (with 74% reduction in RMSE compared to no assimilation) despite it clearly producing the best root-zone soil moisture retrieval. While improvements to *H* were similar, with the reduction in RMSE within 1% of the reductions from both of the thermal related data assimilation experiments. Skin temperature assimilation produced the best retrieval of the "truth" root-zone soil temperature. These percentage values of relative change in RMSE were calculated compared to the RMSE values between Open Loop outputs and the "truth" which were not presented in the original published version of the paper (RMSE between Open Loop outputs and the "truth" for each variable of interest is included in the caption for Fig. 5.6 in this thesis).

This proof-of-concept study therefore demonstrates the potential value of *LE* and *H* data assimilation in producing optimal *LE* and *H* predictions. The comparable level of improvement to these predictions from assimilating skin temperature is an important result from a remote sensing perspective, given that instantaneous *LE* and *H* data products would be derived from skin temperature. It was also a valuable study in establishing an assimilation methodology for the CBM, being the first published sequential data assimilation study with this model. An obvious limitation is that the synthetic observations are not truly independent, having all been derived from the same CBM simulation. Hence any relationship that the near-surface soil moisture, heat fluxes and skin temperature "observations" share would be a function of the formulations of the model that they are assimilated into.

The level of complexity of this study was also limited. The ~3 month experimental period, with minimal vegetation cover (LAI < 0.4), did not cover key seasonal variations such as major changes in root-zone profile soil moisture storage and vegetation cover. The single column point scale simulations means that spatial discrepancies between different remotely sensed products – as represented by synthetic observations – were ignored. Moreover, idealised temporal resolutions for data related to thermal remote sensing (heat fluxes and skin temperature) were also used, consisting of the maximum number of potential observations without factoring the effects of cloud interference.

8.1.2 ONE-DIMENSIONAL FIELD DATA ASSIMILATION

Some of the limitations with the synthetic-twin assimilation study were addressed in the one-dimensional field data study carried out for the Kyeamba Creek flux station site (Chapter 6). Importantly, the assimilation used real data that was measured in-situ with different instruments, so the observed series for each data type are mostly independent of each other – one minor exception being that the measured outgoing longwave radiation used to calculate skin temperature was also used together with a number of other datasets in correcting eddy covariance data (to close the energy balance). The use of real data also meant that model structural errors could influence the results. The simulation experiments spanned the full seasonal cycle over a one-year period, and the *LE*, *H* and skin temperature observations were assimilated on more realistic remote sensing time scales with data series filtered for cloudy conditions.

Observational data series for assimilation were sampled from in-situ measurements to approximate remote sensing time scales. For *LE* and *H* (from eddy covariance data) and skin temperature (from applying the Stefan Boltzmann equation using outgoing longwave radiation data), the sampling was done according to approximate MODIS thermal infrared local overpass (*ET* active) times at ~10:00am and ~2:00pm, followed by filtering for cloud cover. Near-surface soil moisture (from 0-8 cm reflectometry probe data) were sampled for the ~2:00am (descending) AMSR-E local overpass time. To remove annual state variable model/observation bias prior to data assimilation, the sampled soil moisture series annual mean and standard deviation were rescaled to match that of the CBM predicted series without assimilation. This was an important extension to the assimilation approach in the synthetic study that was necessary to meet the underlying assumptions of the EnKF.

In addition to repeating the combined *LE* and *H* assimilation, skin temperature assimilation, and near-surface soil moisture assimilation applied in the synthetic study, other multiple data assimilation scenarios were also examined: combined *LE*, *H* and skin temperature data; and combined *LE*, *H*, skin temperature and near-surface soil moisture data. Ensembles of initial state conditions and meteorological forcing inputs (representing errors estimated from differences between flux station site data and ~30 km distant Bureau of Meteorology station data) were generated to produce prediction ensembles for the EnKF. State ensemble inflation was also applied in this study with perturbations added to a-priori ensemble members at EnKF analysis time steps. To represent damped state error with deeper/thicker soil layers, the standard deviations of perturbations used for inflating each CBM soil layer state were a fraction of the standard deviations applied for the top-most soil layer, based on the relative thicknesses between each soil layer and the top-most soil layer.

Assimilation results were validated against independent site measured data series of root-zone soil moisture, near-surface and root-zone soil temperature, and *ET*. The *ET* validation series was constructed using local data on rainfall and changes in root-zone moisture storage, as a fortnightly data set that was independent of the eddy covariance series (used for assimilation). Some results support findings from the synthetic-twin study, such as *LE* and *H* assimilation producing strong *ET* improvements (20% reduction in RMSE compared to no assimilation), exceeding improvements made from skin temperature assimilation (10% reduction in RMSE compared to no assimilation) and near-surface soil moisture assimilation (14% reduction in RMSE compared to no assimilation). The soil moisture assimilation produced the best overall root-zone soil moisture prediction. Combined skin temperature and near-surface soil moisture assimilation produced the best overall *ET* prediction by a small margin (23% reduction in RMSE compared to no assimilation).

Despite the strong *ET* improvement from *LE* and *H* assimilation, the slightly better *ET* prediction from assimilating skin temperature together with near-surface soil moisture in this study again raised the question of whether *LE* and *H* assimilation is worthwhile from a remote sensing perspective, especially given that these data would need to first be derived from skin temperature. The combined skin temperature and near-surface soil moisture assimilation experiment also balanced improvements to *ET* with improvements to soil moisture and temperature states. This implies that assimilating skin temperature and near-surface soil moisture together may be the most suitable for simultaneously improving LSM states and diagnostic fluxes.

With regard to soil temperature states, there is no direct link with the vegetation transpiration component of fluxes calculated by the CBM. Therefore impacts on soil temperature for the latter part of the year where vegetation cover was high had no direct effect on flux predictions. The top-most soil layer temperature is involved in calculations for soil *LE* and *H* contributions, and therefore earlier in the year where vegetation cover is lowest, assimilation impacts on soil temperature would have had some impact on total heat flux predictions.

The late spring to early summer period was of particular interest in this study. During this period the CBM predictions of *ET* were very low relative to validation data, with the differences between the two datasets at their greatest for the year. Assimilating eddy covariance heat fluxes strongly improved *ET* in this period, with skin temperature and near-surface soil moisture assimilation also making clear improvements. This supports the interpretation of poor heat flux predictions from the model during this period. Spikes in discharge data for Kyeamba Creek (flowing ~300 m from the flux station), and in soil moisture sensor records below the root-zone indicate that temporary interaction between the root zone and groundwater might have occurred in this period. Consequently, the effects of any water supplied to the soil root-zone via capillary effects would be captured in the different field measurements, but would not be represented by the CBM – hence large under-predictions of *ET* would result. Poor *ET* predictions here may also be an artefact of model process errors associated with depleting soil moisture and near maximum vegetation cover, where the total model fluxes are dominated by vegetation flux calculations.

There were some periods across the different experiments where assimilation had a degrading impact on model state and/or flux predictions. This is likely related to sub-optimal representation of model errors from ensemble predictions, particularly if the resulting error correlations between different variables is poor (e.g. between near-surface soil layer moisture and deeper root-zone soil layer moisture, or between *LE* and deeper root-zone moisture states). Seasonal observation/model bias is another factor that may explain the degraded results. Addressing these problems is non-trivial and relates to the issue of limited independent data availability, which inhibits a complete understanding of all aspects of model error and the accurate representation of it for optimal assimilation performance.

8.1.3 REMOTELY SENSED DATA ASSIMILATION

The potential benefits for LSM heat flux prediction from assimilating different observation types, including the rarely examined approach of *LE* and *H* assimilation, has been demonstrated in the synthetic-twin and one-dimensional field data studies. In the remotely sensed data study (Chapter 7), the focus was narrowed to compare *LE* and *H* assimilation (as a very rare approach in the literature) with near-surface soil moisture assimilation (a very common approach in the LSM assimilation literature).

Experimental simulations with the CBM were performed at 5 km spatial resolution for a 25 km by 25 km region covering most of the Kyeamba Creek catchment, and for the same annual period (2005) as the one-dimensional field data study. Remotely sensed LAI (aggregated from ~1 km spatial resolution) and soil hydraulic properties from regionally mapped soil units were input as spatially distributed parameters and a single set of meteorological forcing (measured at Kyeamba Creek flux station) was used for the whole study domain. Spatially varying model predictions without assimilation were therefore due to spatially distributed parameter inputs.

One experiment involved assimilating a single pixel of an AMSR-E near-surface soil moisture product derived from descending overpass observations (approximately daily at ~2:00am), representing ~1-2 cm depth at 25 km pixel resolution (defining the study region boundary), into the top-most CBM soil layer (2.2 cm). The AMSR-E data were prepared by applying a 5-day moving average filter to dampen temporally varying random noise. While model/observation bias was removed by rescaling the AMSR-E data series so that the annual mean and standard deviation matched that of the annual CBM predicted series for the top layer soil moisture. In a second experiment, MODIS thermal infrared based *LE* and *H* data products at 5 km pixel resolution, derived with the SEBS algorithm for the daily ~2:00pm (*ET* active) overpass time, were assimilated.

The EnKF implementation was the same as for the one-dimensional field data study (perturbed initial states, forcing data and additive covariance inflation of a priori states), with ensemble perturbations generated for every 5 km simulation pixel in the 25 km by 25 km study region. The 5 km scale CBM predictions were spatially averaged to match 25 km AMSR-E data for the innovation calculations, while updates using the calculated innovation were applied to the individual 5 km pixels. Uncertainty information for both remotely sensed data products was taken from literature. For AMSR-E this information was based on a past validation study that covered the region used in this study (Draper *et al*., 2009a). While for *LE* and *H* a value was also taken from literature based on a survey of a range of published validation studies (Kalma *et al*., 2008).

Results from assimilating the remotely sensed data were mixed. The *LE* and *H* assimilation clearly improved both *LE* and *H* predictions overall relative to eddy covariance data (with 13% and 9% reductions in RMSE respectively compared to no assimilation), for the single 5 km simulation pixel collocated with the flux station site. This further demonstrated the ability of *LE* and *H* assimilation to make strong heat flux improvements as in the previous two studies. Inconsistent impacts were found throughout the experiment period from AMSR-E assimilation (improvements in some periods and degradation in others). However, this produced slightly better improvement to *LE* and negligible improvement to *H* predictions overall (15% and 1% reductions respectively in RMSE compared to no assimilation). In the absence of robust error estimates for the remotely sensed *LE* and *H* data specifically for the region, it was encouraging that modelled heat fluxes were still improved by *LE* and *H* assimilation using error values at least 60% greater than the generic 50 Wm^{-2} value taken from literature as used in the earlier experiment.

The large discrepancy between modelled and observed *LE* in the late spring period for the flux station site – as corrected for by assimilation at the local/point scale in the one-dimensional field data study – was improved here by assimilating the 5 km SEBS data products, and from the 25 km AMSR-E moisture assimilation. Therefore, with the broad-scale remotely sensed data sets (compared to one-dimensional study data) making improvements to the under-predicted *LE* in late spring, the interpretations in the one-dimensional study of local groundwater interaction being a possible major cause for the large model/observation differences is brought into question. This implies model process errors associated with the dynamics of moderate soil moisture, together with maximum vegetation cover of late spring, may play a more significant role in the poor heat flux predictions during this period.

Point scale data from ten different in-situ monitoring sites across the study region were used to validate root-zone soil moisture predictions for collocated 5 km simulation pixels. Averages of comparison metrics across the sites showed degraded soil moisture output from both assimilation experiments, reflecting the overall degradation or negligible improvement for each site individually. AMSR-E assimilation degraded predictions for the root-zone (and the near-surface when validated against data from six in-situ sites) more than the *LE* and *H* assimilation did.

There was minimal net impact on near-surface soil temperature predictions from both assimilation experiments over the year-long period, based on the average of validation metrics from comparisons with point scale in-situ data from six monitoring sites. A minor decrease/improvement in predicted soil temperature from *LE* and *H* assimilation for flux station site comparisons in late spring, where vegetation cover was at its maximum, coincides with the improvement to heat flux predictions here. Given the lack of a direct relationship in the CBM between soil temperature and heat fluxes for vegetated surfaces – as highlighted in the one-dimensional study results – the impact on temperature in this period would likely be a flow on effect from more direct impacts on soil moisture which was increased. The stronger temperature impact from AMSR-E assimilation in this period (some degradation and some improvement) also reflects strong impacts on soil moisture states.

In addition to reaffirming that *LE* and *H* assimilation may have some value for improving heat flux predictions using remotely sensed data, this study has further highlighted some of the difficulties in improving model predictions from data assimilation. The particularly poor soil moisture results indicate a number of possible issues. These include the likelihood of inadequate observation and model error representation, with sub-optimal error correlations between different state and heat flux variables a likely consequence as discussed in relation to some of the one-dimensional study results. There were also instances where the minimum CBM moisture content (which is defined rigidly by wilting point values) appears to have caused biased ensemble predictions, as a result of ensemble members with moisture values falling below wilting point being reset to wilting point values. Very poor results from AMSR-E soil moisture assimilation may partly be a reflection of scale discrepancies between the 25 km AMSR-E domain, the simulation pixels and point validation data. It was not possible to examine these issues in further detail with the data that were available.

8.2 SYNTHESIS

The relative value of assimilating different remotely sensed data types was demonstrated across the three assimilation studies. This provides useful insights contributing towards optimising LSM predictions as required for NWP initialisation, with implications for improved water balance modelling in general.

8.2.1 DATA ASSIMILATION AND CBM/CABLE

Importantly, the first published implementation and demonstration of sequential data assimilation with the CBM was produced in this thesis. The CBM is the basis for the soil and canopy scheme of the newer CABLE model, which therefore has similar formulations relating soil moisture and temperature states with heat fluxes, and is in ongoing development for use in global climate model simulations and possibly for Australia's NWP. Hence the findings here have relevance for how data assimilation might best be used to maximise the predictive skill of this model for these uses into the future. They also highlight some limitations of LSM data assimilation which can be useful for focussing future research towards improving outcomes from its application.

8.2.2 COMPARATIVE PERFORMANCE OF DIFFERENT DATA TYPES

Of more general interest, assimilating *LE* and *H* data was a key component of this research. The motivation was the minimal published research examining the assimilation of these data types compared with soil moisture or skin temperature data, and the hypothesis that *LE* and *H* assimilation should have the greatest impact on *LE* and *H* prediction improvement. The basis for this hypothesis is that predictions of a particular variable(s) of interest is expected to be best served by assimilating data types that are most directly related to it, due to LSM structural errors which are generally difficult to quantify and represent for assimilation. This hypothesis was tested for soil moisture and temperature states, as well the heat flux predictions, by assimilating the different data types and different combinations of them.

Results from *LE* and *H* assimilation were consistent across each of the studies in producing amongst the greatest improvements to heat flux predictions overall. However, they did not strictly affirm the above stated hypothesis, with joint skin temperature and soil moisture data assimilation producing the best heat flux improvement in some cases. Nonetheless, an important contribution has been made, as remotely sensed heat fluxes have been shown to make improvements; there are only two other known published works that have carried out heat flux data assimilation (with limitations in their results validation). The strong promise shown from using these data, at least for improving heat flux predictions, which is a specific requirement for NWP, indicate that more comprehensive research with them is worthwhile.

With skin temperature data also contributing to some of the best heat flux predictions, the question of whether assimilating heat flux data or skin temperature data is the preferable approach is still unanswered, noting that *LE* and *H* are derived from skin temperature in the first place. Again, more detailed research comparing the assimilation of the two data types is warranted for a more definitive answer to this question. A key result from the one-dimensional field data study was that the strongest improvement of *ET*, with simultaneous improvement of root-zone soil moisture and temperature state predictions, was from combined skin temperature and near-surface soil moisture assimilation. This shows that using data directly linked to the water balance (near-surface soil moisture) and data directly linked to the surface energy balance (skin temperature) may be complimentary and mutually beneficial in constraining different model processes. Beyond potential benefits for NWP initialisation, such improvements to both moisture storage and fluxes will also be valuable for overall water balance modelling, thus benefiting water accounting and soil water analysis/forecasting for a range of resource management applications.

The well-published approach of assimilating only near-surface soil moisture did make improvements to heat fluxes though they were not always amongst the strongest improvements. In the synthetic-twin and one-dimensional field data studies it produced the best overall root-zone soil moisture predictions, which did not translate to the strongest heat flux improvement. This likely relates to imprecise error representation for model structural inaccuracies as mentioned in relation to the hypothesis stated earlier. However the large scale AMSR-E soil moisture assimilation clearly degraded root-zone moisture predictions in relation to the ten separate validation data sites for the remotely sensed data study, while still making strong improvement to *LE* according to the single flux station site pixel. These results underscore the difficulty in achieving consistently robust data assimilation performance for all related LSM states and diagnostic fluxes.

8.2.3 MODEL STRUCTURAL ISSUES

Understanding factors that limit the performance of LSM data assimilation can be informative for focusing future research and maximising the benefits of its application. Difficulties in accurately representing model prediction error is a major limitation, which is a function of structural error (from generalised formulations) and input data errors (in initial state conditions, and parameter and forcing data). These can be due to measurement inaccuracy, poor spatial representation, or use of generalised/default values of model parameters because of a lack of available data. Importantly, this work highlighted some key issues relating to strengths and limitations of the CBM (with some relevance to the newer CABLE model and LSMs in general) in a data assimilation context, which are now discussed.

For full year CBM simulations without assimilation, predicted heat fluxes were best matched with observations (from both eddy covariance and remotely sensed derived data) over the mainly energy limited winter and early spring months, where soil profile moisture content was at or near maximum. It is therefore assumed that water was readily available in this period, such that *ET* was mostly dependent on atmospheric demand and occurred at or near potential, which is thus relatively straight forward to calculate based solely on atmospheric data and canopy characteristics. This implies that modelling heat fluxes is likely to be most reliable for these seasonal conditions (with LSMs incorporating a standard potential *ET* calculation using atmospheric and vegetation cover data) – an interpretation supported by the comparisons between the model and observed data.

The generally poorer heat flux predictions relative to observations where root-zone soil moisture storage was below maximum (from late summer to autumn early in the year, and late spring to summer later in the year), indicates that modelled fluxes are more error prone when they have a greater dependency on modelled moisture dynamics to scale potential *ET* calculations for water limited conditions. Soil moisture states in the CBM are used in a linear water availability term for scaling potential *ET*, hence this may not be an adequate representation. While for vegetation transpiration, the dependency on complex calculations related to plant stomatal conductance and photosynthesis involving additional parameters, may contribute to error. Especially with generalised values for these parameters.

The vegetation component of heat fluxes is particularly challenging to model accurately under soil moisture controlled *ET* conditions. This is supported by the largest differences between observed and modelled heat fluxes occurring in the late spring to early summer period in the year-long experimental studies, where the predominantly grass pasture was at its fullest cover with diminishing soil moisture store. Large discrepancies occur for both the point scale simulation relative to eddy covariance data in the one-dimensional study, and the 5 km scale simulation relative to remotely sensed flux data for the assessed pixel collocated with the flux station.

Point scale ancillary data used in the one-dimensional study indicated that large discrepancies in late spring to summer may have been due to groundwater interaction, which the CBM does not represent. This interpretation highlights an example where the lack of representation of a certain processes in a LSM potentially contributes to predictive error. However, large discrepancies were still evident relative to the much broader scale remotely sensed data (assimilating 25 km scale AMSR-E and 5 km heat flux data each considerably reduced discrepancies between the 5 km heat flux simulations and flux station data), implying a more general issue with poor CBM predictions related to particular seasonal conditions – i.e. water limited *ET* with high vegetation cover – may also play a role.

The lack of a direct relationship between soil temperature states and vegetation heat fluxes is also highlighted in relation to the maximum vegetation cover of late spring to summer. Strong impacts on heat flux predictions here from assimilating heat flux data coincided with minimal impacts on soil temperature. Results from the one-dimensional study showed that with improvements to soil temperature in this period from skin temperature assimilation, corresponding improvement to *ET* prediction could be explained as an indirect effect from impacts on soil moisture. Soil temperature is directly involved in calculating the soil components of *LE* and *H*, which are a larger proportion of total heat fluxes for sparser vegetation cover.

The changing relationships between state variables and heat fluxes across seasons and as vegetation cover changes implies temporally varying errors associated with these relationships. Examples from the CBM (and the newer CABLE model) structure which can contribute to temporally varying errors include having user-assigned fractions of plant roots for each soil layer which are fixed over time. Where there are large seasonal changes in vegetation, such as with pastures in the Kyeamba Creek region in this study, a fixed root depth might over-state transpiration from deeper soil layers for seasons in the annual growth cycle where grass is not fully developed and coverage is sparse. Also, the soil hydraulic properties for all six soil layers are fixed with identical parameter values (i.e. no depth variation), which would likely result in inaccurate vertical water redistribution that will affect *ET*. Quantifying the combination of these examples of structural error together with parameter data errors (e.g. for soil layer root fractions and hydraulic property values) in terms of contribution to overall prediction error over time is not straight forward.

8.2.4 DATA ASSIMILATION TECHNIQUE ISSUES

EnKF data assimilation is fundamentally based on relationships between errors in the observations and model predictions, and thus quantifying the errors is critical. Correlation between different LSM state and diagnostic variable errors is important in determining how the EnKF propagates state updates to different parts of the model. In addition to the difficulty in defining errors for a particular instance in time, temporally varying model prediction error for LSM states and fluxes, and correlations between them, are very difficult to quantify accurately and represent with ensembles. A major reason is the complexity of some non-linear model relationships together with a general lack of independent data to enable detailed analyses of all aspects of error. This is a general limitation to achieving optimal LSM data assimilation performance that would extend beyond this work and the CBM/CABLE models.

Detailed examination of all aspects of model prediction error was beyond the scope of this thesis. However, a general representation of overall error statistics using available information ensured reasonable EnKF performance for most experiments. This involved prescribing errors to initial state conditions, and to forcing data inputs informed by measurement error estimates, and estimates of representative errors between data sets measured at different locations. For the full year experiments where real data were assimilated, additive inflation was also applied to background state ensembles at analysis time steps. Over prolonged periods of state updating, predicted ensemble spreads dependent on forcing perturbation can collapse towards a single value (especially over longer rain-free periods). Consequently, model error may become under-stated such that the EnKF is no longer effective, possibly even leading to divergence between the mean prediction and observations. Ensemble inflation to increase their spread at update times reduces this risk, and accounts for the fact that there are other errors which could not be explicitly defined (e.g. from model structure and parameter data). The relative thicknesses of soil layers were used to scale the ensemble inflation in this work, factoring in the dampening of state errors for deeper/thicker layers – ensuring more realistic error correlation between states in different layers compared to applying uniform inflation.

Another challenge to achieving optimal EnKF performance is accounting for potentially biased ensemble means near state boundary values. This problem was interpreted from some results in the remotely sensed data study and is an artefact of the CBM having the wilting point parameter value as the minimum boundary for soil moisture content (also relevant to CABLE). With perturbed soil moisture content not able to drop below the wilting point value, multiple ensemble members can be fixed at this minimum boundary, leading to a positively biased ensemble mean. Moisture content can drop below the wilting point in reality. The remotely sensed assimilation study also highlighted the added dimension to the challenge of defining error when dealing with spatially distributed modelling and comparing observed and modelled data at different spatial scales. The lack of independent data for different spatial scales limited the ability to analyse errors related to scale discrepancies between data sets in any detail. It was also a limitation to better understanding the nature of the poor results for soil moisture state prediction in this study, especially from assimilating the spatially disparate AMSR-E moisture data.

Model error issues discussed here in relation to the work in this thesis revolve around the challenges of quantifying key aspects of prediction error – from model structure, input data and spatial representation/discrepancies – and accurately representing them with ensembles for optimal EnKF performance. These issues are ubiquitous with LSM data assimilation applications in general, while some model structure issues will be model specific. Non-stationarity of prediction error variances, and of correlations between them for different variables, can add to the difficulty in defining error and should be part of the focus of future research towards improved model error representation.

Observational data error is an important component of the EnKF due to its role in calculating the Kalman gain that weights innovations for state updating. Removing bias between predicted model states and observations of them prior to their assimilation, typically through rescaling approaches such as cdf matching or matching data series means and standard deviations is also important, since a fundamental assumption of data assimilation is that it deals specifically with random differences between observed and modelled anomalies from the true mean state. Non-stationary state bias with seasonal variation (from either model predictions or observations, or both) may not be completely accounted for when applying corrections based on annual statistics of data series, as was done for the year-long experiments in this work using mean and standard deviation rescaling, which could limit data assimilation performance.

Corrections can be applied for observed/modelled state biases as defined for different time scales (e.g. seasonal, annual, multi-annual etc.), though it is not always possible to know if biases defined for a particular time scale within a certain period actually represent true climatological bias between data sets. Defining and removing seasonal 'bias' for a one year period (the maximum experimental length in this work) may result in removal of some differences in true seasonal anomalies relative to longer-term climatological bias, as noted by Draper *et al*. (2009b). Even bias defined for multiple years may not necessarily reflect true climatological bias, or that of the immediate future, when considering periods such as the Millenium Drought which affected south east Australia from ~2001-2009 (van Dijk *et al*., 2013). This implies that for modelling forward in time – whether for NWP in the shorter term or climate in the longer term– rescaling of assimilated data using previous time period definitions of bias could inhibit optimal assimilation. Therefore the lack of long data series for hydrologic states is a limitation in terms of bias removal. For remotely sensed soil moisture data, the operational period of AMSR-E spanned ~2002-2011, which is most of the Millennium Drought period, while SMOS has so far been in operation for less than five years.

Defining and quantifying errors for observed data of course relies on the availability of suitable independent validation data, or on techniques such as triple collocation, which can determine observed data error variances based on three independent estimates of the same quantity (e.g. Scipal *et al*., 2008). Data produced from remotely sensed observations are inherently more difficult to validate than point scale data, given the obvious spatial disparity with in-situ data which is mostly collected at the point scale. Monitoring networks such as OzNet in Australia provide regionally distributed in-situ soil moisture validation data, but are very isolated on a global scale. The relative expense and complexity of eddy covariance systems means that the most accurate in-situ validation data for remotely sensed *LE* and *H* products are even more limited than for soil moisture.

General error estimates for different remotely sensed products, based on various validation studies for a range of locations/environments, are presented in peer-reviewed literature. Relying on such values is an option in the absence of local validation data for a study region (the error quantity used for AMSR-E moisture data in this thesis was from an earlier validation study for this product using OzNet data (Smith *et al*., 2012) distributed across the Kyeamba Creek region). However, general estimates may not be representative of particular regions, and non-stationary error variances cannot be represented with single values. Triple collocation can therefore be a valuable alternative for error estimation that is well suited for remotely sensed data. This is on the assumption that three independent data sets with a large number of coincident observations in time are available for the quantity of interest, with strictly no correlation between their residual error terms – a possible limitation if available data are derived from the same or similar raw observations – and the relationship between the data sets are linear. Bias between data sets due to different observing sensors and derivation algorithms may also be an issue, similar to that discussed above in relation to model/observation bias.

8.3 FINAL CONCLUSIONS

Assimilating key land surface related data types obtainable from remote sensing – near-surface soil moisture, skin temperature, and *LE* and *H* – into the CBM can clearly improve *LE* and *H* predictions as required for NWP. This capability is presumed to also hold for the CABLE model, due to its very similar soil and canopy scheme relating soil moisture and temperature states with heat fluxes. Improved fluxes/*ET* over longer time scales are also important for improved water balance modelling, which will benefit a range of water resource management applications.

Specifically, *LE* and *H* data assimilation, which included a demonstration using remotely sensed products, is shown to consistently produce some of the strongest improvements to heat flux predictions amongst the data types tested, based on the experiments performed. This finding is important given the minimal research afforded to *LE* and *H* assimilation to date in the peer reviewed literature.

Near-surface soil moisture assimilation also improves heat fluxes. Though even when it produced the greatest improvements to root-zone moisture prediction, this did not necessarily translate to better heat flux predictions than from assimilating *LE* and *H* – presumably due to model structural inaccuracies with LSM moisture states and heat flux relationships. Therefore, despite near-surface soil moisture assimilation providing clear value for LSM prediction, on its own it may not be the best option for achieving optimal heat fluxes.

Assimilating skin temperature on its own has potential to improve heat flux prediction to a similar degree as *LE* and *H* assimilation, though there were lesser improvements in some experiments. Thus the degree of improvement may not always be consistent for a model such as CBM (and CABLE), where the strength of the relationship between state variables (particularly soil temperature), skin temperature and heat fluxes varies temporally with vegetation cover.

Assimilating a combination of data types, which individually are more closely related to different parts of a LSM, can be complimentary in balancing their respective impacts on different variables. As highlighted by the combined assimilation of skin temperature and near-surface soil moisture, which improved *ET* prediction more than from *LE* and *H* assimilation, and simultaneously improved root-zone soil moisture and temperature state predictions – which is particularly encouraging from a water balance modelling perspective. This result for *ET* prediction indicates that strategic use of skin temperature data may possibly remove any need for assimilating remotely sensed *LE* and *H* products (derived using skin temperature) where the aim is to improve heat fluxes. Though more comprehensive follow-up research is required to determine this with greater certainty.

8.4 FURTHER WORK

Based on the work in this thesis, a number of key unresolved issues associated with LSM data assimilation were identified. Addressing these was beyond the scope of this thesis, however they provide clear direction for focussing future research.

Insight was gained into which land surface data types(s) have the greatest potential for improving heat flux prediction, and for simultaneous improvement of state variables. Follow-up research that would clarify and verify these findings, and also advance the knowledge acquired from this research include:

- More comprehensive comparisons between *LE* and *H* data assimilation and skin temperature assimilation – specifically with remote sensing data, where the same skin temperature data used to derive the *LE* and *H* products is assimilated. This would clarify whether remotely sensed *LE* and *H* calculated from skin temperature can provide additional skill to LSM *LE* and *H* predictions, compared to directly assimilating the skin temperature into the LSM;

- Conducting comparison experiments over longer time periods with different remotely sensed products for each data type (from different sensor data and retrieval algorithms), and using different LSMs, to determine how generally applicable the findings are;

- Carrying out the comparison experiments with the latest version of the CABLE model to verify the applicability of the conclusions; and

- For land surface observation data types shown to improve offline LSM fluxes and states when assimilated, test the assimilation of them with the LSM coupled to an atmospheric model (i.e. for CABLE within ACCESS), and assess impacts on predicted screen-level air temperature and humidity in addition to heat fluxes and soil states.

A major issue in terms of optimising LSM performance is the need to improve error representation. This requires more research into the following:

- Correlations between errors for different LSM variable predictions – e.g. between near-surface and deeper soil moisture states, or between all state variables and heat fluxes. This would need to be model specific;

- Error non-stationarity – how the error for different predictions vary, which also affects the correlations between them;

- More detailed examination of LSM structural error and quantifying/correcting it;

- Error related to spatial discrepancies between assimilated data and simulated resolutions;

- Better ensemble generation for the EnKF – including whether Gaussian ensembles are always appropriate/realistic, such as for soil moisture values near boundary values (i.e. wilting point);

- More comprehensive examination of bias between data sets – in terms of defining it and better techniques for correcting it;

- Evaluating the design of in-situ monitoring to maximise the benefits for validating spatial data from remote sensors and simulations; and

- A detailed review of the relative benefits of triple collocation to quantify error for different remotely sensed data types.

REFERENCES

Abramowitz, G. 2006. *User guide for the Community Atmosphere Biosphere Land Exchange (CABLE) land surface model*. Aspendale, Australia, CSIRO Marine and Atmospheric Research

Albergel, C., de Rosnay, P., Gruhier, C., Muñoz Sabater, J., Hasenauer, S., Isaksen, L., et al. 2012. Evaluation of remotely sensed and modelled soil moisture products using global ground-based in situ observations. *Remote Sensing of Environment*, 118**,** 215-226.

Allen, R. G., Pereira, L. S., Raes, D. & Smith, M. 1998. *Crop evapotranspiration - Guidelines for computing crop water requirements - FAO Irrigation and drainage paper 56*. Rome, FAO - Food and Agriculture Organization of the United Nations

Allen, R. G., Tasumi, M. & Trezza, R. 2007. Satellite-based energy balance for mapping evapotranspiration with internalized calibration (METRIC): Model. *Journal of Irrigation and Drainage Engineering,* 133**,** 380-394.

Anderson, J. L. 2007. An adaptive covariance inflation error correction algorithm for ensemble filters. *Tellus,* 59A**,** 210-224.

Anderson, J. L. & Anderson, S. L. 1999. A Monte Carlo implementation of the nonlinear filtering problem to produce ensemble assimilations and forecasts. *Monthly Weather Review,* 127**,** 2741-2758.

Balsamo, G., Mahfouf, J.-F., Belair, S. & Deblonde, G. 2007. A land data assimilation system for soil moisture and temperature: An information content study. *Journal of Hydrometeorology,* 8**,** 1225-1242.

Bastiaanssen, W. G. M., Menenti, M., Feddes, R. A. & Holtslag, A. A. M. 1998. A remote sensing surface energy balance algorithm for land (SEBAL) 1. Formulation. *Journal of Hydrology,* 212-213**,** 198-212.

Batjes, N. H. 2002. *Soil parameter estimates for the soil types of the world for use in global and regional modelling (Version 2.1; July 2002).* Wageningen, International Food Policy Research Institute (IFPRI) and International Soil Reference and Information Centre (ISRIC)

Beljaars, A. C. M., Viterbo, P., Miller, H. L. & Betts, A. K. 1996. The anomalous rainfall over the United States during July 1993: Sensitivity to land surface parameterization and soil moisture anomalies. *Monthly Weather Review,* 124**,** 362-383.

Beven, K. 2012. *Rainfall-Runoff Modelling: The Primer,* Chichester, UK, John Wiley & Sons, Ltd.

Black, C. A. 1965. *Methods of Soil Analysis: Part I Physical and mineralogical properties*. Madison, Wisconsin, USA, American Society of Agronomy

Boulet, G., Oliosob, A., Ceschia, E., Marloie, O., Coudert, B., Rivalland, V., et al. 2012. An empirical expression to relate aerodynamic and surface temperatures for use within single-source energy balance models. *Agricultural and Forest Meteorology,* 161**,** 148-155.

Bouttier, F. & Courtier, P. 1999. Lecture notes on data assimilation concepts and methods. Reading, UK: European Centre for Medium-Range Weather Forecasts.

Bouttier, F., Mahfouf, J.-F. & Noilhan, J. 1993. Sequential assimilation of soil moisture from atmospheric low-level parameters. Part I: Sensitivity and calibration studies. *Journal of Applied Meteorology,* 32**,** 1352-1364.

Bowen, I. S. 1926. The ratio of heat losses by conduction and by evaporation from any water surface. *Physical Review,* 27**,** 779-787.

Brooks, R. J. & Corey, A. T. 1964. *Hydraulic properties of porous media*. Fort Collins, Colorado, Colorado State University

Brutsaert, W. 1999. Aspects of bulk atmospheric boundary layer similarity under free-convective conditions. *Reviews of Geophysics,* 37**,** 439-451.

Brutsaert, W. 2005. *Hydrology: An Introduction,* Cambridge, United Kingdom, Cambridge Univ. Press.

Burba, G. 2013. *Eddy Covariance Method: for Scientific, Industrial, Agricultural and Regulatory Applications,* Lincoln, Nebraska, USA, LI-COR, Inc.

Campbell, G. S. 1974. A simple model for determining unsaturated conductivity from moisture retention data. *Soil Science,* 117**,** 311-314.

Campbell Scientific 1996. CS615 Water content reflectometer. *Instruction manual.* Campbell Scientific Inc., Logan, Utah, USA.

Campbell Scientific 2002. CS616 Water content reflectometer. *Instruction manual.* Campbell Scientific Inc., Logan, Utah, USA.

Campbell Scientific 2003. CSAT Three dimensional sonic anemometer. *Instruction manual.* Campbell Scientific Inc., Logan, Utah, USA.

Campbell Scientific 2004. HFT3 Soil heat flux plate. *Instruction manual.* Campbell Scientific Inc., Logan, Utah, USA.

Carlson, T. N. & Ripley, D. A. 1997. On the relation between NDVI, fractional vegetation cover, and Leaf Area Index. *Remote Sensing of Environment,* 62**,** 241-252.

Case, J. L., Crosson, W. L., Kumar, S. V., Lapenta, W. M. & Peters-Lidard, C. D. 2008. Impacts of high-resolution land surface initialization on regional sensible weather forecasts from the WRF model. *Journal of Hydrometeorology,* 9**,** 1249-1266.

Chen, F., Manning, K. W., LeMone, M. A., Trier, S. B., Alfieri, J. G., Roberts, R., et al. 2007. Description and evaluation of the characteristics of the NCAR high-resolution land data assimilation system. *Journal of Applied Meteorology and Climatology,* 46**,** 694-713.

Chen, F., Pielke Sr., R. A. & Mitchell, K. 2001. Development and application of land surface models for mesoscale atmospheric models: Problems and promises. *In:* Lakshmi, V., Albertson, J. D. & Schaake, J. (eds.) *Land surface hydrology, meteorology, and climate: Observations and modeling.* Washington, DC, American Geophysical Union.

Chen, X. Y. & McKane, D. J. 1997. *Soil landscapes of the Wagga Wagga 1:100 000 sheet*. Sydney, Department of Land and Water Conservation

Choudhury, B. J. 1989. Estimating evaporation and carbon assimilation using infrared temperature data: Vistas in modeling. *In:* Asrar, G. (ed.) *Theory and applications of optical remote sensing.* New York, John Wiley and Sons.

Clapp, R. B. & Hornberger, G. M. 1978. Empirical equations for some soil hydraulic properties. *Water Resources Research,* 14**,** 601-604.

Crosson, W. L., Laymon, C. A., Inguva, R. & Schamschula, M. P. 2002. Assimilating remote sensing data in a surface flux-soil moisture model. *Hydrological Processes,* 16**,** 1645-1662.

Crow, W. T. & Wood, E. F. 2003. The assimilation of remotely sensed soil brightness temperature imagery into a land surface model using Ensemble Kalman filtering: a case study based on ESTAR measurements during SGP97. *Advances in Water Resources,* 26**,** 137-149.

Dai, Y., Zeng, X., Dickinson, R. E., Baker, I., Bonan, G. B., Bosilovich, M. G., et al. 2003. The common land model (CLM). *Bulletin of the American Meteorological Society,* 84**,** 1013.

De Lannoy, G. J. M., Houser, P. R., Pauwels, V. R. N. & Verhoest, N. E. C. 2007. State and bias estimation for soil moisture profiles by an ensemble Kalman filter: Effect of assimilation depth and frequency. *Water Resources Research,* 43**,** W06401.

De Ridder, K. 2009. Soil temperature spin-up in land surface schemes. *Theoretical and Applied Climatology,* 95**,** 341-347.

de Rosnay, P., Balsamo, G., Albergel, C., Muñoz-Sabater, J. & Isaksen, L. 2014. Initialisation of Land Surface Variables for Numerical Weather Prediction. *Surveys in Geophysics,* 35**,** 607-621.

de Rosnay, P., Drusch, M., Vasiljevic, D., Balsamo, G., Albergel, C. & Isaksen, L. 2013. A simplified Extended Kalman Filter for the global operational soil moisture analysis at ECMWF. *Quarterly Journal of the Royal Meteorological Society,* 139**,** 1199-1213.

Denman, K. L., Brasseur, G., Chidthaisong, A., Ciais, P., Cox, P. M., Dickinson, R. E., et al. 2007. Couplings between changes in the climate system and biogeochemistry. *In:* Solomon, S., Qin, D., Manning, M., Chen, Z., Marquis, M., Averyt, K. B., Tignor, M. M. B. & Miller, H. L. (eds.) *Climate change 2007: The physical science basis. Contribution of Working Group I to the Fourth Assessment Report of the Intergovernmental Panel on Climate Change.* Cambridge, United Kingdom and New York, NY, USA, Cambridge University Press.

Dharssi, I., Bovis, K. J., Macpherson, B. & Jones, C. P. 2011. Operational assimilation of ASCAT surface soil wetness at the Met Office. *Hydrology and Earth System Sciences,* 15**,** 2729-2746.

Dickinson, R. E. 1984. Modelling evapotranspiration for three dimensional global climate models. *In:* Hansen, J. E. & Takahasi, T. (eds.) *Climate Processes and Climate Sensitivity.* American Geophysical Union.

Dirmeyer, P. A., Schlosser, C. A. & Brubaker, K. L. 2009. Precipitation, Recycling, and Land Memory: An Integrated Analysis. *Journal of Hydrometeorology,* 10**,** 278-288.

Donohue, R. J., Roderick, M. L. & McVicar, T. R. 2008. Deriving consistent long-term vegetation information from AVHRR reflectance data using a cover-triangle-based framework. *Remote Sensing of Environment,* 112**,** 2938-2949.

Douville, H., Viterbo, P., Mahfouf, J. F. & Beljaars, A. C. M. 2000. Evaluation of the optimum Interpolation and nudging techniques for soil moisture analysis using FIFE data. *Monthly Weather Review,* 128**,** 1733-1756.

Draper, C. S., Mahfouf, J.-F. & Walker, J. P. 2009b. An EKF assimilation of AMSR-E soil moisture into the ISBA land surface scheme. *Journal of Geophysical Research,* 114**,** D20104.

Draper, C. S. & Mills, G. 2008. The Atmospheric Water Balance over the Semiarid Murray–Darling River Basin. *Journal of Hydrometeorology,* 9**,** 521-534.

Draper, C. S., Reichle, R. H., De Lannoy, G. J. M. & Liu, Q. 2012. Assimilation of passive and active microwave soil moisture retrievals. *Geophysical Research Letters,* 39**,** L04401.

Draper, C. S., Walker, J. P., Steinle, P., de Jeu, R. & Holmes, T. 2009a. An evaluation of AMSR-E derived soil moisture over Australia. *Remote Sensing of Environment,* 113**,** 703-710.

Drusch, M., Scipal, K., de Rosnay, P., Balsamo, G., Andersson, E., Bougeault, P., et al. 2009. Towards a Kalman Filter based soil moisture analysis system for the operational ECMWF Integrated Forecast System. *Geophysical Research Letters,* 36**,** L10401.

Drusch, M., Wood, E. F. & Gao, H. 2005. Observation operators for the direct assimilation of TRMM microwave imager retrieved soil moisture. *Geophysical Research Letters,* 32**,** L15403.

Ek, M. B., Mitchell, K. E., Lin, Y., Rogers, E., Grunmann, P., Koren, V., et al. 2003. Implementation of Noah land surface model advances in the National Centers for Environmental Prediction operational mesoscale Eta model. *Journal of Geophysical Research,* 108**,** 8851.

Entekhabi, D., Nakamura, H. & Njoku, E. G. 1994. Solving the inverse problem for soil moisture and temperature profiles by sequential assimilation of multifrequency remotely sensed observations. *IEEE Transactions on Geoscience and Remote Sensing,* 32**,** 438-448.

Entekhabi, D., Njoku, E. G., O'Neill, P. E., Kellogg, K. H., Crow, W. T. & Edelstein, W. N., et al 2010. The Soil Moisture Active Passive (SMAP) mission. *Proceedings of the IEEE Transactions on Geoscience and Remote Sensing,* 98**,** 704-716.

Evensen, G. 1994. Sequential data assimilation with a nonlinear quasi-geostrophic model using Monte Carlo methods to forecast error statistics. *Journal of Geophysical Research - Oceans,* 99**,** 10143-10162.

Evensen, G. 2009. *Data assimilation: The Ensemble Kalman Filter,* Berlin; New York, Springer.

Franks, S. W. & Beven, K. 1999. Conditioning a multiple-patch SVAT model using uncertain time-space estimates of latent heat fluxes as inferred from remotely sensed data. *Water Resources Research,* 35**,** 2751-2761.

French, A. N., Jacob, F., Anderson, M. C., Kustas, W. P., Timmermans, W., Gieske, A., et al. 2005. Surface energy fluxes with the Advanced Spaceborne Thermal Emission and Reflection radiometer (ASTER) at the Iowa 2002 SMACEX site (USA). *Remote Sensing of Environment,* 99**,** 55-65.

Gao, H., Wood, E. F., Jackson, T. J., Drusch, M. & Bindlish, R. 2006. Using TRMM/TMI to retrieve surface soil moisture over the southern United States from 1998 to 2002. *Journal of Hydrometeorology,* 7**,** 23-38.

Gibson, J. K., Kallberg, P., Uppala, S., Hernandez, A., Nomura, A. & Serrano, E. 1997. *ERA description*. Reading, UK, European Centre for Medium Range Weather Forecasts

Glenn, E. P., Huete, A. R., Nagler, P. L., Hirschboeck, K. K. & Brown, P. 2007. Integrating remote sensing and ground methods to estimate evapotranspiration. *Critical Reviews in Plant Sciences,* 26**,** 139-168.

Gokmen, M., Vekerdy, Z., Verhoef, A., Verhoef, W., Batelaan, O. & van der Tol, C. 2012. Integration of soil moisture in SEBS for improving evapotranspiration estimation under water stress conditions. *Remote Sensing of Environment,* 121**,** 261-274.

Hain, C. R., Crow, W. T., Anderson, M. C. & Mecikalski, J. R. 2012. An ensemble Kalman filter dual assimilation of thermal infrared and microwave satellite observations of soil moisture into the Noah land surface model. *Water Resources Research,* 48**,** W11517.

Heathman, G., Starks, P. J., Ahuja, L. & Jackson, T. 2003. Assimilation of soil moisture to estimate profile soil water content. *Journal of Hydrology,* 279**,** 1-17.

Holm, E. V. 2003. Lecture notes on assimilation algorithms. Reading, UK: European Centre for Medium-Range Weather Forecasts.

Houser, P. R., De Lannoy, G. & Walker, J. P. 2010. Land surface data assimilation. *In:* Lahoz, W., Khatattov, B. & Menard, R. (eds.) *Data Assimilation: Making sense of observations.* The Netherlands, Springer.

Houtekamer, P. L. & Mitchell, H. L. 1998. Data assimilation using Ensemble Kalman filter techniques. *Monthly Weather Review,* 126**,** 796-811.

Hsieh, C. I., Huang, C. W. & Kiely, G. 2009. Long-term estimation of soil heat flux by single layer soil temperature. *International Journal of Biometeorology,* 53**,** 113-123.

Huang, C., Li, X. & Lu, L. 2008. Retrieving soil temperature profile by assimilating MODIS LST products with ensemble Kalman filter. *Remote Sensing of Environment,* 112**,** 1320-1336.

Imaoka, K., Kachi, M., Kasahara, M., Ito, N., Nakagawa, K. & Oki, T. 2010. Instrument performance and calibration of AMSR-E and AMSR2. *International Archives of the Photogrammetry, Remote Sensing and Spatial Information Science,* XXXVIII**,** 13-16.

Jackson, T. J., Schmugge, J. & Engman, E. T. 1996. Remote sensing applications to hydrology: soil moisture. *Hydrological Sciences Journal,* 41**,** 517-530.

Jiang, L. & Islam, S. 2001. Estimation of surface evaporation map over southern Great Plains using remote sensing data. *Water Resources Research,* 37**,** 329-340.

Johansen, O. 1975. *Thermal conductivity of soils.* Ph.D. thesis, University of Trondheim.

Kaleita, A. L. & Kumar, P. 2000. AVHRR estimates of surface temperature during the Southern Great Plains 1997 Experiment. *Journal of Geophysical Research,* 105**,** 20791-20801.

Kalma, J. D., McVicar, T. R. & McCabe, M. F. 2008. Estimating Land Surface Evaporation: A Review of Methods Using Remotely Sensed Surface Temperature Data. *Surveys in Geophysics,* 29**,** 421–469.

Kalman, R. E. 1960. A new approach to linear filtering and prediction problems. *Transaction of the ASME - Journal of Basic Engineering,* 82**,** 35-45.

Kalnay, E., Kanamitsu, M., Kistler, R., Collins, W., Deavan, D. & Gandin, L., et al. 1996. The NCEP/NCAR 40-Year Reanalysis Project. *Bulletin of the American Meteorological Society,* 77.

Keenan, T. F., Carbone, M. S., Reichstein, M. & Richardson, A. D. 2011. The model–data fusion pitfall: assuming certainty in an uncertain world. *Oecologia,* 167**,** 587-597.

Kerr, Y. H., Waldteufel, P., Wigneron, J. P., Martinuzzi, J. M., Font, J. & Berger, M. 2001. Soil moisture retrieval from space: the Soil Moisture and Ocean Salinity (SMOS) mission. *IEEE Transactions on Geoscience and Remote Sensing,* 39**,** 1729-1735.

Kerr, Y. H., Waldteufel, P., Wigneron, J.-P., Delwart, S., Cabot, F., Boutin, J., et al. 2010. The SMOS mission: New tool for monitoring key elements of the global water cycle. *Proceedings of the IEEE Transactions on Geoscience and Remote Sensing,* 98**,** 666-687.

Kipp & Zonen B.V. 2003. CNR1 net radiometer. *Instruction manual.* Kipp & Zonen B.V., Delft, The Netherlands.

Koster, R. D., Mahanama, S. P. P., Yamada, T. J., Balsamo, G., Berg, A. & Jeong, J.-H., et al. 2011. The Second Phase of the Global Land–Atmosphere Coupling Experiment: Soil Moisture Contributions to Subseasonal Forecast Skill. *Journal of Hydrometeorology,* 12**,** 805-822.

Koster, R. D. & Milly, P. C. D. 1997. The interplay between transpiration and runoff formulations in land surface schemes used with atmospheric models. *Journal of Climate,* 10**,** 1578-1591.

Koster, R. D., Suarez, M. J., Liu, P., Jambor, U., Berg, A., Kistler, M., et al. 2004. Realistic initialization of land surface states: Impacts on subseasonal forecast skill. *Journal of Hydrometeorology,* 5**,** 1049-1063.

Kowalczyk, E. A., Garrat, J. R. & Krummel, P. B. 1994. *Implementation of a soil-canopy scheme into the CSIRO GCM – regional aspects of the model response*. Aspendale, Australia, CSIRO Atmospheric Research. Technical Paper, 32.

Kowalczyk, E. A., Stevens, L., Law, R. M., Dix, M., Wang, Y.-P., Harman, I. N., et al. 2013. The land surface model component of ACCESS: description and impact on the simulated surface climatology. *Australian Meteorological and Oceanographic Journal,* 63**,** 65-82.

Kowalczyk, E. A., Wang, Y.-P., Law, R. M., Davies, H. L., McGregor, J. L. & Abramowitz, G. 2006. *The CSIRO Atmosphere Biosphere Land Exchange (CABLE) model for use in climate models and as an offline model*. Aspendale, Australia, CSIRO Marine and Atmospheric Research. Paper 013.

Kumar, P. & Kaleita, A. L. 2003. Assimilation of near-surface temperature using extended Kalman filter. *Advances in Water Resources,* 26**,** 79-93.

Kumar, S. V., Reichle, R. H., Koster, R. D., Crow, W. T. & Peters-Lidard, C. D. 2009. Role of subsurface physics in the assimilation of surface soil moisture observations. *Journal of Hydrometeorology,* 10**,** 1534-1547.

Kustas, W. P., Anderson, M. C., Norman, J. M. & Li, F. Q. 2007. Utility of radiometric–aerodynamic temperature relations for heat flux estimation. *Boundary-Layer Meteorology,* 122**,** 167-187.

Kustas, W. P. & Norman, J. M. 1996. Use of remote sensing for evapotranspiration monitoring over land surfaces. *Hydrological Sciences Journal-Journal Des Sciences Hydrologiques,* 41**,** 495-516.

Kustas, W. P., Norman, J. M., Anderson, M. C. & French, A. N. 2003. Estimating subpixel surface temperatures and energy fluxes from the vegetation index–radiometric temperature relationship. *Remote Sensing of Environment,* 85**,** 429-440.

Ladson, A. 2008. *Hydrology: An Australian introduction* Oxford University Press.

Lakshmi, V. 2000. A simple surface temperature assimilation scheme for use in land surface models. *Water Resources Research,* 36**,** 3687-3700.

Law, R. M., Raupach, M. R., Abramowitz, G., Dharssi, I., Haverd, V., Pitman, A. J., et al. 2012. *The Community Atmosphere Biosphere Land Exchange (CABLE) model Roadmap for 2012–2017*. Aspendale, Australia, The Centre for Australian Weather and Climate Research (CAWCR). Technical Report 057.

Levis, S. 2010. Modeling vegetation and land use in models of the Earth System. *WIREs Climate Change,* 1**,** DOI: 10.1002/wcc.83.

Li, F., Jackson, T. J., Kustas, W. P., Schmugge, T. J., French, A. N., Cosh, M. H., et al. 2004. Deriving land surface temperature from Landsat 5 and 7 during SMEX02/SMACEX. *Remote Sensing of Environment,* 92**,** 521-534.

Li, H., Kalnay, E. & Miyoshi, T. 2009. Simultaneous estimation of covariance inflation and observation errors within an ensemble Kalman filter. *Quarterly Journal of the Royal Meteorology Society,* 135**,** 523-533.

Li, J. & Islam, S. 1999. On the estimation of soil moisture profile and surface fluxes partitioning from sequential assimilation of surface layer soil moisture. *Journal of Hydrology,* 220**,** 86–103.

LI-COR 2003. LI-7500 CO2/H2O Analyzer. *Instruction manual.* LI-COR Inc., Lincoln, Nebraska, USA.

Liu, Q., Reichle, R. H., Bindlish, R., Cosh, M. H., Crow, W. T., de Jeu, R., et al. 2011. The contributions of precipitation and soil moisture observations to the skill of soil moisture estimates in a land data assimilation system. *Journal of Hydrometeorology,* 12**,** 750-765.

Liu, S., Lu, L., Mao, D. & Jia, L. 2007. Evaluating parameterizations of aerodynamic resistance to heat transfer using field measurements. *Hydrology and Earth System Sciences,* 11**,** 769-783.

Lu, H., Raupach, M. R. & McVicar, T. R. 2001. *A robust model to separate remotely sensed vegetation indices into woody and non-woody cover and its large-scale application using AVHRR NDVI time series*. Australia, CSIRO. technical report 35/01.

Lu, H., Raupach, M. R., McVicar, T. R. & Barrett, D. J. 2003. Decomposition of vegetation cover into woody and herbaceous components using AVHRR NDVI time series. *Remote Sensing of Environment,* 86**,** 1-18.

Mahfouf, J.-F. 1991. Analysis of soil moisture from near surface parameters: A feasibility study. *Journal of Applied Meteorology,* 30**,** 1534-1547.

Mahfouf, J.-F. 2010. Assimilation of satellite-derived soil moisture from ASCAT in a limited-area NWP model. *Quarterly Journal of the Royal Meteorological Society,* 136**,** 784-798.

Mahfouf, J.-F. & Noilhan, J. 1991. Comparative study of various formulations of evaporation from bare soil using in situ data. *Journal of Applied Meteorology,* 30**,** 1354-1365.

Manabe, S. 1969. Climate and the ocean circulation: 1, the atmospheric circulation and the hydrology of the Earth's surface. *Monthly Weather Review,* 97**,** 739-805.

Margulis, S. A. & Entekhabi, D. 2003. Variational assimilation of radiometric surface temperature and reference-level micrometeorology into a model of the atmospheric boundary layer and land surface. *Monthly Weather Review,* 131**,** 1272-1288.

Margulis, S. A., McLaughlin, D., Entekhabi, D. & Dunne, S. 2002. Land data assimilation and estimation of soil moisture using measurements from the Southern Great Plains 1997 Field Experiment. *Water Resources Research,* 38**,** 1299.

Massman, W. J. 1997. An analytical one-dimensional model of momentum transfer by vegetation of arbitrary structure. *Boundary-Layer Meteorology,* 83**,** 407-421.

Maybeck, P. S. 1979. *Stochastic models, estimation, and control,* New York, Academic Press, Inc.

McCabe, M. F. & Wood, E. F. 2006. Scale influences on the remote estimation of evapotranspiration using multiple satellite sensors. *Remote Sensing of Environment,* 105**,** 271-285.

McKenzie, N., Gallant, J. & Gregory, L. 2003. *Estimating water storage capacities in soil at catchment scales*. Australia, Cooperative Research Centre for Catchment Hydrology. Technical report 03/3.

McKenzie, N., Jacquier, D. W., Ashton, L. J. & Cresswell, H. P. 2000. *Estimation of soil properties using the Atlas of Australian Soils*. Canberra, Australia, CSIRO Land and Water. Technical report 11/00.

McNider, R. T., Song, A. J., Casey, D. M., Wetzel, P. J., Crosson, W. L. & Rabin, R. M. 1994. Towards a dynamic thermodynamic assimilation of satellite surface temperature in numerical atmospheric models. *Monthly Weather Review,* 122**,** 2784-2803.

McVicar, T. R., Jupp, D. L. B., Reece, P. H. & Williams, N. A. 1996. *Relating Landsat TM vegetation indices to in-situ Leaf Area Index measurements*. Australia, CSIRO Division of Water Resources. Technical memorandum 96.14.

Meng, C. L., Li, Z.-L., Zhan, X., Shi, J. C. & Liu, C. Y. 2009. Land surface temperature data assimilation and its impact on evapotranspiration estimates from the Common Land Model. *Water Resources Research,* 45**,** W02421.

Merlin, O., Walker, J., Panciera, R., Young, R. I., Kalma, J. D. & Kim, E. Soil moisture measurements in heterogeneous terrain. *In:* Oxley, L. & Kulasiri, D., eds. MODSIM07: International Congress on Modelling and Simulation, 2007 Christchurch, NZ. MSSANZ, Canberra, Australia, 2604–2610.

Mertens, J., Madsen, H., Kristensen, M., Jacques, D. & Feyen, J. 2005. Sensitivity of soil parameters in unsaturated zone modelling and the relation between effective, laboratory and *in situ* estimates. *Hydrological Processes,* 19**,** 1611-1633.

Milly, P. C. D. & Shmakin, A. B. 2002. Global Modeling of Land Water and Energy Balances. Part I: The Land Dynamics (LaD) Model. *Journal of Hydrometeorology,* 3**,** 283-299.

Mitchell, K. E., Lohmann, D., Houser, P. R., Wood, E. F., Schaake, J. C. & Robock, A., et al. 2004. The multi-institution North American Land Data Assimilation System (NLDAS): Utilizing multiple GCIP products and partners in a continental distributed hydrological modeling system. *Journal of Geophysical Research,* 109**,** D07890.

Monteith, J. L., Szeicz, G. & Waggoner, P. E. 1965. The measurement and control of stomatal resistance in the field. *Journal of Applied Ecology,* 2**,** 345-355.

Moran, M. S., Peters-Lidard, C. D., Watts, J. M. & McElroy, S. 2004. Estimating soil moisture at the watershed scale with satellite-based radar and land surface models. *Canadian Journal of Remote Sensing,* 30**,** 805-826.

Njoku, E., Jackson, E., Lakshmi, V., Chan, T. & Nghiem, S. 2003. Soil moisture retrieval from AMSR-E. *IEEE Transactions on Geoscience and Remote Sensing of Environment,* 41**,** 215-229.

Njoku, E. G. & Entekhabi, D. 1995. Passive microwave remote sensing of soil moisture. *Journal of Hydrology,* 184**,** 101-130.

Norman, J. M., Kustas, W. P. & Humes, K. S. 1995. A two-source approach for estimating soil and vegetation energy fluxes from observations of directional radiometric surface temperature. *Agricultural and Forest Meteorology,* 77**,** 263-293.

Northcote, K. H., et al. 1960–1968. *Atlas of Australian Soils, Sheets 1–10, with explanatory data*. Melbourne, Australia, CSIRO Australia and Melbourne University Press

Northcote, K. H. 1979. *A Factual Key for the Recognition of Australian Soils*. Rellim Technical Publications, Glenside, South Australia,

Overgaard, J., Rosbjerg, D. & Butts, M. B. 2006. Land-surface modelling in hydrological perspective – a review. *Biogeosciences,* 3**,** 229-241.

Owe, M., DeJeu, R. A. M. & Holmes, T. R. H. 2008. Multi-sensor historical climatology of satellite-derived global land surface moisture. *Journal of Geophysical Research,* 113**,** F01002.

Pan, M., Wood, E. F., Wojcik, R. & McCabe, M. F. 2008. Estimation of regional terrestrial water cycle using multi-sensor remote sensing observations and data assimilation. *Remote Sensing of Environment,* 112**,** 1282-1294.

Penman, H. L. 1948. Natural evaporation from open water, bare soil and grass. *Proceedings of the Royal Society of London,* 193**,** 120-146.

Peters-Lidard, C. D., Kumar, S. V., Mocko, D. M. & Tian, Y. 2011. Estimating evapotranspiration with land data assimilation systems. *Hydrological Processes,* 25**,** 3979-3992.

Pielke Sr., R. A., Avissar, R., Raupach, M. R., Johannes Dolman, A., Zeng, X. & Denning, S. 1998. Interactions between the atmosphere and terrestrial ecosystems: influence on weather and climate. *Global Change Biology,* 4**,** 461-475.

Pipunic, R. C., Ryu, D. & Walker, J. P. In press. Assessing Near-Surface Soil Moisture Assimilation Impacts on Modeled Root-Zone Moisture for an Australian Agricultural Landscape. *In:* Lakshmi, V. (ed.) *Remote Sensing of the Terrestrial Water Cycle.* USA, Wiley.

Pipunic, R. C., Walker, J. P. & Western, A. W. 2008. Assimilation of remotely sensed data for improved latent and sensible heat flux prediction: A comparative synthetic study. *Remote Sensing of Environment,* 112**,** 1295-1305.

Pitman, A. J. 2003. The evolution of, and revolution in, land surface schemes designed for climate models. *International Journal of Climatology,* 23**,** 479-510.

Potter, C. S., Randerson, J. T., Field, C. B., Matson, P. A., Vitousek, P. M., Mooney, H. A., et al. 1993. Terrestrial ecosystems production: A process model based on global satellite and surface data. *Global Biogeochemical Cycles,* 7**,** 811-841.

Puri, K., Dietachmayer, G., Steinle, P., Dix, M., Rikus, L., Logan, L., et al. 2013. Implementation of the initial ACCESS numerical weather prediction system. *Australian Meteorological and Oceanographic Journal,* 63**,** 265–284.

Raupach, M. R. 1989. A practical Lagrangian method for relating concentrations to source distributions in vegetation canopies. *Quarterly Journal of Royal Meteorology Society,* 115**,** 609-632.

Raupach, M. R., Finkele, K. & Zhang, L. 1997. *SCAM (Soil-Canopy-Atmosphere Model): Description and comparison with field data*. Australia, CSIRO Centre for Environmental Mechanics. Technical report 132.

Reichle, R. & Koster, R. D. 2004. Bias reduction in short records of satellite soil moisture. *Geophysical Research Letters,* 31**,** L19501.

Reichle, R. H., Crow, W. T., Koster, R. D., Sharif, H. O. & Mahanama, S. P. P. 2008. Contribution of soil moisture retrievals to land data assimilation products. *Geophysical Research Letters,* 35**,** L01404.

Reichle, R. H. & Koster, R. D. 2005. Global assimilation of satellite surface soil moisture retrievals into the NASA Catchment land surface model. *Geophysical Research Letters,* 32**,** L02404.

Reichle, R. H., Koster, R. D., Liu, P., Mahanama, S. P. P., Njoku, E. G. & Owe, M. 2007. Comparison and assimilation of global soil moisture retrievals from the Advanced Microwave Scanning Radiometer for the Earth Observing System (AMSR-E) and the Scanning Multichannel Microwave Radiometer (SMMR). *Journal of Geophysical Research,* 112**,** D09108.

Reichle, R. H., Kumar, S. V., Mahanama, S. P. P., Koster, R. D. & Liu, Q. 2010. Assimilation of satellite-derived skin temperature observations into land surface models. *Journal of Hydrometeorology,* 11**,** 1103-1122.

Reichle, R. H., Walker, J. P., Koster, R. D. & Houser, P. R. 2002. Extended versus Ensemble Kalman Filtering for Land Data Assimilation. *Journal of Hydrometeorology,* 3**,** 728-740.

Rhodin, A., Kucharski, F., Callies, U., Eppel, D. P. & Wergen, W. 1999. Variational analysis of effective soil moisture from screen-level atmospheric parameters: Application to a short-range weather forecast model. *Quarterly Journal of the Royal Meteorological Society,* 125**,** 2427-2448.

Richards, L. A. 1931. Capillary conduction of liquids through porous mediums. *Physics,* 1**,** 318-333.

Richter, H., Western, A. W. & Chiew, F. 2004. The Effect of Soil and Vegetation Parameters in the ECMWF Land Surface Scheme. *Journal of Hydrometeorology,* 5**,** 1131-1146.

Rüdiger, C., Western, A. W., Walker, J. P., Smith, A. B., Kalma, J. D. & Willgoose, G. R. 2010. Towards a general equation for frequency domain reflectometers. *Journal of Hydrology,* 383**,** 319-329.

Sabater, J. M., Rudiger, C., Calvet, J.-C., Fritz, N., Jarlan, L. & Kerr, Y. H. 2008. Joint assimilation of surface soil moisture and LAI observations into a land surface model. *Agricultural and Forest Meteorology,* 148**,** 1362-1373.

Schuurmans, J. M., Troch, P. A., Veldhuizen, A. A., Bastiaanssen, W. G. M. & Bierkens, M. F. P. 2003. Assimilation of remotely sensed latent heat flux in a distributed hydrological model. *Advances in Water Resources,* 26**,** 151-159.

Scipal, K., Holmes, T., de Jeu, R., Naeimi, V. & Wagner, W. 2008. A possible solution for the problem of estimating the error structure of global soil moisture data sets. *Geophysical Research Letters,* 35**,** L24403.

Sellers, P. J., Dickinson, R. E., Randall, D. A., Betts, A. K., Hall, F. G., Berry, J. A., et al. 1997. Modeling the Exchanges of Energy, Water, and Carbon Between Continents and the Atmosphere. *Science,* 275.

Sellers, P. J., Mintz, Y., Sud, Y. C. & Dalcher, A. 1986. A Simple Biosphere model (SiB) for use within general circulation models. *Journal of the Atmospheric Sciences,* 43**,** 505-531.

Sellers, P. J., Randall, D. A., Collatz, C. J., Berry, J. A., Field, C. B., Dazlich, D. A., et al. 1996. A revised land-surface parameterization (SiB2) for atmospheric GCMs. Part 1: model formulation. *Journal of Climate,* 9**,** 676–705.

Seuffert, G., Wilker, H., Viterbo, P., Drusch, M. & Mahfouf, J. F. 2004. The usage of screen-level parameters and microwave brightness temperature for soil moisture analysis. *Journal of Hydrometeorology,* 5**,** 516-531.

Seuffert, G., Wilker, H., Viterbo, P., Mahfouf, J.-F., Drusch, M. & Calvet, J.-C. 2003. Soil moisture analysis combining screen-level parameters and microwave brightness temperature: A test with field data. *Geophysical Research Letters,* 30**,** 1498.

Seyfried, M. S. & Murdock, M. D. 2001. Response of a new soil water sensor to variable soil, water content, and temperature. *Soil Science Society of America Journal,* 65**,** 28-34.

Seyfried, M. S. & Murdock, M. D. 2004. Measurement of soil water content with a 50 Hz soil dielectric sensor. *Soil Science Society of America Journal,* 68**,** 394-403.

Shuttleworth, W. J. 2007. Putting the "vap" into evaporation. *Hydrology and Earth System Sciences,* 11**,** 210-244.

Siriwardena, L., Chiew, F., Richter, H. & Western, A. W. 2003. *Preparation of a climate data set for the Murrumbidgee River catchment for land surface modelling experiments*. Australia, Cooperative Research Centre for Catchment Hydrology. Working Document 03/1

Smith, A. B., Walker, J. P., Western, A. W., Young, R. I., Ellet, K. M., Pipunic, R. C., et al. 2012. The Murrumbidgee Soil Moisture Monitoring Network Data Set. *Water Resources Research,* 48**,** W07701.

Snyder, W., Wan, Z., Zhang, Y. & Feng, Y.-Z. 1998. Classification-based emissivity for land surface temperature measurement from space. *International Journal of Remote Sensing,* 19**,** 2753-2774.

Sobrino, J. A., Jiminez-Munoz, J. C. & Paolini, L. 2004. Land surface temperature retrieval from LANDSAT TM 5. *Remote Sensing of Environment,* 90**,** 434-440.

Soil Moisture Equipment Corp. 1989. *TRASE system 1 operating instructions*. Santa Barbara, California, USA

Stauffer, D. R. & Seaman, N. L. 1990. Use of four-dimensional data assimilation in a limited-area mesoscale model. Part I: Experiments with synoptic-scale data. *Monthly Weather Review,* 118**,** 1250-1277.

Su, C.-H., Ryu, D., Young, R. I., Western, A. W. & Wagner, W. 2013. Inter-comparison of microwave satellite soil moisture retrievals over the Murrumbidgee Basin, southeast Australia. *Remote Sensing of Environment,* 134**,** 1-11.

Su, H., McCabe, M. F., Wood, E. F., Su, Z. & Prueger, J. H. 2005. Modeling evapotranspiration during SMACEX: comparing two approaches for local- and regional-scale prediction. *Journal of Hydrometeorology,* 6**,** 910-922.

Su, H., Wood, E. F., McCabe, M. F. & Su, Z. 2007. Evaluation of remotely sensed evapotranspiration over the CEOP EOP-1 reference sites. *Journal of the Meteorological Society of Japan,* 85A**,** 439-459.

Su, Z. 2002. The Surface Energy Balance System (SEBS) for estimation of turbulent heat fluxes. *Hydrology and Earth System Sciences,* 6**,** 85-99.

Sun, D., Pinker, R. T. & Basara, J. B. 2004. Land surface temperature estimation from the next generation of Geostationary Operational Environmental Satellites: GOES M-Q. *Journal of Applied Meteorology,* 43**,** 363-372.

Swinbank, W. C. 1950. The measurement of vertical transfer of heat and water vapour by eddies in the lower atmosphere. *Journal of Meteorology,* 8**,** 135-145.

Topp, G. C., David, J. L. & Annan, A. P. 1980. Electromagnetic determination of soil water content: Measurement in coaxial transmission lines. *Water Resources Research,* 16**,** 574-582.

Turner, M. R. J., Walker, J. P. & Oke, P. R. 2008. Ensemble member generation for sequential data assimilation. *Remote Sensing of Environment,* 112**,** 1421-1433.

Twine, T. E., Kustas, W. P., Norman, J. M., Cook, D. R., Houser, P. R., Meyers, T. P., et al. 2000. Correcting eddy covariance flux underestimates over a grassland. *Agricultural and Forest Meteorology,* 103**,** 279-300.

Ulaby, F. T., Moore, R. K. & Fung, A. K. 1982. *Microwave Remote Sensing: Active and Passive, Volume II: Radar Remote Sensing and Surface Scattering and Emission Theory,* Reading, Massachusetts, Addison-Wesley.

Ulaby, F. T., Moore, R. K. & Fung, A. K. 1986. *Microwave Remote Sensing: Active and Passive, Volume III: Volume Scattering and Emission Theory, Advanced Systems and Applications,* Massachusetts, Artech House, Inc.

Unidata Australia 1997. STARLOG Temperature probes. *User manual supplement.* MacLaren Enterprises.

van den Hurk, B., Doblas-Reyes, F., Balsamo, G., Koster, R. D., Seneviratne, S. I. & Camargo Jr, H. 2010. Soil moisture effects on seasonal temperature and precipitation forecast scores in Europe. *Climate Dynamics***,** DOI 10.1007/s00382-010-0956-2.

van Den Hurk, B. J. J. M., Jia, L., Jacobs, C., Menenti, M. & Li, Z.-L. 2002. Assimilation of land surface temperature data from ATSR in an NWP environment - a case study. *International Journal of Remote Sensing,* 23**,** 5193-5209.

van Dijk, A. I. J. M., Beck, H. E., Crosbie, R. S., de Jeu, R. A. M., Liu, Y. Y., Podger, G. M., et al. 2013. The Millennium Drought in southeast Australia (2001–2009): Natural and human causes and implications for water resources, ecosystems, economy, and society. *Water Resources Research,* 49**,** 1040-1057.

van Genuchten, M. T. 1980. closed-form eqution for predicting the hydraulic conductivity of unsaturated soils. *Soil Science Society of America Journal,* 44**,** 892-898.

Vinukollu, R. K., Wood, E. F., Ferguson, C. R. & Fisher, J. B. 2011. Global estimates of evapotranspiration for climate studies using multi-sensor remote sensing data: Evaluation of three process-based approaches. *Remote Sensing of Environment,* 115**,** 801-823.

Viterbo, P. & Beljaars, A. C. M. 1995. An improved land surface parameterization scheme in the ECMWF model and its validation. *Journal of Climate,* 8**,** 2716-2748.

Viterbo, P. & Beljaars, A. C. M. 2004. Impact of land surface on weather. *In:* Kabat, P. (ed.) *Vegetation, Water, Humans and the Climate: A New Perspective on an Interactive System.* Springer-Verlag.

Vrugt, J., Gupta, H. V., O Nuallain, B. & Bouten, W. 2006. Real-Time Data Assimilation for Operational Ensemble Streamflow Forecasting. *Journal of Hydrometeorology,* 7**,** 548-565.

Wagner, W., et al 2013. The ASCAT Soil Moisture Product: A Review of its Specifications, Validation Results, and Emerging Applications. *Meteorologische Zeitschrift,* 22**,** 5-33.

Wagner, W., Bloschl, G., Pampaloni, P., Calvet, J.-C., Bizzari, B., Wigneron, J. P., et al. 2007. Operational readiness of microwave remote sensing of soil moisture for hydrologic applications. *Nordic Hydrology,* 38**,** 1-20.

Wagner, W., Lemoine, G. & Rott, H. 1999. A method for estimating soil moisture from ERS scatterometer and soil data. *Remote Sensing of Environment,* 70**,** 191-207.

Wagner, W., Lemoine, G. & Rott, H. 1999. A method for estimating soil moisture from ERS scatterometer and soil data. *Remote Sensing of Environment,* 70**,** 191-207.

Walker, J. P. & Houser, P. R. 2001. A methodology for initializing soil moisture in a global climate model: Assimilation of near surface soil moisture observations. *Journal of Geophysical Research,* 106(D11)**,** 11761-11774.

Walker, J. P. & Houser, P. R. 2004. Requirements of a global near-surface soil moisture satellite mission: accuracy, repeat time, and spatial resolution. *Advances in Water Resources,* 27**,** 785-801.

Walker, J. P. & Houser, P. R. 2005. Hydrologic Data Assimilation. *In:* Aswathanarayana, A. (ed.) *Advances in Water Science Methodologies.* Rotterdam, A. A. Balkema.

Walker, J. P., Willgoose, G. R. & Kalma, J. D. 2001a. One-dimensional soil moisture profile retrieval by assimilation of near-surface measurements: A simplified soil moisture model and field application. *Journal of Hydrometeorology,* 2**,** 356-373.

Walker, J. P., Willgoose, G. R. & Kalma, J. D. 2001b. One-dimensional soil moisture profile retrieval by assimilation of near-surface observations: A comparison of retrieval algorithms. *Advances in Water Resources,* 24**,** 631–650.

Walker, J. P., Willgoose, G. R. & Kalma, J. D. 2004. In situ measurement of soil moisture: a comparison of techniques. *Journal of Hydrology,* 293**,** 85-99.

Wan, Z. & Dozier, J. 1996. A generalized split-window algorithm for retrieving land-surface temperature from space. *IEEE Transactions on Geoscience and Remote Sensing,* 34**,** 892-905.

Wan, Z. & Li, Z.-L. 1997. A physics-based algorithm for retrieving land-surface emissivity and temperature from EOS/MODIS data. *IEEE Transactions on Geoscience and Remote Sensing,* 35**,** 980-996.

Wan, Z., Zhang, Y., Zhang, Q. & Li, Z.-L. 2004. Quality assessment and validation of the MODIS global land surface temperature. *International journal of remote sensing,* 25**,** 261-274.

Wang, K. & Dickinson, R. E. 2012. A review of global terrestrial evapotranspiration: Observation, modeling, climatology, and climatic variability. *Reviews of Geophysics,* 50**,** RG2005.

Wang, K. & Liang, S. 2009. Evaluation of Aster and MODIS land surface temperature and emissivity products using long-term surface longwave radiation observations at SURFRAD sites. *Remote Sensing of Environment,* 113**,** 1556–1565.

Wang, Y.-P., Baldocchi, D., Leuning, R., Falge, E. & Vesala, T. 2007. Estimating parameters in a land surface model by applying non-linear inversion to eddy covariance flux measurements from eight FLUXNET sites. *Global Change Biology,* 13**,** 652-670.

Wang, Y.-P., Kowalczyk, E., Leuning, R., Abramowitz, G., Raupach, M. R., Pak, B., et al. 2011. Diagnosing errors in a land surface model (CABLE) in the time and frequency domains. *Journal of Geophysical Research,* 116**,** doi: 10.1029/2010JG001385.

Wang, Y.-P. & Leuning, R. 1998. A two-leaf model for canopy conductance, photosynthesis and partitioning of available energy I. Model description and comparison with a multi-layered model. *Agricultural and Forest Meteorology,* 91**,** 89-111.

Wang, Y.-P., Leuning, R., Cleugh, H. A. & Coppin, P. A. 2001. Parameter estimation in surface exchange models using non-linear inversion: How many parameters can we estimate and which measurements are most useful? *Global Change Biology,* 7**,** 495-510.

Wang, Y.-P., Trudinger, C. M. & Enting, I. G. 2009. A review of applications of model-data fusion to studies of terrestrial carbon fluxes at different scales. *Agricultural and Forest Meteorology,* 149**,** 1829-1842.

Western, A. W. & Seyfried, M. S. 2005. A calibration and temperature correction procedure for the water-content reflectometer. *Hydrological Processes,* 19**,** 3785-3793.

Williams, J., Ross, P. J. & Bristow, K. L. Prediction of the Campbell water retention function from texture, structure and organic matter. *In:* Van Genuchten, M. T., Leij, F. J. & Lund, L. J., eds. Proceedings of the International Workshop on Indirect Methods for Estimating the Hydraulic Properties of Unsaturated Soils, 1992 University of California, Riverside, California. 427-441.

Xu, T. R., Liu, S. M., Xu, Z. W., Liang, S. & Xu, L. 2013. A dual-pass data assimilation scheme for estimating surface energy fluxes with FY3A-VIRR land surface temperature. *Hydrology and Earth System Sciences,* 10**,** 3927-3972.

Yates, D. N., Chen, F. & Nagai, H. 2003. Land Surface Heterogeneity in the Cooperative Atmosphere Surface Exchange Study (CASES-97). Part II: Analysis of Spatial Heterogeneity and its Scaling. *Journal of Hydrometeorology,* 4**,** 219-234.

Yeoh, N., Walker, J., Young, R. I., Rüdiger, C., Smith, A. B., Ellett, K., et al. 2008. *Calibration of the Murrumbidgee Monitoring Network CS616 Soil Moisture Sensors*. Melbourne, Australia, Dept. of Civil and Environmental Engineering, The University of Melbourne.